Does crosstalk occur between neuropilin-1 and platelet-derived growth factor receptors in tumour cells?

A thesis submitted to the University of Manchester

for the degree of Doctor of Philosophy

in the Faculty of Life Sciences

2012

Ellinor Mary Tudge

Contents

Final word count: 57,710 words

List of Tables

List of Figures

Abstract

The platelet-derived growth factor (PDGF) and vascular endothelial growth factor (VEGF) families of receptor tyrosine kinases (RTKs) are evolutionarily related cell-surface receptors which regulate physiological and pathological angiogenesis. Neuropilins (NRPs) are transmembrane glycoproteins which function as co-receptors for VEGFR to mediate vascular development and angiogenesis. RTK signalling has a long established role in tumour-cell biology and downstream cellular effects of RTK activation, such as, sustained cell proliferation and invasion are known hallmarks of cancer. NRPs are also up-regulated in tumour cell lines and clinical specimens, and a major focus of NRP research has been to understand the role of NRPs in cancer, which to date has largely been attributed to NRPs contribution to VEGFR activation. Emerging evidence for NRPs in regulating the activation of adhesion molecules, growth factors and RTKs (other than VEGFR) illustrate that NRP has a much broader role in cancer. In cell types including smooth muscle cells, stem cells and tumour cells, there is now evidence that NRP-1 regulates PDGFR activation and signalling. Identification of the molecules that regulate PDGFR signalling will advance the understanding of tumour cell biology and contribute to the development of targeted therapies.

To date, few studies have evaluated the role of NRP-1/PDGFR signalling in cancer. The objective of this study was therefore, to elucidate the cellular mechanisms of NRP-1/PDGFR signalling, and to investigate how this cellular crosstalk modulates PDGFR-stimulated signalling, survival and migration of tumour cells. A subset of mesenchymal tumour cell lines that expressed NRP-1 and PDGFR-α and/or PDGFR-β and were identified to investigate NRP-1/PDGFR crosstalk. In these cell lines, NRP-1 could associate with PDGFR-α and PDGFR-β independent of PDGF growth factor stimulation. NRP-1 did not regulate PDGF-stimulated phosphorylation of PDGFR-α or PDGFR-β yet, in a subset of the cell lines, NRP-1 contributed to the activation of the MAPK-ERK and PI3K pathways. NRP-1 did not regulate PDGF-stimulated cell proliferation, yet NRP-1 knockdown attenuated PDGF-stimulated cell migration in certain cell lines. Together, this study has provided evidence of NRP-1/ PDGFR crosstalk, which affects the migratory potential of a subset of mesenchymal tumour cells. In these cell lines, NRP-1 knockdown does not inhibit the overall phosphorylation of PDGFR, yet does have subtle effects on specific downstream PDGFR pathways.

Declaration

No portion of the work referred to in the thesis has been submitted in support of an application for another degree or qualification of this or any other university or other institute of learning.

Copyright Statement

Acknowledgements

Firstly, I would like to thank my academic supervisor Professor Cay Kielty. I am indebted to Cay for her patience, encouragement and advice throughout the course of my studies.

I would also like to thank my industrial supervisor, Dr Steve Wedge, for his insightful advice and for kindly providing reagents for the project.

I would also like to thank all the past and present members of the Kielty lab for always creating such a pleasant working environment and for always providing a friendly ear. I particularly wish to thank Dr Stephen Ball for sharing his technical expertise and for his advice throughout the project. I am also very grateful to Dr Stuart Cain for his assistance with the BIAcore analysis and for sharing his extensive knowledge of molecular biology.

I wish to thank Mike Jackson, for providing flow cytometry assistance and Dr Peter March for his helpful bio-imaging advice.

I am also eternally grateful to all the close friends and family who have been an unwavering source of support, help and advice throughout my PhD. I would particularly like to thank, my Mum and Geoff for always believing in me, Phil for his love, never-ending patience and encouragement and my Dad for always listening.

Finally, I would like to thank the Biotechnology and Biological Sciences Research Council and AstraZeneca for funding this work.

Abbreviations

α Alpha
β Beta
γ Gamma
Ab Antibody
AMP Adenosine monophosphate
ANOVA Analysis of variables
ATCC American Type Culture Collection
ATP Adenosine triphosphate
BCA Bicinchoninic acid
bp Base pair
BSA Bovine serum albumin
C- Carboxyl terminus
COOH Carboxyl
Ca^{2+} Calcium
CNS Central nervous system
CO_2 Carbon dioxide
Cu^{1+} Cuprous cation
Cu^{2+} Copper
CUB Complement C1r/C1s, Uegf, Bmp1
CS Chondroitin sulphate
DAG Diacylglycerol
DAPI 4',6-diamidino-2-phenylindole
DEPC Diethyl dicarbonate
DMEM Dulbecco's Modified Eagles Medium
DMSO Dimethyl sulphoxide
DNA Deoxyribonucleic acid
E Embryonic day
ECL Enhanced chemiluminescence
EDC 1-ethyl-3-(3-dimethylaminopropyl) carbodimide hydrochloride
EDTA Ethylenediaminetetraacetic acid
EGF Epidermal growth factor
EGFR Epidermal growth factor receptor
ELISA Enzyme-linked immunosorbent assay
ERK Extracellular signal-regulated kinase
FAK Focal adhesion kinase

FBS Foetal bovine serum
FC Flow cytometry
FGF Fibroblast growth factor
FGFR Fibroblast growth factor receptor
FITC Fluorescein isothiocyanate
Flt-1 Fms-related tyrosine kinase 1
Flk-1 Fetal Liver Kinase 1
GAG Glycosaminoglycan
GDP Guanosine diphosphate
GIPC GAIP-interacting protein C terminus
Grb2 Growth factor receptor-bound protein 2
GTP Guanosine triphosphate
HBS Hepes buffered saline
HCl Hydrochloric acid
HDFs Human dermal fibroblasts
HEPES N-2-Hydroxyethylpiperazine-N'-2-ethane-sulphonic acid
HIF Hypoxia inducible factor
HRP Horse radish peroxidase
HSPG Heparan sulphate proteoglycan
HS Heparan sulphate
IB Immunoblot
IF Immunofluorescence
Ig Immunoglobulin
IP Immunoprecipitation
IP_2 Inositol-1,4,5-trisphosphate
IPTG isopropyl β-D-1-thiogalactopyranoside
kb Kilo base pairs
KCl Potassium chloride
KDR Kinase insert domain receptor
kDa Kilo Daltons
LB Lysogeny broth
mAb Monoclonal antibody
MAPK Mitogen activated protein kinase
MEK MAP kinase kinase
MES 2-(*N*-morpholino) ethanesulfonic acid
Mg^{2+} Magnesium
Mn^{2+} Manganese

MR Maximum resolution

MSC Mesenchymal stem cell

N- Amino terminus

NaCl Sodium chloride

NIP Neuropilin interacting protein

NRP Neuropilin

NSCLC

O_2 Oxygen

OD Optical density

P Phosphorylation

PAGE Polyacrylamide gel electrophoresis

PBS Phosphate buffered saline

PCR Polymerase chain reaction

PDGF Platelet-derived growth factor

PDGFR Platelet-derived growth factor receptor

PE Phycoerythrin

PIP_2 Phosphatidylinositol 4,5-bisphosphate

PIP_3 Phosphatidylinositol-3,4,5-trisphosphate

PI3K Phosphatidylinositol 3'-kinase

PKC Protein kinase C

PLA Proximity ligation assay

PLC Phospholipase C

PNS Peripheral nervous system

Ras-GAP Ras GTPase-activating protein

RNA Ribonucleic acid

RT Reverse transcription

RTK Receptor tyrosine kinase

RT-PCR Real time polymerase chain reaction

SEMA Semaphorin

SDS Sodium dodecyl sulphate

SH Src homology

SMC Smooth muscle cell

siRNA Small interfering ribonucleic acid

Sos Son of sevenless

TAE Tris-acetate EDTA

TBS-T Tris-buffered saline containing Tween 20

TE Tris-EDTA

TGF Transforming growth factor

Tris (hydroxymethyl) aminomethane

Tyr- Tyrosine

V Volts

VEGF Vascular endothelial growth factor

VEGFR Vascular endothelial growth factor receptor

v/v Volume per volume

w/v Weight per volume

Chapter 1– Introduction

1.0 Overview

Receptor tyrosine kinase (RTK) signalling has a long established role in tumourigenesis (Xu and Huang, 2010; Gschwind et al., 2004) and contributes to several of the hallmarks of cancer, such as sustained cell proliferation and invasion (Hanahan and Weinberg, 2011). The vascular endothelial growth factor (VEGF) family of RTKs has been extensively studied in cancer. Vascular endothelial growth factor receptor (VEGFR) signalling exerts multiple effects on cells within the tumour stroma including, endothelial cells and bone marrow-derived vascular precursor cells, culminating in increased tumour angiogenesis (Ellis and Hicklin, 2008; Roskoski, 2007b). This contribution of VEGFR signalling to tumour angiogenesis, has led to the development of VEGFR-targeted therapies, such as bevacizumab, which have been applied with some success in several types of cancer (Hurwitz et al., 2004; Miller et al., 2007; Sandler et al., 2006). Neuropilin-1 (NRP-1), which was established as a co-receptor for VEGFR (Soker et al., 1998), enhances VEGF-A binding to VEGFRs and potentiates VEGFR signalling (Shay Soker et al., 2002). Inhibition of NRP-1 binding to VEGF-A was reported to induce the apoptosis of breast cancer cell lines (Barr et al., 2005), illustrating the vital importance of NRP-1 in VEGFR signalling.

NRP-1 is associated with a poor prognosis and is expressed in many types of cancer (Kawakami et al., 2002; Latil et al., 2000; Ochiumi et al., 2006; Osada et al., 2004; Wey et al., 2005). NRP-1 is also expressed in cancer cells which lack VEGFR expression (Pellet-Many et al., 2008) implicating a wider role for this receptor in tumourigenesis. The diverse functions of NRP-1 have been corroborated in a number of studies outlining the role of NRP-1 in signalling by c-Met (Hu et al., 2007), fibroblast growth factor receptor (FGFR) (West et al., 2005) platelet-derived growth factor receptor (PDGFR) (Ball et al., 2010; Cao et al., 2010; Pellet-Many et al., 2011) and transforming growth factor-beta (TGF-β) (Cao et al., 2010). The intracellular signalling proteins regulated by NRP-1 mediate cellular effects such as cell cycle progression, migration and differentiation, processes that are deregulated in the development of cancer. Amongst these proteins, PDGFRs share the closest relationship with VEGFRs. VEGFR and PDGFR tyrosine kinases share a close phylogenic relationship (Dormer and Beck, 2005; Gu and Gu, 2003) and VEGF-A has been reported to signal through PDGFRs in mesenchymal stem cells (MSCs) (Ball et al., 2007b; Pennock and Kazlauskas, 2012). Using VEGFR targeted therapies, such as sorafenib and sunitinib, kinases including PDGFR are also inhibited (Karaman et al., 2008). Multi-kinase VEGFR and PDGFR inhibitors have been reported to show greater efficacy than single agents targeted against VEGFR in regressing mature tumour vasculature (Erber et al., 2004). Simultaneous inhibition of PDGFR and VEGFR is proposed to inhibit the endothelial and pericyte interactions

which stabilise tumour vessels and contribute to tumour cells evading anti-angiogenic therapies (Erber et al., 2004; Hasumi et al., 2007). These data are substantiated by the reported RTK co-activation networks which exist in multiple drug resistant tumours (Xu and Huang, 2010). Pillay et al (2009) proposed a mechanism whereby a dominant RTK sits at the top of a hierarchy of RTKs. Inhibition of the dominant RTK elevates a secondary RTK to the primary position which in turn compensates for the inhibited RTK (Pillay et al., 2009). Such co-activation networks are based on the emerging knowledge that many RTKs can activate convergent pathways, albeit to different degrees. The close relationship between VEGFR and PDGFR makes it feasible that such co-activation networks exist between these two RTKs. Moreover, one of the mechanisms proposed to mediate resistance to VEGFR-targeted therapies involves a compensatory increase in VEGF-A and PDGF secretion (Ellis and Hicklin, 2009; Fan et al., 2011) which could potentiate PDGFR signalling. The concept that NRP-1 could be involved in regulating the activity of both VEGFR and PDGFR would therefore, make NRP-1 an effective target for anti-angiogenic therapies.

Identification of the molecules that regulate RTK signalling will advance the understanding of tumour cell biology and contribute to the development of targeted therapies. To date, no studies have extensively evaluated how NRP-1 and PDGFR may functionally interact or 'crosstalk' to regulate PDGFR signalling in cancer. This project therefore provided an important opportunity to advance the understanding of NRP-1 and PDGFR crosstalk, and the possible role of this cellular mechanism in tumour cell biology.

1.1 Neuropilins

Neuropilins (NRPs) are transmembrane glycoproteins which have essential roles in the development of the embryonic nervous system and cardiovascular system (Gu et al., 2003; Kawasaki et al., 1999; Kitsukawa et al., 1997; Lee et al., 2002). NRPs are receptors for the class 3 semaphorins, which are a family of secreted polypeptides with essential roles in axon guidance (Neufeld and Kessler, 2008). NRPs also act as co-receptors during VEGFR signalling to mediate vascular development and angiogenesis (Neufeld, 2002). The function of NRPs in physiological and pathological angiogenesis has prompted research into NRPs role in tumourigenesis and tumour progression (Ellis, 2006; Miao et al., 2000). The structure, isoforms, and biological functions of NRPs will be discussed in the forthcoming sections.

1.1.1 Neuropilin domain structure

Both NRP-1 and NRP-2 share a similar domain structure, with three extracellular domains (each~840 residues), a single trans-membrane (TM) domain (~25 residues) and a single short cytoplasmic domain (~40 residues) (Figure 1.0). The overall amino acid homology of the two NRPs is 44%, with 923 and 926 amino acids for NRP-1 and NRP-2, respectively.

The NRP extracellular regions comprise two a domains (a1 and a2), two b domains (b1 and b2) and a single c domain. The NRP a1/ a2 domains are CUB domains and are essential for the binding of the semaphorins. These types of domains were first identified in the complement subcomponents C1r and C1s, followed by Uegf and Bmp1 proteins and thus were defined CUB domains (Bork and Beckmann, 1993). All CUB domains contain four conserved cysteine residues, which form two disulphide bridges. The secondary structure of CUB domains consists of anti-parallel ß-strands folded to resemble an immunoglobulin-like domain structure. CUB domains are often found in developmental proteins such as the A5 antigen and the NRPs (Bork and Beckmann, 1993; Takagi et al., 1991).

The second of the extracellular domains, b1/b2, are members of the coagulation factor family of proteins and are homologous to the coagulation factors V and VIII membrane adhesion (type C2) domains. The b domain tandem repeats have 153 and 151 amino acid residues in b1 and b2, respectively. X-ray crystallography studies of the NRP-1 b domains have identified a conserved six residue b1/ b2 domain linker region, which results in a fixed orientation of the two domains (Vander Kooi et al., 2007). This linker region is part of the inter-domain interface buried surface area and the hydrophobic residues within this inter-domain interface are conserved in both NRP-1 and NRP-2 homologues (Vander Kooi et al., 2007). The b domains bind multiple ligands, including VEGF-A, heparin, and the semaphorins. Serine-612, in the linker region between the b1/b2 and the c

domains of NRP-1, also provides the binding site for heparan sulphate (HS) and chondroitin sulphate (CS) glycosaminoglycans (GAGs). Post-translation, in the Golgi-apparatus, GAG chains are covalently attached to proteins with Gly-Ser consensus sequences. Serine-612 is the only identified GAG attachment site in NRP-1 and thus, NRP-1 only exists as either a HS or CS modified entity (Frankel et al., 2008; Shintani et al., 2006). NRP-1 often exists as a proteoglycan, and in smooth muscle cells and endothelial cells a substantial proportion of cellular NRP-1 is GAG-modified, yet the non-GAG modified NRP-1 is also always detected (Frankel et al., 2008).

The c domain of NRP is a type of domain found in functionally diverse proteins such as meprins and zonadhesins. This type of domain was first discovered in meprin, A5 protein and receptor tyrosine phosphatase μ, which led to the name MAM (meprin, A5, μ) domain (Bork and Beckmann, 1993). MAM domains contain approximately 170 amino acids, with four highly conserved cysteine residues that are predicted to form disulphide bonds and a secondary β-sheet structure. The MAM domain functions to regulate homodimeristion and oligiomerisation. Both NRP-1 and NRP-2 form hetero and homo-oligomers (Takahashi et al., 1998) and it has been reported only negligible oligomerisation of NRP occurs in the absence of the MAM domain (Nakamura et al., 1998).

The small NRP TM and cytoplasmic domains consist of approximately 25 and 40 amino acid residues, respectively. There is controversy over whether or not these domains function in a signalling capacity, and initial studies suggested no functional roles (Nakamura et al., 1998). However, further work suggested that the TM domain, along with the MAM domain, is essential in oligomerisation (Giger et al., 1998). The identification of a NRP-interacting protein (NIP) with a central PSD-95/Dlg/ZO-1 (PDZ) domain, which interacts with the C-terminus of NRP-1, suggested that the cytoplasmic domain of NRP-1 might have a signal transduction role (Cai and Reed, 1999). This possibility is strengthened by the fact that the NRP-1 C-terminus is conserved from *Xenopus* to human, which might suggest that the NRP-1 interaction with NIP is crucial and possibly a means transduce intracellular signals (Roth et al., 2008). Prahst et al (2008) suggested that the NRP-1 PDZ domain interacts with synectin to control VEGFR-2 and NRP-1 complex formation (Prahst et al., 2008) and the C-terminus of NRP-1 is essential for PDGF mediated activation of p130Cas, a protein important in cell migration (Evans et al., 2011; Pellet-Many et al., 2011). The NRP-1 PDZ domain is also reported to interact with the GAIP-interacting protein (GIPC) to control integrin α5β1 internalisation (Valdembri et al., 2009). In the TM domain of NRP, a highly conserved GxxxG motif has also been identified (Senes et al., 2000) which is present in signalling proteins, such as the ErbB family (Bennasroune et al., 2004) and contributes to receptor activation. In NRP-1, mutating the GxxxG motif inhibits semaphorin/ NRP-1 complex formation, suggesting a potential signalling role for the TM domains of NRP (Roth et al., 2008). Overall, although the TM and cytoplasmic

domains of NRP are less well characterised, current evidence indicates a key role for these regions in NRP signal transduction.

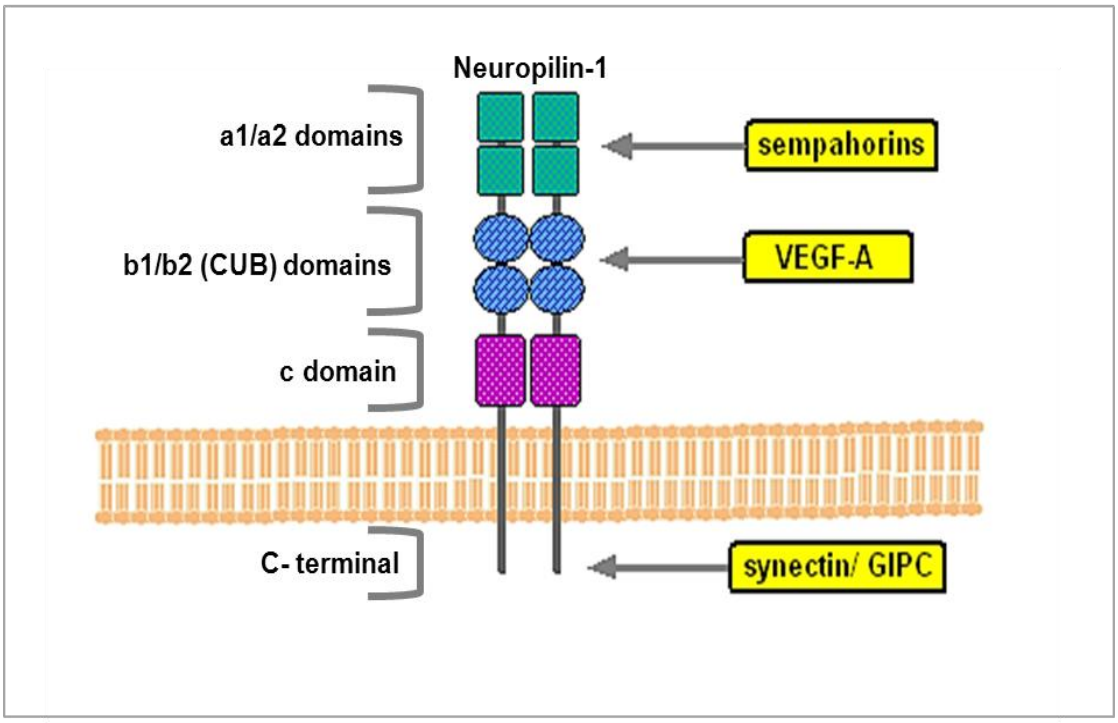

Figure 1.0: The domain structure and associated ligands of neuropilin-1
The diagram illustrates the domain structure of NRP-1. The NRP extracellular regions comprise two a domains (a1 and a2), two b domains (b1 and b2) and a single c domain. The a1/a2 regions of NRP-1 are CUB domains which serve as the main binding site for class 3 semaphorins. The b domains serve as the binding site for VEGF-A. NRP-1 exists as a dimer and the c domain has important roles in oligomerisation. NRP-1 has a TM region and a short intracellular C-terminal extension. The C-terminus of NRP-1 is reported to bind to synectin and GIPC and regulate the activity of proteins including p130Cas, VEGFR-2 and integrin α5β1. The linker-region between the b1/b2 domains and the c domain also contains serine-612, which serves as the attachment site for HS or CS GAGs (see Section 1.1.1).

1.1.2 Neuropilin genes and isoforms

NRPs were first identified in *Xenopus* (Takagi et al., 1991) and since then, NRP expression has been documented in vertebrates including, mammals (Kawakami et al., 1996; Reza et al., 1999), chickens (Takagi et al., 1995) and zebrafish (Bovenkamp et al., 2004). NRP expression across mammalian species is highly conserved (Bovenkamp et al., 2004) owing to their crucial roles in neuronal and cardiovascular development.

In humans, NRP-1 and NRP-2 genes are located on chromosomes 10p12 and 2q34, respectively (Rossignol et al., 1999). These genes span 120 kb for NRP-1 and 112 kb for NRP-2. The NRP-1 gene has 16 introns and 17 exons and the NRP-2 gene has 16 introns and 18 exons (Figure 1.1). In the coding regions of NRP-1 and NRP-2, five out of the seventeen exons are identical in size, with the remainder being very similar, suggesting that the different isoforms of NRP have arisen from a gene duplication event. The most variable regions in the NRP genes are the linker regions between the b and c domains, and the c and TM domains. These linker regions are also the sites of alternative splicing, resulting in the generation of several different membrane-bound and soluble isoforms of NRP-1 and NRP-2 (Figure 1.1) (Rossignol et al., 2000).

In the case of NRP-1, two soluble isoforms (sNRP-1) were initially identified. These isoforms were generated from pre-mRNA processing in intron 11 and 12 and thus were designated, s_{11}NRP-1 and s_{12}NRP-1 (Gagnon et al., 2000; Rossignol et al., 2000). Subsequently, two further soluble NRP-1 isoforms were identified; sIIINRP-1 and sIVNRP-1 (Cackowski et al., 2004), which are relatively less abundant at the mRNA level than s_{11}NRP-1 and s_{12}NRP-1. These soluble forms of NRP-1 lack the c domain, however they retain the ability to bind to VEGF-A and the class 3 semaphorins (Cackowski et al., 2004; Rossignol et al., 2000). As a monomer, the sNRP-1 isoforms have been reported to antagonise VEGF-A_{165} signalling through VEGFR-2, thereby inhibiting angiogenesis (Gagnon et al., 2000; Schuch et al., 2002). However, as a dimer, this function is effectively reversed, with the sNRP-1 promoting VEGF-A binding to VEGFR and angiogenesis (Yamada et al., 2001). A membrane-associated isoform, NRP-1 (△exon16), has also been identified which is generated from alternative pre-mRNA splicing. In NRP-1 (△exon16), the coding region of exon sixteen, located between the c domain and TM domain is replaced by an arginine codon (Figure 1.1) (Tao et al., 2003). NRP-1 (△exon16) isoform accounts for 30% of the mRNA transcript in endothelial cells and tumour cells and functions in a similar capacity to NRP-1 (Tao et al., 2003). NRP-2 has two major membrane-bound isoforms, NRP-2a and NRP-2b and one soluble isoform s9NRP-2 (Figure 1.1) (Rossignol et al., 2000). In summary, although these various isoforms of NRP are expressed in many healthy and cancerous tissues, their functions remain poorly defined.

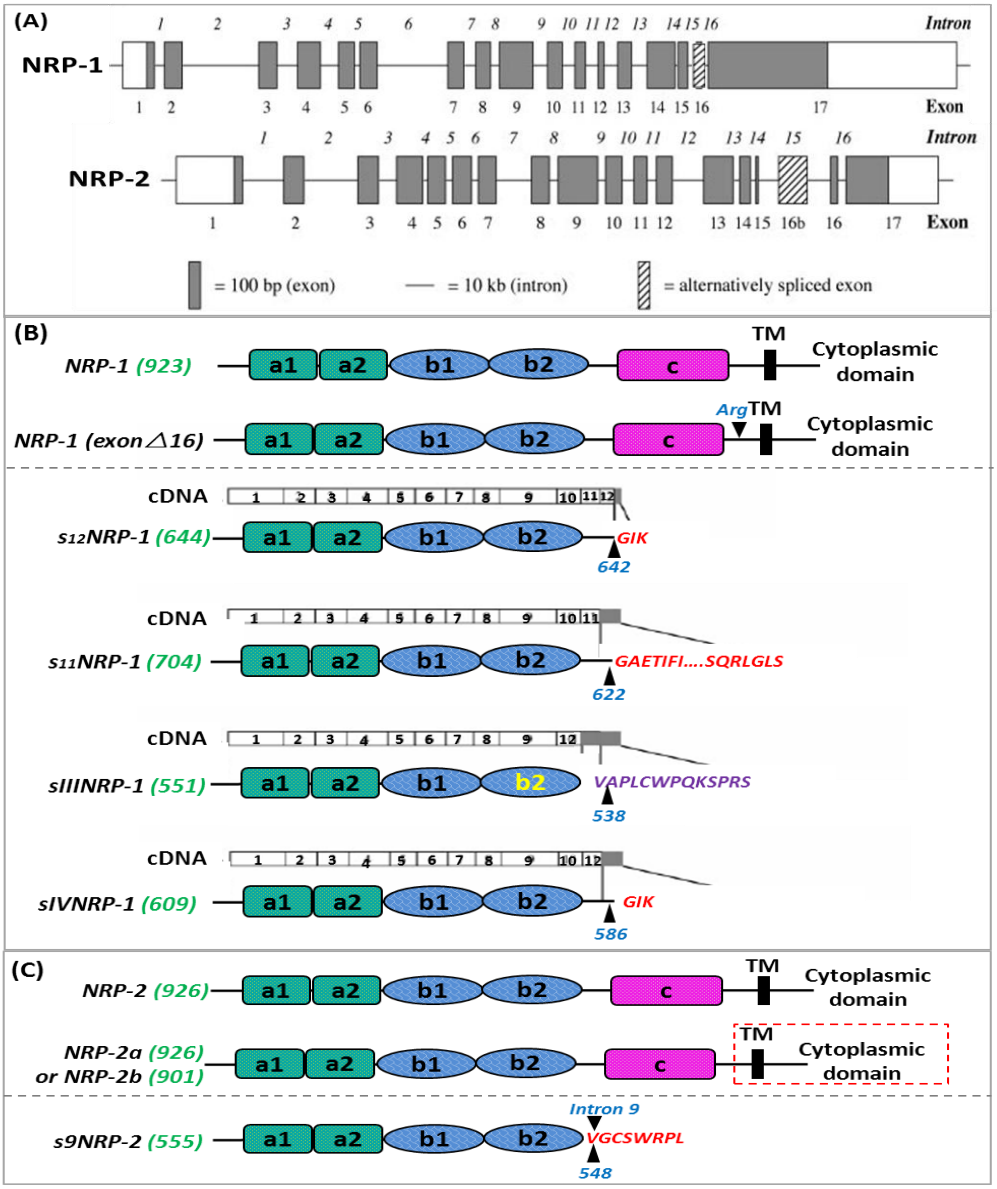

Figure 1.1: The genomic organisation and isoforms of neuropilins

(A) The genomic organisation of the NRP-1 and NRP-2 genes. The lines represent introns and the boxes represent exons, with the coding regions shaded grey and the non-translated regions shaded white. The hashed shading highlights alternatively spliced exons. Both NRP-1 and 2 have 17 exons and 16 introns, with the initiating methionine in exon 1 and the termination sequence/ 3'UTR in exon 17. Figures in **(B)** and **(C)** detail the structure of NRP-1 and 2 isoforms, respectively. The specific isoform is detailed to the left with the amino acid length of each isoform highlighted green, in brackets. Amino acid sequences, encoded by exons, are in purple and intron coded sequences are in red**.** The blue italic indicates the start position of the C-terminal amino acid sequences. **(B)** NRP-1 (Exon△16) is alternatively spliced in the region between the c and TM domain, and arginine is inserted. The s_{11}NRP-1 and s_{12}NRP-1 are truncated soluble isoforms with intron-derived (intron 11 or 12) C-terminal amino acid sequences (red). sIIINRP-1 lacks exon 10 and 11, and thus the b2 domain (yellow text) is truncated by 48 residues. The C-terminal of sIIINRP-1 has a novel 13 amino acid sequence generated from reading exon 12 in an alternative frame. sIVNRP-1 lacks exon 11 and has an intron 12 encoded C-terminus, GIK. Alternative splicing of exon 16b (see A) of NRP-2 generates NRP-2b. NRP-2a and 2b show divergence in the TM and cytoplasmic domains. The s9NRP-2 isoform is truncated in b2 and contains an intron 9 derived C-terminal. Figures have been adapted from Rossignol et al (2000).

1.1.3 Neuropilin ligand binding

1.1.3.1 The semaphorins

As referred to (Section 1.1), one of the ligands which binds to the NRPs are the semaphorins. The semaphorins were initially identified as proteins that mediate growth cone collapse and axon guidance during development of the central nervous system (Luo et al., 1993). Since then, their roles as ligands for the NRP and plexin receptors has been well defined, with these receptors being expressed in many cell types including endothelial cells and various cancer cells. It is, therefore, not surprising that the semaphorins have been implicated in many biological processes including angiogenesis, the immune response and tumour metastasis (Catalano et al., 2006; Neufeld and Kessler, 2008; Neufeld et al., 2005).

The semaphorins are members of an extensive protein family which contains twenty-one vertebrate genes, and a further eight genes which are only found in invertebrates. The sheer size of this protein family has meant that their nomenclature had become confusing up until the development of a standard nomenclature in 1999 (Goodman et al., 1999). Under this new nomenclature, semaphorins are abbreviated to SEMA followed by the subfamily number e.g. SEMA3D. There are both membrane-bound and soluble forms of SEMA and, based on common features such as immunoglobulin (Ig) like domains and carboxyl segments, they are separated into eight sub-classes (Goodman et al., 1999). The SEMAs also share a homology domain of approximately 550 amino acid residues (Kolodkin et al., 1993). Only sub-classes three to seven are expressed in vertebrates (Goodman et al., 1999). The membrane-bound SEMAs, belonging to classes 3 to 7, bind to the plexin receptors, whereas all SEMA3 proteins are secreted soluble forms that bind to NRPs, (with the exception of SEMA3E which can bind directly to plexins)(Neufeld and Kessler, 2008) (Figure 1.2).

All SEMAs contain a conserved five hundred residue sema domain at the N-terminus, within which, a 70 amino acid region was reported to determine the binding and activity of a number of the SEMA3 proteins (Gherardi et al., 2004; Koppel et al., 1997). A cysteine-rich domain, abbreviated as the PSI (denoting its presence in plexins, semaphorins and integrins)(Bork et al., 1999), is located close to the C-terminus of the sema domain (Figure 1.2). The crystal structures of the sema domain were resolved for SEMA3A (Antipenko et al., 2003) and SEMA4D (Love et al., 2003), revealing a conserved seven blade β-propeller structure which is common in both intracellular and extracellular proteins (Jawad and Paoli, 2002; Springer, 2002). The sema domain is unusual in the fact that it is large to be in this fold, with most other propeller folded proteins being approximately 400 residues. Binding of SEMA3A to NRP-1 is predicted to occur at amino acids 355-366,

corresponding to β-propeller loops 4b-c and 5c-5d (Antipenko et al., 2003). This fraction of the sema domain binds to the extracellular CUB domains of NRP, with a basic sema carboxyl domain binding to the NRP b domains (Gu et al., 2002).

Much study has focused on the semaphorins, with the SEMA4, SEMA6 and SEMA7 immunological functions ranging from immunomodulatory roles to an involvement in autoimmune conditions, being recently reviewed (Suzuki et al., 2008). SEMAs have also been implicated in inhibiting platelet function (SEMA3A) (Kashiwagi et al., 2005) and have involvement in neurological conditions such as epilepsy (Gant et al., 2009), highlighting their functional diversity. One of the primary areas of research has focused on SEMA involvement in angiogenesis and tumour progression (Neufeld and Kessler, 2008), with much focus on NRP and the SEMA3 subgroup. SEMA3A was initially termed chick collapsin I, for its role inducing the collapse of specific neural growth cones in developing chicks (Luo et al., 1993). The SEMA3 subgroup have since been well characterised as ligands for the NRPs, however, the binding affinities of SEMA3 to NRP-1 and NRP-2 do differ (Figure 1.2). SEMA3B and 3C binds to both NRPs, however, SEMA3A and SEMA3D bind and signal exclusively through NRP-1. In contrast, SEMA3G binds and signals through only NRP-2. The other well-characterised SEMA3F will bind NRP-1 with low affinity, compared to NRP-2 binding, and all signal transduction occurs via NRP-2 (Chen et al., 1997; Kolodkin et al., 1997; Takahashi et al., 1998; Taniguchi et al., 2005).

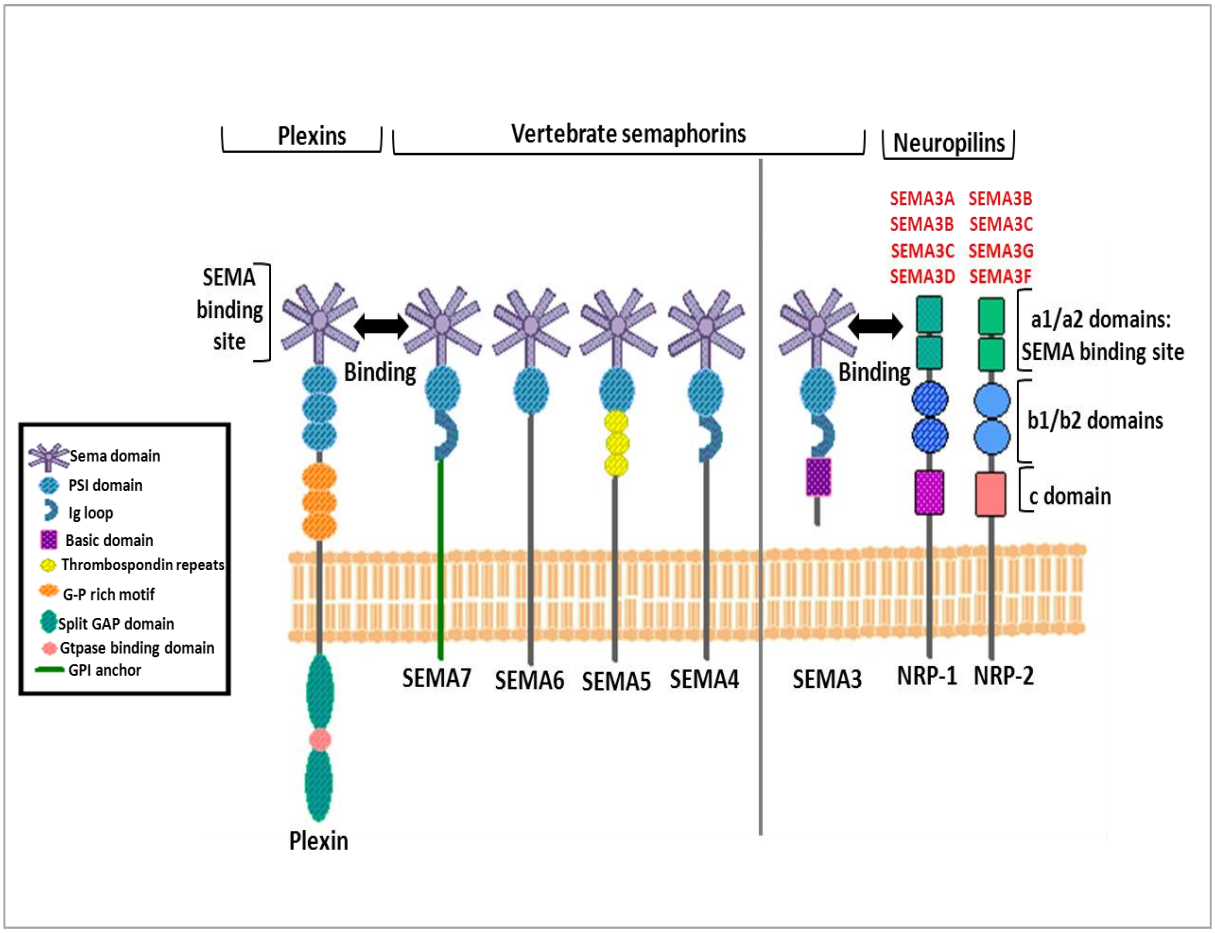

Figure 1.2: The structure and binding specificities of the semaphorins
The figure illustrates the structure of the vertebrate semaphorins, with the different structural features coded by a key in the left of the figure. SEMA4 to SEMA7 are membrane-bound and bind to the plexins via interactions between the SEMA and plexin sema domains. The soluble SEMA3s bind via their sema domain to the a1/a2 domains of NRPs, with the different specificities. The binding specificities of the different SEMA3 to either NRP-1 or NRP-2 are highlighted in red. Figure adapted from Neufeld et al (2008).

1.1.3.2 VEGF isoforms

Vascular endothelial growth factors (VEGF) are members of the cysteine knot superfamily of growth factors, characterised by the presence of eight conserved cysteine residues (Vitt et al., 2001). There are seven identified members of the VEGF family designated; VEGF A, VEGF-B, VEGF-C, VEGF-D, VEGF-E, VEGF-F and placental growth factor (PLGF) and VEGFs have been found in all vertebrates. The seven VEGFs have different binding specificities for VEGFR-1, VEGFR-2, and VEGFR-3, and for NRP-1 and NRP-2 (Figure 1.3). The different VEGF family members have distinct but critical roles in vasculogenesis, angiogenesis and lymphangiogenesis (Holmes and Zachary, 2005; Roskoski, 2007b).

Human VEGFs include VEGF-A, VEGF-B, VEGF-C, VEGF-D and PLGF (Holmes and Zachary, 2005). The VEGF-B gene encodes 188 amino acids and can be alternatively spliced into two different variants encoding proteins,VEGF-B_{186} and VEGF-B_{167}, which are homodimers of 60 kDa and 42 kDa, respectively (Olofsson, 1996a; Olofsson et al., 1996b). VEGF-B_{186} can be proteolytically processed at Arg-127 to generate a 34 kDa dimer (Makinen et al., 1999; Siegfried et al., 2005). The two isoforms of VEGF-B only differ in their C-terminal domains and bind exclusively to VEGFR-1 and NRP-1 (Nash et al., 2006). VEGF-C and VEGF-D are subject to post synthetic proteolytic processing and processed VEGF-C and VEGF-D bind to VEGFR-2, VEGFR-3, and NRP-2 (Figure 1.3) (Joukov et al., 1997a; Stacker et al., 1999). VEGF-C is synthesised as a precursor protein that is activated by the intracellular proprotein convertases, furin, PC5, and PC7. VEGF-C is then secreted and further processed by proteolytic enzymes, for e.g., plasmin, in the extracellular environment to generate the 21 kDa VEGF-C homodimer (Joukov et al., 1997b; Siegfried et al., 2003). VEGF-D is secreted from the cell as a pre-cursor protein which is proteolytically cleaved at the N-terminus and C-terminus by furin, PC5, and PC7 and this processing facilitates the VEGF-D/VEGFR-2 interaction (McColl et al., 2007). Alternative splicing of the human PLGF gene gives rise to four PLGF protein isoforms, PLGF-1, PLGF-2, PLGF-3 and PLGF-4 (Cao et al., 1997; Maglione et al., 1993; Yang et al., 2003). The different PLGF isoforms bind exclusively to VEGFR-1 with high affinity (Park et al., 1994), however, only PLGF-2 binds to the b1/b2 domains of NRP-1 (Mamluk et al., 2002; Migdal et al., 1998) (Figure 1.3).

Alternative splicing of the VEGF-A gene generates at least eight different transcripts resulting in eight protein isoforms (Figure 1.3), distinguished by a number denoting the amino acid length, e.g. VEGF-$A_{165.}$ All the transcripts for each isoform contain exons 1-5 and exon 8, whereas exons 6 and 7 are alternatively spliced, which affects the binding specificities of the different VEGF-A isoforms for VEGFR-1, VEGFR-2, and NRPs (Figure 1.4) (Robinson and Stringer, 2001; Tischer et al., 1991). The larger isoforms, VEGF-A_{183}, VEGF-A_{189}, and VEGF-A_{206} are tightly bound to

heparan sulphate proteoglycans (HSPG) including NRP-1/ NRP-2 and thus, are sequestered at the cell surface and in the extracellular matrix. The extracellular bioavailability and activity of these larger isoforms is thought to be mediated by proteolytic cleavage of their C-terminal by enzymes such as plasmin (Park et al., 1993). Proteolytic cleavage of VEGF-A_{189} allows the release of an active, diffusible 110 amino acid fragment (Lee et al., 2005) which is able to bind to VEGFR-2 (Plouët et al., 1997). VEGF-A_{148} has not been well studied, however VEGF-A_{145} binds to VEGFR-1 and VEGFR-2, HSPG, and NRP-2 (Woolard et al., 2009) (Figure 1.3). The best studied isoforms of VEGF-A, which are involved in NRP interactions, are VEGF-A_{121} (the evidence for VEGF-A_{121}/NRP-1 interactions is not conclusive) and VEGF-A_{165}, and these interactions will now be discussed.

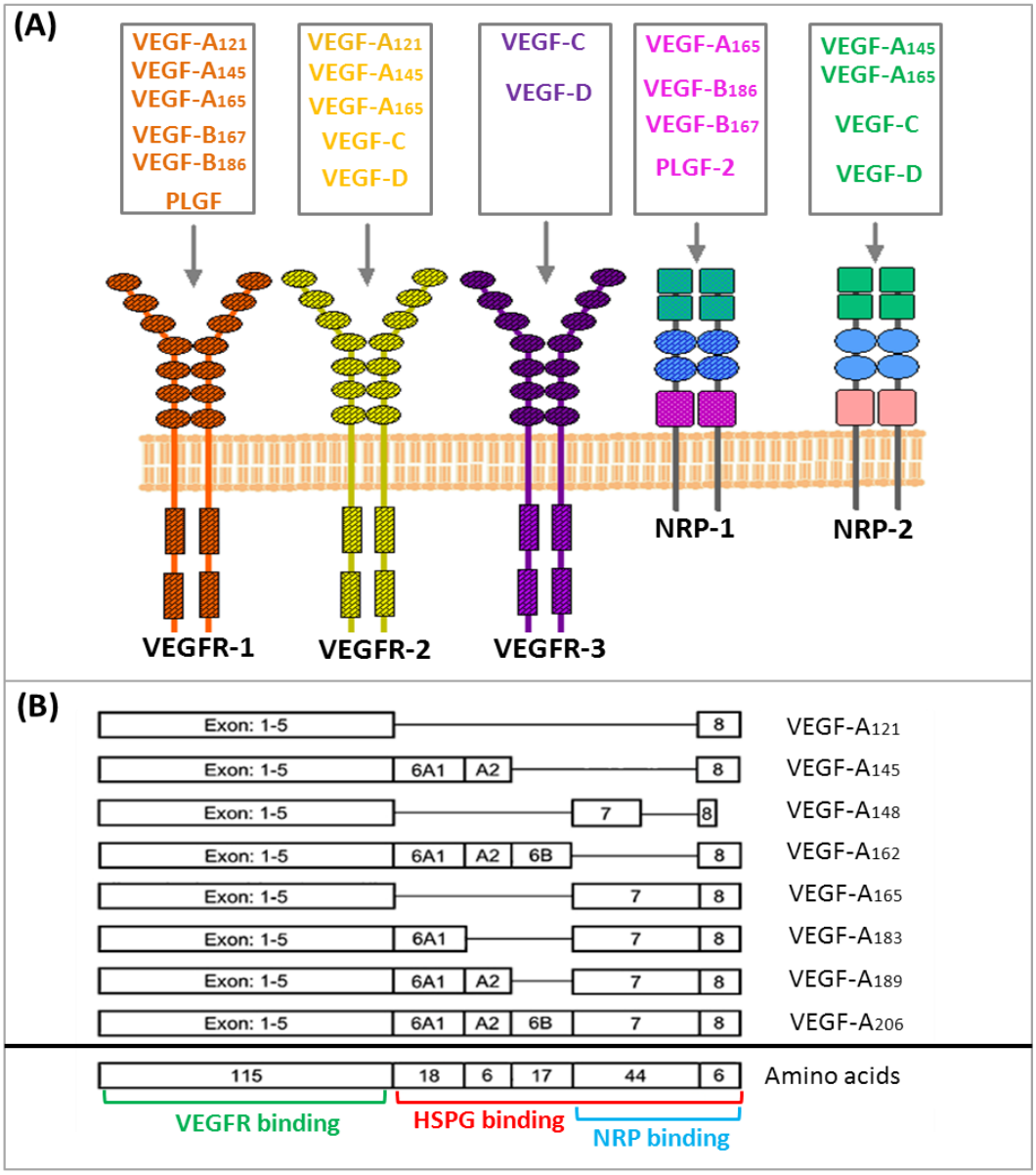

Figure 1.3: The different isoforms of VEGF and their binding specificity for VEGFRs and NRPs

(A) The figure illustrates the binding specificities of the different isoforms of VEGF for VEGFRs and NRPs. VEGFR-1 and VEGFR-2 bind to a larger array of VEGF isoforms than VEGFR-3. VEGF-B shows specificity for NRP-1 whereas; VEGF-C and VEGF-D show specificity for NRP-2. **(B)** The exon arrangement of the different isoforms of VEGF-A are illustrated, with the corresponding amino acid positions indicated in the lower half of the figure. Exons 1-5 encode the VEGFR binding domains of VEGF-A and the NRP binding domain is encoded by exons 7 and 8 (Parker et al., 2012). Alternative splicing of the VEGF-A gene generates the different VEGF-A isoforms, with variability in the exon 6 and 7 region. The figure in **(B)** was adapted from (Eming and Krieg, 2006).

Soker et al (1998) initially described the binding of VEGF-A_{165} to NRP-1, and reported that NRP-1 enhanced the binding of VEGF-A_{165} to VEGFR-2 and subsequent VEGFR-2 signalling. This study also reported the region of VEGF-A_{165}, encoded by exon 7 (amino acids 116-157), binds to the NRP-1 b1/b2 domains (Soker et al., 1998). As the region of VEGF-A_{165} encoded by exon 3 and 4 binds to VEGFR-1 and VEGFR-2, respectively, a model was proposed whereby VEGF-A_{165} acts as a bridging molecule linking VEGFR-1 or VEGFR-2 with NRP-1 (Shraga-Heled et al., 2007; Soker et al., 2002) (Figure 1.4). This VEGF-A_{165} bridge was proposed to bring the NRP and VEGF receptors into close proximity, leading to the formation of a NRP-1/VEGFR complex which potentiates VEGFR signalling. However, this bridging model is by no means universally accepted.

Disputing the exon 7-encoded NRP-1 binding site, Suarez et al (2006) isolated a splice variant of VEGF-A, VEGF-A_{165b}, from kidney epithelial cells. This isoform is identical to VEGF-A_{165}, except that the last 6 amino acids are encoded by exon 9 as oppose to exon 8. Exon 7 is intact in VEGF-A_{165b}, yet, it was concluded that VEGF-A_{165b} did not bind to NRP-1, suggesting that the exon 7 encoded region of VEGF-A is not critical for NRP-1 binding (Suarez et al., 2006). Further evidence, using a bicyclic peptide to antagonise VEGF-A binding to NRP-1, detailed that peptides comprising, the exon 8 encoded region of VEGF-A yet lacking the exon 7 encoded regions, inhibited NRP-1 binding to VEGFR-2. However additive inhibition of NRP-1 binding was documented when peptides blocked the regions of VEGF-A encoded by both exon 7 and exon 8 (Jia et al., 2006). Together these reports suggested that the exon 7 and exon 8 encoded regions of VEGF-A mediate NRP-1 binding and a recent publication by Parker et al (2012) reconciled these findings. This work revealed the co-crystal structure of the exon7/8 -encoded regions of VEGF-A_{165} in complex with the b1 domain of NRP-1. This study determined that both exon 7 and exon 8 encoded regions of VEGF-A physically contribute to NRP-1 binding and interestingly NRP-1 showed a 50-fold stronger binding to VEGF-A_{165} than NRP-2 (Parker et al., 2012). Exon 7 of VEGF-A also encodes the heparin binding domain. Heparin binding to both VEGF-A_{165} and NRP-1 provides an important link between VEGF and NRP which is reported promote the formation of stable complexes between VEGF-A/ NRP-1 and VEGFR (Mamluk et al., 2002; Vander Kooi et al., 2007). Other groups have also suggested that the NRP-1 cytoplasmic PDZ binding domain and its interacting molecule synectin are essential in the formation of stable signalling complexes between NRP-1 and VEGFR (Prahst et al., 2008).

It is subject to debate whether or not the VEGF-A isoform $VEGF_{121}$ binds to NRP-1, as $VEGF_{121}$ lacks the amino acid sequence encoded by exon 7 (Figure 1.3) (Soker et al., 1998). However, direct interaction of VEGF-A_{121} via its C-terminus (encoded by exon eight), with NRP-1 has been reported (Pan et al., 2007). This interaction does not induce complex formation with VEGFR-2, as VEGF-A_{165} does. Instead, it is proposed VEGF-A_{121} may signal directly through NRP-1 to regulate

endothelial cell motility. It has also been reported that a peptide named tuftsin, which has homology to the C-terminal of VEGF-A_{121} and VEGF-A_{165} binds directly to NRP-1 (Von Wronski et al., 2006), whereas, VEGF-A_{109}, which lacks the C-terminus, does not bind to NRP-1 (Pan et al., 2007). Together, these results suggest that NRP-1 may also have additional roles in VEGF-A signalling, which are not dependent on the formation of NRP-1/VEGFR complexes.

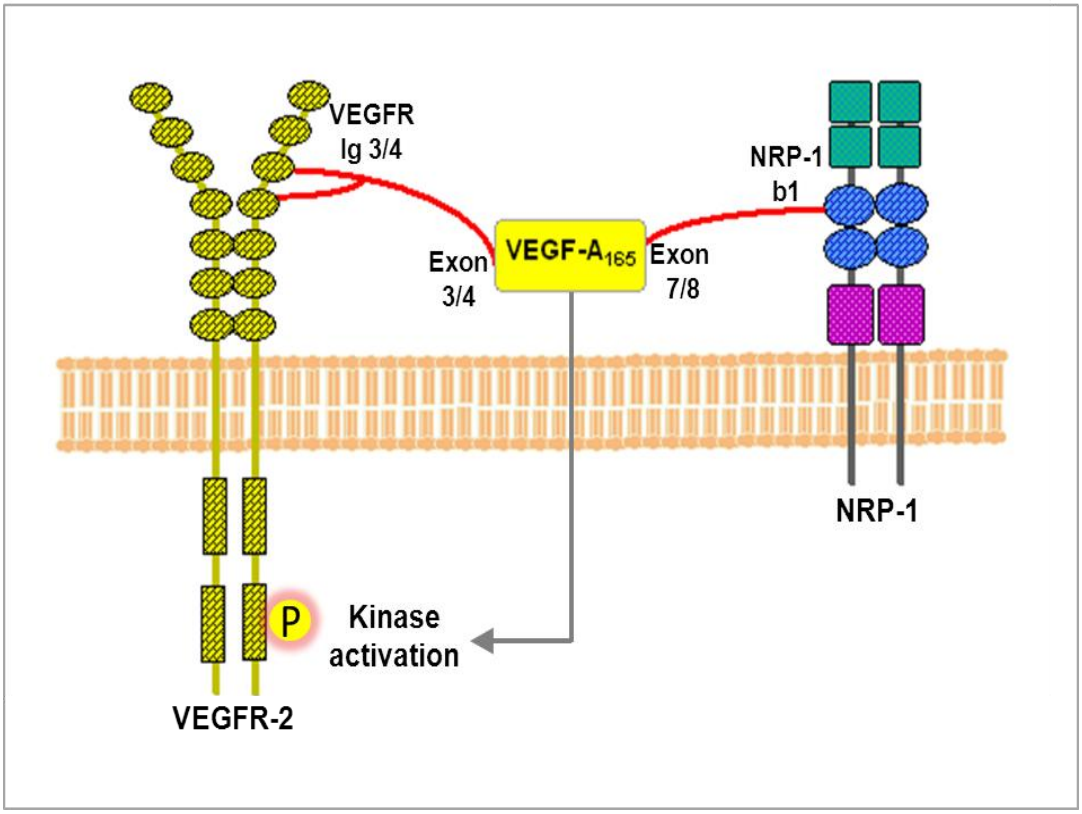

Figure 1.4: VEGF-A_{165} bridges an interaction with NRP-1 to regulate VEGFR kinase activity
The figure illustrates the complex formation between VEGF-A_{165} / VEGFR-2 and NRP-1. The region of VEGF-A_{165} encoded by exon 3/exon 4 binds to Ig-like domains 3 and 4 of VEGFR-2. The amino acid sequence encoded by VEGF-A_{165} exons 7 and 8 binds to the b1 domain of NRP-1. This interaction potentiates the binding of VEGF-A_{165} to VEGFR-2 and promotes VEGFR-2 phosphorylation and signalling (Soker et al., 1998).

1.1.4 Neuropilins: expression and function in health and disease

1.1.4.1 Developmental roles

The involvement of both NRP-1 and NRP-2 in the development of the neurological system has been well documented (He and Tessier-Lavigne, 1997; Kitsukawa et al., 1995; Kolodkin et al., 1997). Early studies used mouse embryonic stem cell clones that constitutively expressed NRP-1. These clones were used to produce chimeric embryos that over-expressed NRP-1, resulting in embryonic lethality. In the dead embryos, abnormalities were localised to tissues where NRP-1 is expressed during development, namely within the cardiovascular and nervous systems. Abnormalities included haemorrhage, heart malformations, excess capillaries and ectopic sprouting of nerve fibres (T Kitsukawa et al., 1995). Overall, this study highlights the importance of NRP-1 in normal development. Further work investigating neurological development in the rat, discovered NRP-2 through identifying clones with sequence homology to NRP-1 (using dbEST data base of human expressed sequence tags) (Kolodkin et al., 1997). Overlapping, yet distinct expression patterns of NRP-1 and NRP-2 were recorded in developing embryonic rat neurons (Chen et al., 1997; Kolodkin et al., 1997) and in early development of the cardiovascular system, NRP-1 is localised in arteries and NRP-2 in veins which was suggested to influence arterial and venous blood vessel differentiation (Herzog et al., 2001; Yuan et al., 2002). In mouse knockout models, NRP-1 or NRP-2 knockout mice die by embryonic day (E.10), whereas, double NRP-1 and NRP-2 knockout mice died in utero on day E8.5 (Takashima et al., 2002). These studies suggest that NRP-1 and NRP-2 share important but distinct roles at specific stages of neuronal development.

The role of the two NRPs in neuronal development has been studied in murine models. Kitsukawa and colleagues reported NRP-1 null mice die by embryonic day E13.5 with abnormalities in both the central nervous system (CNS) and peripheral nervous system (PNS) (T Kitsukawa et al., 1997). In contrast, NRP-2 null mice survive to adulthood, however, fasciculation of both cranial and spinal nerves, and either absent or disorganised brain fibre tracts were documented in these adults (Giger et al., 2000). More recently NRP-2 has been documented as an important mediator of peripheral nerve regeneration (Bannerman et al., 2008).

In the cardiovascular system, NRPs play important biological roles in development. The generation of NRP-1-deficient mutant mice embryos highlighted the importance of NRP-1 in embryonic vessel formation. Deficient embryos showed a partial disorganisation of extra-embryonic vessels, impaired neuronal vascularisation, and abnormalities in the dorsal aorta and arch arteries (Kawasaki et al.,

1999). Over-expression of NRP-1 in chimeric mice caused excess capillaries/ blood vessels, malformed hearts, and ectopic sprouting which was lethal (T Kitsukawa et al., 1995). However, these phenotypes were not as severe as VEGFR-2 deficient mutants, which had impaired early vessel formation resulting in death at E8.5 (Fong et al., 1995; Shalaby et al., 1995). The more severe phenotype of VEGFR-2 mutants led to the theory that functional VEGFR is a prerequisite for early vessel formation, with NRP-1/ VEGFR interactions being central in remodelling and maturation of the embryonic vasculature (Kawasaki et al., 1999). In support of this observation, Lee and colleagues (2002) showed that NRP-1 knockouts in zebrafish did not inhibit early vessel formation. Instead, NRP-1 was shown to have a crucial later role in angiogenic vessel formation (Lee et al., 2002). Yuan et al (2002) reported the vascular phenotype of NRP-2 is less severe and mice survive; however, there are abnormalities in both small lymphatic and capillary vessel formation. As alluded to, NRP-2 is expressed in veins in early development, however this expression depletes later in development and NRP-2 is predominantly localised to lymphatic vessels. In NRP-2 deficient lymphatic endothelial cells, a reduction in DNA synthesis is also documented (Herzog et al., 2001; Yuan et al., 2002). Overall, these experiments illustrate that NRP-1 and NRP-2 have distinct functions in early and later stages of vascular development.

1.1.4.2 Physiological roles

As well as their importance in nerve and blood vessel development, NRPs have been implicated in several physiological functions. NRPs are expressed in a range of cell types including endothelial cells, bone marrow cells, T and dendritic cells, and tumour cells. The expression of both NRPs can be modulated in response to oestrogen and progesterone, suggesting a role in physiological angiogenesis in menstruation (Germeyer et al., 2005; Pavelock et al., 2001). Within blood vessels, changes in flow can affect expression patterns of NRP-1 (Jones et al., 2008; le Noble et al., 2004). In support of flow rates affecting NRP expression, occlusion of the middle cerebral artery has been shown to induce the expression of NRP-1 and NRP-2 (Fujita et al., 2001) whilst ischaemia /hypoxia resulting from reduced flow, up-regulated NRP expression. In hypoxia, both endothelial and embryonic stem cells showed increased NRP-1 levels that promoted cell survival (Brusselmans et al., 2005; Ottino et al., 2004).

NRP-1 has also been documented to mediate chemotaxis of bone marrow cells to sites of neo-angiogenesis in mice. Although bone marrow derived myeloid cells are not arteriogenic, they function in a paracrine manner to promote proliferation of smooth muscle cells and endothelial cells. This mechanism required the presence of NRP-1 to ensure both endothelial cell proliferation and angiogenic arterial development (Zacchigna et al., 2008). In embryonic stem cells, NRP-1 and VEGFR-2 positive cells have also been shown to differentiate into endothelial vascular cells with microenvironmental cues (Gualandris et al., 2009). NRP-1 has also been reported to affect

osteoblast function (Harper et al., 2001), and the interaction between stromal and haemopoietic cells (Tordjman et al., 1999). NRPs also have important immunological functions, namely in regulating the interactions between dendritic cells and immature T cells, both of which are central to the primary immune response (Mizui and Kikutani, 2008; Wülfing and Rupp, 2002). NRP-1 has also been shown to be involved in early thymocyte differentiation (Corbel et al., 2007). In wound healing, NRP-1 is highly expressed, with inhibition of NRP-1 resulting in reduced vascularisation to the wound (Matthies et al., 2002). Similarly, in *Xenopus* models with crushed optic nerves, NRP-1 levels were elevated and remained high for three weeks up until healing had occurred (H Fujisawa et al., 1995). This regenerative role is also evident for NRP-2, with Bannerman et al (2008) reporting that the regeneration of crushed sciatic nerves in rats took significantly longer in NRP-2-deficient rats compared to normal controls (Bannerman et al., 2008). The functional diversity of the NRPs is increasingly evident with the huge body of literature surrounding them. However, within the literature, many studies have focused on NRPs roles in angiogenesis and tumour biology.

1.1.4.3 Roles in cancer

1.1.4.3.1 Expression of neuropilins in cancer

The NRPs affect tumour angiogenesis, metastasis, and growth by mediating the signalling effects of VEGF and SEMA family members. Pellet-Many et al (2008) reported the expression of both NRP-1 and NRP-2 in a number of tumour cell lines including lung, breast, kidney, and ovary thus, illustrating that NRP expression in cancer is not localised to a small number of tissues but is a common feature in many cancers (Pellet-Many et al., 2008) (Table 1.0). In patient samples, NRP-1 was found in cancerous but not in healthy tissues, again suggesting a specific tumour role (Kawakami et al., 2002; Lantuéjoul et al., 2003; Parikh et al., 2004; Vanveldhuizen et al.,2003). Furthermore, NRP expression has been associated with the metastatic potential of tumours and considered as a possible marker for tumour progression. Correlation of higher NRP expression with cancer progression has been highlighted in glioma (Hu et al., 2007; Osada et al., 2004), pancreatic (Wey et al., 2005), prostate (Latil et al., 2000; Vanveldhuizen et al., 2003), lung (Kawakami et al., 2002), colon (Ochiumi et al., 2006), leukaemia (Kreuter et al., 2006) plus many other cancerous tissues (Table 1.0). Interestingly, Osada et al (2004) identified that it was expression of the NRP-1 gene, not the genes for flt-1 (VEGFR-1), KDR (VEGFR-2) or NRP-2, which contributed to the rate of tumour progression in 37 glioma patients (Osada et al., 2004). Overall, these studies highlight NRP expression in both cancer cell lines and clinical cancerous tissue is correlated with an invasive, aggressive phenotype.

Tumour type	NRP-1	NRP-2	Reference
Bladder		◆	(Sanchez-Carbayo et al., 2003)
Brain	◆	◆	(Osada et al., 2004) (Hamerlik et al., 2012) (Karayan-Tapon et al., 2008)
Breast	◆	◆	(Yasuoka et al., 2009) (Stephenson et al., 2002) (Bachelder et al., 2001)
Colon	◆◆	◆	(Parikh et al., 2004) (Grandclement et al., 2011) (Kamiya et al., 2006) (Zhang et al., 2011)
Leukaemia	◆	◆	(Kreuter et al., 2006a) (Vales et al., 2007) (Lu et al., 2008)
Lung	◆	◆	(Kawakami et al., 2002) (Chen et al., 2006) (Hong et al., 2007a)
Liver	◆		(Raskopf et al., 2010)
Melanoma	◆	◆	(Straume and Akslen, 2003) (Rushing et al., 2012)
Prostate	◆		(Latil et al.,2000) (Pallaoro et al., 2011)
Pancreatic	◆	◆	(Fukahi, 2004) (Fukasawa and Matsushita , 2007) (Matsushita et al.,2007) (Dallas et al., 2008) (Zhang, 2010)
Sarcoma		◆	(Handa et al., 2000)
Stomach	◆	◆	(Akagi et al., 2003) (Samuel et al., 2011)

Table 1.0: NRP-1 and NRP-2 are expressed in many different types of tumour
A large body of literature outlines the involvement of NRP-1 or NRP-2 in a number of cancers. The (◆) in the table illustrates that NRP-1 or NRP-2 is expressed and correlates with malignancy/ tumour progression. The (◆) also outlines the expression of NRP-1 or NRP-2, however in these instances NRP-1 was found to have an anti-cancer effect. It can be clearly seen that many tumours express both isoforms of NRP-1 and in the majority of cases this correlates with tumour progression.

1.1.4.3.2 Neuropilins regulate cellular signalling and are therapeutic targets in cancer

In recent years, evidence has emerged that NRP-1 interacts with a diverse array of proteins, some of which are important in tumourigenesis. Using MSCs, Ball et al (2010) first documented that NRP-1 could interact with PDGFRs to mediate PDGFR phosphorylation and associated cellular effects including, cell migration and proliferation (Ball et al., 2010). Subsequent studies also suggested that signalling interactions between NRP-1 and PDGFR (Banerjee et al., 2006; Cao et al., 2010; Pellet-Many et al., 2011) and thus, it is feasible that NRP-1 may regulate PDGFR signalling. Given the close phylogeny between PDGFR and VEGFR (Dormer and Beck, 2005; Gu and Gu, 2003), it is possible to speculate that an extracellular growth factor mediated interaction may mediate PDGFR/NRP-1 interactions. However, a study by Evans et al (2011) has suggested that the C-terminus of NRP-1 may be particularly important in specific PDGFR/NRP-1 signalling. In this study, PDGF-BB stimulated the phosphorylation of p130Cas, which mediated the migration of glioma cells. Expression of a deletion mutant of NRP-1, lacking the C-terminus or NRP-1 knockdown, inhibited PDGF-BB/p130Cas induced glioma cell migration. Interestingly, the proteins which usually mediate migration downstream of PDGFR, extracellular signal-regulated kinase (ERK) and AKT, were unaffected by NRP-1 knockdown, suggesting that a distinct pathway is mediated by PDGFR/NRP-1 in U87MG cells (Evans et al., 2011).

Further studies in glioma models have suggested that a novel mechanism whereby NRP-1 potentiates the activity of HGF/SF and the c-Met signalling pathway. Using prostate cancer cells, Zhang et al (2010) highlighted that VEGF-A_{165} induced NRP-1 to associate directly with HGF, stimulating the activation of c-Met. This study hypothesised that this NRP-1 dependent mechanism may regulate the activity of the anti-apoptotic protein Mcl-1, thereby conferring a survival advantage to prostate cancer cells (Zhang et al., 2010). NRP-1 was also reported to potentiate the HGF/c-met pathway, which enhanced both the proliferation and survival of glioma cells (Hu et al., 2007) and the invasive potential of pancreatic cancer cells (Matsushita et al., 2007).

Recent studies have identified that both NRP-1 and NRP-2 are able to bind to both latent and active transforming growth factor receptor beta (TGF-β), and that NRPs are able to activate latent TGF-β. NRPs are also able to bind to TGF-β receptors (TβR); TβR I, TβR II TβR III, and act as co-receptors to augment TGF-β signalling (Glinka et al., 2010). In epithelial colon cancer cells, NRP-2 promoted TβR I signalling and constitutive phosphorylation of downstream Smad 2/3. This aberrant TGF-β signalling induced the colon cancer cells to undergo epithelial-to-mesenchymal transition, which is associated with increased malignancy (Grandclement et al., 2011).

Synergy between NRP-1 and other mitogenic proteins has also been implied in a series of studies. West et al (2005) discovered that NRP-1 could bind to fibroblast growth factor (FGF) 1, 2 and 3,

and potentiate the stimulatory potential of FGF-2 (West et al., 2005). Epidermal growth factor was also able to induce the expression of NRP-1 via a mechanism involving the activation of ERK and AKT (Akagi et al., 2003), and inhibition of EGFR inhibited NRP-1 expression (Parikh et al., 2004). Interestingly, in tumour-associated endothelial cells, EGF receptor inhibition again down-regulated NRP-1, yet surprisingly VEGFR-2 signalling was up-regulated (Amin et al., 2008). Together these studies suggest a complex regulation of NRP-1 expression, which may have developed to regulate the multiple interactions between NRPs and other signalling molecules.

The integrin-mediated adhesion of cells to extracellular matrix components is an important mediator of cell motility. NRP-1 has been documented to interact with integrin α5β1 (Valdembri et al., 2009), integrin β1 (Fukasawa et al., 2007) and integrin α5β3 (Robinson et al., 2009), and NRP-2 has been reported to interact with integrin α6β1 (Goel et al., 2012). In cancer, NRP/ integrin interactions have been shown to have both protective and oncogenic cellular effects. Using *in vivo* and *in vitro* models, Robinson et al (2009) outlined that integrin α5β3 could negatively regulate NRP-1/ VEGF-A angiogenesis in endothelial cells. It was found that NRP-1 could physically interact with integrin α5β3 in a VEGF-dependent manner; this interaction maybe responsible for sequestering NRP-1, preventing interactions with VEGFR-2. Interestingly, it was the β3 cytoplasmic tail which was essential to disrupt VEGFR-2: NRP-1 interaction, which might suggest an intracellular interaction with the C-terminus of NRP-1 and integrin β3, particularly as such intracellular interactions have also been proposed between NRP-1 and α5β1 (Valdembri et al., 2009). In pancreatic cancer cells, a mechanism involving NRP-1 and integrin β1 promotes the adhesion of tumour cells, which increases cancer cell growth and survival (Fukasawa et al., 2007). In invasive breast cancer cells, (MDA MB 231) a semaphorin 3A/ NRP-1 mechanism was found to promote integrin α2β1-mediated adhesion to collagen and suppress cell migration/ invasion (Pan et al., 2008). However, in a more recent study using breast cancer cells, Goel et al (2012) revealed that NRP-1 regulated the formation of α6β1 focal adhesions on laminin and that this regulated the activation of mitogenic FAK and Src signalling pathways (Goel et al., 2012). Interestingly, NRP-2 was localised at focal adhesion sites, suggesting NRP-2 is actively involved in the spreading and adhesive potential of breast cancer cells. Together, these studies outline that NRPs have the capacity to regulate integrin functions in both tumour cells and vascular stromal cells. The cell type and expression levels of NRP-1/ integrin may determine whether crosstalk between these receptors confers pro-or anti-oncogenic effects in cancer. However, given the role of in NRPs in tumourigenesis, such interactions with adhesion molecules provide insights into how NRP-1 signalling may contribute to promoting the motility and invasive potential of cancer cells.

Another interesting role for NRPs in cancer, was revealed by the finding that NRP helps to maintain a de-differentiated tumour phenotype and thus contributes to the cancer stem cell hypothesis.

NRP-1 and NRP-2 have been shown to enhance hedgehog signalling (Cao et al., 2008; Hillman et al., 2011), which is associated with controlling self-renewal and migration of cells, and similarly hedgehog can up-regulate NRP-1 (Hochman et al., 2006). Other groups have suggested that VEGFR-2/ NRP-1 signalling in specific subsets of glioma (Hamerlik et al.,2012), and in skin cancer cells (Beck et al., 2011), is essential for the establishment and maintenance of cancer stem cells. Many studies have focused on cancer stem cells as the cells of origin in many cancers and primary drivers of tumour progression (Vermeulen et al., 2012). The discovery that NRPs may regulate this cancer phenotype adds to the evidence that NRPs regulate a diverse array of cellular behaviours in tumourigenesis and therefore, contribute to several of the hallmarks of cancer (Figure 1.5).

Targeted cancer therapies against NRP-1 have revealed interesting results. Work using xenograft models revealed that peptide inhibition of NRP-1 and VEGFR complex formation inhibited both tumour angiogenesis and growth. More specific inhibition, targeted against the NRP-1 b1 domain binding to VEGF-A, also had a range of effects, including prevention of complex formation, inhibition of cell migration and inhibition of xenograft growth and vascularisation. Blocking NRP-1 also has additive effects when used in combination with VEGFR targeted therapies such as, avastin or bevacizumab. Treating tumours with antibodies to VEGF alone reduced angiogenesis yet vessels still showed a close association with pericytes, whereas both anti VEGF and NRP-1 antibodies blocked this vascular remodelling (Pan et al., 2007). In the case of NRP/VEGFR signalling, a soluble isoform of NRP inhibits normal angiogenic pathways, providing an interesting model for drug design. Monomeric sNRP-1 sequesters VEGFR, thereby inhibiting VEGF signalling and angiogenesis (Gagnon et al., 2000; Schuch et al., 2002). To date, no large-scale trials have evaluated NRP-1 as a therapeutic cancer target, however, the studies described predict that targeting NRP-1 alone or in combination can induce anti-cancer effects.

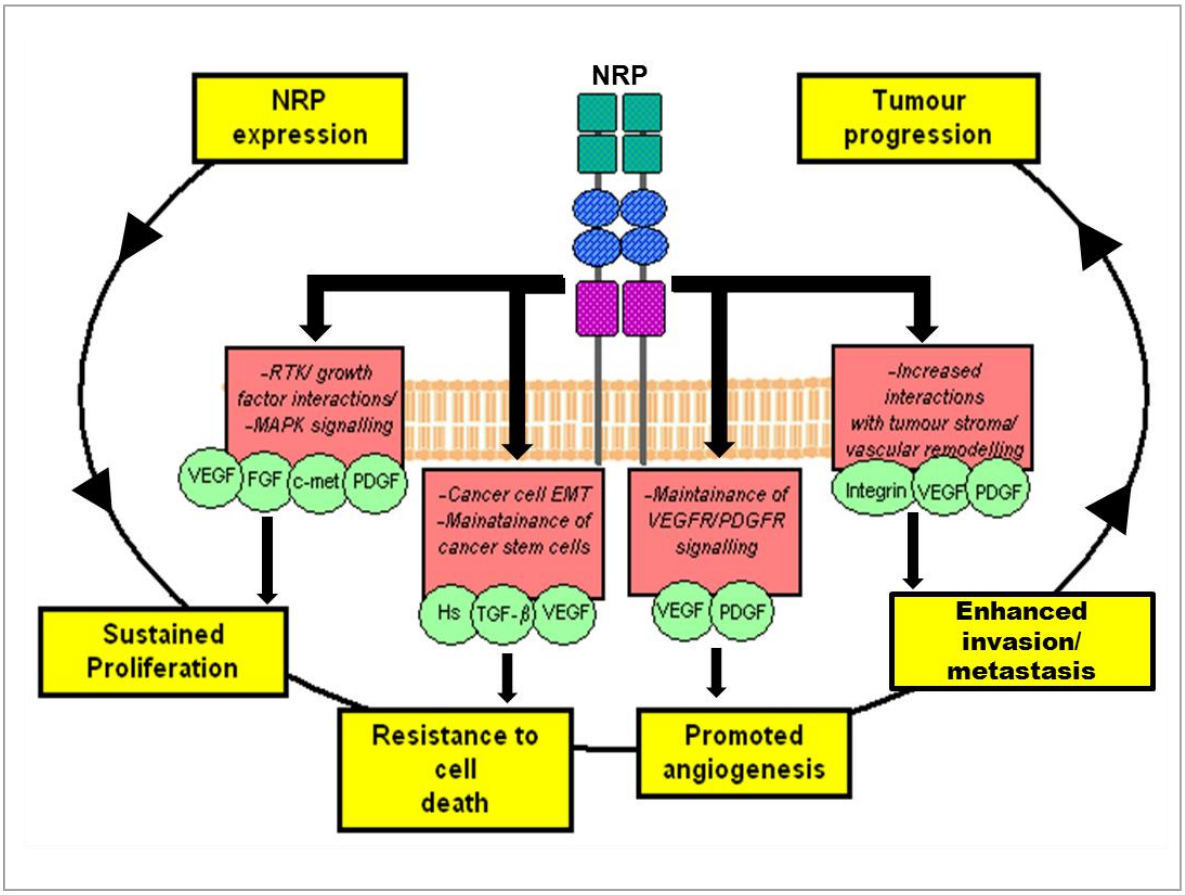

Figure 1.5: NRP signalling regulates several important hallmarks of cancer
The molecules highlighted in green are all reported to share interactions with either NRP-1 or NRP-2. The red boxes highlight some of the biological effects induced by NRP interactions with the associated molecules (highlighted in green) and how these biological effects may regulate some of the hallmarks of cancer: sustained proliferation, resistance to cell death, angiogenesis and enhanced invasion/ metastasis. Some of the molecules associated with NRPs include: RTK growth factors (e.g. VEGF, PDGF), integrins and heparan sulphate (HS). Together, these molecular interactions with NRP-1 and the cellular consequences may affect early and late hallmarks of cancer and accumulate to promote tumour progression.

1.2 The platelet-derived growth factor family of receptors and ligands

1.2.1 PDGF isoforms and biosynthesis

PDGF was initially identified as serum-derived growth factor which promoted the proliferation of fibroblasts (Kohler and Lipton, 1974), smooth muscle cells (Ross et al., 1974), and glial cells (Westermark and Wasteson, 1976). Following its identification, PDGF was purified from platelets (Antoniades et al., 1979; Heldin et al., 1979), which act as a major storage site for PDGF.

In humans, the genes for the A and B chains of PDGF are located on chromosomes 7 and 22, respectively (Betsholtz et al., 1986; Dalla-Favera et al., 1982; Swan et al., 1982). The PDGF-C and D chains, which were discovered more than a decade later (LaRochelle et al., 2001; Li et al., 2000), are located on chromosome 4 and 11, respectively (Uutela et al., 2001). The gene organisation of all four PDGF growth factors is similar, particularly the exons encoding the growth factor domain. PDGF-A, B and C chains have seven exons, with exon 7 being non-coding in PDGF-A and B (Bonthron et al., 1988; Johnsson et al., 1984; Rorsman et al., 1988). The PDGF-C chain has six exons. The growth factor domain is highly conserved in all the PDGF chains and the same motif is also present in VEGF isoforms (Fredriksson et al., 2004; Holmes and Zachary, 2005; McDonald and Hendrickson, 1993). The homology of the growth factor domain across the four PDGF chains is 25%, with PDGF-A and B sharing 50% homology and PDGF-C and D sharing 50% homology. Interestingly, although the exon organisation of the four PDGF genes is similar, the introns of PDGF-C and D are much larger, such that the genomic DNA for PDGF-A and B spans around 20 kb but for PDGF-C and D it spans around 200 kb. Based on these data, it is suggested that the PDGF chains arose from a common ancestor containing both the growth factor domains and CUB domains. Duplication of the ancestral gene generated two branches, with one branch generating PDGF-A and B chains and the second branch generating PDGF-C and D chains (Fredriksson et al., 2004).

All four chains of PDGF are synthesised as inactive precursor molecules. Dimerisation of PDGF occurs in the endoplasmic reticulum and five disulphide-bonded dimers have been described to date; PDGF-AA, PDGF-AB, PDGF-BB, PDGF-CC and PDGF-DD (Fredriksson et al., 2004). Proteolytic processing of N-terminal amino acids of PDGF-A and B chains by the trans-Golgi network results in the secretion of the mature growth factor (Ostman et al., 1992). The immature form of PDGF-A is 50 kDa, and the proprotein convertase, furin, is proposed to cleave PDGF-A to generate the mature 30 kDa protein (Siegfried et al., 2003). Siegfried et al (2005) proposed furin, PACE4, PC5, and PC7 as the primary proprotein convertases involved in the cleavage of the immature (~60 kDa) PDGF-BB to the mature 27 kDa product (Siegfried et al., 2005). Interestingly,

this report also suggested that the formation of PDGF heterodimers was favoured over homo-dimers in the endoplasmic reticulum. The C-termini of PDGF-A and B chains have a number of basic residues, known as retention motifs, which are documented to mediate extracellular interactions with glycosaminoglycans (García-Olivas et al., 2003) and matrix proteins (Pollock and Richardson, 1992). Alternative splicing of exon 6, which encodes the C-terminus of PDGF-A, generates a long and short PDGF-A chain, with the short chain lacking the basic C-terminal residues. Following synthesis, the C-terminal residues of PDGF-B are cleaved to generate a short and long PDGF-B chain. The long PDGF-A and PDGF-B chains, containing the C-terminal basic motifs, interact with cell surface molecules such as, HSPG, and the extracellular matrix, thereby retaining PDGF at the cell surface. In contrast, the short chains of PDGF-A and B, lacking the C-terminal motifs, do not interact at the cell surface which promotes the secretion and wider localisation of the short isoforms (LaRochelle et al., 1991; Ostman et al., 1991; Raines and Ross, 1992).

The processing of the PDGF-C and D chains differs from the A and B chains, in that PDGF-C and D are thought to undergo extracellular cleavage. PDGF-C and D are secreted as inactive dimers, and proteolytic removal of their CUB domain generates the mature growth factor which is able to bind to PDGFRs (Bergsten et al., 2001; LaRochelle et al., 2001; Li et al., 2000). Recent work by Hurst et al (2012) using breast cancer cells, has suggested that the proteolytic activation of PDGF-C is a two-step process, which results in the generation of a dimer encompassing the growth factor domains of PDGF-C. In this study, tissue plasminogen activator and matriptase were identified as the major proteases involved in the cleavage and activation PDGF-C (Hurst et al., 2012). A similar mechanism has been proposed for PDGF-D activation, again involving two-step proteolytic cleavage of PDGF-D and the generation of a PDGF-D growth factor binding domain dimer (Ustach et al., 2010). In pancreatic cancer cells, matriptase and urokinase plasminogen activator are primary candidates involved in the cleavage and activation of PDGF-D (Ustach and Kim, 2005; Ustach et al., 2010).

1.2.2 The PDGF and VEGF receptor tyrosine kinase superfamily

PDGFRs and VEGFRs are members of the same superfamily of receptor tyrosine kinases. Both receptors have a split intracellular kinase domain and are activated by extracellular ligand binding to their immunoglobulin (Ig) homology domains. PDGFRs are defined as class III RTKs and contain five Ig homology domains, whereas VEGFRs are class V RTKs, which contain seven Ig homology domains. The sequence homology and structural similarities of PDGFRs and VEGFRs suggest that these RTKs arose from a common ancestor, like their growth factor ligands (Gu and Gu, 2003; Kondo et al., 1998).

1.2.2.1 Vascular endothelial growth factor receptors

VEGFR-1 is also referred to as fms (refers to the feline McDonough sarcoma virus) -like tyrosine kinase (flt-1) due to its homology with the fms family of proteins (Shibuya et al., 1990). Structurally, VEGFR-1 has seven extracellular Ig homology domains, a single transmembrane domain and an intracellular tyrosine kinase signalling domain.

VEGFR-1 binds to VEGF-A, VEGF-B and PLGF (Figure 1.6) with high affinity, resulting in phosphorylation of intracellular tyrosine residues and induction of MAPK signalling cascades. Although both VEGF-A and PLGF bind to the second Ig domain of VEGFR-1, X-ray crystallography studies revealed no conformational differences when VEGF-A or PLGF were bound (Christinger et al., 2004; Wiesmann et al., 1997). With this detail in mind, it is interesting that binding of PLGF or VEGF-A exerts distinct biological effects through binding to VEGFR-1. $PLGF_{152}$ binding to VEGFR-1 stimulates phosphorylation of Tyr-1309, whereas VEGF-A_{165} stimulates Tyr-1213. This distinction is further exemplified in studies using mice primary capillary endothelial cells, where $PLGF_{152}$ binding altered the expression of more than 50 genes, whereas binding of VEGF-A_{165} had no detectable effects on gene expression (Autiero et al., 2003).

Functionally, VEGFR-1 is expressed in endothelial cells and early in embryogenesis, suggesting an important developmental role. In hypoxia, up-regulation of VEGFR-1 expression is mediated by hypoxia inducible factor -1 (HIF-1), making it an important pro-angiogenic mediator in tumour hypoxia (H. P. Gerber et al., 1997). Other diverse functions have been implicated for VEGFR-1 including, monocyte migration (Barleon et al., 1996), angiogenesis (Fong et al., 1995), and endothelial cell maturation (Lyden et al., 2001). Downstream signalling induced by PLGF/VEGFR-1 in monocytes activates the PI3K/AKT and ERK-1/2 pathways (Selvaraj et al., 2003), which are important in both inflammatory diseases and cancer. A further soluble form of VEGFR-1, generated from alternative splicing, has been documented (Kendall and Thomas, 1993). This form is thought to bind to, and inhibit the effects of VEGF-A.

VEGFR-2 (otherwise known as kinase insert domain receptor (KDR)) was first isolated in 1991 and primers directed against type III RTKs were used to identify KDR (Terman et al., 1991). The murine form of VEGFR-2 is otherwise known as foetal liver kinase-1 (Flk-1) and shares 85% amino acid sequence homology in the extracellular domains with human VEGFR-2 (Popkov et al., 2004). The VEGFR-2 gene is located on chromosome 4q11-12 and encodes 1356 amino acids (Sait et al., 1995). Intracellular translation generates a 150 kDa protein that undergoes glycosylation to produce mature 230 kDa VEGFR-2, which is expressed on the cell surface (Takahashi and

Shibuya, 1997). VEGFR-2 has seven extracellular Ig homology domains, a single transmembrane domain and two intracellular kinase domains that are split by a 70 amino acid insert.

VEGF-A, C and D bind to VEGFR-2 (Figure 1.6), however, the most studied interaction is with VEGF-A. VEGF-A binds to the second and third extracellular Ig domains of VEGFR-2 (Shinkai et al., 1998) with a lower affinity than it binds to VEGFR-1. Binding of VEGF-A induces the phosphorylation of tyrosine residues within the intracellular kinase domain, exposing docking sites on VEGFR-2 that are specific for intracellular proteins. Proteins with Src Homology 2 (SH2) domains bind to these docking sites initiating intracellular signalling. Five major tyrosine phosphorylation sites were initially identified for VEGFR-2, Tyr-951, Tyr-996, Tyr-1054 and Tyr-1059 (Dougher-Vermazen et al., 1994). Further research, using mammalian cells, which over-express VEGFR-2, has revealed other tyrosine sites and identified their location. Phosphopeptide analysis revealed: Tyr-951, Tyr-1054 and Tyr-1059 in the kinase-insert domain and Tyr-1175 and Tyr-1214 in the C-terminal of the receptor (Matsumoto et al., 2005; Takahashi et al., 2001). Phosphorylation of these residues creates docking sites for: VEGF receptor associated protein (VRAP) on Tyr-951 (Wu et al., 2000) and the adaptor protein Nck on Tyr-1214 (Lamalice et al., 2006), with the latter activating the p38 MAPK pathway and promoting cell migration. Tyr-1175 is phosphorylated on VEGF-A binding and activates phospholipase-C-γ (PLC-γ), which results in activation of the protein kinase-C (PKC) and ERK-1/2 pathways (Takahashi et al., 2001). This interaction has been shown to be essential for VEGF induced endothelial cell proliferation.

The final receptor in the VEGF family is VEGFR-3, sometimes called flt-4 (fms like tyrosine kinase 4). This 170 kDa receptor is alternatively spliced to generate two isoforms with differences in the C-terminal region (Hughes, 2001). VEGFR-3 binds to both VEGF-C and VEGF-D (Figure 1.6) and plays important roles in angiogenesis and lymphangiogenesis in adults (Kaipainen et al., 1995). Like VEGFR-1, VEGFR-3 is up-regulated by HIF-1 under hypoxic conditions (I. Nilsson et al., 2004) It is predicted that VEGFR-3 alone does not induce Tyr-phosphorylation, instead it forms a heterodimer with VEGFR-2 presenting an interesting mechanism of VEGFR crosstalk (Alam et al., 2004; Dixelius et al., 2003).

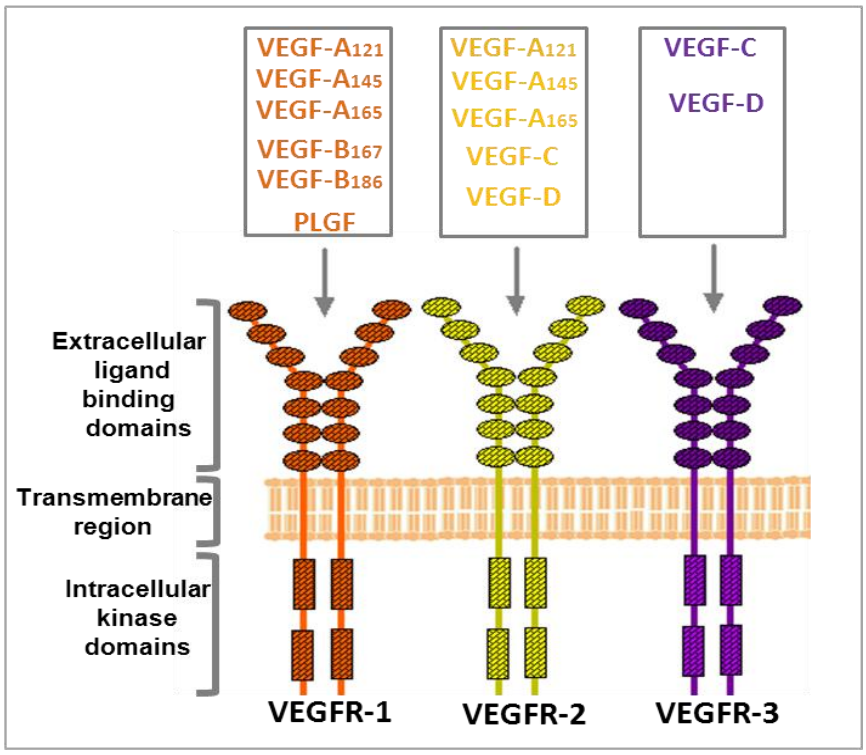

Figure 1.6: The domain structure of VEGFRs and binding interactions with VEGF isoforms
The figure illustrates that VEGFR-1, VEGFR-2 and VEGFR-3 homodimers contain, extracellular ligand binding regions consisting of 7 Ig homology domains, a transmembrane region and a split intracellular kinase domain. Specific isoforms of VEGF associate with the three different VEGFRs. VEGFR-1 binds to PLGF and multiple isoforms of VEGF-A or VEGF-B. VEGFR-2 binds to VEGF-C, VEGF-D and multiple isoforms of VEGF-A. VEGFR-3 binds specifically to VEGF-C and VEGF-D. VEGF binding induces the autophosphorylation of tyrosine residues in the split kinase domains of VEGFRs which initiates specific intracellular signalling cascades that regulate distinct cellular effects.

1.2.2.2 Platelet-derived growth factor receptors-α and β

PDGFR-α and PDGFR-β genes are localised on chromosome 4q12 and 5q33, respectively. PDGFR-α and β share 31% amino acid homology in the ligand binding domain, 27% in the kinase insert domain and 28% in the C-terminus (Gronwald et al., 1988; Matsui et al., 1989).

The kinase domain of PDGFRs is split into two lobes, which are divided by a polypeptide linker known as the kinase insert. In the absence of PDGF ligands, three regions of PDGFR are important in maintaining the receptor in an inactive conformation (Figure 1.7). The maintenance of the juxtamembrane region of both PDGFR-α (Stover et al., 2006) and PDGFR-β (Irusta et al., 2002) inhibits the activation of PDGFRs in the absence of ligand. In leukaemia, truncation of the PDGFR-α juxtamembrane region is reported to induce constitutive activation of PDGFR-α, which is independent of ligand and receptor dimerisation (Stover et al., 2006). The C-terminus of PDGFR-β was also reported to maintain the receptors inactive conformation. Chiara et al (2004) outlined that, deletion of a C-terminal 46 amino acid motif, rich in glutamic acid and proline residues, dramatically increased the auto-activation of PDGFR-β in the absence of ligand (Chiara et al., 2004a). The final region, which is important for the auto-inhibition of PDGFRs, is the activating loop, which is located in the C-terminal lobe of the kinase domain. This region contains one to three tyrosine residues which, when phosphorylated, disrupt the closed, inactive conformation of the activation loop. Phosphorylation induces the activation loop to adopt an open conformation which is conducive for ATP and substrate binding (Huse and Kuriyan, 2002). Tyrosine residues 849 (Chiara et al., 2004b) and 857 (Wardega et al., 2010) have been proposed as candidates for the regulation of the PDGFR-β activation loop, however strong lines of evidence favour Tyr-849 as the principal Tyr-residue (Chiara et al., 2004b; Krampert et al., 2008; Magnusson et al., 2007; Suzuki et al., 2007). Several studies have shown that mutation of Tyr-849 induces ligand-independent activation of PDGFR-β and phosphorylation of a Tyr-857 is associated with regulating PDGFR-β catalytic activity (Chiara et al., 2004b; Magnusson et al., 2007). In PDGFR-α, a tyrosine residue in a similar position, Tyr-842, has been identified as the regulatory element within the activation loop. Mutation of Tyr-842 is reported in several malignancies (Hirota et al., 2003; Lierman et al., 2009; Makinen et al., 1999; Zheng et al., 2007) and is a mechanism for leukaemia cells to acquire drug resistance (Lierman et al., 2009), presumably through maintaining the activation loop in an open conformation.

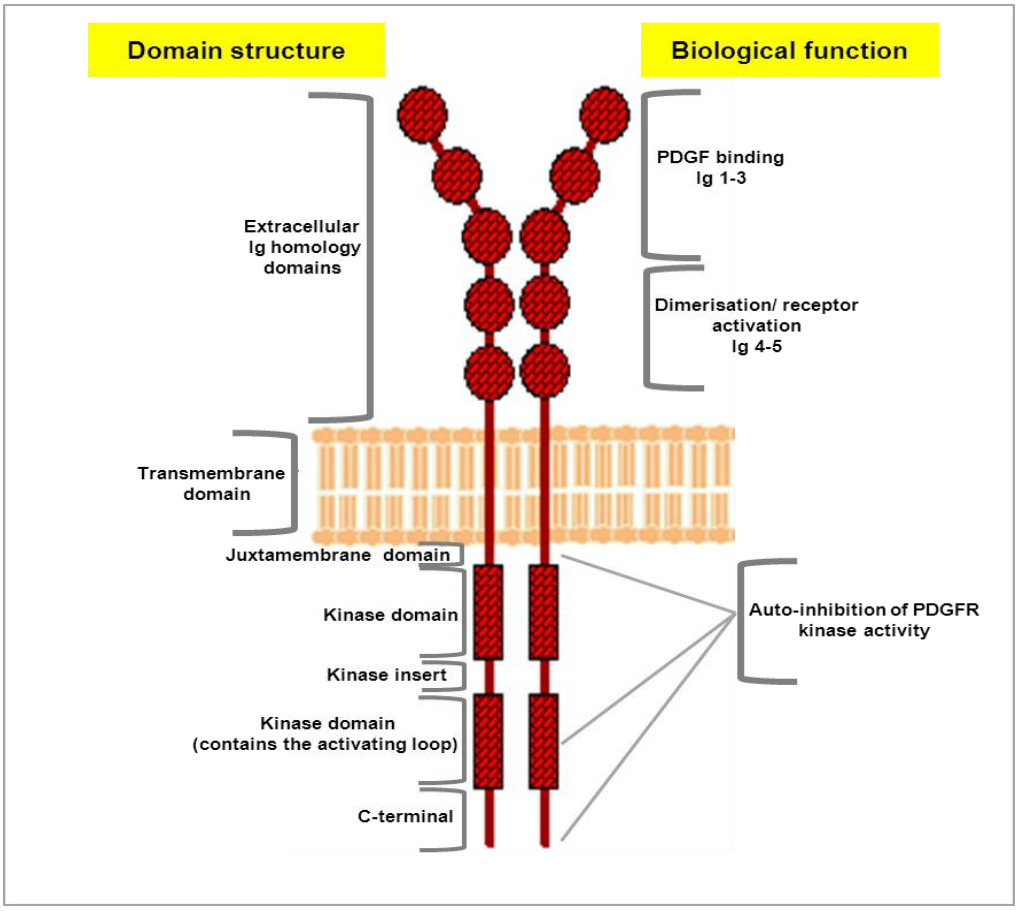

Figure 1.7: PDGFR domain structure and biological significance

Each PDGFR contains 5 extracellular Ig like domains which are important in mediating ligand binding and receptor dimerisation/ activation. Intracellularly, several regions (highlighted above) of PDGFR are important in controlling the auto-inhibition of PDGFR kinase activity in the absence of PDGF ligand. On PDGF ligand binding, autophosphorylation of tyrosine residues in the split kinase domains of PDGFRs is induced which initiates specific intracellular signalling cascades that control distinct cellular effects.

PDGF ligand binding to the extracellular Ig homology domains mediates the dimerisation and autophosphorylation of PDGFRs. Early studies outlined that Ig domains 1-3 were sufficient for maximal PDGF-BB binding to PDGFRs (Heidaran et al., 1995) and Lokker et al (1997) further defined the PDGF binding site to Ig domains 2 and 3 (Lokker, 1997) (Figure 1.7). The Ig domains 4 and 5 were implicated in mediating the dimerisation of PDGFR in early studies (Omura et al., 1997; Miyazawa et al., 1998). However latter work by Yang et al (2008) has outlined that Ig domain 4 is not required for PDGFR dimerisation but it is required for receptor activation (Yang et al., 2008). Recent co-crystallisation of PDGFR-β Ig domains 1-3 bound to PDGF-BB elucidated the mechanism of PDGF binding (Shim et al., 2010). This report revealed that, on association with PDGFR-β, the L1 loop of PDGF-BB adopts a highly ordered conformation which mediates hydrophobic interactions with Ig domain 3 of PDGFR-β. Interestingly, Ig domains 4 and 5 negatively regulate the binding affinity between PDGFR-β and PDGF-BB, yet, Ig domains 4 and 5 are still necessary for the activation of the receptor (Shim et al., 2010; Yang et al., 2008).

The isoform of PDGF binding to PDGFRs induces the formation of PDGFR homodimers or heterodimers. PDGF-AA only activates the PDGFR-αα, whereas PDGF-AB and PDGF-CC can activate PDGFR-αα or PDGFR-αβ. PDGF-BB has a wider specificity and can activate all three dimeric isoforms of PDGFR, whereas PDGF-DD is only reported to activate PDGFR-ββ (Figure 1.8) (Bergsten et al., 2001; Claesson-Welsh et al., 1988; Claesson-Welsh, 1994; Gilbertson et al., 2001; Li et al., 2000; Matsui et al., 1989).

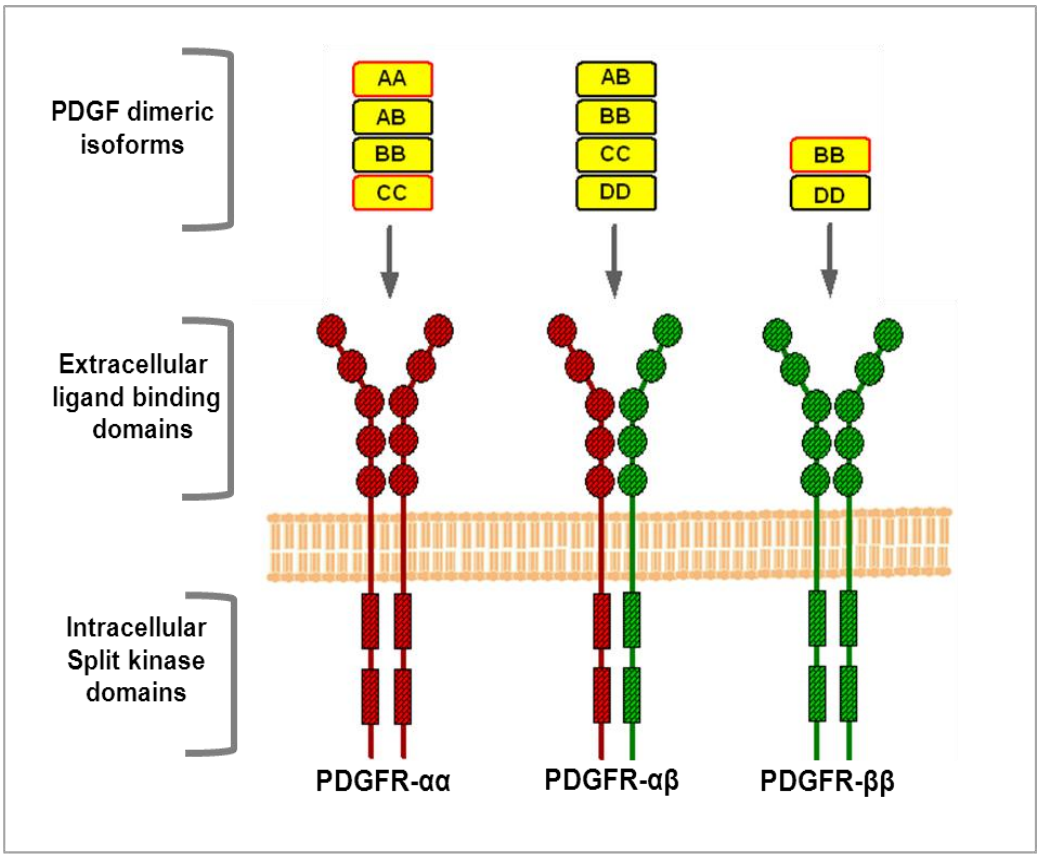

Figure 1.8: Specific binding interactions of PDGF isoforms with PDGFRs
Via the extracellular ligand binding domains, PDGFR homodimers or heterodimers bind to specific PDGF isoforms. The yellow PDGF dimers with a red outline represent interactions which have been demonstrated *in vivo*, with remainder of the interactions been demonstrated *in vitro*. The above figure was adapted from Andrea et al (2008).

1.3 PDGFR signalling in health and disease

1.3.1 Core signalling pathways regulated by PDGFR

PDGF binding induces the dimerisation of PDGFR, which stimulates auto-phosphorylation of conserved tyrosine residues within the kinase domains, Tyr-849 for PDGFR-α and Tyr-857 for PDGFR-β (Fantl et al., 1989; Heldin and Westermark, 1999; Kazlauskas and Cooper, 1989; Kelly et al., 1991). Phosphorylation of these conserved tyrosine residues is critical to activate the catalytic activity of PDGFR-α and PDGFR-β. Fantl et al (1989) reported mutation of Tyr-857 to phenylalanine severely impairs the kinase activity of PDGFR-β and that Tyr-849 and Tyr-857 are the only conserved auto-phosphorylation sites located inside the kinase domain. Evidence from reports examining hepatocyte growth factor receptor (Naldini et al., 1991) and insulin receptor (White et al., 1988) suggest that tyrosine residues in this position have crucial roles in regulating the kinase activity of receptors (Figure 1.9).

Additional tyrosine residues outside the kinase domain also undergo auto-phosphorylation. Phosphorylation of these tyrosine residues exposes binding sites allowing several molecules, including phosphatidylinositol 3'-kinase (PI3K) and PLC-γ to bind directly to PDGFRs. Other adaptor molecules including, growth factor receptor bound protein 2 (Grb2) also bind to phosphorylated tyrosine residues and facilitate indirect PDGFR interactions with other catalytic proteins, such as Ras. Ultimately, these interactions initiate downstream signalling which mediates cellular events.

1.3.1.1 Ras/MAP kinase signalling

PDGFR mediated activation of the Ras-MAP kinase signalling pathway is initiated through the adaptor protein, Grb2, binding to phosphorylated PDGFR. Grb2 contains one Src homology (SH) SH2 and two SH3 domains. Via its SH2 domain, Grb-2 binds directly to PDGFR-β Tyr-716 (Arvidsson et al., 1994) and to PDGFR-α Tyr-720 (Bazenet et al., 1996). Grb-2 can also bind indirectly to PDGFRs via the tyrosine phosphatase SHP-2 (Li et al., 1994). Following association with the active PDGFRs, Grb2 binds via its SH3 domains to the guanine nucleotide exchange factor Son of Sevenless 1 and/or 2 (Sos-1/2). Sos-1/2 then catalyses the replacement of GDP with GTP, to activate Ras, which then initiates the MAP kinase signalling cascade. Sequential phosphorylation and activation of Raf and mitogen activated protein kinase (MEK) cumulates in the activation of the extracellular signal regulated kinase (ERK) (Schlessinger and Bar-Sagi, 1994; Seger and Krebs, 1995). ERK then activates multiple transcription factors which positively regulate cell proliferation, survival and differentiation. As a consequence of these cellular effects, the MAPK

signalling cascade has long been a focus in cancer research (Dhillon et al., 2007; Sebolt-Leopold and Herrera, 2004)(Figure 1.9).

1.3.1.2 Phosphatidylinositol-3-kinase (PI3K) signalling

Following phosphorylation of PDGFR, SH2 domains within the p85 regulatory subunit of PI3K can bind directly to phosphorylated PDGFR tyrosine residues. PI3k binds to PDGFR-β Tyr-751 and Tyr-740 (Kashishian et al., 1992; Kazlauskas and Cooper, 1989; Kazlauskas et al., 1992) and PDGFR-α Tyr-740 or Tyr-731 (Yu et al., 1991). Binding of the p85 subunit stimulates the release of the catalytic subunit of PI3K (Carpenter et al., 1993) which targets its major substrate phosphatidylinositol 4,5-bisphosphate (PIP_2). PI3K phosphorylates PIP_2 and generates the second messenger phosphatidylinositol 3,4,5-trisphosphate (PIP_3) which activates the serine threonine kinase, AKT (Bos, 1995; Marte and Downward, 1997). AKT is documented to phosphorylate multiple proteins involved in cell death, ultimately leading to increased cell survival and proliferation. AKT also has documented roles in regulating cell differentiation and migration (Manning and Cantley, 2007; Marte and Downward, 1997; Vivanco and Sawyers, 2002; Yoeli-Lerner et al., 2009). A second target of PI3K was identified by Hawkins et al (1995) as the small GTPase Rac-1 (Hawkins et al., 1995) which regulates actin polymerisation, membrane ruffling, and cell motility (Nobes and Hall, 1995; Ridley and Hall, 1992; Ridley et al., 1992). Subsequent work has provided insights into a positive feedback mechanism that regulates PIP_3 production. However, this mechanism is only triggered if PI3K is active and Rac-induced actin polymerisation has occurred (Inoue and Meyer, 2008) (Figure 1.9).

1.3.1.3 Phospholipase C-γ signalling

Via its two SH2 domains, PLC-γ binds directly to tyrosine residues in the C-terminus of PDGFR. PLC-γ is reported to associate with PDGFR-α Tyr-988 and Tyr-1018 (Eriksson et al., 1995) or PDGFR-β Tyr-1021 and Tyr-1091 (Valius et al., 1993). The association of PLC-γ with PDGFR initiates the phosphorylation of PLC-γ at three tyrosine sites. Phosphorylation of Tyr-783 is reported to be essential for the catalytic activity of PLC-γ (Kim et al., 1991). Activated PLC-γ acts on the same substrate as PI3K, PIP_2, and interestingly molecular crosstalk between PI3K and PLC-γ exists to regulate PLC-γ activity (Falasca et al., 1998). Activated PLC-γ targets PIP_2 and generates two products, inositol-1,4,5-trisphosphate (IP_3) and diacylglycerol (DAG). DAG activates protein kinase C (PKC) and IP_3 increases the accumulation of intracellular calcium (Kim et al., 2000). Activation of PLC-γ is reported to be a rate-limiting step that mediates the chemotaxis of cells towards PDGF(Rönnstrand et al., 1999). PLC-γ signalling is also reported to be involved in cell spreading, motility and cancer cell invasion (Jones et al., 2005; Rönnstrand et al., 1999) (Figure 1.9).

1.3.1.4 Src family kinase signalling

Src family kinases are defined by the presence of a kinase domain and an SH2 and SH3 domain. Src family kinases bind to PDGFR-α Tyr-574 and Tyr-572 (Gelderloos et al., 1998; Hooshmand-Rad et al., 1998) and PDGFR-β Tyr-579 and Tyr-581 (Mori et al., 1993). The association of src with PDGFR initiates the phosphorylation of key tyrosine residues within the src SH2 and SH3 domains; these include Tyr-138 and Tyr-579. These phosphorylation events are necessary to promote the intrinsic kinase activity of src and maintain stable src interactions with PDGFRs (Alonso et al., 1995; Broome and Hunter, 1997). Src has been implicated in mitogenic signalling, activating c-myc and positively regulating cell-cycle progression. However this mitogenic signalling is dependent on the cell type, and PDGFR-β (rather than PDGFR-α) has been implicated as the primary receptor responsible for src signal transduction (DeMali et al., 1999). Later reports by Veracini et al (2006) suggested PDGFR signalling stimulates two spatially distinct pools of src family kinases, which also exert distinct biological effects that control cell growth or cell morphology (Veracini et al., 2006). Such insights help to explain the diverse effects of src kinase activation in different cell types (Figure 1.9).

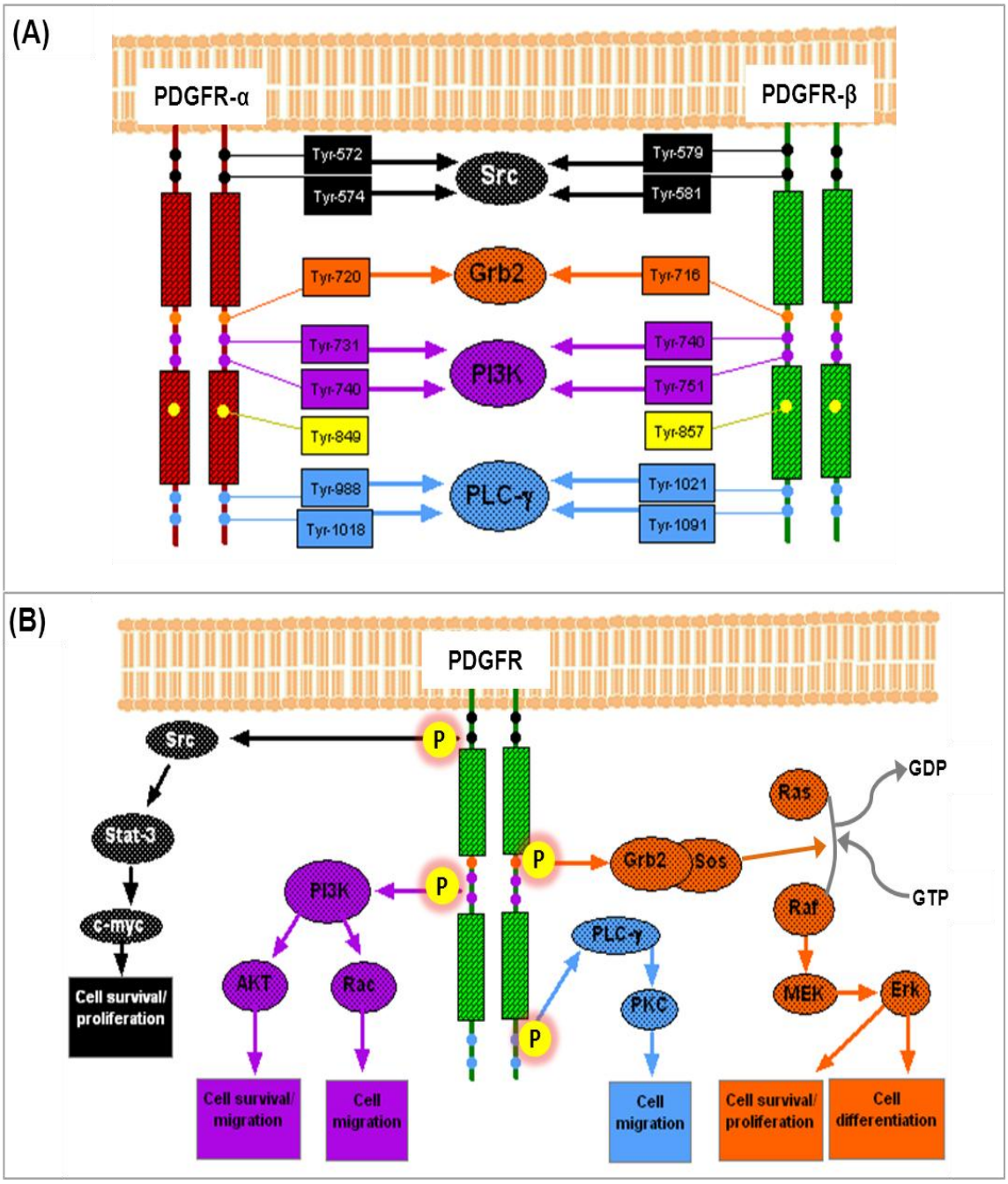

Figure 1.9: Core signalling pathways regulated by PDGFR kinase activity
The schematic diagram in **(A)** illustrates the split kinase domains of PDGFR-α and PDGFR-β and the specific tyrosine residues phosphorylated to create docking sites for distinct signalling molecules. Within the kinase domain, the PDGFR-α and PDGFR-β auto-phosphorylation sites, are also highlighted in yellow. **(B)** The schematic diagram outlines the key PDGFR downstream signalling pathways and cellular effects induced by PDGFR signalling. The colour of each pathway corresponds to specific tyrosines highlighted by the same colour in **(A)**.

1.3.2 The physiological importance of PDGFR signalling

1.3.2.1 Developmental roles

Studies using murine models have demonstrated the essential role of both PDGFR-α and PDGFR-β in embryonic development. PDGFR-α knockout is embryonic lethal between E8 and E16, with defects including cleft face, spina bifida and skeletal/vascular defects (Soriano, 1997). PDGFR-β null embryos die between E16 and 19, with abnormalities including placental defects, widespread oedema and haemorrhage, hypotrophy of the cardiac muscle, and abnormal kidney glomeruli (Hellström et al., 1999; Lindahl et al., 1998; Soriano, 1994).

During murine embryonic development, PDGFR-α expression is induced very early, pre-implantation of the embryo (Palmieri et al., 1992) and PDGFR-α and PDGF-AA are co-expressed in the blastocyst inner cell mass. However, even at the early stages of development, distinct patterning of PDGFR-α and PDGF-AA expression is observed, with PDGFR-α localised to the mesenchyme and PDGF-AA localised in adjacent epithelial layers, suggesting a paracrine mechanism of PDGFR signalling (Orr-Urtreger and Lonai, 1992). As development progresses, PDGF-AA expression becomes widespread in the tissues of the nervous system, the epithelia, and muscles, whereas PDGFR-α is largely localised to the mesenchyme (Ataliotis and Mercola, 1997). However, some epithelia do express PDGFR-α, notably the lens epithelium and apical ectodermal ridge (Morrison-Graham et al., 1992; Schatteman et al., 1992; Yeh et al., 1991). It has been suggested that PDGF secretion from adjacent or distant epithelia is a mechanism that regulates both the positioning and cellular behaviour of PDGFR-α positive mesenchyme cells during development.

High expression of both PDGF-C and PDGF-A is documented in the epithelia of brachial arches and facial processes (Ding et al., 2000; Tallquist et al., 2000), which act as chemoattractants to recruit PDGFR-α positive neural cells, which are important for normal skeletal development. In skin and hair development, PDGF-A is expressed in the epidermis and hair follicle epithelium with PDGFR-α localised in the lower mesenchyme layer. PDGFR-α knockout mice show severe defects, with detached epidermis and dermal hypoplasia, whereas PDGF-A knockout mice show a progressive reduction in the dermal mesenchyme with age. These abnormalities are explained by observations that paracrine secretion of PDGF-A from the epithelium induces the proliferation of the mesenchyme dermal cells, which stimulates the development of mesenchymal sheaths, dermal fibroblasts and dermal papillae (Karlsson et al., 1999). PDGF-A also mediates the proliferation and spreading of alveolar precursor smooth muscle cells in the murine lung. Mice lacking PDGF-A are null for mature alveolar smooth muscle cells. Clusters of PDGFR-α positive

mesenchymal cells gather during the pseudoglandular stage of lung development, yet without PDGF-AA, these cells fail to proliferate and do not distally spread to the developing alveolar saccules (Boström et al., 1996; Lindahl et al., 1997b). Consequently, mice develop an emphysema-like condition, through abnormalities in the alveoli (Boström et al., 1996). The myelination of neurons is severely impaired in PDGF-AA negative mice (Fruttiger et al., 1999). Oligodendrocytes are responsible for the formation of myelin sheaths and precursor cells express high levels of PDGFR-α, however these precursor cells are significantly reduced in PDGF-A-null embryos. It is therefore proposed PDGF-AA promotes the migration and expansion of oligodendrocytes precursor cells. High levels of PDGF-A are also expressed by neurons, which may provide the chemoattractant for oligodendrocyte precursor cells (Calver et al., 1998; Fruttiger et al., 1999). Further developmental defects were related to PDGF-AA: PDGFR-α mediated proliferation of precursor cells and include a progressive decrease in testicular size (Gnessi et al., 2000) and impaired formation of intestinal villi (Karlsson et al., 2000).

PDGFR-β and PDGF-BB are of primary importance in development of the vasculature. The highest expression of PDGF-BB is documented in sprouting immature vessels, denoting the role of PDGFR-β in blood vessel maturation (Lindahl, et al., 1997a). PDGF-BB is secreted by endothelial cells to promote the proliferation of surrounding vascular smooth muscle cells (vSMC) and pericyte precursor cells (Hellström et al., 1999; Lindahl et al., 1997a). Mice null for PDGFR-β and PDGF-BB display arterial smooth muscle cell hypoplasia, reduced cardiac muscle size, and widespread haemorrhages and oedema (Leveen et al., 1994; Soriano, 1994). In these mice, the number of pericyte and vSMC precursor cells is significantly depleted at sites such as, the brain, but not at sites such as, the pancreas. These tissue-specific effects are proposed to be related to the rate or stimuli which induce the precursor cell towards vSMC or pericyte lineages which express PDGFR-β. Thus, tissues such as the pancreas are proposed to have a higher rate of PDGFR-β induction than the brain (Hellström et al., 1999; Lindahl et al., 1997a). In the developing kidney, PDGFR-β or PDGF-BB knockout results in severe glomerular abnormalities. Specialised pericyte, meningeal cells, are no longer recruited to capillaries and as a result, capillary branching fails and the kidney only has one or a few capillary tufts occupying the entire Bowman's space (Levéen et al., 1994; Lindahl et al., 1998).

1.3.2.2 PDGFR signalling in wound healing

At the wound site, early studies revealed that PDGF is released from platelets and macrophages (Shimokado et al., 1985), thrombin activated endothelial cells (Harlan et al., 1986), arterial vSMCs (Walker et al., 1986), and epidermal keratinocytes (Ansel et al., 1993). At sites of inflammation, PDGFR-β is also up-regulated in vSMCs and expression has been documented in epithelial cells

(Antoniades et al., 1991; Rubin et al., 1988). Moreover, PDGF-BB stimulates human dermal fibroblasts to produce collagenase (Bauer et al., 1985) and at the wound interface PDGF-BB or PDGF-AB stimulate fibroblasts to contract the collagen matrix (Clark et al., 1989). In animal models, increased healing was documented following the local application of PDGF-BB at the site of incision or excision wounds (Mustoe et al., 1991; Pierce et al., 1988), burns (Danilenko et al., 1995), or periodontal injury (Rutherford et al., 1992). In humans, topical application of PDGF-BB enhanced the healing of pressure ulcers, accompanied by increased fibroblast proliferation and differentiation (Pierce et al., 1994). In patients with compromised healing, such as diabetics, PDGF-BB is well tolerated and effectively promotes the healing of lower extremity ulcers (Embil et al., 2000; Steed, 1995). PDGF-BB has also been evaluated in patients with periodontal disease, and has shown some success in promoting periodontal regeneration following surgery (Nevins et al., 2003) and increasing markers of bone regeneration (Sarment et al., 2006). Collectively, these studies outline a critical role for PDGF-BB in promoting wound healing, which is proving to be of clinical benefit.

1.3.3 PDGFR signalling in disease

1.3.3.1 Vascular diseases

Several factors associated with cardiovascular disease increase the expression of PDGF ligands. These include reduced blood flow and high cholesterol (Mondy et al., 1997), and hypertension (Negoro et al., 1995). Given these findings, it is unsurprising that high concentrations of PDGF-A and PDGF-B have been identified in atherosclerotic plaques, coupled with the increased expression of PDGFR-α and PDGFR-β by vSMCs in the vessel wall (Raines, 2004). In the inflammatory model of atherosclerosis, vSMC migration from the media to the intima, followed by vSMC proliferation, is proposed to be a key event in atherosclerosis. *In vivo* studies blocking either PDGFR-β or PDGF ligands, inhibited the accumulation of vSMCs in the intima and PDGF-BB was shown to stimulate the proliferation of vSMCs and intima thickening (Banai et al., 1998; Ferns et al., 1991; Jawien et al., 1992; Lewis et al., 2001; Yamasaki et al., 2001). More recent work has helped to elucidate possible mechanisms by which PDGFR-β signalling modulates vSMC migration and proliferation in atherosclerosis. PDGFR-β was documented to associate with low density lipoprotein receptor-related protein 1 (LRP-1) and the kinase domain of PDGFR-β was essential for LRP-1 phosphorylation. This association is reported to regulate the endocytosis and recycling of PDGFR-β. However, there are contradictory results as to whether LRP-1 negatively or positively regulates PDGFR-β, and whether this interaction is protective or harmful in atherosclerosis (Boucher et al., 2002, 2003; Newton et al., 2005; Takayama et al., 2005). More recently, another LDL protein, LRP-6 was reported to associate with PDGFR-β which promoted the lysosomal

degradation of PDGFR-β and inhibited vSMC cell proliferation in response to PDGF-BB. Mutant LRP-6 induced the activation of distinct PDGFR-β downstream signalling pathways and early onset atherosclerosis (Keramati et al., 2011). PDGFR signalling has also been implicated in pulmonary hypertension (Balasubramaniam et al., 2003; Humbert et al., 1998) and imatinib treatment has been shown to reverse pulmonary hypertension in animal models (Schermuly et al., 2005). Together these studies provide important insights into the mechanisms regulating PDGFR function and pathogenicity in vascular disease.

1.3.3.2 PDGFR signalling in cancer

Abnormalities in PDGFR signalling have been documented in many types of cancer. Such abnormalities have been correlated to factors including over-expression of PDGFRs and ligands, and activating mutations in the kinase domain of PDGFR (Holden et al., 2007; Martinho et al., 2009; Szerlip et al., 2012; Tsao et al., 2011). However, one of the primary mechanisms in which cancer cells exploit PDGFR signalling is through simultaneous expression of PDGF ligands and receptors, establishing autocrine PDGFR signalling loops (Ostman, 2004).

1.3.3.2.1 Glioma and autocrine PDGFR signalling

Such autocrine PDGFR signalling loops have been described in glioma (Hoelzinger et al., 2007; Lokker et al., 2002). Gliomas are classified based on their histology/ cell type, and their grade (Grade I-IV) denotes increased malignancy. The most prolific gliomas are; astrocytic, oligodendroglial, oligoastrocytic and ependymal tumours (Louis et al., 2007). PDGFR and PDGF expression is found in low and high grade gliomas and secondary tumours (Calzolari and Malatesta, 2010). In mice, Uhrborn et al (1998) outlined that recombinant PDGF-BB was able to induce gliomagenesis (Uhrbom et al., 1998), and Dai et al (2001) later suggested autocrine PDGFR signalling was able to generate gliomas through driving the proliferation and de-differentiation of glial pre-cursor cells.(Dai et al., 2001). The idea that precursor cells contribute to gliomagenesis was corroborated in later studies where PDGF stimulated the formation of heterogeneous gliomas, from adult white matter, with the majority of cells expressing glial precursor biomarkers. In a second study, PDGFR-α positive B cells were identified in the sub-ventricular zone (SVZ) of the adult brain. PDGFR-α was essential for oligodendrogenesis but not neurogenesis and infusion of PDGF generated large hyperplasias with glioma-like features. This study demonstrated that, in the human and murine SVZ, PDGFR-α signalling can determine the lineage differentiation of neural stem cells and induce early hallmarks of gliomagenesis (Jackson et al., 2006). Interestingly, PDGFR-α expression decreases during oligodendrocyte and astrocyte differentiation and is barely detectable in mature cells. Post-translational modification of PDGFR-α mRNA by cyclic AMP was responsible for the down-regulation of PDGFR-α in mature glial cells,

however, glioma cells were insensitive to cAMP and maintained PDGFR-α expression (Li and Wang, 2011). It is advantageous for the glioma cells to maintain a de-differentiated phenotype with a capacity for self-renewal as exemplified in a recent study detailing that glioma-derived cancer initiating cells have stem cell-like properties. PDGF-BB depletion caused these cells to arrest proliferation, lose their self-renewal capacity and begin to express biomarkers of oligodendrocytes. The glioma-derived cancer initiating cells could no longer form tumours without PDGF-BB (Jiang et al., 2011). Collectively these data suggest that the glioma cell of origin may derive from deregulation of neural precursor cells, which actively involves PDGFR autocrine signalling (Hambardzumyan et al., 2011) (Figure 1.10).

Progression of glioma is thought to involve the sequential accumulation of mutations in a clonal cell population derived from the cell of origin (Mueller et al., 2001; Zhu et al., 1997). Such mutations include PTEN, which causes aberrant activation of PI3K signalling (Endersby and Baker, 2008). A characteristic of gliomas is their highly heterogeneous cell population and some studies suggest the presence of genetically distinct clonal cell populations (Gömöri et al., 2002; Piccirillo et al., 2009), which challenges the idea of a single cell of origin. In cancer, tumour-derived PDGF mediates the infiltration PDGFR expressing stromal cells, promoting the development of the tumour vasculature (Pietras et al., 2008). In addition, tumour-derived PDGF mediates the tropism of adult mesenchymal stem cells (MSCs) (Doucette et al., 2011; Hata et al., 2010) and human umbilical vein stem cells (Gondi et al., 2010) towards gliomas. Whether or not cells infiltrating into gliomas become transformed, was recently interrogated by Fomchenko and colleagues (2011). This study used a murine model of PDGF-BB induced gliomagenesis and outlined that a population of cells, distinct from the cell of origin, is recruited to gliomas. In the glioma microenvironment, these recruited cells undergo transformation, with loss of tumour suppressors and an established self sufficiency of growth, eventually dominating areas of the tumour. The recruited cells were also able to initiate gliomas following transplantation and showed genetic changes typical of glioma cells (Fomchenko et al., 2011). Such studies suggest the cellular composition of glioma may derive from multiple cell types that are corrupted to mimic the glioma cell of origin (Figure 1.10). Several studies are also looking to exploit the PDGF-driven tropism of MSCs towards gliomas as drug delivery vehicles, and much of the literature suggests a positive role for MSCs (Hamada et al., 2005; Sasportas et al., 2009). However, other studies have shown that MSCs within the tumour microenvironment differentiated towards a tumour associated fibroblast phenotype (Mishra et al., 2008) and that autocrine PDGFR crosstalk between leukemic cells and MSCs may contribute to initiating the angiogenic switch (Ding et al., 2010). Given the recent observations by Fomchenko et al (2011), more studies are required to understand how PDGFR signalling might affect specific cell types recruited to the glioma microenvironment.

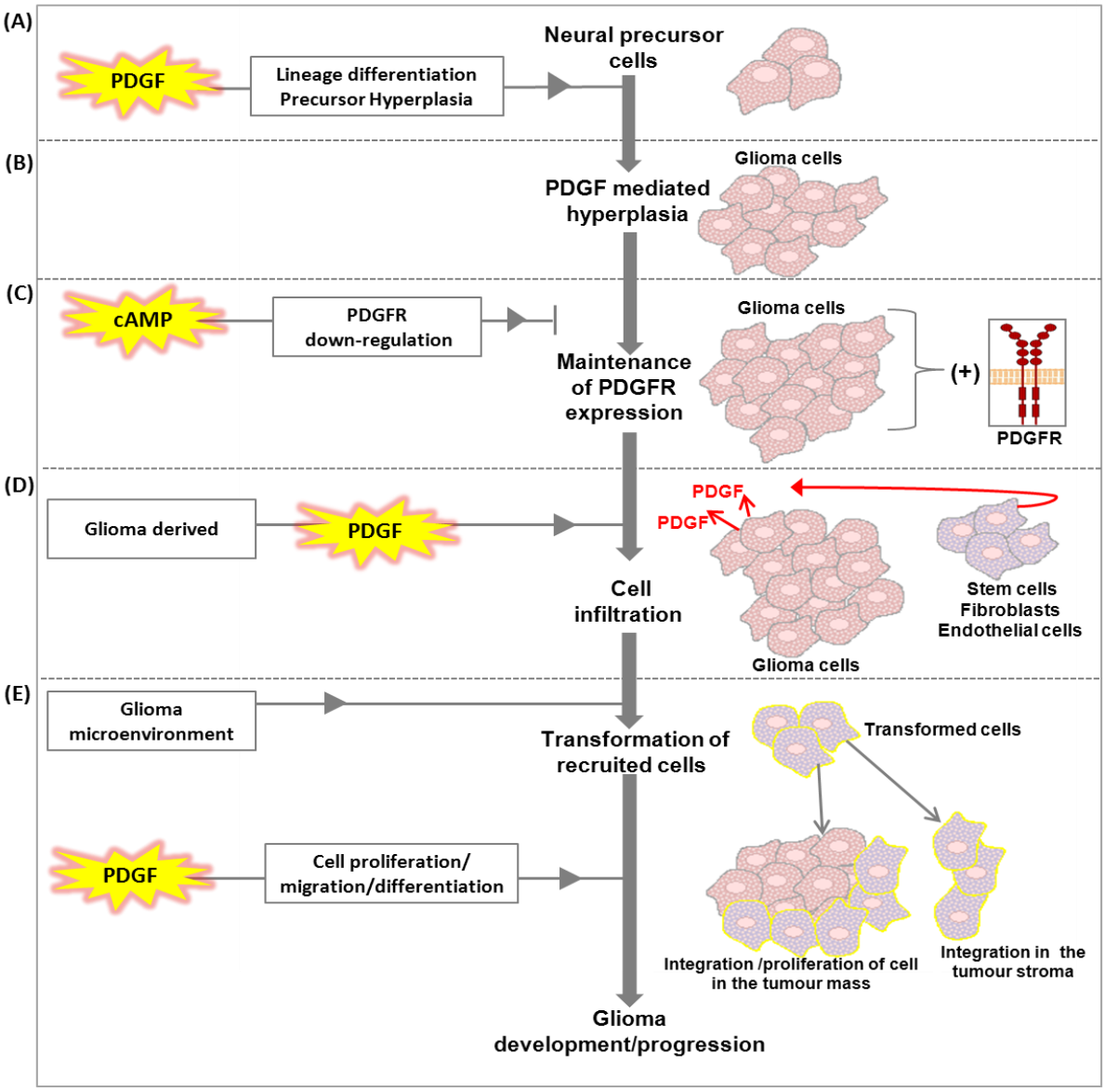

Figure 1.10: The contribution of PDGFR signalling to glioma development and progression
The schematic outlines how PDGFR is reported to contribute to gliomagenesis and glioma progression. **(A)** PDGF can mediate early precursor cells to differentiate along specific lineages (e.g. oligodendrocyte) which then undergo PDGF dependent hyperplasia **(B)**. **(C)** The expression of cAMP induces cells to down-regulate PDGFR expression during normal differentiation yet glioma cells continue to express PDGFR as part of their de-differentiated phenotype. **(D)** Glioma cells secrete PDGFs to recruit exogenous cells including, stem cells, fibroblasts and endothelial cells. **(E)** Within the glioma microenvironment, recruited cells are transformed and can integrate into the glioma tumour mass or form part of the glioma vascular stroma Together these PDGFR-dependent mechanisms of signalling promote the maintenance and progression of gliomas.

1.3.3.2.2 PDGFR signalling in other cancers

In other mesenchymal tumours, PDGFR and ligand expression is also correlated to a poor prognosis. Concurrent PDGFR-α and PDGF-AA expression was detected in 75% of human osteosarcoma specimens and this correlated negatively with event-free survival (Kubo et al., 2008). In other sarcomas, the expression of PDGFR and ligand has also been documented, with suggested autocrine signalling contributing to malignant behaviours (Stürzl, 1992; Sulzbacher et al., 2000; Wang et al., 1994).

Many epithelial tumours are reported to secrete PDGF ligands (Bronzert, 1987; Hsu et al., 1995; Tejada, 2006), whereas PDGFRs are highly expressed in the stroma surrounding carcinomas (Ostman, 2004). The stroma in a carcinoma generally consists of a vascular region populated by endothelial cells/ associated mural cells, and a fibrous region populated by mesenchymal cells. In the vascular tumour stroma, pericyte recruitment is important to stabilise tumour vessels. In Lewis lung carcinoma or B16 melanoma cells, tumour-derived PDGF-BB or PDGF-DD was essential for effective pericyte recruitment to the tumour vasculature. In the melanomas, the level of pericyte coverage was positively correlated to tumour growth and inhibition of PDGF-BB caused a regression in tumour vessels in Lewis lung carcinoma (Furuhashi, 2004; Sennino et al., 2007). Such studies have promoted the use of VEGF and PDGF targeted therapies, which have had some success in regressing tumour vasculature (Erber et al., 2003; Roskoski, 2007a). However, the importance of evaluating such therapeutics in individual cancers was highlighted in a recent study using colorectal and prostate carcinoma cells. This study showed that over-expression of PDGF-BB increased the pericyte content of vessels, which inhibited the growth of tumours (McCarty et al., 2007). Dhar et al (2010) also identified that an interaction involving tumour-derived PDGF-BB and NRP-1 was essential in driving the recruitment and differentiation of murine MSCs into pericytes in the tumour stroma (Dhar et al., 2010). Subsequent studies have shown that a mechanism involving stromal-derived factor -1 and tumour-derived PDGF-BB is able to differentiate bone marrow cells into pericytes (Hamdan et al., 2011). Carcinomas have also been reported to exploit fibroblasts in the tumour stroma to promote malignancy. PDGF-driven recruitment of fibroblasts has been documented in lung and cervical carcinomas (Pietras et al., 2008; Tejada, 2006). The paracrine PDGFR signalling between the tumour cells and fibroblasts can directly induce tumour growth. However, in the cervical cancer mouse model, PDGFR signalling up-regulated FGF in the fibroblasts, which was hypothesised to directly stimulate the cervical cancer cells (Pietras et al., 2008). Cancer cells, deficient in VEGF-A, were also documented to use PDGF to recruit fibroblasts, and fibroblast derived VEGF-A then rescued angiogenesis (Dong et al., 2004).

Together these studies outline that the paracrine and autocrine mechanisms of PDGFR signalling co-operate in early and later stages of tumourigenesis in a diverse array of tumours. The multi-faceted effects of PDGFR on tumour cells, and within the tumour microenvironment contribute to several of the hallmarks of cancer and PDGFR, therefore, remains an important anti-cancer target. Some of these mechanisms are summarised in Figure 1.11.

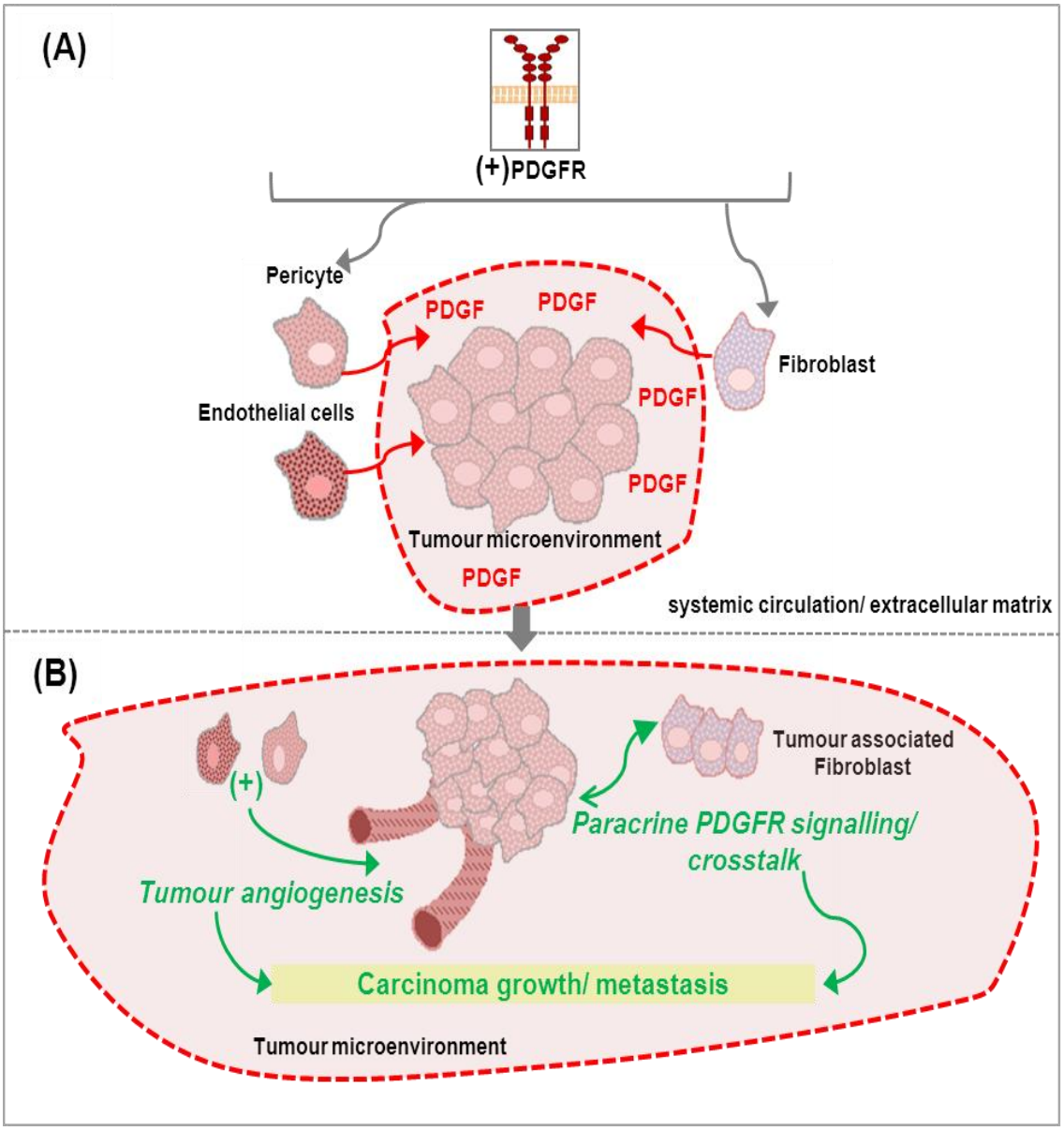

Figure 1.11: The contribution of PDGFR signalling to carcinoma progression
(A) Many epithelial tumours do not express PDGFRs yet commonly secrete high levels of PDGF growth factors to establish a tumour microenvironment rich in PDGF. PDGF in the tumour microenvironment chemotactically attracts PDGFR (+) cells such as fibroblasts, pericytes and endothelial cells to carcinomas. **(B)** Pericytes and endothelial cells contribute to the establishment of stable tumour vasculature and promote angiogenesis. Also in the tumour stroma, paracrine PDGFR signalling can occur between PDGFR expressed on tumour-associated stromal cells and tumour cell-derived PDGF ligands. PDGFR signalling in the tumour microenvironment functions to directly and indirectly promote the growth of carcinomas.

1.4 Summary

It is evident from the body of literature surrounding both NRP-1 and PDGFR that, in their own right, each of these receptors has conserved roles in development, physiology and tumourigenesis. As crosstalk between PDGFR and NRP-1 was only recently identified (Ball et al., 2010), the mechanism of this interaction has not been fully elucidated and questions remain as to whether this is a cell-type specific crosstalk. Other studies have corroborated the principal findings (Evans et al., 2011; Pellet-Many et al., 2011), however the NRP-1/PDGFR driven signalling varies in these different cell types. To date, no extensive studies of NRP-1/PDGFR crosstalk have been undertaken in tumour cells. Yet, given the contribution of both NRP-1 and PDGFR to tumourigenesis, identification of such a crosstalk in tumours would be particularly important and may contribute to a rationale for targeted therapies. Thus, this study provides an exciting opportunity to advance understanding of NRP-1/PDGFR crosstalk and the potential role of this mechanism in tumour cell biology.

1.4.1 Specific project aims

◆ **Identify tumour cell lines to study the crosstalk between NRP-1 and PDGFRs**

The complement of cell surface receptors is likely to be an important factor in mediating NRP-1/ PDGFR crosstalk in tumour cells. It is established that NRP-1 interacts with VEGF to facilitate VEGFR activation, however NRP-1 also interacts with multiple other proteins; c-Met (Hu et al., 2007), FGF (West et al., 2005) PDGFR (Cao et al., 2010; Ball et al., 2010; Pellet-Many et al., 2011) and TGF-β (Cao et al., 2010). Whether NRP-1 preferentially controls the activation of particular tyrosine kinase receptors may be defined by the relative expression of each receptor, the cell type and the culture conditions. In the study by Ball et al (2010) MSCs, cultured in 2-D, did not express detectable levels of VEGFR-1, VEGFR-2 or VEGFR-3 yet expressed PDGFR-α, PDGFR-β and NRP-1. An initial aim of the project was therefore to identify and profile tumour cell lines which expressed NRP-1 and/or PDGFR-α/ PDGFR-β with low or no detectable expression of VEGFRs.

◆ **Establish the biomolecular interactions that mediate NRP-1/PDGFR crosstalk**

The factors that mediate the crosstalk between NRP-1 and PDGFRs have not been elucidated. In MSCs, Ball et al (2010) documented that NRP-1 co-immunoprecipitation with both PDGFR-α and β was significantly enhanced in the presence of PDGF growth factors (Ball et al., 2010). NRP-1 is also reported to bind to both PDGF-AA (Ball et al., 2010) and PDGF-BB (Banerjee et al., 2006). Collectively these studies suggest that PDGF growth factors might mediate an indirect interaction between NRP-1 and PDGFR, in a similar way as VEGF-A_{165} bridges the interaction between NRP-1 and VEGFRs (Soker et al., 2002). Contrary to this hypothesis, Pellet-Many et al (2011) reported

that NRP-1 and PDGFR-α co-immunoprecipitated at similar levels in the absence or presence of PDGF growth factors. Yet, NRP-1 was still essential for the phosphorylation of PDGFRs (Pellet-Many et al., 2011), suggesting an interaction between NRP-1 and PDGFRs in the absence of PDGF growth factors. Previous reports examining NRP-1/VEGFR crosstalk also implied that the growth factor bridging model was insufficient to explain NRP-1's ability to potentiate VEGFR signalling. In these studies, NRP-1 enhanced VEGFR signalling in the absence of VEGF-A binding to NRP-1, and the complex formation between NRP-1 and VEGFR-2 was documented in the absence of VEGF-A (Shraga-Heled et al., 2007). In view of these reports, it is feasible that NRP-1 enhances PDGFR signalling in the absence or presence of PDGF growth factors, depending on the cell type. As no conclusive evidence defining the nature of the interaction between PDGFR and NRP-1 exists, a specific aim of the project was to determine if PDGF growth factors mediated a biophysical interaction between NRP-1 and PDGFRs.

◆ **Determine if PDGFR kinase activity and signalling is mediated by NRP-1/PDGFR crosstalk**

As outlined, the specific interactions between different isoforms of PDGFR and PDGFs govern the activation of distinct and overlapping intracellular signalling pathways. Subtle differences in signalling induced by the different dimers of PDGFR may be important in NRP-1/PDGFR crosstalk, as changes in the phosphorylation pattern of PDGFR may influence which adaptor molecules can interact with PDGFRs. Previous reports outlined that PDGF-AA induced phosphorylation of PDGFR- α is most significantly affected by NRP-1. In these studies, NRP-1 siRNA significantly decreased both the total phosphorylation of PDGFR-α (Pellet-Many et al., 2011) and the phosphorylation of the PI3K binding site, Tyr-742 (Ball et al., 2010). NRP-1 also had a significant effect on PDGF-BB induced phosphorylation of the PDGFR-β PI3K binding site, Tyr-751, however, Pellet-Many et al suggested NRP-1 did not significantly affect the overall phosphorylation of PDGFR-β. Together these studies suggest that the PDGFR-α homodimer may be the predominantly regulated by NRP-1. A specific aim of this study was to therefore, examine the influence of NRP-1 on the overall phosphorylation of PDGFR-α and PDGFR-β in tumour cells and the effects on key signalling pathways downstream of PDGFR.

◆ **Identify specific cellular effects that are mediated by NRP-1/PDGFR crosstalk**

Studies by Ball et al (2010) reported that the NRP-1/PDGFR crosstalk significantly affected PDGFR-mediated MSC proliferation and chemotaxis (Ball et al., 2010). Given the importance of cell migration and proliferation in the establishment of an oncogenic phenotype, it was important to establish if NRP-1 crosstalk with PDGFR could modulate these behaviours in tumour cells. A final aim of the project was therefore, to examine tumour cell survival and migration in the context of NRP-1/PDGFR crosstalk.

Chapter 2- Materials and Methods

2.0 Cells and cell culture

All tumour cell lines used in this study were obtained from AstraZeneca and originally derived from the American type culture collection (ATCC). Tumour cell lines were maintained in Dulbecco's Modified Eagles Medium (DMEM) growth medium (Sigma-Aldrich) supplemented with 10% (v/v) foetal bovine serum (FBS) and 1% (v/v) L-glutamine (Lonza). Unless otherwise stated, this was the standard culture media. Human epithelial non-small cell lung cancer (NSCLC) cell lines; A549, H1703, H1299, CALU-6, H23, H460, H522 and H1793 were used in this study. Colon epithelial cancer cell lines; HCT116, COLO-205, SW620 and LoVo were also used in the initial phase of this study. Mesenchymal cancer cell lines included seven glioma cell lines; T98G, A172, U87MG, U118MG, LN229, M059J, M059K and three osteosarcoma cell lines; Saos-2, KHOS-240S and MG63.

As part of this study, human MSCs were also used as a positive control as these cells had been well characterised within the group (Appendix, Figure 8.0) and were known to exhibit NRP-1 and PDGFR crosstalk (Ball et al., 2010). MSCs were obtained from normal bone marrow of five different individuals (Lonza) and cells were always assayed at passage five. Cells were maintained in MSC growth medium (MSCGM^{TM}) (Invitrogen) supplemented with 10% (v/v) FBS, 1% L-glutamine, and 1% (v/v) penicillin/streptomycin (Lonza).

All cell lines were cultured in 75 cm^2 tissue culture treated flasks (Corning, Costar) with vented lids in a humidified atmosphere of 37°C/5% CO_2. Unless otherwise stated these were the standard incubation conditions. Once cells had reached a maximum of 80% confluence they were sub-cultured using 0.05% trypsin-0.02% ethylenediaminetetraacetic acid (EDTA) (Sigma-Aldrich). The cancer cell lines were split at a 1:10 ratio. Briefly, to trypsinise cells, cell culture media was removed and the cell monolayer was washed in 10 mL of phosphate buffered saline (PBS) (Sigma Aldrich). PBS was discarded and 3 mL of 0.05% trypsin-0.02%-EDTA was added to cells and cells were incubated for no more than 5 minutes. Flasks were agitated through gentle tapping and trypsin was neutralised through the addition of 10 mL standard culture media. The cell suspension was then split between appropriate numbers of 75 cm^2 flasks. During cell culture, growth medium was replenished every 2-3 days.

2.1 siRNA transfection

Cells were allowed to reach 50% confluence and media was replenished with an appropriate volume of fresh standard culture media. To prepare siRNA solutions, 10nM of validated NRP-1

siRNA (Qiagen: S102663213/siRNA sequence 5'-CACGCGATTCATCAGGATCTA-3') was used to silence the expression of NRP-1.

As a control, cells treated with 10 nM of scrambled oligonucleotides (Qiagen) were also used in each assay. The scrambled oligonucleotides or siRNA solutions were added to 100 µL of Opti-MEM® (Invitrogen) and, in a separate tube, 2 µL of Lipofectamine® RNAiMAX (Invitrogen) was added to 100 µL of Opti-MEM®. The two Opti-MEM® solutions were mixed to give a total volume of 200 µL and incubated for 30 minutes at room temperature. The Opti-MEM® solution was then added to cells, giving a final concentration of 10 nM of siRNA or scrambled oligonucleotides. The cells were incubated with the siRNA for a maximum of 72 hr.

2.2 Flow cytometry

Cells were removed from flasks by trypsinisation and cell suspensions were centrifuged at 1500 rpm for 4 minutes. Cell pellets were resuspended in 5 mL fresh culture media and cells were counted using an electronic cell counter (CASY counter, Roche Diagnostics). Briefly, 50 µL of cell suspension was added to 10 mL CASYton solution (Roche Diagnostics) and viable cell counts were estimated using the CASY counter. Cell counts were recorded and cells were allowed to recover cell surface receptor expression at, 37°C/5% CO_2 for 30 minutes. Cell suspensions were adjusted to 1 x10^5 and cells were centrifuged at 1200 rpm to pellet cells. From this point onwards the cells were kept on ice. Cells were re-suspended in 500 µL of cold PBS containing 0.5% (v/v) bovine serum albumin (BSA) (Sigma-Aldrich). This wash step was repeated before cells were re-suspended in either 10 µg/mL anti-human phycoerythrin (PE)-conjugated or unconjugated antibodies (Table 2.0 and 2.1). Selected cells were also incubated with identical concentrations of conjugated isotype-matched anti-IgG-PE or unconjugated isotype-matched anti-IgG (Table 2.0 and 2.1). Cells were incubated for 1 hour on ice. Cells were then centrifuged at 1200 rpm for 4 minutes and washed in 500 µl PBS/0.5% (w/v) BSA, for a total of 3 washes. For un-conjugated antibodies, secondary labelling was performed by suspending cells in the appropriate fluorescein isothiocyanate (FITC) or PE-conjugated antibody (diluted 1/200 in PBS/0.5% (w/v) BSA) (Table 2.0 and 2.1) and incubating cells for 30 minutes. Following incubation, a further 3 washes, using 1 mL PBS/ 0.5% BSA, were performed. The University of Manchester flow cytometry facility was used to analyse the cells. Briefly, 1×10^5 cells were counted using a FACscan cytometer (Becton Dickinson) at a flow rate of <200 events/second.

2.3 Immunoblot analysis

2.3.1 Isolation of cell lysates

On a bed of ice, cell monolayers were washed twice in cold PBS. PBS was aspirated followed by the immediate addition of an appropriate volume of cold cell lysis buffer (20 mM tris(hydroxymethyl)aminomethane-hydrochloride (Tris-HCl); pH 8/ 150 mM sodium chloride (NaCl), 1% (v/v) Tergitol-type NP-40 (NP-40) /2.5 mM EDTA) supplemented with protease inhibitor cocktail (Roche Diagnostics). The cell layer was scraped to remove all cell material. Cell lysates were then transferred to 1.7 mL eppendorf and lysates were then rotated end-over-end for 60 minutes at 4°C. Lysates were centrifuged at 10,000 rpm for 10 minutes at 4°C to remove cell debris, before the supernatant was transferred to a fresh eppendorf. Lysates were either used immediately or stored at -80°C until required.

2.3.2 Determination of protein concentration (BCA assay)

To quantify the total protein in lysates the bicinchoninic acid (BCA) protein assay (Thermo Scientific) was used. The BCA assay relies on the fact that in an alkaline medium protein reduces Cu^{2+} to Cu^{1+} and BCA addition can accurately quantify the amount of Cu^{1+} in a sample. On BCA addition, a purple reaction product is formed which exhibits a linear absorbance at 562 nm and is proportional to the protein concentration (Smith *et al*., 1985).

To perform the BCA assay, known albumin protein standards were prepared in lysis buffer to give 9 standards in increments ranging from 25 µg/mL to 2 mg/mL. The standards and unknown protein samples were added (25 µL/well) to a 96-well microplate (Corning, Costar) and BCA reagent was added (200 µL/well). Plates were incubated at 37°C for 30 minutes and the absorbance at 570 nm was measured using a Dynex MRX II microtitre plate reader with Revolution software. The unknown protein concentrations were calculated using the standard curve values.

2.3.3 Co-immunoprecipitation reaction

For co-immunoprecipitation, the cancer cell lysates were diluted to 500 µg, however, the MSCs gave a lower protein yield and were, therefore, diluted to 250 µg in lysis buffer. Lysates were pre-cleared for 1 hour at 4°C under gentle rotation using 20 µL of protein-G sepharose beads (Zymed, Invitrogen). Samples were centrifuged at 1000 rpm for 2 minutes at 4°C. The pre-cleared lysate was transferred to a fresh tube and 0.5 µg/mL of either NRP-1 primary antibody or a rabbit IgG control antibody (Table 2) was added and lysates were incubated overnight at 4°C under gentle rotation. The following day, 40 µL of protein G sepharose beads was added to each sample,

followed by incubation overnight at 4°C under gentle rotation. Samples were centrifuged 1000 rpm for 2 minutes at 4°C and lysates were removed and retained. The pelleted protein-G sepharose beads were washed (X2) in 1 mL of PBS and then centrifuged 1000 rpm for 2 minutes at 4°C to allow removal of the wash. Beads were then resuspended in 60 µL of 4X NuPAGE® SDS sample buffer (Invitrogen) and 2.5 µL of reducing agent (Invitrogen). As an additional control (to assess the amount of NRP-1 retained in the cell lysate) 25 µL of lysate was prepared by adding 6 µL 4X NuPAGE® SDS sample buffer and 1 µL of reducing agent. All samples were boiled for 5 minutes before being centrifuged at 2000 rpm. The supernatant was transferred to a fresh tube and the beads discarded before samples were used for immunoblots analysis. The antibodies used for the co-immunoprecipitation and immunoblots are detailed (Table 2).

2.3.4 Immunoblot

Whole cell lysates were diluted in lysis buffer (final concentration 20-100 µg), reduced by the addition of 1.0 µL of sample reducing agent (containing 500 mM dithiothreitol (DTT) (Invitrogen) and prepared for electrophoresis through the addition of 7 µL 4X NuPAGE® sodium dodecyl sulphate (SDS) sample buffer (Invitrogen) to a final volume of 30 µL. Samples were heated to 90-100°C for 5 minutes, briefly centrifuged and resolved by SDS polyacrylamide gel electrophoresis (PAGE). Gels used for SDS-PAGE were 4-12% Bis-Tris (Invitrogen) with 1X 2-(*N*-morpholino) ethanesulfonic acid (MES) SDS running buffer (Invitrogen). To determine the size of the resolved proteins, precision plus all blue protein marker (Bio-Rad) with a molecular weight range from 10 to 250 kDa was loaded in one lane of each gel. Proteins were resolved for 90 minutes at 150 volts (V). Using the NuPAGE® Western transfer system (Invitrogen) proteins were transferred to a 0.45 µm nitrocellulose membrane (Whatman, GE Healthcare) Transfer was performed in transfer buffer (48 mM Tris/39 mM glycine/0.37% SDS/10% methanol) for 2 hours at 40 V. Transfer efficiency was assessed through staining the nitrocellulose membranes with 0.1% (w/v) Ponceau S (Sigma-Aldrich) in 4% (v/v) acetic acid. Membranes were de-stained in Tris-buffered saline with added Tween-20 (TBS-T) (10 mM Tris, 150 mM NaCl, 0.05% (v/v) Tween-20, pH 7.4) before being blocked in either 4% (w/v) BSA (diluted in TBS-T) and incubated for 1 hour at room temperature. Primary antibodies were then prepared in blocking solution (see Table 2.0) and incubated at 4°C overnight with gentle agitation. Membranes were washed 3 times in 10 mL of TBS-T with gentle agitation for 10 minutes/ wash. Appropriate HRP-conjugated secondary antibodies (see Table 2.1) were diluted in 4% (w/v) in milk Marvel® /TBS-T and incubated with membranes for 2 hours at room temperature with gentle agitation. Membranes were washed 4 times in 10 mL of TBS-T with gentle agitation for 15 minutes/ wash with a final wash in 20 mL of Milli-Q water (Merck Millipore) for 20 minutes. Immunoblots were developed through incubating nitrocellulose membranes in the dark for 4 minutes with either, UptiLight™HS or the more sensitive UptiLight™US HRP substrates

(both from Interchim). Kodak BioMax MR or BioMax XAR film was used to visualise proteins. Gene Tools v3 software was used to determine the pixel density of protein bands and β-Actin was used as loading control for relative quantification of proteins.

2.3.5 Cell treatments/ antibodies for the PDGFR signalling immunoblots

In a 12-well tissue culture plate, tumour cells and MSCs were cultured to 40% confluence and cells were treated with either 10 nM of NRP-1 siRNA or scrambled oligonucleotides as described (Section 2.0). The following day after siRNA treatment, the cell media was replaced with 0.75 mL starvation media and selected cells were treated with 100 nM of PDGFR inhibitor V (Merck Millipore) or 80 nM of PDGFR inhibitor IV. PDGFR inhibitor V and IV are ATP competitive, reversible small molecule inhibitors and inhibitor IV inhibits the kinase activity of PDGFR-α, PDGFR-β and c-Abl kinase whereas PDGFR inhibitor V specifically inhibits PDGFR-α and PDGFR-β. All cells were incubated with the compounds for 24 hours. The following day, cells were washed in starvation media, before being treated with either 0.4 mL of 25ng/mL PDGF-AA or PDGF-BB or starvation media for 10 minutes. Cells were lysed and protein concentrations were quantified (see below). The samples were then analysed by immunoblot (see Section 2.2.3) and the nitrocellulose membranes were cut into segments and incubated with primary antibodies against: pERK-1/2 (dilution: 1/4000), pAKT (dilution: 1/20,000), pPLC-γ (dilution: 1/15,000), NRP-1 (dilution: 1/20,000) or pPDGFR (Tyr-849/ Tyr-857) (dilution: 1/25,000) (see Table 2.0).

2.4 pPDGFR-α and pPDGFR-β ELISA assays

2.4.1 Cell preparation for ELISA assays

In a 6-well tissue culture plate, tumour cells and MSCs were cultured to 40% confluence and cells were treated with either 10 nM of NRP-1 siRNA or scrambled oligonucleotides using the Lipofectamine® RNAiMAX protocol as previously described (Section 2.0). The following day the cell media was replaced with 2 mL starvation media and selected cells treated with 100 nM of PDGFR inhibitor V (Merck Millipore). Cells were incubated overnight. Cells were washed once in 2 mL of starvation media, before being treated with either 0.5 mL of PDGF-AA, PDGF-BB or starvation media. Treated cells were incubated for 10 minutes then immediately placed on ice and washed in 3 mL of ice-cold PBS. PBS was aspirated and 0.2 mL of lysis buffer was added/ well. Cell scrapers were used to dissociate cells before the total lysate was pipetted into a fresh 1.7 mL eppendorf. Lysates were left at 4°C, rotating on a medium speed, for 1 hour. Lysates were then centrifuged at 4°C at 10,000 rpm for 5 minutes and the supernatant was transferred to a fresh eppendorf tube. Protein concentrations were quantified by BCA assay, as previously described (Section 2.4.2).

2.4.2 pPDGFR-α (Tyr-849) sandwich ELISA

All samples were assayed in duplicate within a 96-well immulon high bind flat bottom plate (Thermo Scientific). For this assay, the Pathscan® PDGFR-α and pPDGFR-α antibody pair was employed. The pPDGFR-α (Tyr-849) capture antibody (Cell Signalling Technology) (see Table 2.0) was diluted 1/100 in PBS and 50 µL/ well was added before the plate was sealed and incubated overnight at 4°C. The antibody solution was tapped from the plate and wells were washed (X5) in wash buffer (PBS/ 0.05% Tween-20) using a volume of 200 µL/ well. Plates were blotted on blue roll to remove excess wash solution between washes (this was the standard wash procedure unless otherwise stated). Non-specific binding sites were blocked by the addition of 150 µL/ well of 1% (w/v) BSA diluted in PBS (blocking buffer). Plates were sealed and incubated at 37°C for 2 hours. Plates were washed and 50 µL/well of pre-prepared lysate (Section 2.4.1) was added at a concentration of 200 µg/ well (x2 wells containing lysis buffer only were included as negative diluent only controls). Plates were sealed and incubated overnight at 4°C. Plates were washed and total PDGFR-α mouse detection antibody (see Table 2.0) was diluted 1/100 in blocking buffer and 50 µL/well was added. Plates were sealed and incubated for 90 minutes at 37°C. Plates were washed and anti-mouse HRP-linked secondary antibody (Table 2.1) was diluted 1/1000 in blocking buffer and 50 µL/ well was added. Plates were sealed and incubated for 60 minutes at 37°C. Plates were washed and 50 µL of TMB substrate (#7004) (Cell Signalling Technology) was added/ well. Plates were protected from light and incubated for 10-15 minutes at room temperature, before 20 µL stop solution (2 N sulphuric acid) (R&D systems) (#DY994) was used to terminate the reaction. Plates were agitated for 20 seconds and immediately read at 450 nm absorbance using Dynex MRX II microtitre plate reader with Revolution software.

2.4.3 pPDGFR-β Duoset® IC sandwich ELISA

The human pPDGFR-β Duoset® IC sandwich ELISA (R&D Systems) was used to quantify the total phosphorylation of PDGFR-β. The pPDGFR-β capture antibody (see Table 2.0) was diluted to a 4 µg/mL in PBS and 50 µL/well was added to a 96-well immulon high bind flat bottom plate. Plates were sealed and incubated overnight at 4°C. The antibody solution was tapped from the plate and wells were washed (X5) in wash buffer (PBS/ 0.05% Tween-20) using a volume of 200 µL/ well. Plates were blotted on blue roll to remove excess wash solution between washes (this was the standard wash procedure unless otherwise stated). Non-specific binding sites were blocked by the addition of 150 µL/ well of 1% (w/v) BSA diluted in PBS (blocking buffer). Plates were sealed and incubated at 37°C for 2 hours. Plates were washed and 50 µL/well of pre-prepared lysate (Section 2.4.1) was added at a concentration of 200 µg/ well (x2 wells containing lysis buffer only were included as negative diluent only controls and x2 wells containing Duoset® positive pPDGFR-β

controls #841424). Plates were sealed and incubated overnight at 4°C. Anti-mouse HRP-linked p-Tyr detection antibody (Table 2.1) was diluted 1/1500 in diluent #14 (20 mM Tris/ 137 mM NaCl/ 0.05% Tween-20/ 0.1% BSA/ pH 7.2-7.4) and 50 µL/ well was added. Plates were incubated for 2 hours at 37°C protected from light. Plates were washed and 50 µL of TMB substrate (R&D Systems, UK) (#DY999) was added/ well. Plates were protected from light and incubated for 10-15 minutes at room temperature, before 20 µL stop solution was used to terminate the reaction. Plates were agitated for 20 seconds and immediately read at 450 nm absorbance using Dynex MRX II microtitre plate reader with Revolution software.

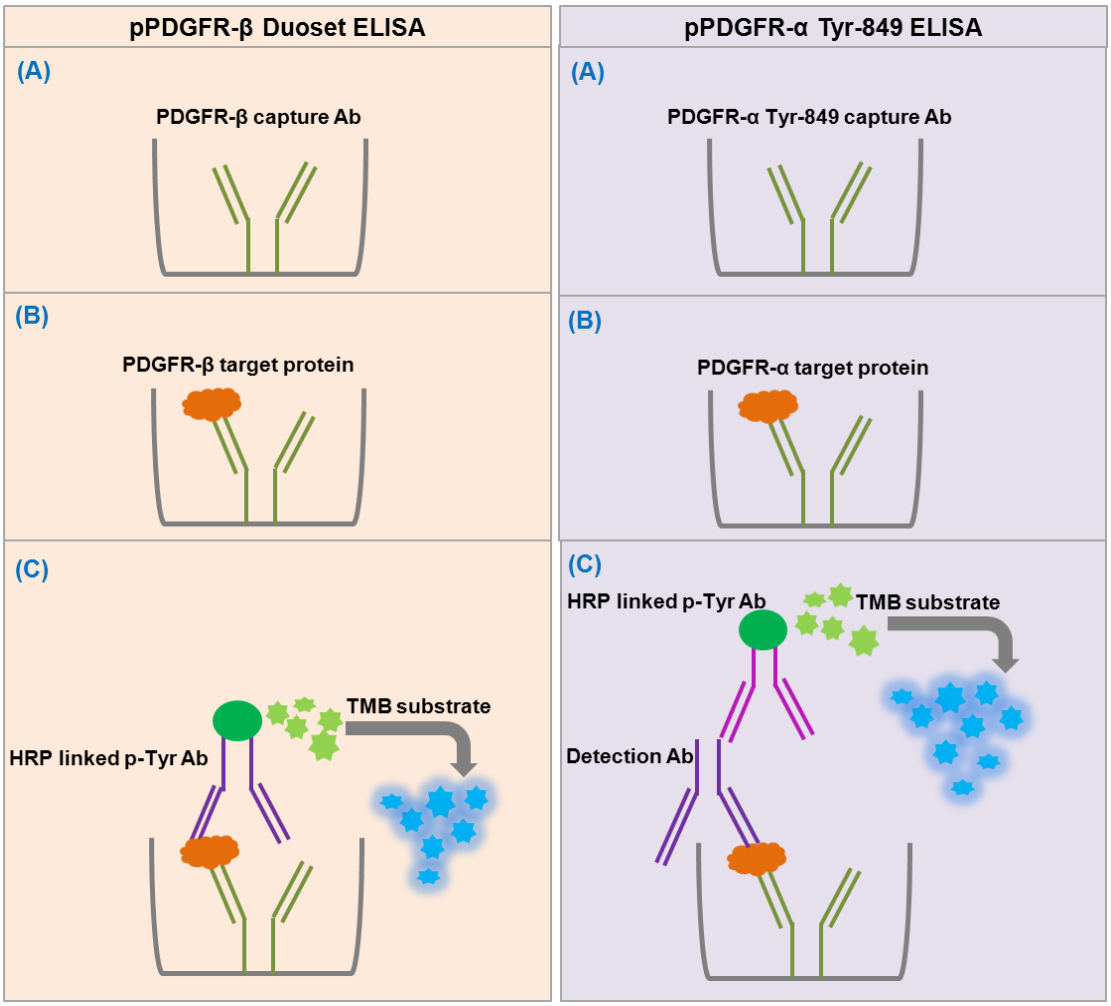

Figure 2.0: Schematic of the pPDGFR-α and pPDGFR-β ELISAs
In each well of a 96-well microtiter plate, capture antibodies for each ELISA were incubated overnight. The PDGFR-β antibody detected both phosphorylated and total PDGFR-β. The PDGFR-α antibody specifically detected pPDGFR-α Tyr-849. **(B)** Cell lysates, which had been treated (+/-) PDGF, were added and incubated overnight. **(C)** For the PDGFR-β ELISA, a HRP-conjugated p-Tyr secondary antibody was added. For the PDGFR-α ELISA, a detection antibody against total PDGFR-α was added followed by the addition of the HRP-conjugated secondary antibody. TMB substrate was added to the ELISA plates and incubated. An acidic stop solution was added to quench the reaction prior to reading plates at 450 nm absorbance using Dynex MRX II microtitre plate reader with Revolution software.

2.5 Analysing PDGFR:NRP-1 mediated cell survival and migration

2.5.1 Cyquant assay

The CyQuant® cell proliferation assay (Invitrogen, UK, C7026) was used to determine if NRP-1 crosstalk with PDGFRs could affect cell proliferation. Cells were seeded and treated with NRP-1 siRNA or scrambled oligonucleotides as described (Section 2.1). During the seeding process, a cell pellet containing 100,000 cells was frozen at -80°C. The day following siRNA treatment, cell media was replaced with starvation media and PDGF-AA or PDGF-BB (25 ng/mL) was added to selected scrambled or NRP-1 siRNA treated cells (growth factors were replenished every 24 hours). Cells were incubated with PDGF growth factors for a total of 48 hours.

Media was aspirated and cells were incubated at -80°C for a minimum of 3 hours. A solution containing CyQuant® GR dye (Invitrogen) diluted in CyQuant lysis buffer (Invitrogen) was prepared. CyQuant GR dye is a green fluorescent dye, which emits enhanced fluorescence when bound to cellular nucleic acids. Cells were thawed at room temperature and 200 µL of CyQuant GR dye/lysis buffer was added/ well. Cells were incubated for 5 minutes at room temperature, protected from light, before fluorescence was quantified using a FLx800 fluorescence microtitre plate reader with excitation at 480 nm and emission detection at 540 nm, using KC Junior software. To generate a standard curve/ cell line, cell pellets containing 100,000 cells were thawed at room temperature. The Cyquant GR dye solution was used to re-suspend cell pellets. Serial dilutions were then performed to generate standards containing between 1000-50,000 cells/ 200 µL volume. The CyQuant assay has a linear range between 50-50,000 cells per 200 µL volume. Standard curves were used to determine cell numbers within individual samples. Cell numbers were expressed as ratios relative to scrambled un-stimulated controls.

2.5.2 The cell exclusion migration assay

A cell exclusion migration assay was used. Selected cells had been pre-treated 24 hours before with 10 nM of either NRP-1 siRNA or scrambled oligonucleotides (Section 2.1). Cells were harvested by trypsinisation and suspensions containing $4x10^5$ cells/mL were prepared in DMEM standard culture media. A sterile adhesive cell culture insert (ibidi) with 2 wells was placed in each well of 24-well tissue culture plate. In each well of the culture insert, 80 µL of the prepared cell suspension was aliquoted and cells were allowed to adhere for 24 hours. Cell culture inserts were removed to create a cell free area with a width of 500 µm (+/-) 50 µm. Following removal of the culture insert cells were allowed to recover for 30 minutes before cells were washed in 500 µL starvation media and selected cells were then treated with either 25 ng/mL of PDGF-AA or PDGF-BB +/- 100 nM of PDGFR inhibitor V. Negative control cells were treated with starvation media

only. Using defined points marked on the 24-well plates, the cell free area was imaged in the same position at time 0, 4, 8 and 24 hours. The images were quantified using the Image J polygon function to define the cell free area. The polygon was then over-laid at subsequent time points to determine the percentage cell free area relative to the 0 hour time-point.

2.6 Analysis of NRP-1:PDGFR interactions using immunofluorescence and the proximity ligation assay (PLA)

2.6.1 Cell preparation

Cells used for the NRP-1 antibody validation had been pre-treated with NRP-1 or scrambled oligonucleotides 24 hours prior to seeding the cells (see Section 2.1 for methods). Sterile 13 mm glass coverslips were positioned in each well of a 24-well tissue culture plate (Corning, Costar, UK). MSCs (passage 5) or cancer cells (passage 6-10) were harvested by trypsinisation. MSCs were seeded at a density 10,000 cells/ well and cancer cells were seeded at 20,000 cells/well. Cells were allowed to adhere overnight and the following day cells were washed in starvation media (DMEM/1% L-glutamine/0.5% FBS) and then starved for 6 hours. Cells used for the proximity ligation assay were also labelled with 1 µg/mL of wheat germ agglutinin (WGA) conjugated to Alexa Fluor®488 (Molecular Probes®, Invitrogen™). WGA selectively bind *N*-acetylglucosamine and sialic acid residues and thus primarily labels the plasma membrane of cells (Chazotte, 2011).

PDGF-AA or PDGF-BB (R&D Systems) were diluted in starvation media to a concentration of 25 ng/mL. Cells were washed in 500 µL of starvation media and then treated with 300 µL/ well of the prepared PDGF-AA, PDGF-BB or starvation media. Cells were incubated for 10 minutes and then immediately placed on ice. Media was aspirated, cells were washed in 500 µL of PBS and then 500 µL/well of 3% (w/v) para-formaldehyde was added to fix cells. Cells were incubated for 15 minutes under gentle agitation before para-formaldehyde was aspirated and cells were washed (X3) in 500 µL/ well of PBS. To quench un-reacted aldehydes, 500 µL/well of 0.2 M glycine was added for 10 minutes. Cells were washed (X2) in 500 µL PBS before 500 µL of 0.1% (v/v) Triton-X-100™(Sigma Aldrich) was added for 2-3 minutes. Cells were washed (X3) in 500 µL/ well of PBS followed by the addition of 500 µL of 0.25µm filtered 3% fish skin gelatin (Sigma-Aldrich). Cells were incubated under gentle agitation at room temperature for 1 hour. Primary antibodies (Table 2.1) were diluted 1/200 in 3% fish skin gelatin and 40 µL aliquots were placed on para-film in a humidity chamber. For the PLA control samples either the NRP-1, PDGFR-α or PDGFR-β primary antibodies were incubated in isolation. Coverslips were placed face down on the primary antibody and incubated in the humidity chambers overnight at 4°C.

2.6.2 Immunofluorescence secondary labelling

For the NRP-1 primary antibody validation and co-localisation immunofluorescence analysis, secondary labeling of the coverslips was performed. Coverslips were washed by transferring them sequentially through four 200 mL beakers of PBS and two 200 mL beakers of Milli-Q water. In humidity chambers, coverslips were placed face-down on 40 µL aliquots of appropriate Alexa Fluor™ (Invitrogen) conjugated secondary antibodies (Table 2.1). Alexa-Fluor's had been diluted 1/800 in 3% fish skin gelatin and filtered through a 0.22 µm filters (Millipore). Coverslips were incubated with secondary antibodies for 90 minutes at room temperature protected from light. Coverslips were washed as described for the primary antibodies. Coverslips were then mounted onto glass slides using 10 µL ProLong® Gold with DAPI (Invitrogen) and sealed using nail varnish. Images were collected on a widefield microscope (Leica DM RXA) using a 20x or 40x objective and captured using a Coolsnap EZ camera driven by MetaVue software.

2.6.3 Proximity ligation assay (PLA)

The PLA assay uses the Duolink ®II Fluorescence assay kit (Olink Bioscience, Sweden), however, the protocol has been optimised. The following buffers were prepared and vacuum filtered through a 0.25 µm filter: 1X Buffer A (0.01 M Tris / 0.15 M NaCl/ 0.05% Tween-20 (pH 7.4)) and 1X Buffer B (0.2 M Tris /0.1M NaCl). Primary antibodies were washed from the coverslips by transferring them sequentially through 6 200 mL beakers of 1X Buffer A, unless otherwise stated this wash procedure was followed. The PLA anti-rabbit and PLA anti-mouse probes were prepared by diluting them together (1/5) in Duolink II antibody diluent. In a humidity chamber, 20 µL of the PLA probe solution was aliquoted onto para-film and coverslips were placed face down onto the solution. The coverslips were incubated for 90 minutes at 37°C. The ligation solution was prepared on ice by diluting the 5X ligation stock to 1X in Milli-Q water. Per reaction, 19.5 µL of 1X ligation stock was combined with 0.5 µL of ligase solution. Coverslips were washed in Buffer A then 20 µL of the ligation solution was aliquoted onto para-film in the humidity chamber. Coverslips were placed face down onto the ligation solution and incubated for 1 hour at 37°C. From this point onwards the samples were protected from light. The amplification solution was prepared on ice by diluting the 5X amplification stock to 1X in Milli-Q water. Per reaction 19.75 µL of 1X amplification stock was combined with 0.25 µL of polymerase solution. Coverslips were washed in Buffer A and 20 µL of the amplification solution was aliquoted onto para-film. Coverslips were placed face down onto the amplification solution and incubated for 2 hours at 37°C in the humidity chamber. The coverslips were washed by transferring them through 6 200 mL beaker of 1X Buffer B and two 200 mL beakers of 0.01X Buffer B. The coverslips were placed face up, protected from light and allowed to completely dry. Coverslips were then mounted onto glass slides using 10 µL ProLong® Gold with DAPI (Invitrogen, UK) and sealed using nail varnish. Images were collected on a widefield

microscope (Leica DM RXA) using a 20x or 40x objective and captured using a Coolsnap EZ camera driven by MetaVue software.

2.6.4 Image analysis

For the co-localisation analysis the co-localisation colour map macro on image J was implemented. This analysis determines correlation of intensities between pairs of individual pixels with the same spacial co-ordinates (Jaskolski et al., 2005). This value is then used to generate a correlation index (Icorr*)* which quantifies the fraction of positively correlated pixels in a field of view and, as reported (Apostolova et al., 2011; Lo Buono et al., 2011) quantifies the degree of co-localisation. One advantage of this analysis is that it avoids setting a manual image threshold which can introduce bias. This colour map analysis was also reported to accurately differentiate subtle changes in co-localisation which other analysis methods such as the Pearson r index could not detect.

For the analysis of the PLA images the BlobFinder V3.2 software (Centre for Image Analysis, Uppsula University)(Allalou and Wählby, 2009) was used. The average count function on the software was used to quantify the number of fluorescent signals and nuclei in each image. The number of PLA signals/ cell was determined through dividing the number of nuclei by the total number of PLA signals in a field of view. For each sample, images were taken at 20x magnification in triplicate to encompass the widest field of view and ensure images were representative of the sample. At least two experimental repeats were performed.

2.7 Cloning, expression and binding analysis of the NRP-1 b domains

2.7.1 RNA isolation

CALU-6 NSCLC cells were cultured as described (Section 2.0) and had been sub-cultured into a 25 cm^2 tissue culture flask (Corning, Costar, UK). Culture media was aspirated from cells and residual media was removed through washing the cell mono-layer with PBS before RNA was isolated using TRIzol® reagent (Invitrogen). Briefly, 1 mL of TRIzol® was added to the flask and cells were left at room temperature under gentle agitation for 5 minutes. Flasks were vortexed and TRIzol®, containing the lysed cell material, was pipetted into a 1.7 mL eppendorf. To the eppendorf, 200 µL of chloroform (VWR International) was added before tubes were vortexed for 30 seconds and then incubated for 3 minutes at room temperature. To allow phase-separation, the solution was centrifuged at 4°C for 15 minutes at 12,000 rpm. The upper aqueous phase, containing the RNA, was carefully pipetted into a fresh 1.7 mL eppendorf. RNA was precipitated through adding 0.5 mL of isopropanol (Fisher Scientific) and incubating samples for 15 minutes on

ice. The precipitated RNA was pelleted through centrifuging samples at 4°C for 15 minutes at 12,000 rpm. The supernatant was discarded and the RNA pellet was washed (X2) in 75% (v/v) ethanol (Fisher Scientific) and then centrifuged at 4°C for 5 minutes at 7500 rpm. The ethanol was completely removed and the RNA pellet was allowed to air dry before being re-suspended in 50 µL diethyl dicarbonate (DEPC) treated water (Invitrogen). RNA concentration and purity was quantified using the NanoDrop ND 1000 spectrophotometer (NanoDrop Products).

2.7.2 Reverse transcription (RT)

On ice, using thin-wall PCR tubes, CALU-6 RNA was diluted in Milli-Q water to a concentration of 1 µg and mixed with 1 µL of oligo DT primer (Promega). To anneal the RNA and oligo DT, the mixture was incubated at 65°C for 10 minutes. The following reagents were then added: 4 µL 5X RT buffer, 2 µL 100 mM DTT, 2 µL 10 mM dNTP (Promega) before adding 0.5 µL of AMV reverse transcriptase and 0.5 µL RNAse inhibitor (Roche Diagnostics). The final volume was adjusted to 20 µL using Milli-Q water and RT was initiated through incubating samples in a GeneAmp PCR system thermocycler 2700 (Applied Biosystems) for 10 minutes at 30°C, then 90 minutes at 42°C.

2.7.3 Polymerase chain reaction

Primer mixes containing equal volumes of 100 µM forward (GAGGATCCACCGGTTGTATGGAA GCTCTGGGCATG) and reverse (GCCTCGAGTTAATTAATCAACAGCCCAGCAGCTCC) NRP-1 b domain primers were prepared (oligonucleotides were ordered from Eurofins MWG Operon). Within the primer sequences, the following restriction sites are highlighted: Bam HI (blue), Age I (red), Xho I (green) and Pac I (purple). From the RT reaction, 5 µL of cDNA was added to a fresh thin wall PCR tube and the following reagents were added: 1 µL dNTP (Roche Diagnostics), 0.5 µL pfu Ultra II Fusion HS DNA polymerase, 2 µL 10X PCR buffer (Stratagene) and 1 µL of the primer mix. The volume was adjusted to 20 µL using Milli-Q water before reactions were incubated for 2 minutes at 94°C, followed by 25 cycles of: 30 seconds at 94°C, 30 seconds at 55°C and 1 minute at 72°C. This was followed by a final incubation at 72°C for 7 minutes.

To prepare the PCR product for ligation into the pCR2.1-TOPO 2.1 vector, an adenine extension was added to the 3' end of the product. To do this, 1 µL of Taq DNA polymerase and 1 µL of polymerase buffer (New England Biolabs) were added to the PCR reaction and reactions were incubated at 72°C for 20 minutes. All PCR reactions were performed using the GeneAmp PCR system thermocycler 2700.

2.7.4 Ligation of the NRP-1 b domains into the pCR2.1-TOPO 2.1 vector

The PCR product was resolved on 1% (w/v) ultra-pure agarose gel (Invitrogen) along with a molecular weight marker, Hyperladder I, which detects products in the range of 200-10037 base pairs (Bioline). The gel was run in 1X TAE buffer (40 mM Tris-acetate/1 mM EDTA, pH 8) for 1 hour at 100 V. Gels were immersed in 100 mL 1X TAE buffer containing 1 µL of Gel Red™ (Biotium) nucleic acid stain for 1 hour. The products were visualised using an ultraviolet trans-illuminator and the 924 base pair product corresponding to the NRP-1 b domains was excised using a scalpel. The DNA was extracted from the agarose using the QIAX II gel extraction kit (Qiagen) according to the manufacturer's protocol.

Ligation mixtures consisting of, 4 µL purified PCR product, 1 µL salt solution and 1 µL pCR2.1-TOPO 2.1 vector, were incubated for 5 minutes at room temperature, before being placed on ice. This ligation step allowed the adenine extension at the 3' end of the PCR product to ligate with the complementary thymidine sequence at the 3' end of the pCR2.1-TOPO 2.1 vector.

On ice, 3 µL of the ligation mixture was added to 50 µL of XL1-Blue super-competent *E.coli* cells (Stratagene) and incubated for 30 minutes on ice. The cells were heat-shocked at 42°C for 45 seconds before being placed immediately back on ice for 2 minutes. Finally, 200 µL of pre-warmed (37°C) SOC media (Invitrogen) was added to the tubes which were then incubated at 37°C under agitation (200 revolutions/ minute) for 1 hour. During the incubation, sterile Lysogeny broth (LB) agar (Novagen, Merck Chemicals) plates, supplemented with 50 µg/mL carbenicillin, were pre-warmed to 37°C. Agar plates were then coated with 125 mM isopropyl β-D-1-thiogalactopyranoside (IPTG) and 40 mg/mL X-gal (Bioline) to allow for blue-white screening. The super-competent cell solutions were then sterility plated onto the prepared agar, inverted and incubated overnight at 37°C. White colonies indicated the presence of the pCR2.1-TOPO 2.1 vector with the b domain sequence inserted. Single colonies were picked using sterile pipette tips and incubated in pre-warmed autoclaved LB-Broth (Novagen, Merck Chemicals), supplemented with 50 µg/mL carbenicillin. Flasks containing inoculated LB-Broth were incubated overnight at 37°C with agitation (200 revolutions/ minute).

A Mini-prep kit (Qiagen) was used, according to the manufacturer's protocol, to extract the plasmid DNA from the bacterial cell suspensions. Briefly, bacterial suspensions were centrifuged at 5000 rpm and pellets were re-suspended in Buffer P1, followed by the sequential addition of Buffer P2 and Buffer P3. Samples were then centrifuged at 13,000 rpm for 10 minutes at 4°C and supernatants were transferred to QIAprep spin columns, which incorporate a silica membrane for plasmid DNA binding. To wash the plasmid DNA, Buffer PB was added to the spin column which

was centrifuged for 1 minute at 13,000rpm, the flow through was discarded and this was repeated for Buffer PE. The spin column was then transferred to a 2 mL fresh eppendorf tube and 30 µL of Buffer EB was added to the silca membrane and incubated for 2 minutes. The spin column was centrifuged at 13,000 rpm for 1 minute and the plasmid DNA was collected in the flow through. To confirm the correct size of the pCR2.1-TOPO 2.1 vector and the b domain construct, double restriction digests were performed. In a 1.7mL eppendorf tube, 1µL of Age I, 1 µL of Pac I and 2 µL of Buffer 1 (New England Biolabs) were added to 4 µL of plasmid DNA and 12 µL of Milli-Q water. Samples were incubated for 3 hours at 37°C before samples were resolved on a 1% (w/v) ultra-pure agarose gel alongside the molecular weight marker, Hyperladder I. Gels were immersed in 100 mL 1X TAE buffer containing 1 µL of Gel Red™ (Biotium) nucleic acid stain for 1 hour. The products were visualised using an ultraviolet trans-illuminator to confirm the presence of the 924 bp b domain product and the 3931 bp pCR2.1-TOPO 2.1 vector product.

A sample of the plasmid DNA was sent for DNA sequencing to confirm the fidelity of the NRP-1 b domains. Sequencing reactions were prepared in thin wall PCR tubes by adding: 1 µL BigDye, 2.5 µL BigDye buffer (BigDye Terminator v1.1 Cycle Sequencing Kit from Applied Biosystems) and 4 µL DNA. Per reaction, a single sequencing primer was added. These sequencing primers were pCR2.1-TOPO 2.1 vector primers; 1 µL M13 reverse primer or 1 µL M13 forward (-20) primer (Invitrogen); or 1 µL of the internal b domain sequencing primer (5'-TGTCCGAATCAAGC CTGCAAC-3')(Eurofins MWG Operon). Reaction volumes were adjusted to 20 µL using Milli-Q water. Samples were incubated at 96°C for 1 minute, followed by 25 cycles of: 96°C for 40 seconds, 50°C for 15 seconds, 60°C for 4 minutes; with a final 10 minute hold at 4°C. Reactions were performed using the GeneAmp PCR system thermocycler 2700. DNA was then ethanol precipitated in preparation for sequencing. The following reagents were added to the sample: 25 µL 96% ethanol (v/v), 3 µL 3M Na Acetate (pH 4.5), 1 µL GlycoBlue (Ambion), 2 µL 125 mM EDTA (pH 8.0). Samples were vortexed, incubated at room temperature for 15 minutes and then centrifuged at 13,000 rpm for 25 minutes. Supernatant was discarded and the pellet was washed in 100 µL of 70% (v/v) ethanol. Samples were centrifuged for 5 minutes at 13,000 rpm and the 70% ethanol wash was repeated. Ethanol was removed and DNA pellets were allowed to air dry before being submitted to the in house sequencing facility.

2.7.5 Ligation of the NRP-1 b domains into the PQCXIP-V5-His expression vector

Using, the b domain: pCR2.1-TOPO 2.1 DNA construct and the PQCXIP v5 His vector, double restriction digests were performed, as described (Section 2.8.4). The products were visualised using an ultraviolet trans-illuminator and the bands corresponding to the 924 bp NRP-1 b-domains

or the 7312 bp PQCXIP V5 His vector were excised. The DNA was extracted from the agarose using the QIAX II gel extraction kit (Qiagen).

Ligation reactions with either a 1:1 or 3:1 vector: insert DNA ratio were prepared in thin wall PCR tubes. Per reaction: 1 µL DNA T4 Ligase and 2 µL DNA T4 Ligase buffer (New England Biolabs) was added and reaction volumes were adjusted to 10 µL using Milli-Q water. Samples were incubated overnight at 17°C in the GeneAmp PCR system thermocycler 2700. On ice, 5 µL of the ligation mixture was added to 50 µL of XL1-Blue super-competent *E.coli* cells and incubated for 30 minutes on ice. The cells were heat shocked at 42°C for 45 seconds before being placed immediately back on ice for 2 minutes. Finally, 200 µL of pre-warmed SOC media was added to the tubes which were then incubated at 37°C under agitation (200 revolutions/ minute) for 1 hour. During the incubation, sterile LB agar plates supplemented with 50 µg/mL carbenicillin were pre-warmed to 37°C. The super-competent cell solutions were then sterility plated onto the prepared agar, inverted and incubated overnight at 37°C. The subsequent: expansion of single clones, Mini-Prep and DNA sequencing are as described for pCR2.1-TOPO 2.1 (Section 2.8.4).

2.7.6 Expression of the NRP-1 b domains in HEK-293-EBNA mammalian cells

Initially the PQCXIP: b domain construct was transfected into the packaging cell line, HEK-293-T. HEK-293-T cells were cultured in in a humidified atmosphere of 37°C/5% CO_2 using DMEM culture media supplemented with 10% (v/v) FBS and 1% (v/v) L-glutamine. HEK-293-T cells were harvested by trypsinisation and $1x10^6$ cells were seeded and allowed to adhere overnight in a 6-well tissue culture plate (Corning, Costar). To precipitate the vectors, 5 µg of the retroviral packaging components, pVPack–GP and pVSV-G (Stratagene) together with 5 µg of the PQCXIP: b domain construct were mixed. To this reaction, 1 mL of 70% (v/v) ethanol was added, followed by 100 µL of 3 M sodium acetate. The solution was inverted to mix and then incubated at -80°C for 30-60 minutes. The sample was centrifuged at 4°C, 12,000 rpm for 10 minutes and the supernatant was discarded. The pellet was washed in 70% (v/v) ethanol and then centrifuged at 4°C 12,000 rpm for 5 minutes. The excess ethanol was removed and the pellet was stored overnight at 4°C.

The following day, the HEK-293-T media was replenished and the transfection reagents were prepared for calcium phosphate transfection. The precipitated DNA pellet was resuspended in 15 µL of TE buffer (10 mM Tris-HCl/1 mM EDTA) (pH 8.0) to give a total DNA concentration of 1 mg/mL. The DNA was mixed with 37 µL of 2 M calcium chloride and the volume was made up to 300 µL using sterile Milli-Q water. To a separate 15 mL falcon tube, 300 µL of 2X Hepes buffered saline (HBS)(12 mM Dextrose/50 mM HEPES/ 50 mM potassium chloride (KCl)/ 280 mM NaCl/ 1.5 mM sodium hydrogen phosphate dihydrate ($Na_2HPO_4 \bullet 2H_2O$)) was added. Whilst the HBS solution

was vortexed, the DNA solution was added drop-wise to the 2X HBS and this was followed by 30 minutes incubation at room temperature. The DNA: HBS solution was then added drop-wise to the HEK-293-T cells followed by 25 µL of 25 mM chloroquine (Sigma-Aldrich). Chloroquine stabilises cell lysosomes and increases the fraction of DNA reaching the cell nucleus during transfection (Gavrilescu and Van Etten, 2007). Cells were incubated at 37°C/5% CO_2 for 5 hours before the culture media was replenished.

The following day $5x10^4$ HEK-293 EBNA cells were seeded in a 6-well tissue culture plate (Corning, Costar) in DMEM culture media (Sigma-Aldrich) supplemented 10% (v/v) FBS and 1% (v/v) L-glutamine and 1% penicillin-streptomycin solution (Invitrogen) and left to adhere overnight. The next day, viral media was aspirated from the HEK-293-T cells and sterile filtered through a 0.45 µm HV PVDF filter (Millipore) to remove any cells. The media was then used to transduce HEK-293-EBNA cells and 8 µg/mL of polybrene (Sigma Aldrich) was added to promote transduction, by neutralising the charge repulsion between sialic acid on the cell surface and the virions. The transduction protocol was repeated the following day. Finally the HEK-293-EBNA cells were expanded and the DMEM culture media was supplemented with 2 µg/mL puromycin (Invitrogen) to select transduced cells. Non-transduced cells were allowed to die back before the HEK-293-EBNA cells were expanded into four triple layer tissue culture vented flasks (Corning, Costar), each containing 100 mL of DMEM. When the cells reached confluence, cell media was collected and then replenished every 3-4 days until the cells began to die. Collected media was centrifuged at 5000 rpm for 5 minutes and the supernatant was retained and supplemented with 0.04% (v/v) protease inhibitor cocktail P8340 (Sigma-Aldrich). The supernatant was stored at -80°C until required.

2.7.7 Purification and characterisation of the NRP-1 b domains

The collected supernatant containing the NRP-1 b domains removed from the -80°C freezer and thawed at room temperature. A 500 mL solution containing 200 mM sodium bicarbonate and 2 mM EDTA (diluted in Milli-Q water) was used to boil dialysis tubing for 10 minutes. The supernatant was then added to the dialysis tubing and dialysed overnight at 4°C against a gradient of: 20 mM Tris/400 mM NaCl/10 mM imidazole (pH 8.0). The dialysed supernatant was then filtered through a 0.45µm (Pall Corporation) vacuum filter (to remove debris and de-gas the media) and stored on ice. A His-Trap FF column (GE Healthcare) attached to an AKTA purifier (GE Healthcare) was charged with $NiSO_4$ and then equilibrated with: 20 mM Tris/400 mM NaCl/10 mM imidazole (pH 8.0). The dialysed supernatant was passed through the His-Trap FF column. The bound His-tagged fraction of the supernatant was eluted off the His-Trap column with: 20 mM Tris/ 400 mM NaCl and 400 mM imidazole. The fractions were resolved by SDS-PAGE using a 4-12%

polyacrylamide gel (Expedeon) at 150 V for 1 hour. The gel was stained with Instant Blue stain (Expedeon) to confirm the products corresponded to the theoretical size of the NRP-1 b domains with a molecular weight of 37 kDa.

The fractions containing the b domains were pooled and further purified using the sepharose S200 size exclusion column (GE Healthcare) attached to an AKTA purifier (GE Healthcare UK). Briefly, the column was equilibrated using HBS (10 mM HEPES, 150 mM NaCl) (pH 7.4) which had been filtered through a 0.45 µm vacuum filter (Pall Corporation) and de-gassed. The pooled supernatant was concentrated to a 500 µL volume using a VIVASPIN column (Sartorius Stedim Ltd) and injected onto the S200 column. The protein fractions were eluted through passing HBS through the column. Again, fractions were resolved by SDS-PAGE using a 4-12% polyacrylamide gel (Expedeon) at 150 V for 1 hour. The gel was stained with Instant Blue (Expedeon) stain to confirm the products corresponded to the theoretical size of the NRP-1 b domains with a molecular weight of 37 kDa. To confirm the identity/ purity of the NRP-1 b domains, the Instant Blue stained gel was submitted to the in house mass spectrometry facility for analysis.

2.7.8 Surface plasmon resonance: BIAcore analysis

The BIAcore 3000 and control software (GE Healthcare) were used for binding analysis of the NRP-1 b domains. A carboxymethyldextran, CM5 sensor chip, was equilibrated HBS-T (10 mM Hepes/ 150 mM NaCl, 0.005% Tween-20) (pH 7.4) which had been filtered and de-gassed. To determine the optimal pH for protein immobilisation onto the CM5 chip, a pH scout was performed. Briefly, 50 mM sodium acetate solutions (pH: 2, 3, 4 and 5.5) or HBS-T were used to prepare a 3 µg/mL dilution of the b domains. Samples were injected over the surface of the CM5 chip for 2 minutes at 20 µL/ minute and response units were recorded. For immobilisation, the surface of the CM5 chip was first activated using 120 µL 0.1 M 1-ethyl-3-(3-dimethylaminopropyl) carbodimide hydrochloride (EDC) (GE Healthcare) and 120 µL 0.4 M N-hydroxysuccinimide (NHS) (GE Healthcare). Using the pre-determined optimal pH 5.5 sodium acetate solution, 3µg/mL of the b domains were injected at 12 µL/minute for 12 minutes over the surface of the CM5 chip and the reaction was quenched using ethanolomine-HCl (pH 8.5). A paired control cell on the chip was treated in the same way, with the omission of the NRP-1 b domain protein.

Analytes: PDGF-AA, PDGF-BB, PDGF-CC, PDGF-AB (all R&D Systems), VEGF-A_{165} and VEGF-A_{121} (recombinantly expressed in the group by Maybo Chiu) were all diluted in HBS-T to a concentration of 25 nM. Diluted analytes were injected over the CM5 chip at a rate of 20 µL/ minute for 3 minutes. In between different analytes, a solution of 0.8M NaCl: HBS was used to dissociate

bound analytes followed by a 5 minute injection of HBS-T to regenerate the binding surface. For kinetic analysis of VEGF-A_{165} and VEGF-A_{121} a range of analyte concentrations from 0-200 nM were prepared in HBS-T, whereas for PDGF-BB and PDGF-AB the concentration range was 0-100 nM. Analytes were injected over the surface of the CM5 chip at a 30 µL/minute for 3 minutes, followed by regeneration of the chips surface (as described for the analyte scan). The analyte response in the control cell was treated as non-specific background and was subtracted from the analyte response in the cell containing the immobilised NRP-1 b domains.

Antibody/Clone	Specificity	Reactivity	Application	Supplier
446921	Mouse anti-human	Neuropilin-1	FC	R&D Systems (FAB3870P)
D62C6	Rabbit-anti human	Neuropilin-1	IB/IP	Cell signalling technology (#3725)
polyclonal	Rabbit-anti human	Neuropilin-1	IF	Santa Cruz Biotechnology (sc-5541)
446915	Mouse anti-human	Neuropilin-1	IF	R&D Systems (MAB-38701)
D13C6	Rabbit-anti human	PDGFR-α	IB	Cell signalling technology (#5241)
polyclonal	Rabbit-anti human	PDGFR-α	IF	Santa Cruz Biotechnology (sc-338)
16A1	Mouse anti-human	PDGFR-α	IF	Santa Cruz Biotechnology (sc-21789)
polyclonal	Rabbit-anti human	PDGFR-α	IF	Cell signalling technology (#3164)
35248	Mouse anti-human	PDGFR-α	IF	R&D Systems (MAB-322)
	Mouse anti-human	PDGFR-α	Pathscan® ELISA	Cell Signaling Technology (#7317)
	Rabbit-anti human	pPDGFR-α (Tyr-849)	Pathscan® ELISA	Cell Signaling Technology (#7317)
2B3	Mouse anti-human	PDGFR-β	IF	Cell signalling technology (#3175)
polyclonal	Rabbit-anti human	PDGFR-β	IF	Santa Cruz Biotechnology (sc-339)
28E1	Rabbit-anti human	PDGFR-β	IF	Cell signalling technology (#3169)
	Mouse anti-human	pPDGFR-β	Duoset® ELISA	R&D Systems (Part:841422)
	Mouse anti-human	pPDGFR-β	Duoset® ELISA	R&D Systems (Part:841422)
polyclonal	Rabbit-anti human	pERK1/2 (Tyr-202/ Tyr-204)	IB	Santa Cruz Biotechnology (sc-16982-R)
193H12	Rabbit-anti human	p-Akt (Serine-473)	IB	Cell Signaling Technology (#4058)
AF321	Goat anti-human	VEGFR-1	IB	R&D Systems (AF321)
55B11	Mouse anti human	VEGFR-2	IB	Cell Signalling Technology (#2479)
polyclonal	Rabbit-anti human	p-PLCγ-1 (Tyr-783)	IB	Cell Signaling Technology (#2821)
C43E9	Rabbit-anti human	pPDGFR-α (Tyr-849)/ pPDGFR-β (Tyr-857)	IB	Cell Signaling Technology (#3170)
AC-15	Mouse anti-human	B-Actin	IB	Sigma Aldrich (A1978)

Table 2.0: Primary antibodies

The table details the primary antibodies used during the project. The application in which the antibodies were used is highlighted in the fourth column (IB=immunoblot/ IP=immunoprecipitation/ FC=flow cytometry /IF=immunofluorescence/ Duoset® ELISA / Pathscan® ELISA).

HRP-conjugated	Goat anti-mouse	Secondary label	IB	Dako (P0447)
HRP-conjugated	Goat anti-rabbit	Secondary label	IB	Dako (P0448)
HRP-conjugated	Rabbit anti-goat	Secondary label	IB	Dako (P0449)
Alexa Fluor 488	Donkey anti-mouse	Secondary label	IF	Invitrogen (A-21202)
Alexa Fluor 594	Donkey anti-rabbit	Secondary label	IF	Invitrogen (A-21207)
	Rabbit-IgG	Negative control	IP	Dako (X0903)
HRP linked	Anti-mouse IgG	Secondary label	Pathscan® ELISA	Cell Signaling Technology (#7317)
HRP linked	Anti-mouse	Secondary label	Duoset® ELISA	R&D Systems (Part:841403)

Table 2.1: Secondary antibodies and negative controls
The table details the secondary and negative control antibodies used during the project. The application in which the antibodies were used is highlighted in the fourth column (IB=immunoblot/ IP=immunoprecipitation/ FC=flow cytometry /IF=immunofluorescence/ Duoset® ELISA / Pathscan® ELISA).

Chapter 3 – Results

Identification of tumour cell lines to study NRP-1/PDGFR crosstalk

3.0 Introduction

The expression of NRP-1 has been documented in many types of primary tumours and cancer cell lines. Pellet-Many et al (2008) reported the expression of both NRP-1 and NRP-2 in a number of tumour cells including lung, breast, kidney and ovarian cells illustrating that NRP expression in cancer is not localised to a small number of tissues (Pellet-Many et al., 2008). In cancer, NRP-1 has been identified as a potential biomarker for tumour progression and NRP-1 can affect tumour angiogenesis, metastasis and growth by mediating the signalling effects of the VEGF and SEMA family members (Neufeld, 2002).

The complement of cell surface receptors is likely to be a critical factor in determining the specific molecular interaction involving NRP-1 in cancer cells. It is well established that NRP-1 interacts with VEGF to facilitate VEGFR activation (Fuh et al., 2000; Soker et al., 2002). However NRP-1 also regulates the activity of other RTKs including; c-Met (Hu et al., 2007), PDGFR (Ball et al., 2010; Cao et al., 2010; Pellet-Many et al., 2011) and interacts with growth factors including; TGF-β (Cao et al., 2010) and FGF (West et al., 2005). In cancer, RTKs are involved in activating intracellular signalling pathways and thus, directing tumour cell behaviour (Bennasroune et al., 2004; Xu and Huang, 2010). Whether NRP-1 preferentially controls the activation of particular RTKs may be controlled by the relative expression of each receptor, the cell type and the culture conditions.

An initial aim of the project was to identify tumour cell models, expressing both NRP-1 and PDGFRs, to investigate NRP-1/PDGFR crosstalk in cancer. Using a cell line database (AstraZeneca), gene expression of NRP-1 and/or PDGFR was identified in a panel of epithelial and mesenchymal tumour cell lines. These cells were than assayed to determine the relative protein expression of NRP-1 and PDGFR-α. PDGFR-α was the initial focus, as the literature had suggested that the α subunit of PDGFR may be of greater importance in the crosstalk with NRP-1 (Ball et al., 2010; Pellet-Many et al., 2011).

3.1 The expression of PDGFRs and NRP-1 in epithelial cancer cell lines

3.1.1 Colon cancer cell lines

A panel of four colon adenocarcinoma cell lines were selected (Table 3.0). HCT116 cells were isolated together with HCT116a and HCT116b from a colon carcinoma. HCT116 cells were more abundant in the tumour (than HCT116a or HCT116b) and showed intermediate tumourigenic potential in athymic nude mice (Brattain et al., 1981). SW620 cells were isolated together with SW480 cells from the same patient, with SW620 cells isolated from the patient's lymph node and classified as a metastasis from the primary adenocarcinoma. Compared to the SW480 cells, SW620, were more de-differentiated and SW620 cells were tumourigenic in athymic nude mice (Leibovitz et al., 1976). LoVo cells were isolated from a metastatic nodule from a patient with colorectal adenocarcinoma. LoVo cells were reported to retain *in vivo* histological and physiological characteristics of colon cancer, such as, acinar structures and the secretion of carcinoembryonic antigen (Drewinko et al., 1976). The semi-adherent, COLO-205 cells were isolated from an ascites fluid specimen from a patient with colorectal adenocarcinoma (Semple et al., 1978).

Cell Line	Tumour/Histology	Growth/Morphology	Isolated from/ date	ATCC number/Reference
HCT116	Colorectal/ adenocarcinoma	adherent/ epithelial	Primary tumour/ 1981	(ATCC:CCL-247™) (Brattain et al., 1981)
LoVo	Colorectal/ adenocarcinoma	adherent/ epithelial	Metastasis/ 1976	(ATCC: CCL-229™) (Drewinko et al., 1976)
SW620	Colorectal/ adenocarcinoma	adherent/ epithelial	Metastasis/ 1976	(ATCC: CCL-227™**)** (Leibovitz et al., 1976)
COLO-205	Colorectal/ adenocarcinoma	mixed, adherent & suspension	Primary tumour ascites fluid/ 1978	(ATCC: CCL-222™) (Semple et al., 1978)

Table 3.0: The table details the colon cancer cell lines selected for characterisation
Four colon cell lines were selected to characterise the expression of NRP-1 and PDGFRs. The cell lines had been isolated from primary tumours and metastasis. The table includes the specific ATCC numbers/cell line and the references detail the isolation and establishment of the different cell lines.

In colon cancer NRP-1 is documented to be highly expressed (Parikh et al., 2004) and correlated to the grade and progression of the tumour (Hansel et al., 2004). The expression of PDGFR has also been documented in colon cancer in tumour-associated stromal cells (Kitadai et al., 2006) and in patient biopsies (Craven et al., 1995; Erben et al., 2008; Wehler et al., 2008). PDGFR has also been recorded in colorectal tumour cell lines (Wehler et al., 2008) however, the expression appears to be highly variable across different cell lines.

When grown under standard culture conditions, HCT116, LoVo, and SW620 cells were fully adherent and formed monolayers with clear cell-to-cell adherence. COLO-205 cells displayed a rounded morphology and were semi-adherent (Appendix, Figure 8.0.). Flow cytometry analysis revealed that LoVo and COLO-205 cell lines expressed very low levels of NRP-1 but NRP-1 could not be detected in the HCT116 or SW620 cell lines (Appendix, Figure 8.1). PDGFR-α expression could not be detected in any of the colon cancer cells (Appendix, Figure 8.2). Consequently, these cell lines were discounted to study the NRP-1/PDGFR crosstalk and were not analysed further.

3.1.2 Lung cancer cell lines

A panel of lung cancer cells were selected, which included eight non-small cell lung cancer (NSCLC) cell lines with varied histological classifications (Table 3.1). A549 cells were isolated from a patient with lung alveolar carcinoma (Giard et al., 1973; Lieber et al., 1976). CALU-6 were isolated in 1975 and form poorly differentiated tumours in nude, athymic mice (Fogh et al., 1977; Fogh, 1978). The poor differentiation of CALU-6 cells may account for the discrepancies in published data, with contrary studies describing them as large cell (Brower et al., 1986; Yamada et al., 2008) or epidermoid NSCLC (Giovannetti et al., 2005). H1299 cells were isolated from the lymph node of a patient (ATCC CRL-5803™) and have large cell carcinoma histology (Giaccone et al., 1992), as do H460 cells. The remainder of the adenocarcinoma cells included; H23, H1703 and H1793.

Cell Line	Tumour/Histology	Growth/ Morphology	Isolated from/ date	ATCC number/Reference
A549	NSCLC/ adenocarcinoma	adherent/ epithelial	Primary tumour /1972	(ATCC:CCL-185™)/ (Giard et al., 1973)
CALU-6	NSCLC/ epidermoid carcinoma (or) large cell carcinoma	adherent/ epithelial	Lung/ 1977	(ATCC: HTB-56™)/ (Fogh et al., 1977; Fogh, 1978; Wright et al., 1981)
H1299	NSCLC/ large cell carcinoma	adherent/ epithelial	Lymph node Metastasis	(ATCC:CRL-5803™)/ (Giaccone et al., 1992)
H23	NSCLC/adenocarcinoma	adherent/ epithelial	Primary lung tumour/1976	(ATCC: CRL-5800™)/ (Brower et al., 1986; Gazdar et al., 1980)
H1703	NSCLC/ squamous cell carcinoma	adherent/ epithelial	Primary lung tumour/1986	(ATCC:CRL-5889™)
H1793	NSCLC/adenocarcinoma	adherent/ epithelial	Primary lung tumour/1987	(ATCC:CRL-5896™)
H522	NSCLC/ adenocarcinoma	adherent/ epithelial	Primary lung tumour/1985	(ATCC:CRL-5810™) (Banks-Schlegel et al., 1985)
H460	NSCLC/ large cell carcinoma	adherent/ epithelial	pleural fluid, pericardial fluid/1982	(ATCC: HTB-177™) (Brower et al., 1986)

Table 3.1: The table details the NSCLC cell lines selected for characterisation
Eight lung NSCLC cell lines were selected to characterise the expression of NRP-1 and PDGFRs. The cell lines had been isolated from primary tumours and metastasis and had varying histological classifications. The table includes the specific ATCC number per cell line and references (where possible) detail the isolation and establishment of the lung cancer cell lines.

In lung cancer, NRP-1 has been shown to contribute to the invasion, migration and metastasis of tumour cells (Hong et al., 2007a) and NRP-1 expression has been documented in both NSCLC cell lines (Castro-Rivera et al., 2008; Tomizawa et al., 2001) and patient samples (Hong et al., 2007a; Kawakami et al., 2002). PDGFR expression has been negatively correlated to patient survival in NSCLC (Kawai et al., 1997) and PDGFR expression has been documented in NSCLC patient samples, the surrounding tumour stroma (Donnem et al., 2008) and NSCLC cell lines (Thomson et al., 2008). Thus, several studies have now examined PDGFRs as a therapeutic target in NSCLC (Bauman et al., 2007; Reinmuth et al., 2009; Vlahovic et al., 2006).

All of the selected NSCLC cell lines were fully-adherent when cultured under standard conditions on tissue culture plastic and cell lines with the same histological classification did not always display similar morphology. The H460 cells displayed the most rounded morphology with visible cell-cell junctions, characteristic of an epithelial cell phenotype. The A549 and H1299 cells were larger and less rounded but still displayed clear cell-cell adherence whereas, the H23, H522 and H1299 cells showed a less ordered pattern of growth with less cell-cell adherence. The H1703, H1793 and CALU-6 cells were larger with a more spindle like morphology (Appendix, Figure 8.3).One of the factors which may reflect the variation in cell morphology is the degree to which these cells have undergone the epithelial-to-mesenchymal transition (EMT), which has been documented in lung tumours (Mendez et al., 2010; Xiao and He, 2011). EMT is characterised by an increased expression of mesenchymal markers such as, vimentin and down-regulation of epithelial markers such as, E-cadherin. Subsequently, cells acquire a spindle-like mesenchymal morphology and EMT has been associated with an invasive phenotype and drug resistance in NSCLC (Thomson et al., 2008; Xiao and He, 2011).

Flow cytometry was used to determine the cell surface expression of NRP-1 (Appendix, Figure 8.4) and PDGFR-α (Appendix, Figure 8.5) in the NSCLC cell lines. Out of the selected cell lines, CALU-6, A549 and H1793 cells, expressed the highest levels of NRP-1. Relative to these cell lines, H460 expressed low levels of NRP-1 and the remainder of the cell lines were negative for NRP-1. PDGFR-α expression could be detected in CALU-6, A549 and H1299 cells. In the rest of the NSCLC cell lines PDGFR-α was not detected and these cells were discounted from the study. H1299 cells were discounted as they lacked the expression of NRP-1.

3.2 The expression of PDGFRs and NRP-1 in mesenchymal cancer cell lines

3.2.1 Osteosarcoma cell lines

Three osteosarcoma cell lines were selected (Table 3.2). KHOS-240S closely resemble the parental, non-transformed human osteosarcoma (HOS) cell line. HOS cells were transformed by Kirsten murine sarcoma virus to generate the KHOS cell line (Rhim et al., 1975). KHOS-240S cells are revertant sub-clones of the KHOS cells, which have lost the viral DNA and reverted back to a phenotype resembling HOS cells which are non-tumourigenic in athymic nude mice (Cho et al., 1976; McAllister et al., 1971; Yang et al., 1979). MG63 cells were isolated and propagated from a primary tumour in 1975. MG63 have fibroblast morphology and can be induced to secrete high levels of interferon (Billiau et al., 1977, 1975). Sarcoma osteogenic (Saos-2) cells are a non-transformed cell line isolated by Fogh et al (1972) from a primary osteosarcoma (Fogh et al., 1977). Saos-2 cells display many features of osteoblasts and can be fully differentiated along the same lineage as osteoblasts. Saos-2 cells are tumourigenic in athymic nude mice (Hausser and Brenner, 2005; Rodan et al., 1987).

Cell Line	Tumour	Growth /morphology	Isolated from/date	ATCC number/ Reference
KHOS-240S	osteosarcoma	Adherent /fibroblast	Femur primary tumour/1971	(ATCC: CRL-1545™) (Cho et al., 1976; McAllister et al., 1971; Rhim et al., 1975; Yang et al., 1979)
MG63	osteosarcoma	Adherent /fibroblast	Primary tumour/1975	(ATCC: CRL-1427™) (Billiau et al., 1977, 1975)
Saos-2	osteosarcoma	Adherent /epithelial	Primary tumour/1972	(ATCC: HTB-85™) (Fogh et al., 1977; Hausser and Brenner, 2005; Rodan et al., 1987)

Table 3.2: The table details the osteosarcoma cell lines selected for characterisation
Three osteosarcoma cell lines were selected to characterise the expression of NRP-1 and PDGFRs. The cell lines had been isolated from primary tumours and the table details the ATCC morphological classification of cells. The table includes the specific ATCC number per cell line and references (where possible) detail the isolation and establishment of the different cell lines.

PDGFRs are documented to be expressed in osteosarcoma. Kubo et al (2008) described PDGFR-α and/or β expression in over 79% of tumours tested and co- expression of PDGFR-α and PDGF-AA significantly worsened disease-free survival (Hassan et al., 2012; Kubo et al., 2008; Raica and Cimpean, 2010). More research has focused on NRP-2 (Handa et al., 2000), rather than NRP-1, in osteosarcoma, however Saos-2 cells are reported to express both NRP-1 and NRP-2 transcripts (Mayr-Wohlfart et al., 2002).

When cultured under standard conditions (see Section 2.0), all the osteosarcoma cell lines were fully adherent and formed monolayers. KHOS-240S and MG63 cells displayed similar fibroblast-type morphology (Figure 3.0). The Saos-2 are characterised (by ATCC) as having an epithelial morphology however the cells appear larger than epithelial cells with a more spindle like morphology (Figure 3.0). This may be accounted for by the observations that Saos-2 cells have many features of osteoblasts (Hausser and Brenner, 2005; Rodan et al., 1987) and therefore, Saos-2 may also have a degree of fibroblastic-morphology which is characteristic of osteoblasts.

Flow cytometry analysis determined that NRP-1 was detected in all of osteosarcoma cell lines, with KHOS-240S cells expressing the highest level of NRP-1 (Figure 3.1). All of the osteosarcoma cells also expressed PDGFR-α (Figure 3.1), which would be anticipated due to the mesenchymal origin of these cell lines (Hassan et al., 2012)

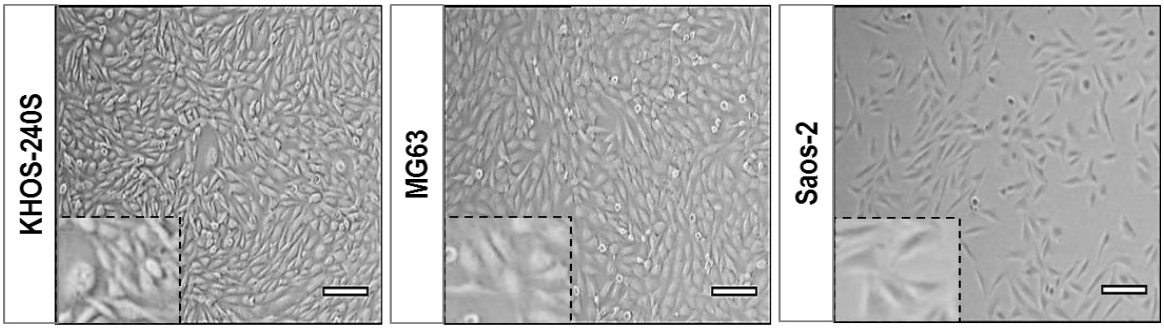

Figure 3.0: The morphology of the selected osteosarcoma cancer cell lines
Osteosarcoma cell lines were cultured under standard conditions (Chapter 2, 2.0). Images were collected using a phase-contrast microscope (Olympus CK X41) set at 10x magnification. Enlarged cell images are illustrated in the bottom left corner of each image outlined by the dashed line (- - -). In the bottom right corner of each image Scale bar=100 µm. Directly below the osteosarcoma cell images, images of human dermal fibroblasts and human periodontal ligament fibroblasts are illustrated at x20 magnification (images sourced from ScienCell™). It is clear to see that human dermal fibroblasts are much larger than human periodontal ligament fibroblasts and that the osteosarcoma cell lines more closely resemble the fibroblast phenotype of the human periodontal ligament fibroblasts.

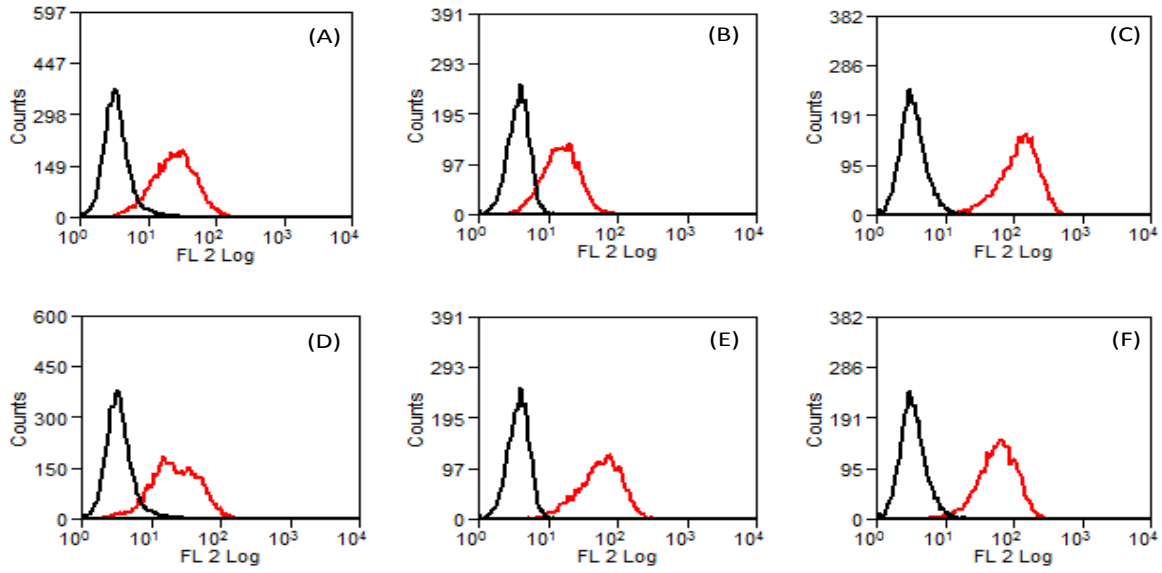

Figure 3.1: Cell surface expression of NRP-1 and PDGFR-α in the osteosarcoma cell lines
Osteosarcoma cell lines were cultured under standard conditions and the expression of NRP-1 and PDGFR-α was determined by single colour flow cytometry. Analysis of **(A)** Saos-2; **(B)** MG63; **(C)** KHOS-240S cell lines was performed using anti-human polyclonal PDGFR-α Ab or a specific IgG control antibody (Chapter 2, Table 2.0). Analysis of **(D)** Saos-2; (**E)** MG63; **(F)** KHOS-240S cell lines was performed using anti-human NRP-1 mAb or a specific IgG control (Chapter 2,Table 2.1). In each histogram, the fluorescent peak for PDGFR-α (red) has been superimposed onto the peak for the isotype-matched IgG control (black).

3.2.2 Glioma cell lines

Gliomas were the second mesenchymal tumour-type selected to characterise the expression of NRP-1 and PDGFRs. Seven glioma cell lines were selected for this analysis (Table 3.3). The T98G glioblastoma multiform cell line, derives from T98 cells which were isolated from the primary tumour and serially sub-cultivated for 300 population doublings (Stein, 1979). Since T98G and T98 display different karyotypes and growth, Stein et al (1979) hypothesised that T98G may have arisen from T98 by a random genetic event or from a distinct cell population present in the primary tumour in small numbers. Interestingly, T98G cells have characteristics of normal cells and tumour cells in that, they arrest growth in G1 phase of the cell cycle under conditions such as, high density yet they display anchorage independent growth and immortality. T98G cells do not form tumours in athymic nude mice (Stein, 1979). The A172 cell line was first established by Giard et al (1973)(Giard et al., 1973). Studies have reported A172 cells have a glial-like cell morphology and are non-tumourigenic in athymic nude mice (Bigner et al., 1981). M059K and M059J were isolated from the same primary glioblastoma and are defined by their different sensitivity to radiation and cytotoxic drugs, with M059J being 30 fold more sensitive than M059K to radiation (Allalunis-Turner et al., 1993). U87MG and U118MG were amongst a number of glioma cell lines established by Ponten and Westermark between 1966 and 1969 (Bigner et al., 1981). U118MG have a mixed morphology and both U87MG and U118MG are tumourigenic in athymic nude mice (Bigner et al., 1981; Fogh et al., 1977). LN229 cells were established by de Tribolet and colleagues. LN229 are tumourigenic in athymic nude mice and display an epithelial morphology (Cordes et al., 2003; Ishii et al., 1999).

Cell Line	Tumour/ Histology	Grade	Growth/ morphology	Isolated from/date	ATCC number/ Reference
T98G	Glioblastoma/ multiforme	-	Adherent/ fibroblast	Primary tumour/ 1979	(ATCC: CRL-1690™) (Stein, 1979)
A172	Glioblastoma/ multiforme	Grade IV	Adherent/ fibroblast	Primary Tumour/ 1973	(ATCC: CRL-1620™) (Bigner et al., 1981; Giard et al., 1973)
M059K	Glioblastoma/ multiforme	Grade IV	Adherent/ fibroblast	Primary tumour/ 1993	(ATCC: CRL-2365™) (Allalunis-Turner et al., 1993)
M059J	Glioblastoma/ multiforme	Grade IV	Adherent/ fibroblast	Primary tumour/ 1993	(ATCC: CRL-2366™) (Allalunis-Turner et al., 1993)
U118MG	Glioblastoma/ astrocytoma	Grade IV	Adherent /mixed glioblastoma and astrocytoma	Primary tumour/ 1966 to 1969.	(ATCC: HTB-15™) (Bigner et al., 1981; Fogh et al., 1977)
U87MG	Glioblastoma/ astrocytoma	Grade IV	Adherent /mixed glioblastoma and astrocytoma	Primary tumour/ 1966 to 1969.	(ATCC: HTB-14™) (Bigner et al., 1981; Fogh et al., 1977)
LN229	Glioblastoma/ multiforme	Grade IV	Adherent/ epithelial	Primary frontal parieto-occipital tumour/ 1979	(ATCC: CRL-2611™) (Cordes et al., 2003; Ishii et al., 1999)

Table 3.3: The table details the glioma cell lines selected for characterisation
Seven glioma cell lines were selected to characterise the expression of NRP-1 and PDGFRs. The cell lines had been isolated from primary tumours and the table details the tumour type, histological classification, grade and morphology of the different cell lines. Gliomas are classified based on their histology/ cell type, and their increased grade (Grade I-IV) denotes increased malignancy The table includes the specific ATCC number per cell line and references (where possible) which detail the isolation, establishment and characterisation of the glioma cell lines.

PDGFR and PDGF ligand expression has been documented in both glioma cell lines and primary tumour specimens (Calzolari and Malatesta, 2010; Hägerstrand et al., 2006; Lokker et al., 2002; Martinho et al., 2009) and PDGFR is thought to be a principal driver of gliomagenesis (Chapter 1, 1.3.3.2.1). NRP-1 expression has also been reported in both glioma clinical specimens and glioma cell lines (Chapter 1, Table 1.0) and is correlated to gliomagenesis and glioma progression (Osada et al., 2004; Hamerlik et al., 2012; Hu et al., 2007).

When cultured under standard conditions, the different glioma cell lines had distinct morphology, although most are classified as fibroblasts. LN229 cells displayed an organised pattern of growth and appeared typical of their epithelial classification (Figure 3.2). U118MG and U87MG readily formed networks and when they reached confluence they formed spheroids and grew simultaneously as a mixture of detached/ attached spheroids and a cell mono-layer. The star shaped networks and protrusions may be attributed to the astrocytoma cell population of U87MG

and U118MG cell lines. At confluence, the spheroids were positioned at the centre of a spider-web like network (Figure 3.2). M059K and M059J grew less aggressively than the other glioma cell lines and displayed a similar spindle shaped fibroblast morphology which resembled other neural fibroblasts, such as choroid plexus fibroblasts (Figure 3.2). Other glioma cell lines including the A172, U118MG and U87MG also showed some similarity to neural fibroblasts. T98G and A172 were highly prolific and displayed no contact inhibition, with the A172 cells forming disorganised overlaid monolayers (Figure 3.2).

Flow cytometry analysis of the glioma cell lines determined that NRP-1 was expressed by U87MG, T98G and A172 cell lines. A low level of NRP-1 could also be detected in M059K cells (Figure 3.3). PDGFR-α was expressed in T98G, U87MG, LN229 and M059K cells (Figure 3.4).

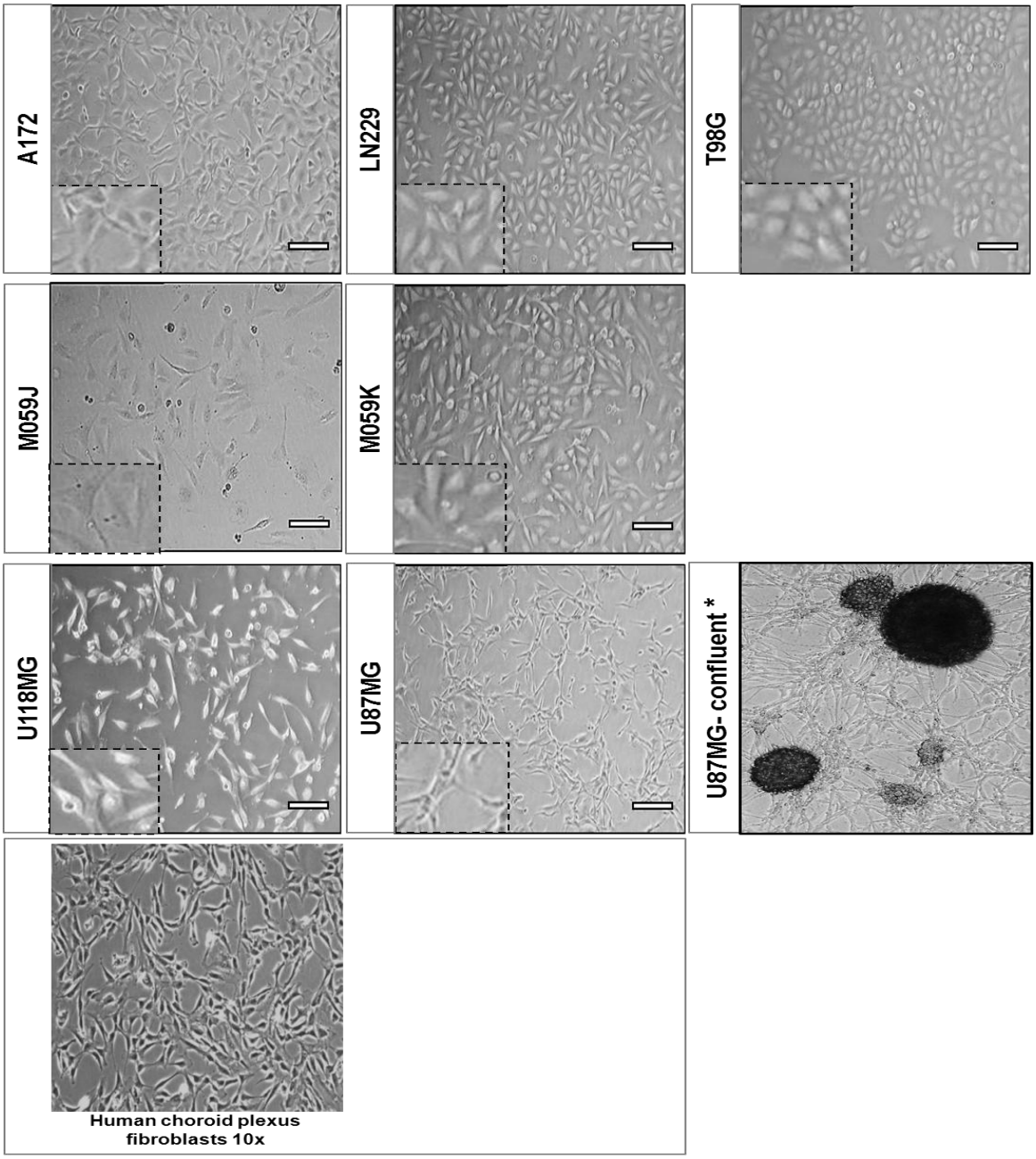

Figure 3.2: The morphology of the selected glioma cancer cell lines

Glioma cell lines were cultured under standard conditions (Chapter 2, 2.0.1). Images were collected using a phase-contrast microscope (Olympus CK X41) set at 10x magnification. Enlarged cell images are illustrated in the bottom left corner of each image outlined by the dashed line (- - -). In the bottom right corner of each image, Scale bar=100 µm. The (*) image is representative of the spheroids/ networks formed by confluent U87MG and U118MG cells. Some of the cell lines with fibroblast morphology show a similar morphology to other neural fibroblasts, e.g. human choroid plexus fibroblasts (bottom left, x10 magnification) (images sourced from ScienCell™).

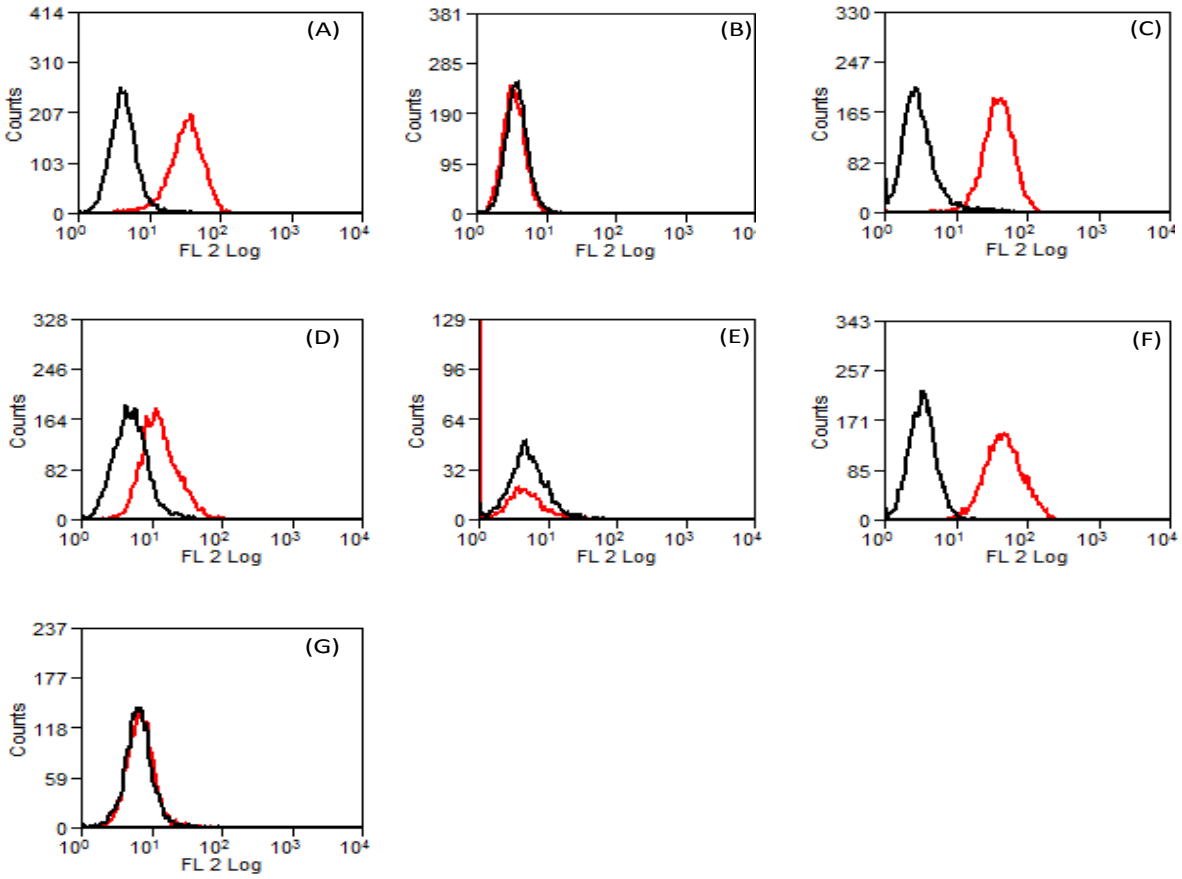

Figure 3.3: Cell surface expression of NRP-1 in the selected glioma cell lines

Glioma cell lines were cultured under standard conditions (Chapter 2, 2.0.1) and the expression of NRP-1 was determined by single colour flow cytometry (see Chapter 2, 2.0.2). Analysis of **(A)** A172; **(B)** LN229; **(C)** T98G; **(D)** M059K; **(E)** M059J; **(F)** U87MG; **(G)** U118MG cell lines was performed using anti-human NRP-1 mAb or a specific IgG control antibody (Chapter 2, Table 2.0). In each histogram, the fluorescent peak for NRP-1 (red) has been superimposed onto the peak for the isotype-matched IgG control (black).

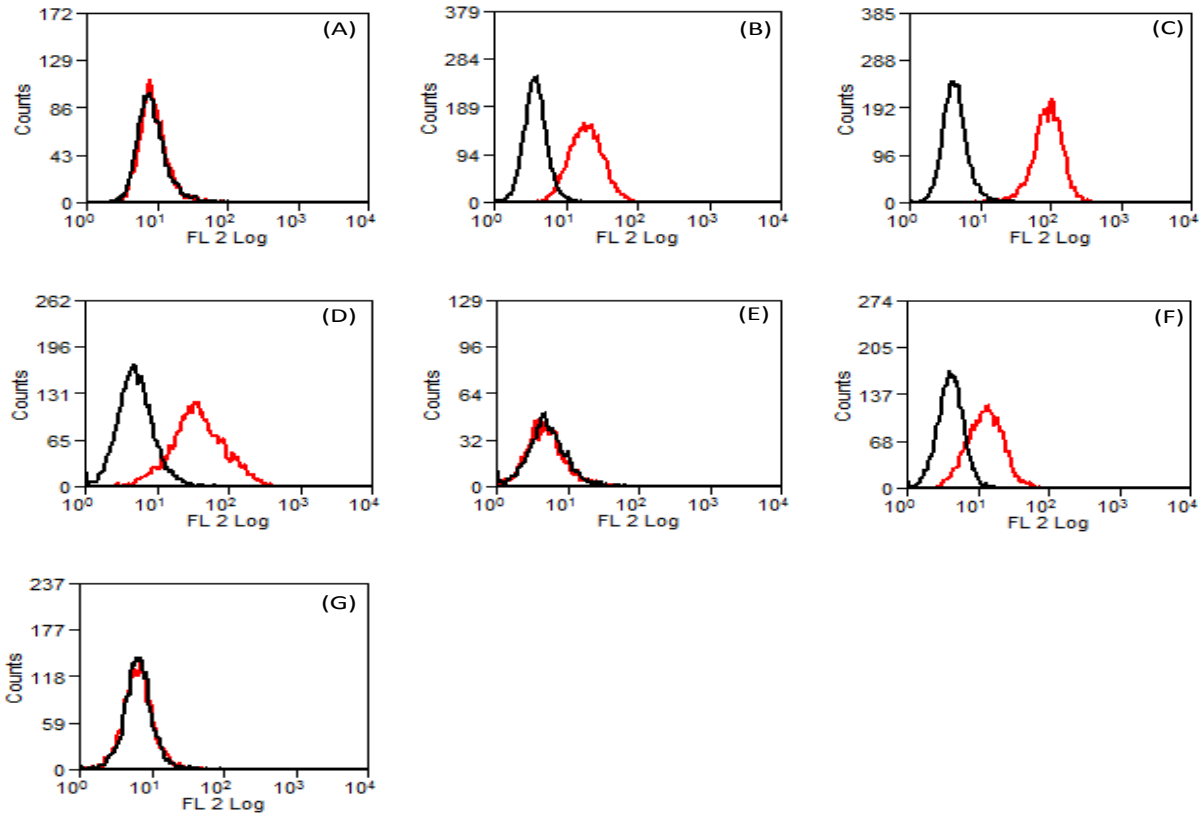

Figure 3.4: Cell surface expression of PDGFR-α in the selected glioma cell lines
Glioma cell lines were cultured under standard conditions and the expression of PDGFR-α was determined by single colour flow cytometry. Analysis of **(A)** A172; **(B)** LN229; **(C)** T98G; **(D)** M059K; **(E)** M059J; **(F)** U87MG; **(G)** U118MG cell lines was performed using a polyclonal PDGFR-α Ab or a specific IgG control antibody (Chapter 2, Table 2.1). In each histogram the fluorescent peak for PDGFR-α (red) has been superimposed onto the peak for the isotype-matched IgG control (black).

3.3 Tumour cell line selection and further characterisation

3.3.1 Tumour cell line selection

Table 3.4 details the results from the initial flow cytometry analysis of NRP-1 and PDGFR-α expression in the epithelial and mesenchymal cancer cell lines. Out of all the epithelial cell lines, only A549 and CALU-6 NSCLC expressed both PDGFR-α and NRP-1. A greater proportion of the mesenchymal tumour cell lines expressed both PDGFR-α and NRP-1 and therefore, mesenchymal tumour cell lines were selected for further characterisation and the epithelial cell lines were discounted from the study.

Cell Line	Cancer	NRP-1	PDGFR-α
COLO-205	Colon	(+)	(-)
HCT116	Colon	(-)	(-)
LoVo	Colon	(+)	(-)
SW620	Colon	(-)	(-)
A549	NSCLC	(+)	(+)
CALU-6	NSCLC	(+)	(+)
H1299	NSCLC	(-)	(+)
H1703	NSCLC	(-)	(-)
H1793	NSCLC	(+)	(-)
H23	NSCLC	(+)	(-)
H460	NSCLC	(-)	(-)
H522	NSCLC	(-)	(-)
KHOS-240S	osteosarcoma	(+)	(+)
MG63	osteosarcoma	(+)	(+)
Saos-2	osteosarcoma	(+)	(+)
T98G	Glioma	(+)	(+)
A172	Glioma	(+)	(-)
M059K	Glioma	(+)	(+)
M059J	Glioma	(-)	(-)
U118MG	Glioma	(-)	(-)
U87MG	Glioma	(+)	(+)
LN229	Glioma	(-)	(+)

Table 3.4: PDGFR-α and NRP-1 expression in epithelial and mesenchymal tumour cell lines
The table details the expression of NRP-1 and PDGFR-α (as determined by flow cytometry analysis) in the selected epithelial and mesenchymal tumour cell lines. The (+) indicates expression whereas (-) indicates no expression.

3.3.2 Further characterisation of the mesenchymal tumour cell lines

Using the osteosarcoma and glioma cell lines, NRP-1, PDGFR-α and PDGFR-β expression was quantified by immunoblot analysis. MSCs were also included as positive control cells in this analysis. MSCs have previously been well characterised within the group (Appendix, Figure 8.6)

and express NRP-1, PDGFR-α and PDGFR-β. The immunoblot analysis revealed that all of the osteosarcoma (Table 3.2) and glioma (Table 3.3) cell lines expressed NRP-1, however MG63 cells only expressed low levels of NRP-1 relative to the other cell lines (Figure 3.5). High levels of NRP-1 could be detected in the MSC control lane. Interestingly, there were also differences in the ratios of soluble: full-length NRP-1 protein expressed in the different cell lines. Soluble NRP-1 is a truncated isoform, with the c domain, transmembrane domain, and intracellular domain absent (see Chapter 1, Section 1.1.2).

There is also evidence from several studies that PDGFR-β and NRP-1 crosstalk occurs (Cao et al., 2010; Ball et al., 2010; Dhar et al., 2010), thus PDGFR-β expression was quantified by immunoblot analysis (Figure 3.5). Saos-2 and LN229 cells did not express PDGFR-β, however PDGFR-β could be detected in the remainder of the osteosarcoma and glioma cell lines. PDGFR-β expression was lowest in the M059J cells and the remainder of the cancer cell lines showed a comparable expression of PDGFR-β. PDGFR-β expression was markedly higher in the MSC control cells relative to any of the cancer cell lines.

Immunoblot analysis of PDGFR-α expression illustrated that, KHOS-240S, MG63 and U118MG cells all expressed high levels of PDGFR-α. High levels of PDGFR-α could be detected in the MSC control lane (Figure 3.6). When the film was exposed to the chemiluminescent substrate for an extended period of time (1 hour) PDGFR-α expression could be detected in, T98G, LN229, U87MG and M059K. However, only trace amounts of PDGFR-α were detected in M059J and A172 cells and PDGFR-α was not detected in Saos-2 cells (this data is shown in the Appendix, Figure 8.7).

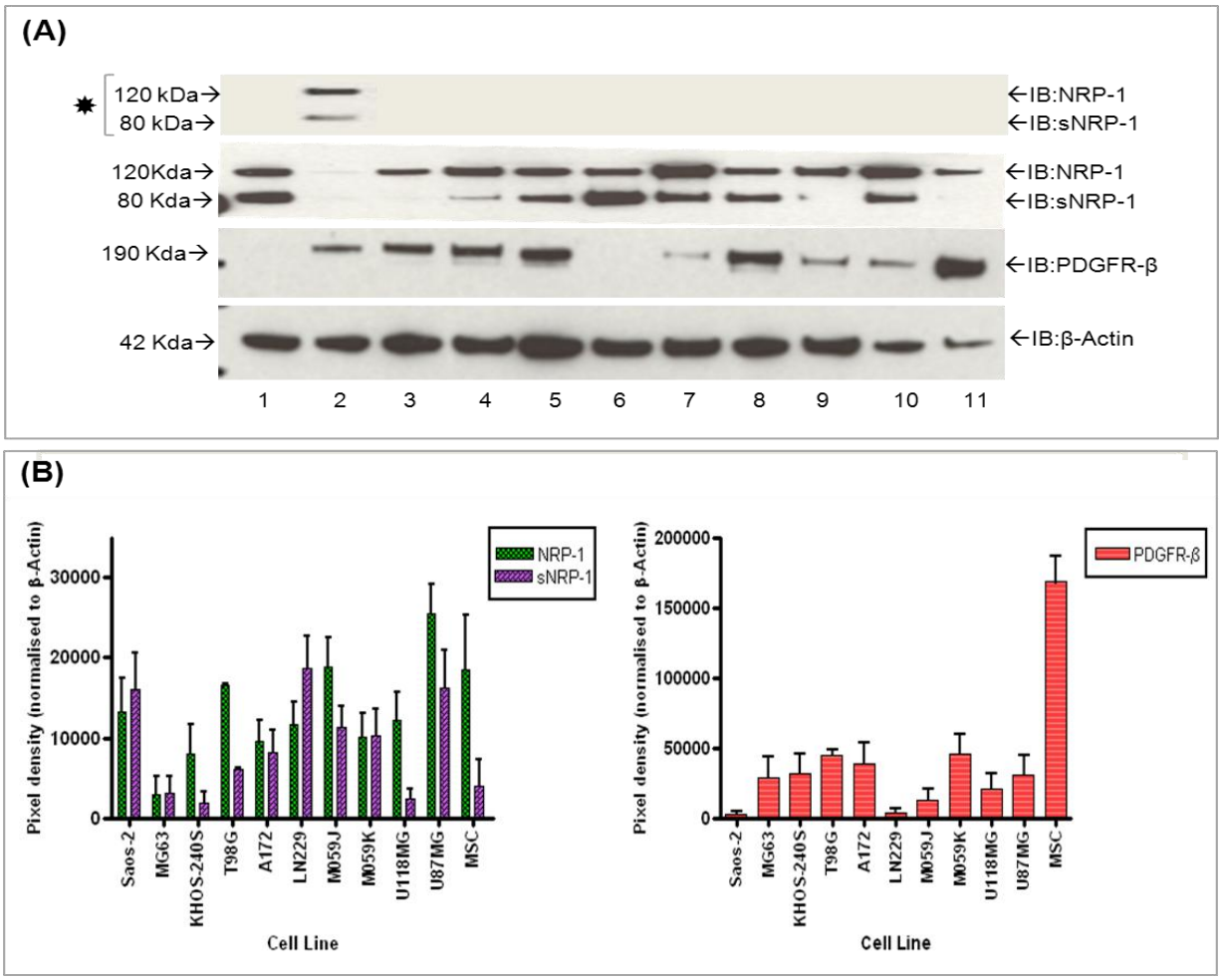

Figure 3.5: NRP-1 and PDGFR-β expression in glioma and osteosarcoma cell lines
(A) Using total cell lysates, immunoblot analysis was performed using the following osteosarcoma and glioma cell lines: **(1)** Saos-2; **(2)** MG63; **(3)** KHOS 240-S; **(4)** T98G; **(5)** A172; **(6)** LN229; **(7)** M059J; **(8)** M059K; **(9)** U118MG; **(10)** U87MG. Lane **(11)** shows the result for the MSC control. The NRP-1 antibody (Chapter 2, Table 2.0) detected both NRP-1 and sNRP-1. For detection of the NRP-1 bands, the film exposure time was 5 minutes, however, due to low expression of NRP-1 in MG63 cells, this segment of the membrane had to be exposed for 30 minutes which is denoted by the (✸). On the same nitrocellulose membrane, the PDGFR-β antibody (Chapter 2, Table 2.0) was used to detect relative levels of PDGFR-β in the cancer cell lines and MSC control cells. **(B)** The histograms show the relative expression of NRP-1/ sNRP-1 and PDGFR-β, which has been calculated through analysis the pixel density and normalised to the β-Actin loading control. It is evident from this that the MSC control cells express much higher levels of PDGFR-β than the cancer cell lines. Results have been calculated from two independent experiments.

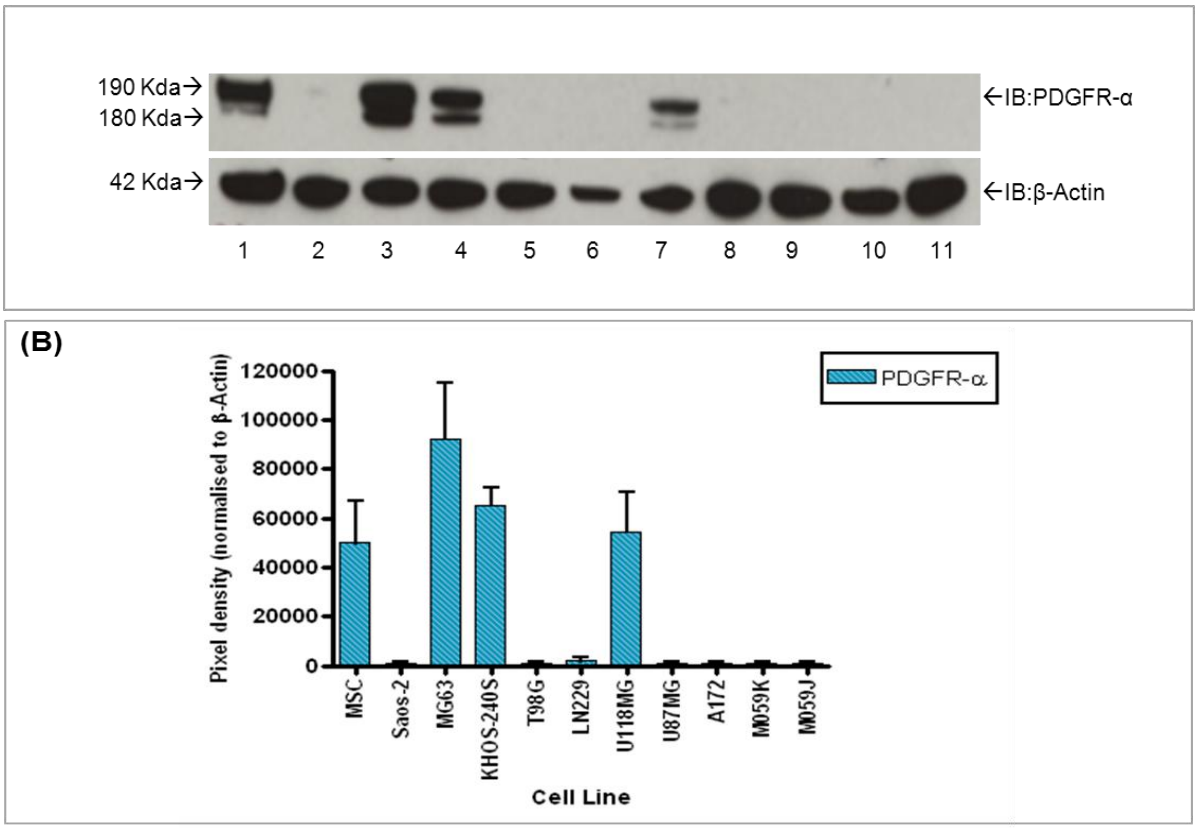

Figure 3.6: PDGFR-α expression in glioma and osteosarcoma cell lines

(A) Using total cell lysates, immunoblot analysis was performed using the following osteosarcoma and glioma cell lines: **(2)** Saos-2; **(3)** MG63; **(4)** KHOS 240-S; **(5)** T98G; **(6)** LN229; **(7)** U118MG; **(8)** U87MG; **(9)** A172; **(10)** M059K; **(11)** M059J. Lane **(1)** shows the result for the MSC control. The PDGFR-α antibody (Chapter 2, Table 2.0) was used to detect relative levels of PDGFR-α in the cancer cell lines and MSC control cells. For detection of the PDGFR-α bands, the film exposure time was 5 minutes, however, PDGFR-α could only be detected in some of the other cell lines after 1 hour exposure (Appendix, Figure 8.1). (B) The histograms show the relative-expression of PDGFR-α, which has been calculated through analysis the pixel density (Chapter 2, 2.0.3.3) and normalised to the β-Actin loading control. Results have been calculated from two independent experiments.

3.4 Summary

The immunoblot results showed some discrepancies compared to the flow cytometry data (Table 3.5), for example, the immunoblot analysis detailed that NRP-1 was expressed in all of the glioma cell lines, whereas in M059J, U118MG and LN229 cell lines NRP-1 was not detected by flow cytometry analysis. Overall, the immunoblots analysis revealed that the expression of both NRP-1 and PDGFR-α was more widespread across the different tumour cell lines than initially suggested by the flow cytometry data. These discrepancies could have been related to the sensitivity of the two techniques as, immunoblots are able to detect the total protein within a cell, whereas, flow cytometry only detects the fraction of the total protein which is expressed the cell surface. The fraction of PDGFRs or NRP-1 on the cell surface would have been dependent on the growth factors within the cellular microenvironment. Prior to flow cytometry analysis, cells were cultured for a minimum of 24 hours under standard culture conditions. Therefore, the cells were exposed to 10% (v/v) FBS, a fraction of which may have contained PDGF or VEGF ligands. In addition to this both osteosarcoma cells and glioma cells secrete PDGF and VEGF ligands (Lokker et al., 2002; Sulzbacher et al., 2000; Westermark et al., 1995). Together these factors may have created a PDGF/VEGF rich culture environment which may have negatively regulated the cell surface expression of PDGFR and NRP-1 through positively regulating receptor activation and endocytosis (Mukherjee et al., 2006; Salikhova et al., 2008).

As detailed in the introduction to this Chapter (Section 3.0), NRP-1 is known to interact with RTKs including; VEGFR (Fuh et al., 2000; Soker et al., 2002), c-Met (Hu et al., 2007), PDGFR (Ball et al., 2010; Cao et al., 2010; Pellet-Many et al., 2011) and growth factors including; TGF-β (Cao et al., 2010) and FGF (West et al., 2005). Out of these growth factors and RTKs, PDGFR and VEGFR family members share the closest phylogenic relationship (Gu and Gu, 2003; Kondo et al., 1998) and it feasible these RTKs may competitively interact with NRP-1. Studies by Ball et al (2010) and Pellet-Many et al (2011) reported NRP-1/PDGFR crosstalk and used cell types with no detectable expression of VEGFR-1 and VEGFR-2 (Ball et al., 2010; Pellet-Many et al., 2011). However, Cao et al (2010) presented evidence of NRP-1/PDGFR crosstalk in hepatic stellate cells (Cao et al., 2010), which are known to constitutively express both VEGFR-1 and VEGFR-2 (Novo et al., 2007). Similarly, Banjeree et al (2006) reported evidence of NRP-1/PDGFR crosstalk in human aortic SMCs (Banerjee et al., 2006), which are documented to express both VEGFR-1 and VEGFR-2 (Banerjee et al., 2008; Lorquet et al., 2010). Together, these lines of evidence suggest that VEGFR expression may be an important determinant of NRP-1/PDGFR crosstalk in some cell types but not others. Given the fact that NRP-1/PDGFR crosstalk has not been investigated in osteosarcoma and glioma cell lines, it was important to gain some insight into VEGFR expression, as this may have proved a critical factor in mediating the possible NRP-1/PDGFR crosstalk in

these cell lines. Preliminary immunoblots analysis of the cell lines (Appendix, Figure 8.2 and 8.3) revealed that all of the tumour cell lines, except KHOS-240S, expressed VEGFR-1 and only U87MG cells expressed VEGFR-2. This VEGFR expression data, together with the PDGFR-α, PDGFR-β and NRP-1 data, was cross-referenced with published data to further verify the expression of these key receptors in the osteosarcoma and glioma cell lines (Table 3.5).

Two of the osteosarcoma cell lines, KHOS-240S and MG63, were selected to study the potential NRP-1/ PDGFR crosstalk. Both of these cell lines expressed high levels of PDGFR-α and PDGFR-β and published data also outlined protein expression of PDGFR-α and β in MG63 cells (Table 3.5). It was not possible to cross-reference published KHOS-240S data, however studies examining the parental cell line HOS (which is very similar to KHOS-240S, see Section 3.2.1) reported the expression of both PDGFR-α and PDGFR-β (Hassan et al., 2012; Loizos et al., 2005). MG63 and KHOS-240S expressed low and high levels of NRP-1, respectively. This provided an interesting distinction between the cell lines which would be useful to interrogate whether or not the relative expression of NRP-1 was a factor determining the NRP-1/PDGFR crosstalk. The KHOS-240S cells also showed a very similar receptor complement to the MSC controls, with high levels of PDGFR-α, PDGFR-β, NRP-1 and no detectable VEGFRs, whereas the preliminary data (Appendix, Figure 8.2) suggested that all the other cancer cell lines expressed VEGFR-1. Thus, the KHOS 240-S cells were a unique cell model to address the questions surrounding VEGFR expression and NRP-1/PDGFR crosstalk in mesenchymal tumour cells. Saos-2 osteosarcoma cells were discounted from the study as PDGFR-β expression was absent and coupled with this PDGFR-α expression was inconclusive/ low or absent. Although published data outlined the expression of PDGFR-α in Saos-2, the expression was negligible compared to, for e.g. the MG63 cells which were described in the same manuscript (Table 3.5).

The following glioma cell lines were selected to study the NRP-1/PDGFR crosstalk: T98G, A172 and U87MG. The flow cytometry and immunoblot data confirmed that T98G and U87MG cells expressed PDGFR-α, PDGFR-β and NRP-1 and this was corroborated by the published data. However, unlike the T98G cells, the U87MG cells also expressed VEGFR-2 and thus, were a valuable cell model to investigate if VEGFR-2 expression affected NRP-1/PDGFR crosstalk in mesenchymal tumour cells. The expression of PDGFR-α in the glioma cell lines was also much lower than in the osteosarcoma cell lines and this provided an interesting comparison between the two tumour types. The A172 cells expressed PDGFR-β but lacked PDGFR-α and therefore, were valuable cells to specifically examine NRP-1/PDGFR-β crosstalk. It was feasible the remainder of the glioma cell lines (detailed in Table 3.5) may have also been useful cell models to investigate NRP-1/PDGFR crosstalk. However, the expression data for these cell lines was less conclusive and for practical reasons the number of cell lines had to be reduced for the study.

Cell Line	NRP-1			PDGFR-α			PDGFR-β		VEGFR-1		VEGFR-2		References
	FC	IB	Ref.	FC	IB	Ref	IB	Ref	IB	Ref.	IB	Ref.	
KHOS-240S	(+)	(+)		(+)	(+)		(+)				(-)		
MG63	(+)	(+)		(+)	(+)	(+)	(+)	(+)	(+)		(-)		(Chen et al., 2009b) (McGary et al., 2002) (Alonso et al., 2008)
Saos-2	(+)	(+)		(+)	(-)	(+) #	(-)	(-)	(+)		(-)		(McGary et al., 2002) (McGary et al., 2002)
T98G	(+)	(+)	(+)	(+)	(+)	(+)	(+)	(+)	(+)		(-)		(Hu et al., 2007) (Jane et al., 2009) (Yang et al., 2007)
A172	(+)	(+)	(+)	(-)	(+)	(-)	(+)	(+)	(+)	(+)	(-)	(+)	(Bagci et al., 2009) (Lokker et al., 2002) (Heidaran.,et al 1991) (Hong et al., 2007b)
M059K	(+)	(+)		(+)	(+)		(+)		(+)		(-)		
M059J	(-)	(+)		(-)	(+)		(+)		(+)		(-)		
U118MG	(-)	(+)	(+)	(-)	(+)	(+)	(+)	(+)	(+)		(-)		(Hu et al., 2007) (Potapova et al., 2006) (Brave et al., 2011)
U87MG	(+)	(+)	(+)	(+)	(+)		(+)	(+)	(+)	(+)	(+)	(+)	(Hu et al., 2007) (Bagci et al., 2009) (Ping Guo et al., 2003) (Hong et al., 2007b)
LN229	(-)	(+)	(+)	(+)	(+)		(-)		(+)		(-)		(Hu et al., 2007)

Table 3.5: The expression of PDGFRs, VEGFRs and NRP-1 in mesenchymal tumour cell lines

The table details the expression of NRP-1, PDGFR-α, PDGFR-β and the VEGFRs in the selected mesenchymal cancer cell lines, as determined by immunoblot (IB) and flow cytometry (FC) analysis. The data has been cross-referenced with published data (Ref). The (+) details positive expression and the (-) details no expression. The # highlights low expression of PDGFR-α in Saos-2 cells. The references are colour coded according to the receptor they refer to; purple (NRP-1), Blue (PDGFR-α), Orange (PDGFR-β), Pink (VEGFR-1 or VEGFR-2).

This Chapter determined that NRP-1 expression is localised to both mesenchymal and epithelial tumour cell lines. However, PDGFR expression is only expressed in tumours with a mesenchymal phenotype. As detailed in Table 3.5, the cell lines selected show a varied expression of NRP-1, PDGFRs and VEGFRs and are valuable models to interrogate how the receptor complement of the mesenchymal tumour cell lines may influence NRP-1/PDGFR crosstalk. As alluded to, the contribution of VEGFR expression to NRP-1/PDGFR crosstalk seems to be cell-type specific. These cell-type specific interactions involving NRP-1 may be defined by the relative importance of each RTK within different cell types. For example, if c-Met, as oppose to VEGFR, is primarily driving cellular behaviour, NRP-1 may interact with the dominant c-Met RTK rather than VEGFR. Alternatively, NRP-1 may interact with different RTKs in a hierarchal fashion for e.g. in the absence of VEGFR, NRP-1 preferentially interacts with PDGFR and in the absence of PDGFR NRP-1 then interacts with c-Met. However, both these mechanisms assume RTKs compete for NRP-1, yet it is possible different RTKs interact distinctly with NRP-1 and that these interactions are concurrent. The next Chapter aims to interrogate these mechanistic interactions between NRP-1 and PDGFRs which in turn will help to determine if the cell surface receptor complement of tumour cell lines is a critical determinant of NRP-1/PDGFR crosstalk.

3.4.1 Chapter 3: principal findings

- NRP-1 is widely expressed in tumour cell lines with either an epithelial or mesenchymal phenotype.
- PDGFR expression was only detected in the mesenchymal tumour cell lines.
- The majority of mesenchymal tumour cell lines express either VEGFR-1 or VEGFR-2, with the exception of KHOS-240S cells, which have no detectable VEGFRs.

.

Chapter 4 – Results

The mechanistic interactions between NRP-1 and PDGFRs in mesenchymal tumour cells

4.0 Introduction

As discussed in Chapter 3, tumour cell lines express multiple RTKs and NRP-1, and it is not clear how the receptor complement of these cells may impact on NRP-1/PDGFR crosstalk. This is because the mechanisms that mediate the crosstalk between NRP-1 and PDGFRs have not been fully elucidated. Chapter 4, therefore, explores if and how PDGFR and NRP-1 physically interact and whether or not these interactions occur in the mesenchymal tumour cell lines.

Several lines of evidence suggest PDGF growth factors are critical in controlling the NRP-1/PDGFR interactions. In MSCs, Ball et al (2010) reported that NRP-1 co-immunoprecipitation with PDGFR-α or PDGFR-β was significantly enhanced in the presence of PDGF growth factors (Ball et al., 2010). Previous work within our group also found that NRP-1 could not bind directly to the extracellular Ig-like domains of PDGFR-α, which suggests that an intermediary factor must be involved if the NRP-1/PDGFR crosstalk is mediated by extracellular interactions. NRP-1 is also reported to bind to both PDGF-AA (Ball et al., 2010) and PDGF-BB (Banerjee et al., 2006). Collectively, this data suggests that extracellular binding of PDGF to both NRP-1 and PDGFR may bridge an association between NRP-1 and PDGFR (as described in the VEGF bridging model (Shay Soker et al., 2002), Figure 1.4).

Not all reports support the hypothesis that PDGF is an essential factor for NRP-1/PDGFR crosstalk. Pellet-Many et al (2011) reported that NRP-1 and PDGFR-α co-immunoprecipitated at similar levels in the absence or presence of PDGF growth factors. Yet, NRP-1 was still essential for the phosphorylation of PDGFRs (Pellet-Many et al., 2011), suggesting factors other than PDGF were mediating the NRP-1:PDGFR crosstalk. Previous reports examining NRP-1/VEGFR crosstalk also implied that the growth factor bridging model was insufficient to explain NRP-1's ability to potentiate VEGFR signalling. In these studies, NRP-1 enhanced VEGFR signalling in the absence of VEGF-A binding to NRP-1 and complex formation between NRP-1 and VEGFR-2 was documented in the absence of VEGF-A (Shraga-Heled et al., 2007).

As alluded to in the previous Chapter, the nature of NRP-1/PDGFR interactions may be cell-type specific. Thus the contrary reports detailing PDGF is/ is not an essential mediator of NRP-1/PDGFR crosstalk may be related to the different cell types used in the respective studies. Although PDGF has been reported to associate with NRP-1, the specific NRP-1 domains involved

in PDGF binding have not been described. This Chapter therefore, investigates which of the NRP-1 domains are involved in PDGF binding and examines the relative contribution of PDGF growth factors in mediating NRP-1 and PDGFR interactions in mesenchymal tumour cell lines.

4.1 The b domains of NRP-1 bind to PDGF growth factors

Due to the close homology between the PDGF growth factors and VEGF-A (Dormer and Beck, 2005; Muller, 1997), it was hypothesised that PDGF may also bind to the b domains of NRP-1. To examine this possibility, the b domains of NRP-1 were recombinantly expressed in a mammalian system, and the binding of the b domains to commercially obtained PDGF growth factors was examined. This section describes the cloning, expression, and purification of the NRP-1 b domains and the subsequent growth factor binding studies.

4.1.1 The NRP-1 b domains were cloned into the PQCXIP expression vector

RNA extracted from CALU-6 cells (which express high levels of NRP-1) was used to generate a cDNA template encoding the b domains of NRP-1. PCR was performed to amplify the DNA construct. The theoretical size of a DNA construct encoding the b domains of NRP-1 is 924 base pairs and Figure 4.0 illustrates that the PCR product was the correct size.

This b domain construct was then ligated into the pCR2.1-TOPO TA cloning vector using a double digest method. Ligation was confirmed through resolving the digested pCR2.1-TOPO: b domain construct on a 1% agarose gel and observing a 3931 bp product which corresponded to the vector and a 924 bp product corresponding to the NRP-1 b domains (Figure 4.0).

The product encoding the NRP-1 b domains was then ligated into the retroviral PQCXIP expression vector. This vector also encoded both a histidine and V5 tag. Following ligation, the PQCXIP: b domain construct was digested using Age1 and Pac1 restriction enzymes. The digested DNA was resolved on a 1% agarose gel and products of the correct size were visualised, confirming that the b domains had successfully ligated into PQCXIP (Figure 4.0). DNA sequencing confirmed the fidelity of the vector and b domain construct. Detailed cloning methods are described in Chapter 2, Section 2.8.

4.1.2 The NRP-1 b domains were expressed and purified

Mammalian HEK-293-EBNA cells were chosen to express the b domains of NRP-1 using the calcium phosphate transfection method (see Chapter 2, Section 2.8.6). Although mammalian expression generally produces lower titres of protein than bacterial protein expression, the advantage is that the mammalian cells possess the both the organelles and enzymes to ensure protein is correctly folded and glycosylated. This is important as studies have shown that NRP-1 undergoes N-linked and O-linked glycosylation (Frankel et al., 2008; Fukahi, 2004) and at least one site of N-linked glycosylation (and a further potential site) is located in the b domains of NRP-1

(Chen et al., 2009a). Thus, the protein produced by mammalian cells is more likely to be functional.

Media containing the recombinant NRP-1 b domains was collected from the transduced HEK-293-EBNA cells. A His-Trap FF column charged with $NiSO_4$ was used to extract the histidine-tagged NRP-1 b domains from the cell media and the NRP-1 b domains were eluted from the His-Trap FF column using an increasing gradient of imidazole, from 0-500 nM (for methods see Chapter 2, Section 2.8.7). The b domains eluted from the His-Trap FF column in fractions 11-15 with an evident peak on the chromatograph (Figure 4.1). The eluted fractions were resolved on a 4-12% polyacrylamide gel and the bands were visualised using instant blue stain. The products resolved from fractions 11-15 corresponded to the theoretical size of the NRP-1 b domains with a molecular weight of 37 kDa (Figure 4.1).

Fractions 11-15 eluted from the His-Trap FF column were pooled and further purified using a Sepharose S200 size exclusion column. This column separated the proteins based on their molecular weight, thus separating any aggregated protein from monomeric protein. A single large peak was visible on the chromatograph between fractions 16-24 (Figure 4.2), indicating that the protein was probably monomeric. Fractions 16-24 were resolved by SDS-PAGE and the bands were visualised using instant blue stain. A double band was visible at 37 kDa which corresponded to the theoretical size of the NRP-1 b domains, previous reports had also suggested the b domains of NRP-1 resolved as a doublet (Mamluk et al., 2002). Because N-glycosylation of the b domains had been previously documented (Chen et al., 2009a), a digest of the b domains using the PNgase-F enzyme was undertaken. Following treatment with PNgase-F, only the lower band could be visualised which indicated that the upper band of the doublet was due to N-glycosylation (Figure 4.2).

Finally to confirm the identity of the purified protein, trypsin digests were performed and the peptide composition of the protein was then analysed by mass spectrometry (Figure 4.3). Results showed 100% identity for human NRP-1 and the peptides identified were localised to the b domains of NRP-1.

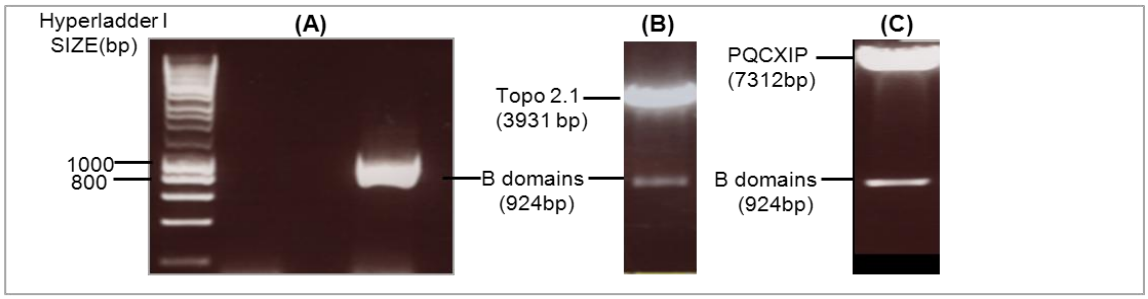

Figure 4.0: Cloning of the NRP-1 b domains

During the cloning of the NRP-1 b domains, all samples were resolved on a 1% agarose gel supplemented with Gel Red for the UV visualisation of products. **(A)** The cDNA encoding the b domains of NRP-1 was amplified by PCR generating a 924 bp product. **(B)** The b domains were ligated into the pCR TOPO 2.1 TA cloning vector. Double digest by Age-1 and Pac-1 restriction enzymes generated the 924bp b domain product and a 3931 bp product corresponding to Topo 2.1. **(C)** The b domains were ligated into PQCXIP. Double digest by Age-1 and Pac-1 restriction enzymes generated the 924 bp product, corresponding to the NRP-1 b domains, and a 7312 bp product corresponding to PQCXIP.

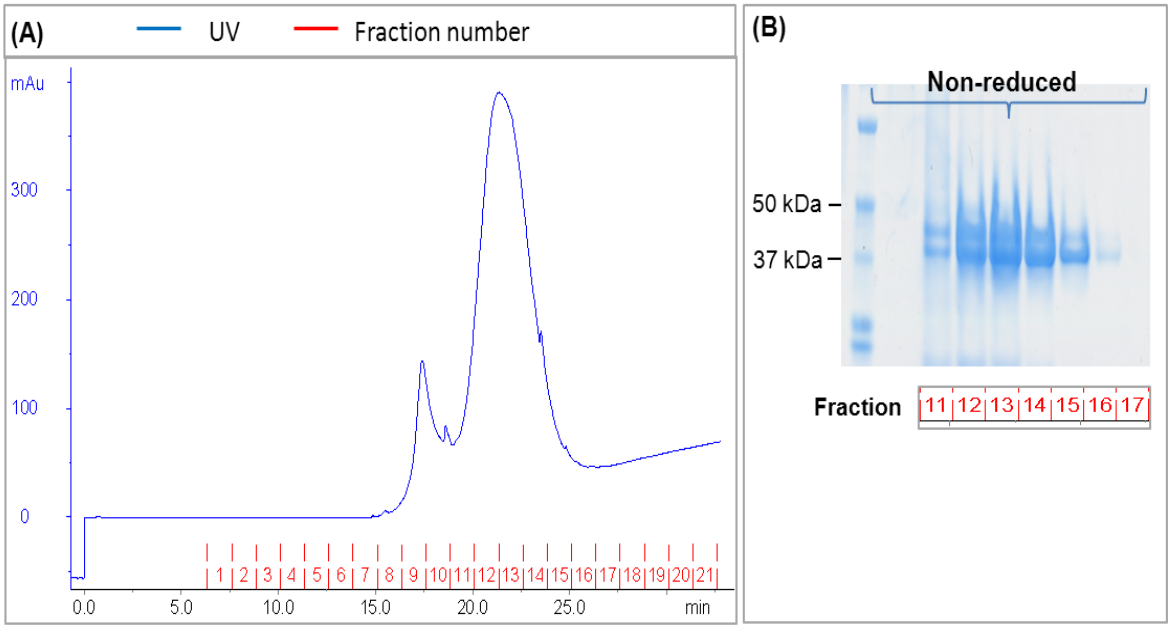

Figure 4.1: The extraction of the recombinant NRP-1 b domains from HEK-293-EBNA cell media using the His-Trap FF column

HEK-293-EBNA cell media containing the His tagged NRP-1 b domains was passed through a His-Trap FF column charged with $NiSO_4$. **(A)** The peak on the chromatogram between fractions11-15 signified that increasing concentrations of imidazole induced elution of the NRP-1 b domains from the His-Trap FF column. Eluted fractions 11-15 were resolved using SDS-PAGE, under non-reduced conditions, and stained with instant blue. **(B)** A 37 kDa product was detected which corresponded to the theoretical molecular weight of the NRP-1 b domains.

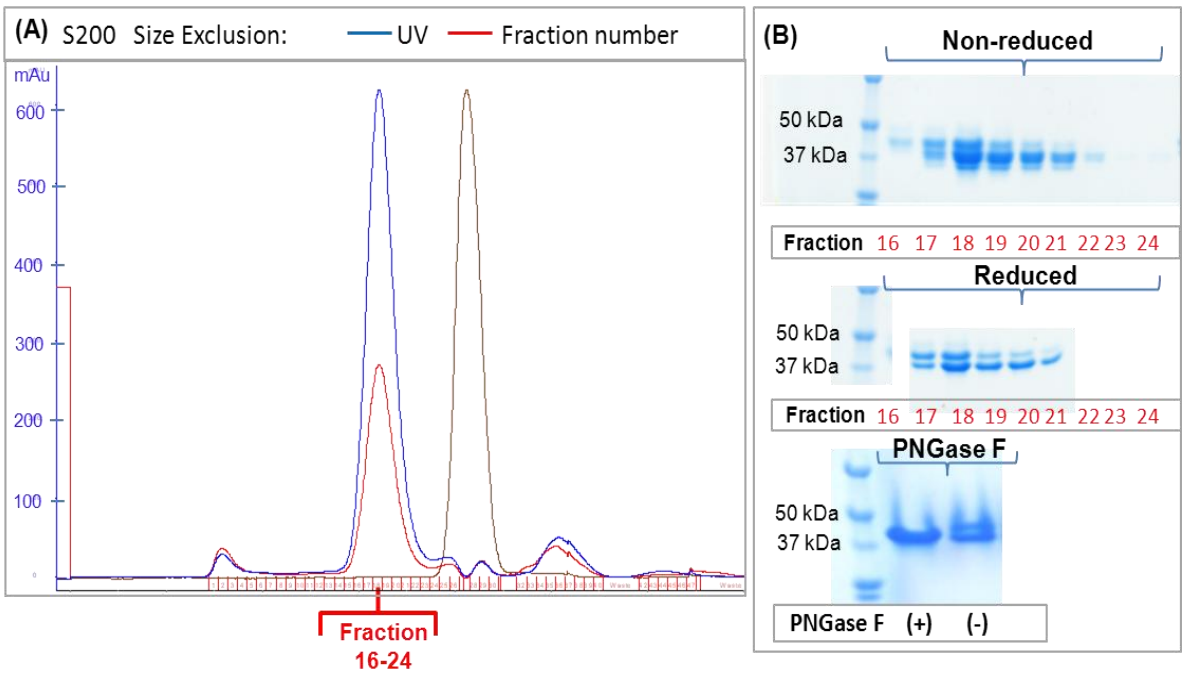

Figure 4.2: Purification of the NRP-1 b domains using the S200 size exclusion column
Protein fractions 11-15 eluted from the His-Trap FF column were pooled and passed down the sepharose S200 size exclusion column. **(A)** Fractions 16-24 signified by the UV absorbance peak (600mA) on the chromatogram were eluted and resolved by SDS-PAGE. Products were visualised by instant blue staining. **(B)** A 37 kDa product was detected which corresponded to the theoretical molecular weight of the NRP-1 b domains. Without reducing agent, the resolution of products decreased, suggesting the presence of protein folding and disulphide bonding. The PNgase-F enzyme eliminated the higher molecular weight product which indicated that the b domains were N-glycosylated.

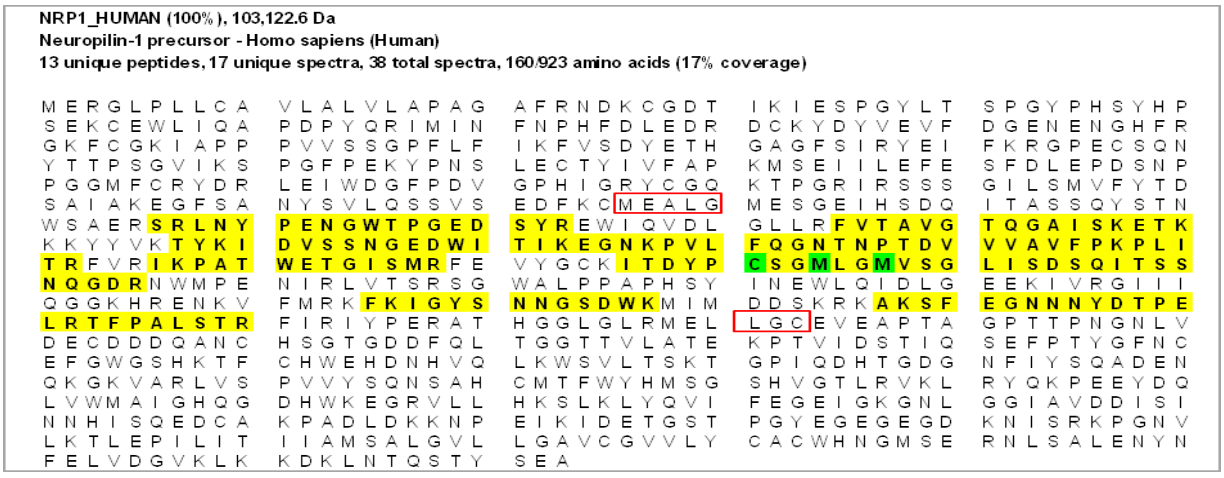

Figure 4.3: Mass spectrometry analysis of the recombinant NRP-1 b domains
The amino acid sequence outlines the peptides (yellow) positively identified by mass spectrometry analysis of the recombinant NRP-1 b domains. The analysis confirmed that the peptides shared 100% identity with human NRP-1 and that all the peptides were localised between the start (MEALG) and end (LGC) of the b domain sequence.

4.1.3 VEGF-A and PDGF growth factors bind to the b domains of NRP- 1

BIAcore is based on surface plasmon resonance technology and allows the analysis of protein interactions and binding affinity in real-time. The recombinant b domains of NRP-1 were immobilised on a CM5 chip and selected VEGF-A and PDGF growth factors were flowed over the chip surface to assess binding to NRP-1.

BIAcore analysis showed that VEGF-A_{165} and VEGF-A_{121} bound to the b domains of NRP-1 and, consistent with published data, VEGF-A_{121} bound with a lower affinity than VEGF-A_{165} (Fuh et al., 2000; Pan et al., 2007). The calculated dissociation constants (K_d) for VEGF-A_{165} and VEGF-A_{121} was 19.6 and 61.8 nM respectively (Figure 4.4). Previous published reports examined the three extracellular domains or the b domains plus the CUB domains of NRP-1 binding to VEGF-A. In these studies, (K_d) values were higher with 100-200 nM for VEGF-A_{165} and 220 nM for VEGF-A_{121} (Fuh et al., 2000; Pan et al., 2007). As the b domains are the binding site for VEGF-A, it is feasible that VEGF-A binding to the b domains, as isolated constructs, is of higher affinity than to the complete ectodomain of NRP-1 which may have caused the lower (K_d) values recorded in this study.

PDGF-AA, BB, CC and AB all bound to the b domains of NRP-1 (Figure 4.5). PDGF-AA bound to the b domains and generated a large response relative to the other isoforms of PDGF. PDGF-AA would not also dissociate from the CM5 chip and this may have been partly due to non-specific binding as PDGF-AA generated a relatively high response (500 RU) in the control flow cell. Previous reports have also highlighted a high non-specific binding response with PDGF-AA which was attributed to electrostatic interactions between negatively charged carboxymethyl dextran on the CM5 chip and cationic PDGF-AA (Goretzki et al., 1999). PDGF-BB and PDGF-AB bound with similar affinities to the b domains and the response induced by binding was comparable to VEGF-$A_{121.}$ PDGF-CC associated less rapidly with the b domains and generated a lower overall response.

Due to the binding characteristics of PDGF growth factors, it was not possible to collect kinetic data. This was for two reasons, the first being the concentration of PDGF growth factors tested was too low for the binding curve to plateau. Secondly, due to the curves not reaching a plateau, it was difficult to fit any conventional binding models to the data and calculate accurate (K_d) values (Figure 4.6). This concentration of PDGF growth factors was a limiting step as the PDGF growth factors were commercially sourced and the quantities required for accurate kinetic data were not feasible for the project.

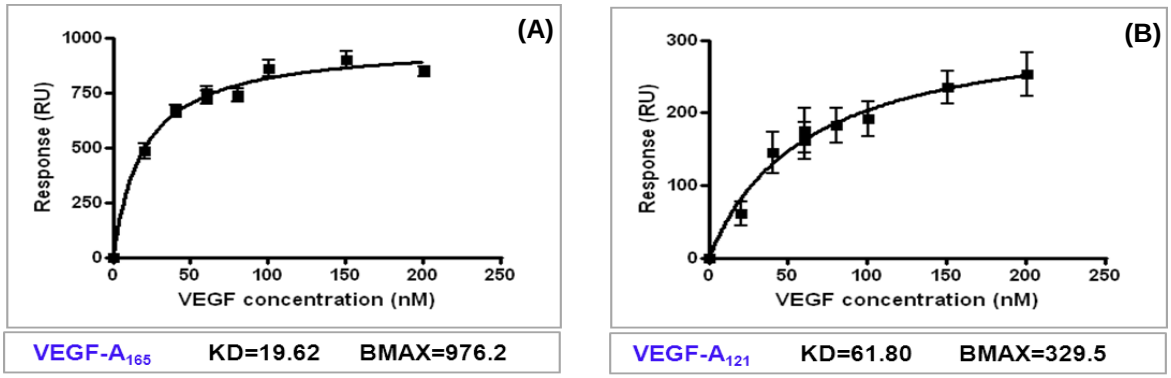

Figure 4.4: The kinetics of VEGF-A_{165} and VEGF-A_{121} binding to the b domains of NRP-1
BIAcore analysis assayed VEGF-A concentrations from 0-200 nM binding to the b domains of NRP-1. Data were plotted in Graph Pad Prism and graphs represent 3 experimental repeats. The one-site binding hyperbola equation (Y=Bmax*X/ (*Kd*+X)) was used to calculate Bmax and K_d values in Graph Pad Prism. **(A)** VEGF-A_{165} bound to the b domains of NRP-1 with fast association and a recorded K_d of 19.62 nM. **(B)** VEGF-A_{121} bound to the b domains of NRP-1 with slower kinetics with a recorded K_d of 61.8 nM.

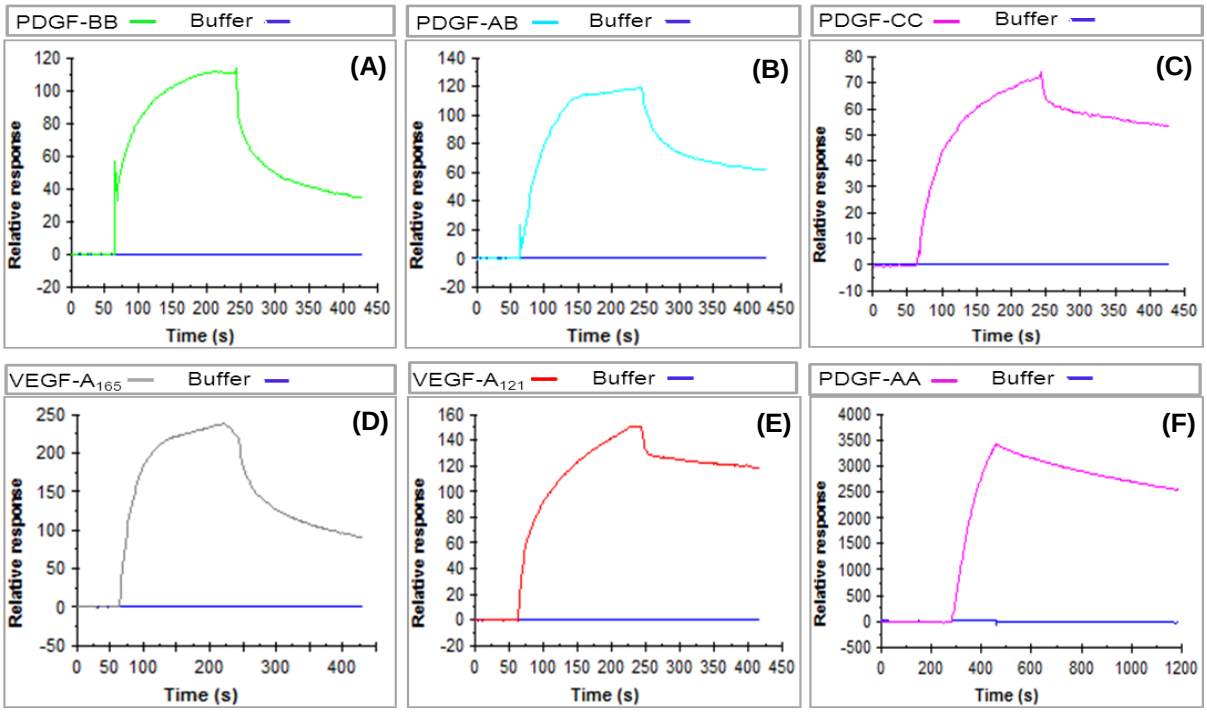

Figure 4.5: BIAcore analysis of VEGF-A or PDGF binding to the b domains of NRP-1
The b domains of NRP-1 were immobilised on a CM5 chip and binding of 25 nM of PDGF or VEGF-A growth factors was evaluated. Analyte scans revealed that, **(A)** PDGF-BB;**(B)** PDGF-AB; **(C)** PDGF-CC and **(F)** PDGF-AA all bound to the b domains. **(F)** Both **(D)** VEGF-A_{165} and **(E)** VEGF-A_{121} also bound to the b domains of NRP-1. Analyte scans were repeated at least twice and generated similar responses and binding curves.

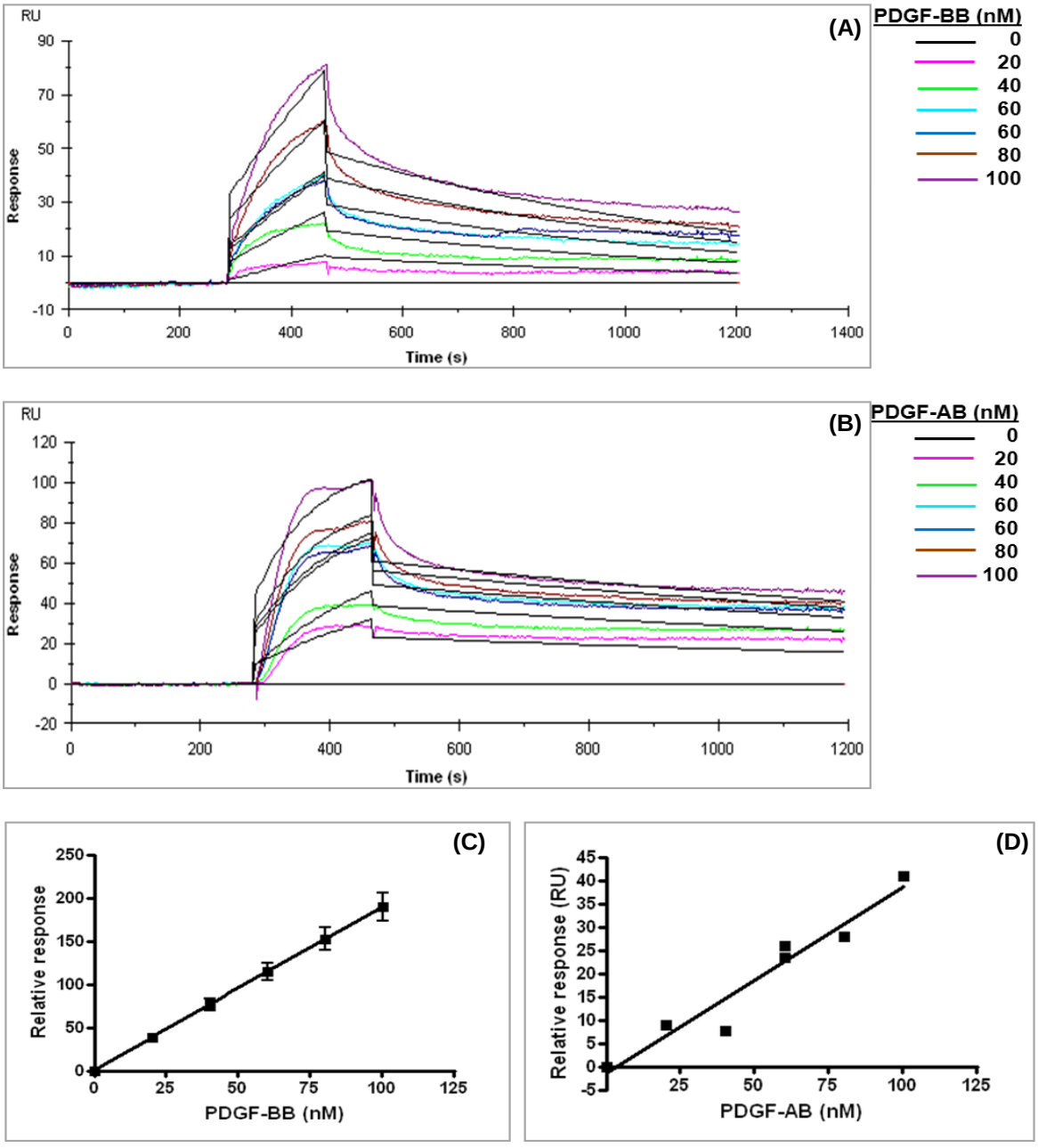

Figure 4.6: Kinetic data showing PDGF-AB or PDGF-BB binding to the b domains of NRP-1
The b domains of NRP-1 were immobilised on a CM5 chip and the binding of 0-100 nM of PDGF growth factors was examined. The BIAcore kinetic analysis revealed that **(A)** PDGF-BB bound to the b domains however, the curves did not fit well with the Langmuir 1:1 binding model. **(B)** PDGF-AB also bound to the b domains and showed an uncharacteristic dip at the plateau of the curve. The curves did not fit with the 1:1 Langmuir binding model and other binding models; (e.g. the one-site binding hyperbola) could not be fit to the PDGF curves. Kinetic data were plotted in Graph Pad Prism and both **(C)** PDGF-BB and **(D)** PDGF-AB showed a dose-dependent increase in binding to the b domains of NRP-1. As curves did not plateau, Bmax and K_d values could not be calculated.

4.1.4 Tuftsin inhibits VEGF-A but not PDGF growth factors binding to the b domains of NRP- 1

Tuftsin (TKPR) is a naturally occurring peptide which binds to the b domains of NRP-1 and selectively blocks VEGF-A_{165} binding (von Wronski et al., 2006). Co-crystallisation studies of NRP-1 and tuftsin helped to define that the C-terminus of VEGF-A_{165} interacts selectively with the b1 domain of NRP-1 (Vander Kooi et al., 2007). Tuftsin was used in this study to determine whether VEGF-A_{165} and the PDGF growth factors both bound to the b1 domain of NRP-1. Initially, tuftsin alone was flowed over the CM5 chip to assess the response, and due to the peptide only being four amino acids in length, a small response was generated (Figure 4.7). When VEGF-A_{165} was flowed over the b domains (+/-) tuftsin, tuftsin clearly inhibited the binding of VEGF-A_{165} to the b domains (Figure 4.7). When the PDGF growth factors were added (+/-) tuftsin, there was no inhibition of PDGF binding. PDGF-BB and PDGF-AB showed an increased response in the presence of tuftsin, which is indicative of the combined response of tuftsin and PDGF binding, generating the overall increased response (Figure 4.7). Together, these results suggest that the PDGF and VEGF growth factors bind to distinct sites within the b domains of NRP-1. These distinct binding specificities may therefore, allow PDGF and VEGF to bind simultaneously to NRP-1 and thus, not compete for the available NRP-1 on the cell surface.

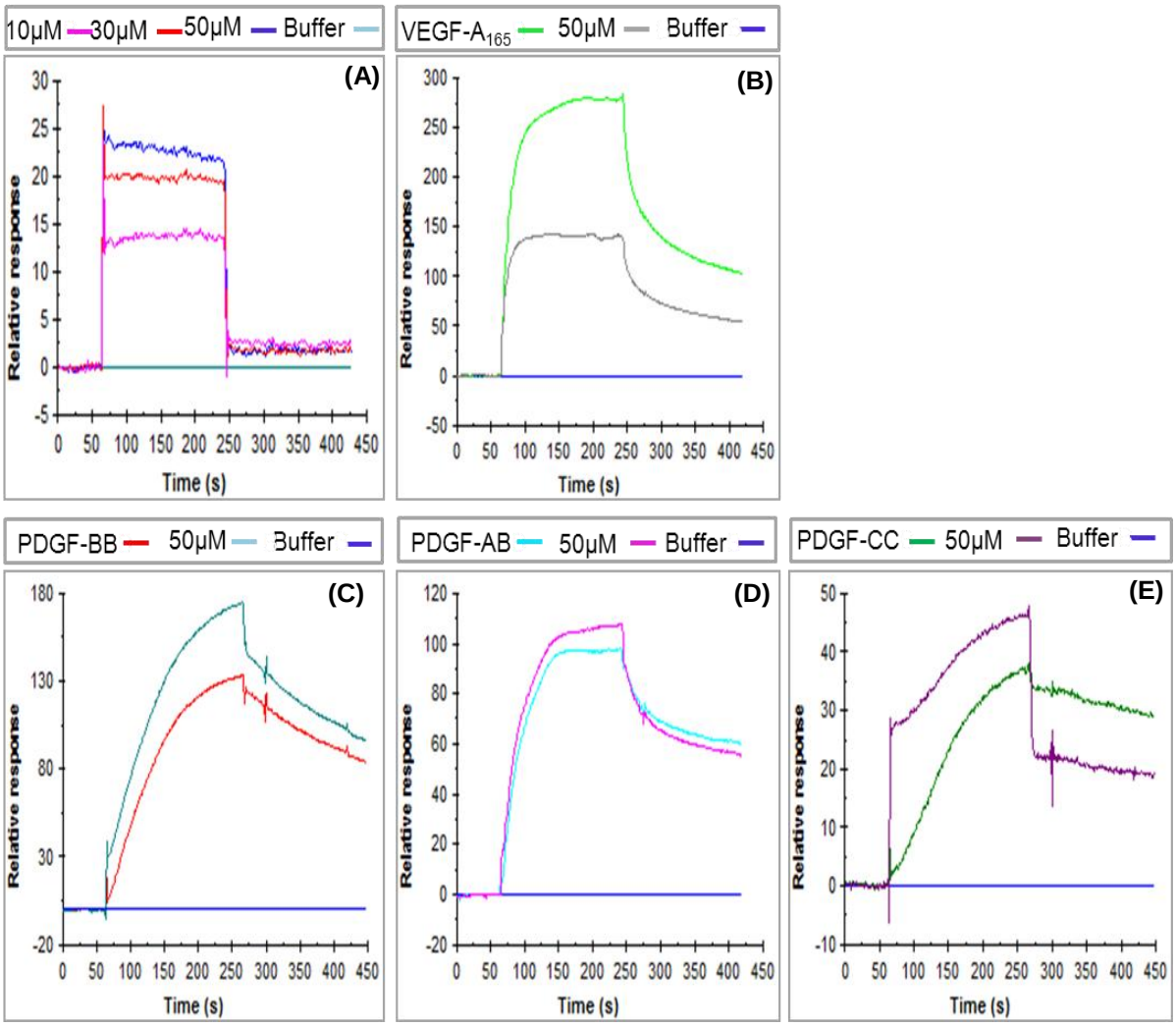

Figure 4.7: Tuftsin inhibits VEGF-$_{165}$ but not PDGF growth factor binding to the b domains of NRP-1

The b domains of NRP-1 were immobilised on a CM5 chip and the binding of VEGF-A_{165} or PDGF growth factors was assessed (+/-) 50 μM of tuftsin. **(A)** The binding of the b domains to 10, 30 and 50 μM of tuftsin were examined. The 50 μM concentration of tuftsin generated a maximal response of ~25 (RU). **(B)** 50 μM tuftsin inhibited VEGF-A_{165} binding to the b domains; however, 50 μM of tuftsin did not inhibit **(C)** PDGF-BB **(D)** PDGF-AB or **(E)** PDGF-CC binding to the b domains of NRP-1 suggesting that PDGF growth factors bind distinctly to VEGF-A_{165}. Analyte scans were repeated twice and generated similar responses and binding curves.

4.2 The interactions between NRP-1 and PDGFR in the selected mesenchymal tumour cell lines

Having established that PDGF growth factors have the capacity to bind to the b domains of NRP-1, the next aim was to determine whether PDGFs mediated an indirect interaction between NRP-1 and PDGFR-α or PDGFR-β in the selected mesenchymal tumour cell lines. Two methods were used to examine PDGF-mediated interactions between NRP-1 and PDGFRs, co-immunoprecipitation and proximity ligation assays.

4.2.1 Immunoblot analysis of NRP-1 immunoprecipitates +/- PDGF

As discussed in the introduction (Section 4.0), previous studies, using different cell types, have outlined that PDGF growth factors are/ are not required for NRP-1/PDGFR crosstalk (Ball et al., 2010; Pellet-Many et al., 2011). These studies suggest that the interactions between NRP-1 and PDGFR may be mediated differently depending on the cell type. The aim of this section was therefore, to examine whether PDGF growth factors were essential in mediating NRP-1/PDGFR interactions in the selected mesenchymal tumour cell lines.

Glioma cell lines, T98G and A172, and osteosarcoma cell lines, MG63 and KHOS-240S, were tested to determine if PDGF-AA or PDGF-BB mediated the association between NRP-1 and PDGFR-α or PDGFR-β. Briefly, serum-starved cells were treated either with 25 ng/mL of PDGF-AA, PDGF-BB or serum-free media before cell lysis. Total cell lysates were then incubated overnight with a NRP-1 monoclonal antibody (#3725 Cell Signaling Technology) and protein-G sepharose beads to isolate NRP-1 immune-complexes. Immune complexes were centrifuged and the lysate supernatant was removed and retained for immunoblot analysis. SDS loading buffer was added, and the immunoprecipitates and the cell lysates, were examined by immunoblot analysis. Primary antibodies against PDGFR-α or PDGFR- β were used in the immunoblots to assess if PDGFRs had co-immunoprecipitated with NRP-1. Immunoblots for NRP-1 were performed concurrently, on the same nitrocellulose membrane, to ensure that the immunoprecipitation (IP) reaction had isolated NRP-1 from the total lysate. The retained lysate (+ PDGF) was included in the immunoblot control to assess: (1) the proportion of NRP-1 which remained in the lysate after NRP-1 IP (2) if PDGFRs still remained in the lysate after NRP-1 IP. Detailed methods are described (Chapter 2, Section 2.4.3).

4.2.2 PDGFRs do not co-immunoprecipitate with NRP-1 in the osteosarcoma cell lines

KHOS-240S cells, which express abundant PDGFR-α and β, were chosen as the control cell line to determine if PDGFR-α or PDGFR-β remained in the cell lysate following NRP-1 IP. The immunoblot analysis of NRP-1 expression revealed that, following IP, only low levels of NRP-1 remained in the KHOS-240S cell lysates (Figure 4.8), yet a high level of NRP-1 could be detected in KHOS-240S NRP-1 IP samples (Figure 4.9). Following NRP-1 IP, PDGFR-α and PDGFR-β remained in the KHOS-240S cell lysate (Figure 4.8) and no PDGFR-α or PDGFR-β could be detected in the NRP-1 IP samples (Figure 4.9). In KHOS-240S cells, PDGF-AA or PDGF-BB stimulation did not alter the level of PDGFR-α or PDGFR-β in the NRP-1 IP samples. In the PDGFR-α immunoblots, the IgG lane showed the detection of a non-specific 100 kDa product, not corresponding to the molecular weight of either NRP-1 (120 and 80 kDa) or PDGFR-α (190 kDa), however this was not visible in the PDGFR-β immunoblot (Figure 4.9). Together these results suggest that in KHOS-240S cells (treated +/- PDGFs) PDGFRs remain in the cell lysate after NRP-1 is extracted by IP and thus, PDGFRs do not associate with NRP-1 in this cell line.

The MG63 cells express low levels of NRP-1 and reflecting this low expression, the immunoblot analysis detected a weak NRP-1 band in the NRP-1 IP samples. No NRP-1 protein remained in the MG63 cell lysate following the NRP-1 IP (Figure 4.10). In the PDGFR-α immunoblot, a non-specific 100 kDa product, that did not correspond to the molecular weight of either NRP-1 (120 and 80 kDa) or PDGFR-α (190 kDa), was detected in the IgG lane. No bands were detected in the IgG control for the PDGFR-β immunoblot. Following the NRP-1 IP of cell lysates, strong bands for PDGFR-α and PDGFR-β were detected in the cell lysate of MG63 cells, suggesting a high proportion of PDGFR remained in the cell lysate post NRP-1 IP. In the MG63 cells, no PDGFR-α or PDGFR-β could be detected in the NRP-1 IP samples, despite all the NRP-1 being extracted from the MG63 lysate (Figure 4.10). PDGF-AA or PDGF-BB stimulation did not alter the level of PDGFR-α or PDGFR-β in the NRP-1 IP samples. Together these results reveal that, in MG63 cells (+/- PDGF stimulation), no proportion of NRP-1 is associated with PDGFRs, as PDGFRs remain in the cell lysate after NRP-1 is extracted by IP.

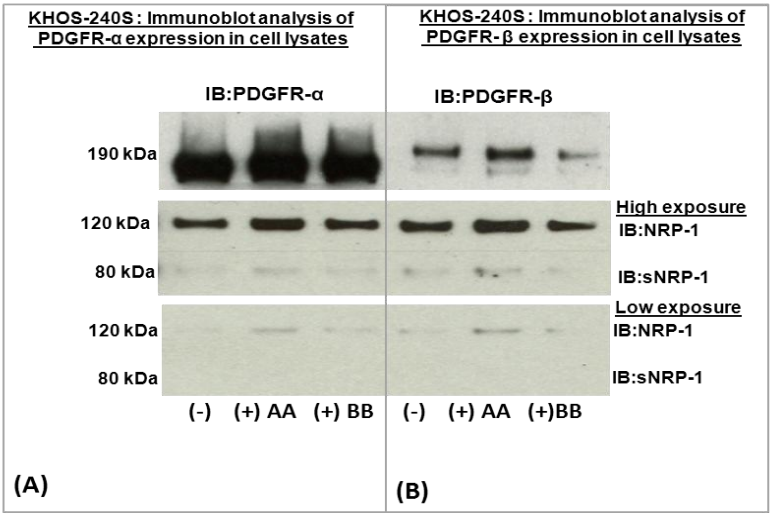

Figure 4.8: PDGFR-α and PDGFR-β were detected in the KHOS-240S total cell lysates
KHOS-240S cells were treated (+/-) PDGF-AA or PDGF-BB and total cell lysates were used in the NRP-1 IP reaction. Following the IP reaction, NRP-1 IP samples were isolated from the total cell lysate by centrifugation and the cell lysate was analysed by immunoblot. (**A)** and **(B)** illustrate that low levels of NRP-1 remained in the total cell lysate (+) or (-) PDGF-AA or BB and NRP-1 could only be detected after high exposure (1 hour). **(A)** PDGFR-α was abundantly expressed in cell lysates (+/-) PDGF and could be detected after an exposure time of 5 minutes. **(B)** PDGFR- β was also detected in the cell lysates. Immunoblots are representative of 2 experimental repeats.

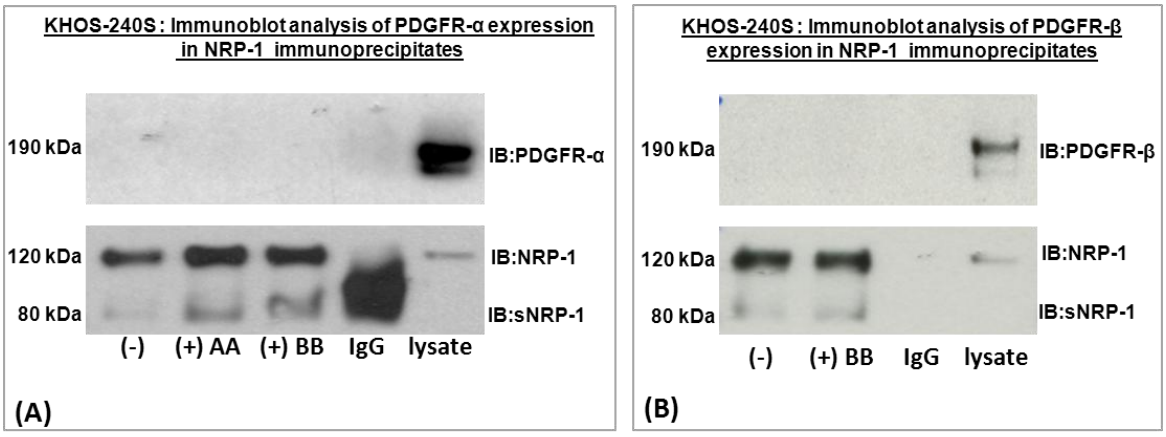

Figure 4.9: PDGFR-α and PDGFR-β did not co-IP with NRP-1 in KHOS-240S cells (+/-PDGF)
Immunoblot analysis of NRP-1 IP samples illustrated that (**A)** similar levels of NRP-1, but no detectable PDGFR-α, could be detected by immunoblot in samples (+/-) PDGF-AA or PDGF-BB. A non-specific 100 kDa product was detected in the IgG lane. Following the isolation of the NRP-1 immunoprecipitates from the cell lysates (by centrifugation), the cell lysate was also analysed by immunoblot. The results illustrated that, there were very low levels of NRP-1 but abundant PDGFR-α in the total cell lysate. **(B)** In the NRP-1 IP samples, similar levels of NRP-1 but no detectable PDGFR-β could be detected (+/-) PDGF-BB. No bands could be detected in the IgG control lane. Following the isolation of the NRP-1 immunoprecipitates from the cell lysates (by centrifugation), the cell lysate was also analysed by immunoblot. The results illustrated that, PDGFR-β remained in the total cell lysate; however, only very low levels of NRP-1 were retained in the cell lysate, indicating that the IP reaction had extracted the majority of NRP-1. Immunoblots are representative of 2 experimental repeats.

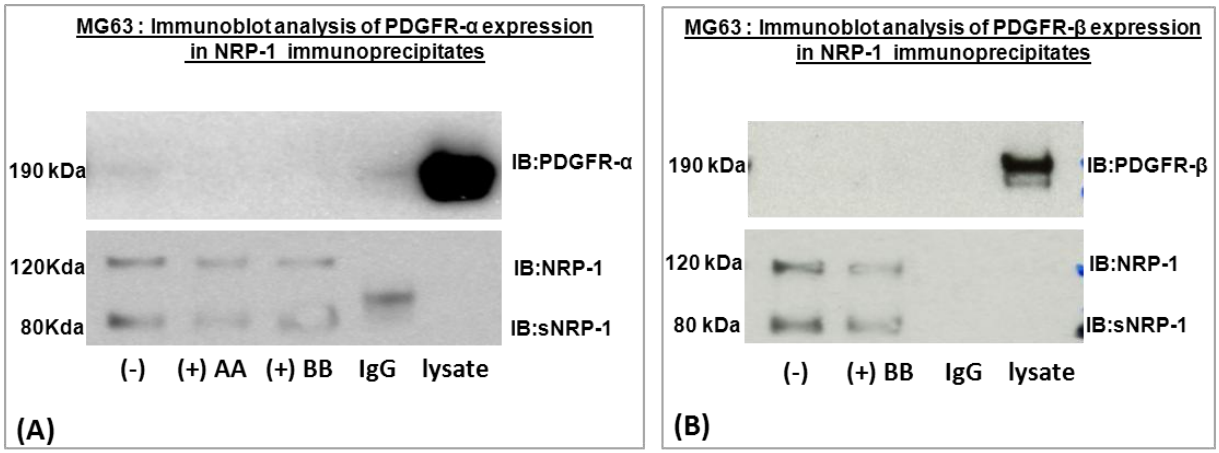

Figure 4.10: PDGFR-α and PDGFR-β did not co-IP with NRP-1 in MG63 cells (+/-PDGF)
Immunoblot analysis of NRP-1 IP samples illustrated that **(A)** similar levels of NRP-1, but no detectable PDGFR-α, could be detected by immunoblot in samples (+/-) PDGF-AA or PDGF-BB. A non-specific 100 kDa product was detected in the IgG lane. Following the isolation of the NRP-1 immunoprecipitates from the cell lysates (by centrifugation), the cell lysate was also analysed by immunoblot. The results illustrated that no detectable NRP-1, but abundant PDGFR-α remained in the lysate. **(B)** In the NRP-1 IP samples, similar levels of NRP-1 but no detectable PDGFR-β could be detected by immunoblot in samples (+/-) PDGF-BB. No bands could be detected in the IgG control lane. Following the isolation of the NRP-1 immunoprecipitates from the cell lysates (by centrifugation) the cell lysate was also analysed by immunoblot. The results illustrated that PDGFR-β remained in the total cell lysate; however, no detectable NRP-1 was retained in the cell lysate, indicating that the IP reaction had extracted NRP-1 but not PDGFR-β. Immunoblots are representative of 2 experimental repeats.

4.2.3 PDGFRs do not co-immunoprecipitate with NRP-1 in the glioma cell lines

ELISA experiments (see Chapter 5) had suggested that T98G cells were primarily responsive to PDGF-BB and not to PDGF-AA. Thus, T98G cells were only treated (+/-) PDGF-BB (prior to lysis). Immunoblot results showed that high levels of NRP-1 could be detected in the T98G NRP-1 IP samples (+/-) PDGF-BB. Both PDGFR-α and PDGFR-β could not be detected in the NRP-1 IP samples (+/-) PDGF-BB, suggesting no significant association between NRP-1 and PDGFRs in T98G cells. No bands were detected in the IgG negative control lane (Figure 4.11), showing that the NRP-1 pull down was specific and could not be attributed to, for example, the protein-G beads binding non-specifically to proteins within the cell lysates. Following the isolation of the NRP-1 immunoprecipitates (by centrifugation) from the T98G cell lysates, lysates were also analysed by immunoblot. The results showed that, following NRP-1 IP, a very low level of NRP-1 remained in the cell lysate, however, a significant level of PDGFR-α and PDGFR-β was retained in the T98G cell lysate (Figure 4.11).

The A172 cells predominantly express PDGFR-β and trace levels of PDGFR-α (see Chapter 3, Section 3.3.1), so again A172 cells were only treated (+/-) PDGF-BB (prior to lysis) for the NRP-1 IP assays. The immunoblot results illustrated that NRP-1 was abundantly expressed in NRP-1 IP samples (+/-) PDGF-BB. In A172 cells, PDGFR-β could not be detected in the NRP-1 IP samples (+/-) PDGF-BB. Following the removal of NRP-1 IP samples (by centrifugation) from the A172 total lysates, lysates were analysed by immunoblot. The immunoblot results illustrated that following NRP-1 IP, a low proportion of NRP-1 was retained in the cell lysate although high levels of PDGFR-β remained in the cell lysate (Figure 4.12). Together these results suggest that PDGFR-β does not co-IP with NRP-1 in A172 cells. No bands for either NRP-1 or PDGFR-β were detected in the IgG negative control lane (Figure 4.12).

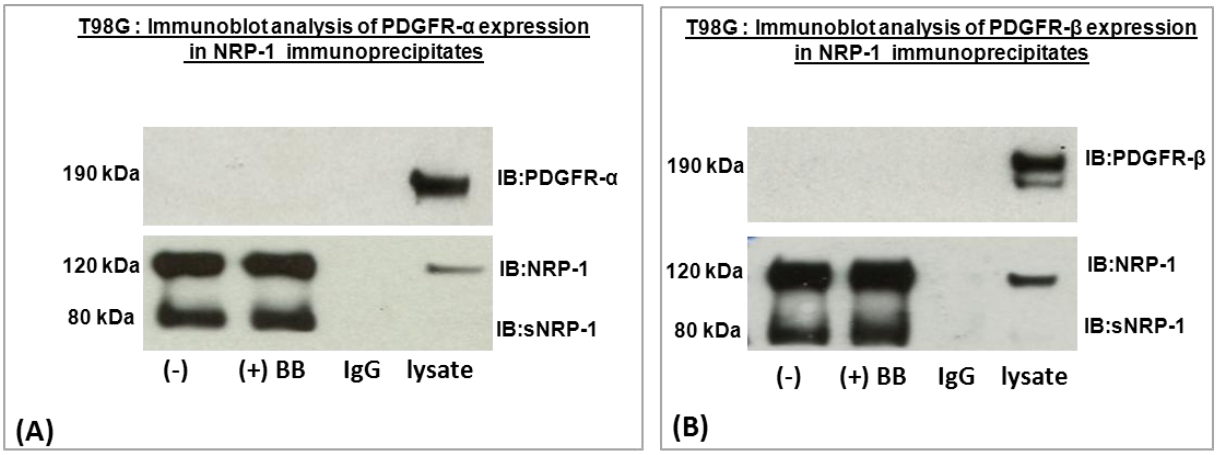

Figure 4.11: PDGFR-α or PDGFR-β did not co-IP with NRP-1 in T98G cells
Immunoblot analysis of NRP-1 IP samples illustrated that **(A)** similar levels of NRP-1, but no detectable PDGFR-α, were detected in samples (+/-) PDGF-BB. No bands were detected in the IgG lane. Following the isolation of the NRP-1 immunoprecipitates from the cell lysates (by centrifugation), the cell lysate was also analysed by immunoblot. The results illustrated that there were very low levels of NRP-1 but abundant PDGFR-α in the total cell lysate. **(B)** In the NRP-1 IP samples, similar levels of NRP-1 but no detectable PDGFR-β could be detected (+/-) PDGF-BB. No bands could be detected in the IgG control lane. Following the isolation of the NRP-1 immunoprecipitates from the cell lysates (by centrifugation), the cell lysate was also analysed by immunoblot. The results illustrated that, PDGFR-β remained in the total cell lysate although only very low levels of NRP-1 were retained in the cell lysate, indicating that the IP reaction had extracted the majority of NRP-1. Immunoblots are representative of 2 experimental repeats.

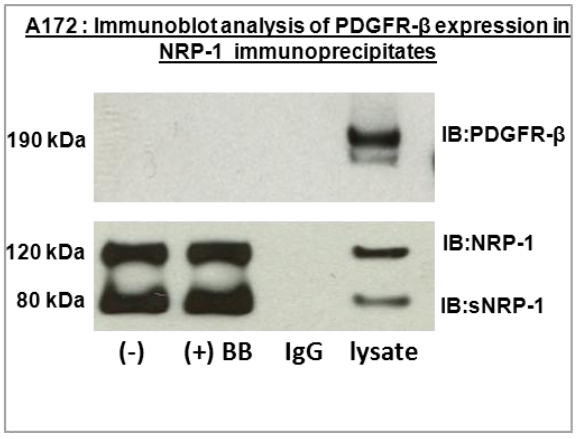

Figure 4.12: PDGFR-β did not co-IP with NRP-1 in A172 cells (+/-PDGF-BB)
Immunoblot analysis of NRP-1 IP samples illustrated that (A) In the NRP-1 IP samples, similar levels of NRP-1 but no detectable PDGFR-β could be detected (+/-) PDGF-BB. No bands could be detected in the IgG control lane. Following the isolation of the NRP-1 immunoprecipitates from the cell lysates (by centrifugation), the cell lysate was also analysed by immunoblot. The results illustrated that, PDGFR-β remained in the total cell lysate; however, only very low levels of NRP-1 were detected in the cell lysate, indicating that the IP reaction had extracted the majority of NRP-1. Immunoblots are representative of 2 experimental repeats.

4.2.4 Examination of NRP-1 and PDGFR interactions in situ

Two methods were used to investigate PDGF mediated NRP-1/PDGFR crosstalk in situ. The proximity ligation assay (PLA) was used to quantify the interaction between NRP-1 and PDGFR. Immunofluorescence analysis was used to determine the degree of cellular co-localisation between NRP-1 and PDGFR.

The PLA technology has been developed to allow the detection and quantification of individual proteins and protein interactions in situ (Söderberg et al., 2006, 2008). The schematic of the assay is outlined in Figure 4.13 (detailed methods can be found in Chapter 2, Section 2.1.3). Using the PLA, the cellular localisation of protein interactions can be visualised and the method is extremely sensitive (due to the amplification step in the protocol). The sensitivity of the PLA assay, therefore, allows the detection of even transient and weak protein interactions which cannot be detected by co-IP. The sensitivity of the PLA technique was exemplified in a report by Nilsson et al (2010) where heterodimeric interactions between VEGFR2/3 were detected by PLA and not co-IP (I. Nilsson et al., 2010). In view of such findings, it was possible that the increased sensitivity of the PLA may detect NRP-1 and PDGFR interactions in mesenchymal tumour cells.

In addition to using the PLA, slides were stained with the same primary antibodies for conventional immunofluorescence to assess the degree of co- localisation between NRP-1 and PDGFRs (+/-) PDGF growth factors (for methods see Chapter 2, Section 2.1.3). The Image J co-localisation colour-map function was used to analyse and quantify the co-localisation. This analysis determines correlation of intensities between pairs of individual pixels with the same spacial co-ordinates (Jaskolski et al., 2005). This value is then used to generate a correlation index (Icorr*)* which quantifies the fraction of positively correlated pixels in a field of view and, as reported (Apostolova et al., 2011; Lo Buono et al., 2011), quantifies the degree of co-localisation. One advantage of the colour-map analysis is that it avoids setting a manual image threshold which can introduce bias. This colour-map analysis was also reported to accurately differentiate subtle changes in co-localisation which other analysis methods such as the Pearson r index could not detect. Therefore, Icorr values were used to detect differences in NRP-1 and PDGFR co-localisation (+/-) PDGF growth factors.

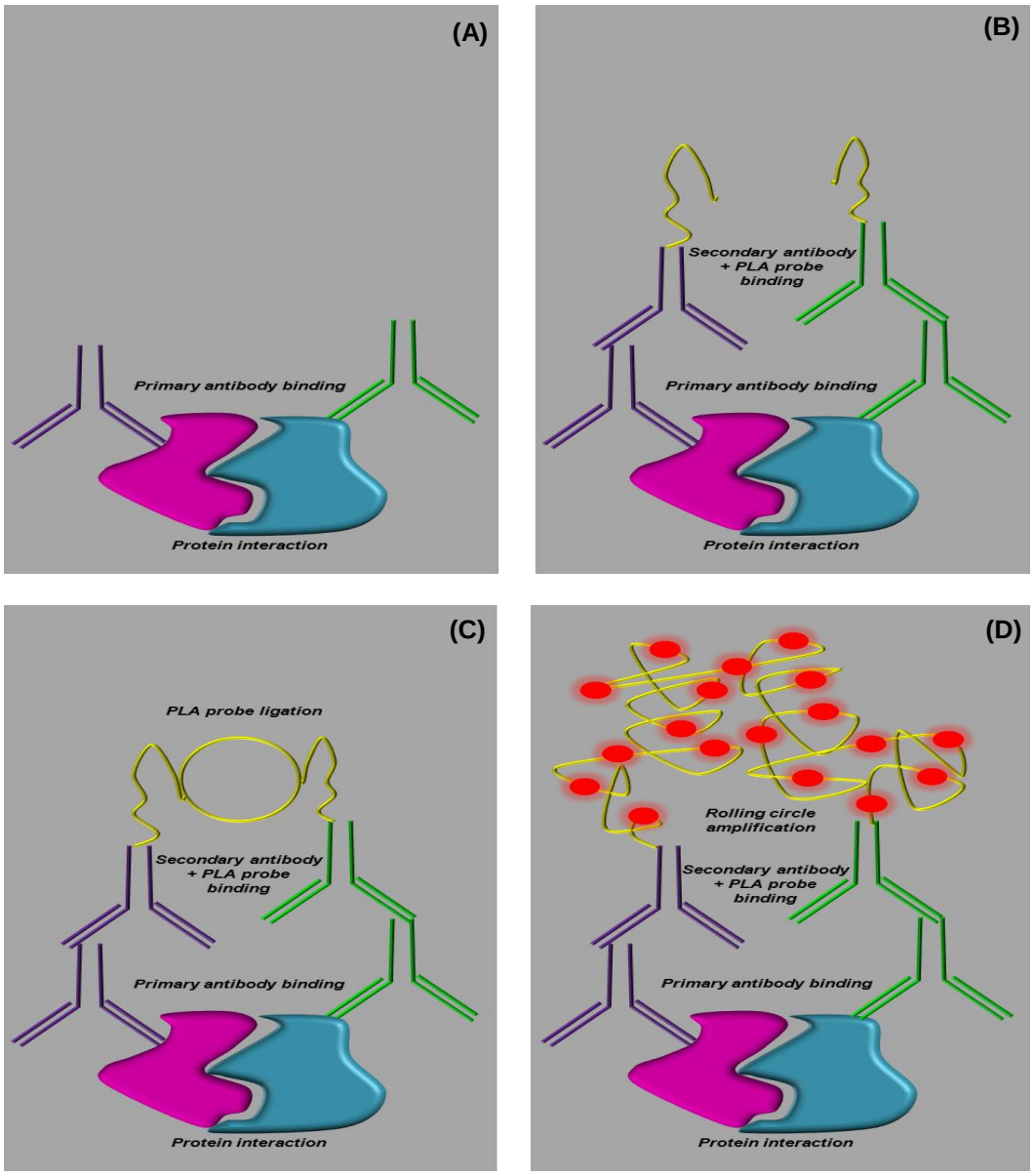

Figure 4.13: Detecting protein interactions using the in situ proximity ligation assay
A schematic of the proximity ligation assay protocol. **(A)** Primary antibodies, raised in different species, are incubated and bind to target proteins. **(B)** Secondary antibodies conjugated to oligonucleotides (known as PLA probes) are added. **(C)** Ligation solution, containing ligase and the complementary oligonucleotides, is added to the reaction. The oligonucleotides hybridise to the PLA probes and, if the 2 proteins are in close proximity, the oligonucleotides bind together to form a closed circle. **(D)** Amplification solution, containing polymerase and fluorescently labelled oligonucleotides, is added. The ligated circle is used as a template and rolling circle amplification (RCA) generates multiple copies. The fluorescently-labelled oligonucleotides then hybridise to the RCA product, generating a signal which can be visualised as a distinct fluorescent spot.

It was essential that the primary antibodies used for the PLA analysis specifically detected the protein of interest, to avoid the amplification of nonspecific signals; consequently, the primary antibodies were validated. Using KHOS-240S cells, which express abundant PDGFR-α and PDGFR-β (see Chapter 3, Section 3.3), the specificity of the PDGFR antibodies was analysed by immunofluorescence (Figure 4.14). Antibodies against PDGFR-α and PDGFR-β showed a very similar pattern of staining, with widespread staining in the cytoplasm and stronger staining around the perinuclear region (Figure 4.14). The similar staining pattern of all the different PDGFR antibodies suggested that they were detecting the same protein and reflecting the true cellular localisation of PDGFR. For the PLA assay, an anti-human mouse antibody had to be paired with an anti-human rabbit antibody, due to the specificity of the PLA probes. The selected NRP-1 antibody was an anti-human mouse antibody (as detailed below), thus the PDGFR antibodies had to be anti-human rabbit. Based on the staining observed (Figure 4.14) and previously published data using the antibodies for immunofluorescence or the PLA, the rabbit anti-human PDGFR-α (sc-339) polyclonal antibody (Santa Cruz Biotechnology) (Ball et al., 2010) and the rabbit anti-human PDGFR-β monoclonal antibody (#3169 Cell Signaling Technology) was selected (Koos et al., 2009).

Using the MSCs, the NRP-1 antibodies were evaluated. The results illustrate that the two NRP-1 antibodies showed different staining patterns with the polyclonal sc-5541 antibody (Santa Cruz Biotechnology) staining primarily around the perinuclear region and the monoclonal MAB38701 antibody (R&D Systems) staining throughout the cell, with some cell membrane staining. Due to the diversity of the staining patterns, the specificity of the antibodies was verified through silencing NRP-1 expression (see Chapter 2, Section 2.1.3.1). Total cell fluorescence for the images was quantified in Image J, as described by Burgess et al (A. Burgess et al., 2010). NRP-1 siRNA induced a significant decrease in fluorescence in MSCs labelled with the MAB-38701 antibody (R&D Systems) However, in MSCs labelled with the sc-5541 antibody (Santa Cruz Biotechnology) NRP-1 siRNA induced no significant change in fluorescence (Figure 4.15). NRP-1 siRNA was confirmed by Western blot analysis (Figure 4.15). Together, these results suggested that the MAB-38701 NRP-1 antibody (R&D Systems) had a greater degree of specificity and thus, this antibody was selected for the PLA and immunofluorescence assays.

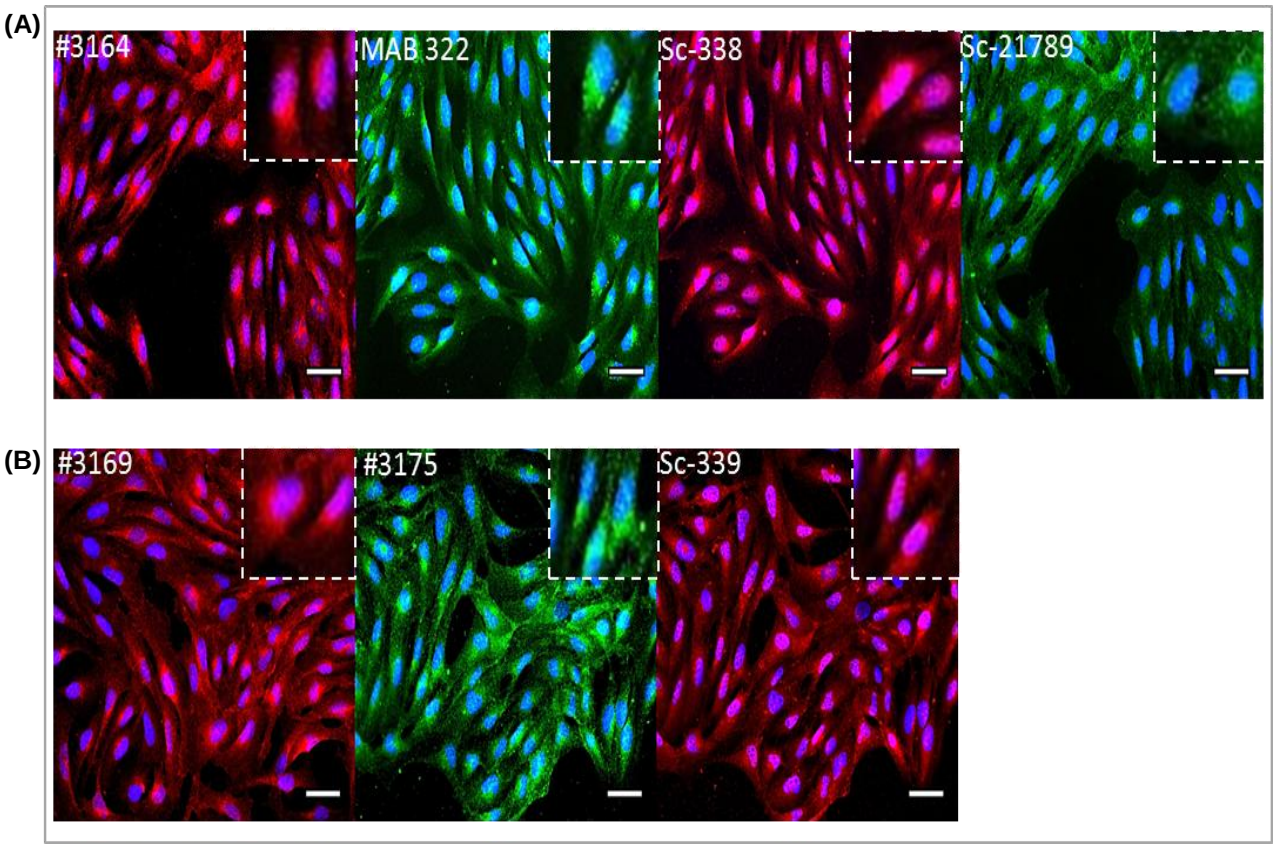

Figure 4.14: Evaluation of PDGFR antibody specificity using KHOS-240S cells

All PDGFR antibodies were diluted 1/200 in 3% (w/v) fish-skin gelatin before being incubated overnight at 4°C and secondary labelling was performed using either Alexa Fluor 488 conjugated secondary antibody (green) or Alexa Fluor 598 conjugated secondary antibody (Red) (see, Section 2.1). Nuclei appeared blue following DAPI staining. **(A)**The PDGFR-α antibodies; #3164, MAB-322 and sc-338; all stained weakly throughout the cytoplasm with strong staining concentrated around the cell nucleus. Using the sc-21789 antibody, perinuclear staining was less evident. Enlarged images are illustrated in the top right-hand corner of each image. **(B)** PDGFR-β antibodies: #3169, #3175, sc-339 showed widespread cytoplasmic staining, however, stronger staining could be visualised around the cell nucleus. Enlarged images are illustrated in the top right-hand corner of each image. Scale bar=50 μm. Images were collected on a widefield microscope (Leica DM RXA) using a 20x objective and captured using a Coolsnap EZ camera driven by MetaVue software. Results are representative of at least two independent experiments.

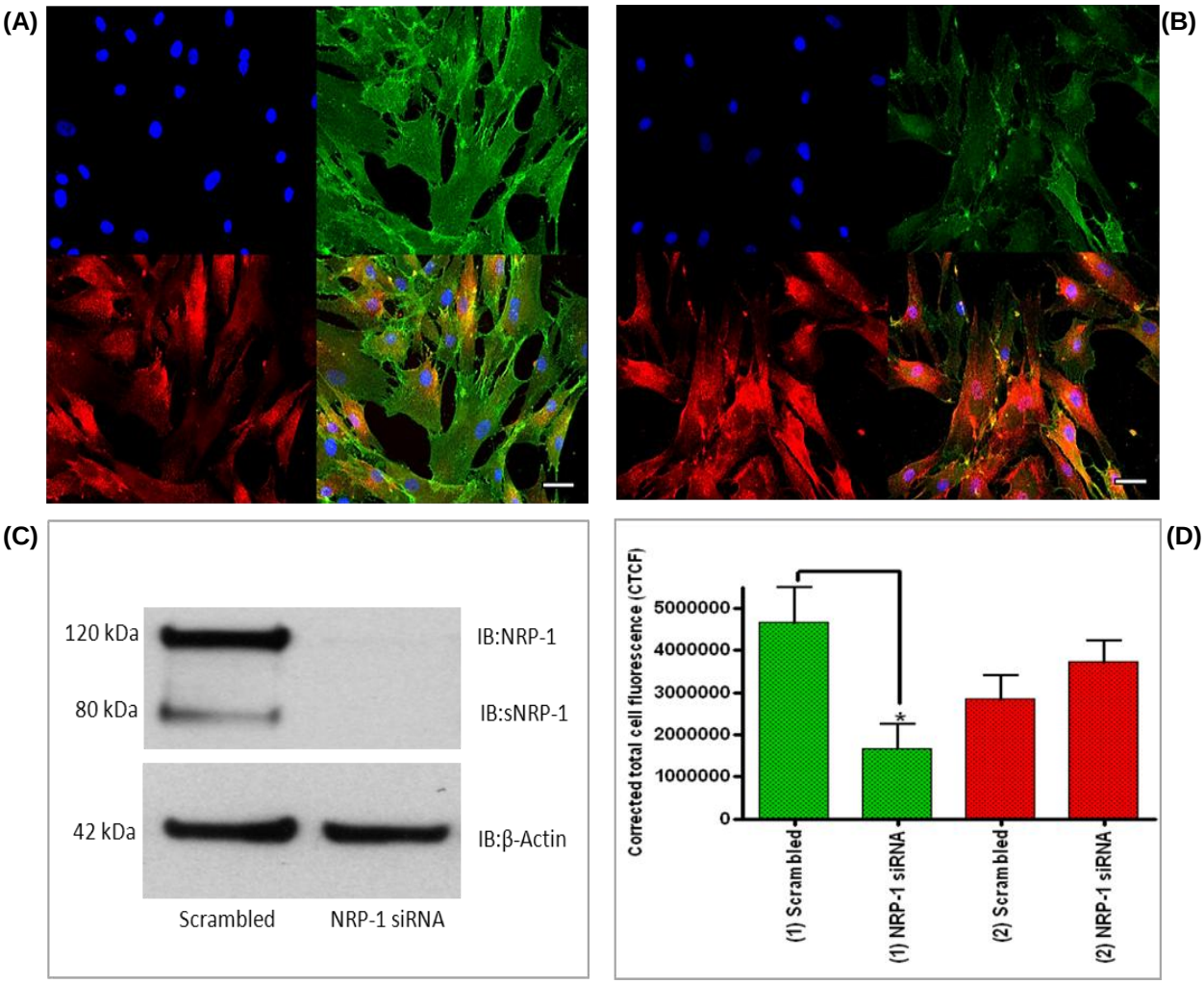

Figure 4.15: Evaluation of NRP-1 antibody specificity

MSCs were used to evaluate the NRP-1 primary antibodies. NRP-1 antibodies were diluted 1/200 in 3% (w/v) fish-skin gelatin, added to the fixed MSCs and incubated overnight at 4°C. NRP-1 MAB-38701 was detected by Alexa Fluor 488 conjugated secondary antibody (green) and NRP-1 sc-5541 detected using Alexa Fluor 598 conjugated secondary antibody (Red) (see, Section 2.1). Nuclei appeared blue following DAPI staining. **(A)** In MSCs treated with control scrambled oligonucleotides MAB-38701 detected widespread NRP-1, with some evident membrane staining. The sc-5541 antibody detected NRP-1 staining largely in the perinuclear region. **(B)** In MSCs treated with NRP-1 siRNA a decrease in staining intensity could be observed using the MAB-38701 NRP-1 antibody, however, no change in staining intensity was observed with the sc-5541 NRP-1 antibody. **(C)** Immunoblot blot analysis confirmed NRP1 siRNA in MSCs **(D)** The histogram plots the corrected total cell fluorescence (CTCF) calculated using Image J. CTCF using MAB-38701 is represented by the green bars, and the red bars represent CTCF using sc-5541. Asterisks * indicate significance (*P<0.05, calculated by one way ANOVA)**.** Scale bar=50 µm. Images were collected on a widefield microscope (Leica DM RXA) using a 20x objective and captured using a Coolsnap EZ camera driven by MetaVue software. Results are representative of at least two independent experiments.

In all experimental repeats for all the cells (A172, T98G, MG62 and KHOS-240S), technical controls were included to confirm the specificity of the results. For the immunofluorescence analysis, secondary antibody only controls; anti-mouse Alexa Fluor 488 and anti-rabbit Alexa Fluor 594; were tested. No staining could be detected in the absence of primary antibody, confirming that the secondary antibodies were not binding non-specifically to the cells (Figure 4.16). For the PLA analysis, single primary antibody controls were tested; NRP-1 (MAB-38701) only, PDGFR-α (sc-338) only, PDGFR-β (#3169) only. When only one primary antibody was incubated, PLA signals were not detected (Figure 4.17), indicating that the PLA signal is specific and reliant on the hybridisation of the two PLA probes. Having established that both the PLA and immunofluorescence analysis are specific, the mesenchymal tumour cell lines were assayed to determine whether PDGF mediated an interaction between NRP-1 and PDGFR.

Using T98G cells, the immunofluorescence analysis illustrated that NRP-1 localised to the cell membrane, whereas PDGFR-α showed strong cytoplasmic staining. PDGF-AA did not affect the localisation of NRP-1 or PDGFR-α. Although some co-localisation between NRP-1 and PDGFR-α was detected (indicated by the hotter colours on the co-localisation colour-map), this was not widespread and not significantly increased by PDGF-AA stimulation. PDGFR-α staining was also only detected in a sub-population of the T98G cells, indicating a heterogeneous expression of PDGFR-α. PDGFR-β staining was more widespread throughout the T98G cell population and PDGFR-β localisation was intracellular and concentrated around the nucleus. Again, some co-localisation was evident between PDGFR-β and NRP-1; however, PDGF-BB stimulation did not significantly increase the level of co-localisation (Figure 4.18).

The PLA analysis revealed an interaction between NRP-1 and PDGFR-α, denoted by the detection of PLA fluorescent signals in T98G cells. When T98G cells were stimulated with PDGF-AA, no significant increase the number of PLA signals was detected, suggesting that PDGF-AA did not increase the interactions between NRP-1 and PDGFR-α. The PLA revealed that PDGFR-β and NRP-1 interacted to a lesser extent than NRP-1 and PDGFR-α, denoted by a decrease in the PLA signal number/cell. PDGF-BB stimulation did not significantly increase the number of PLA signals, which suggested that the interaction between NRP-1 and PDGFR-β was also not increased (Figure 4.19). Together these data illustrated that there was an interaction between NRP-1 and PDGFR-α and β in T98G cells, however NRP-1/PDGFR interactions were not dependent on PDGF.

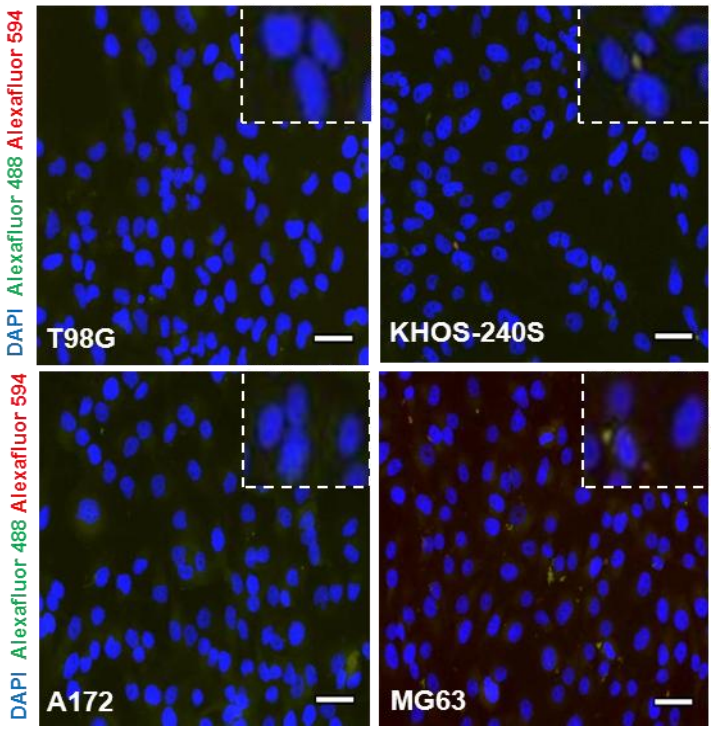

Figure 4.16: The mesenchymal cell lines were labelled with secondary antibodies only
Tumour cell lines were treated in accordance with the immunofluorescence protocol (see Chapter 2, Section 2.1.3) except that the primary antibody was omitted. Cells were instead incubated overnight in 3% (w/v) fish skin gelatin without primary antibody. Only the DAPI nuclear stain could be visualised, indicating that the secondary antibody did not show non-specific binding to cells and that the cells displayed little auto-fluorescence. Enlarged images are illustrated in the top right-hand corner of each image. Images were collected on a widefield microscope (Leica DM RXA) using a 20x objective and captured using a Coolsnap EZ camera driven by MetaVue software. Results are representative of at least two independent experiments.

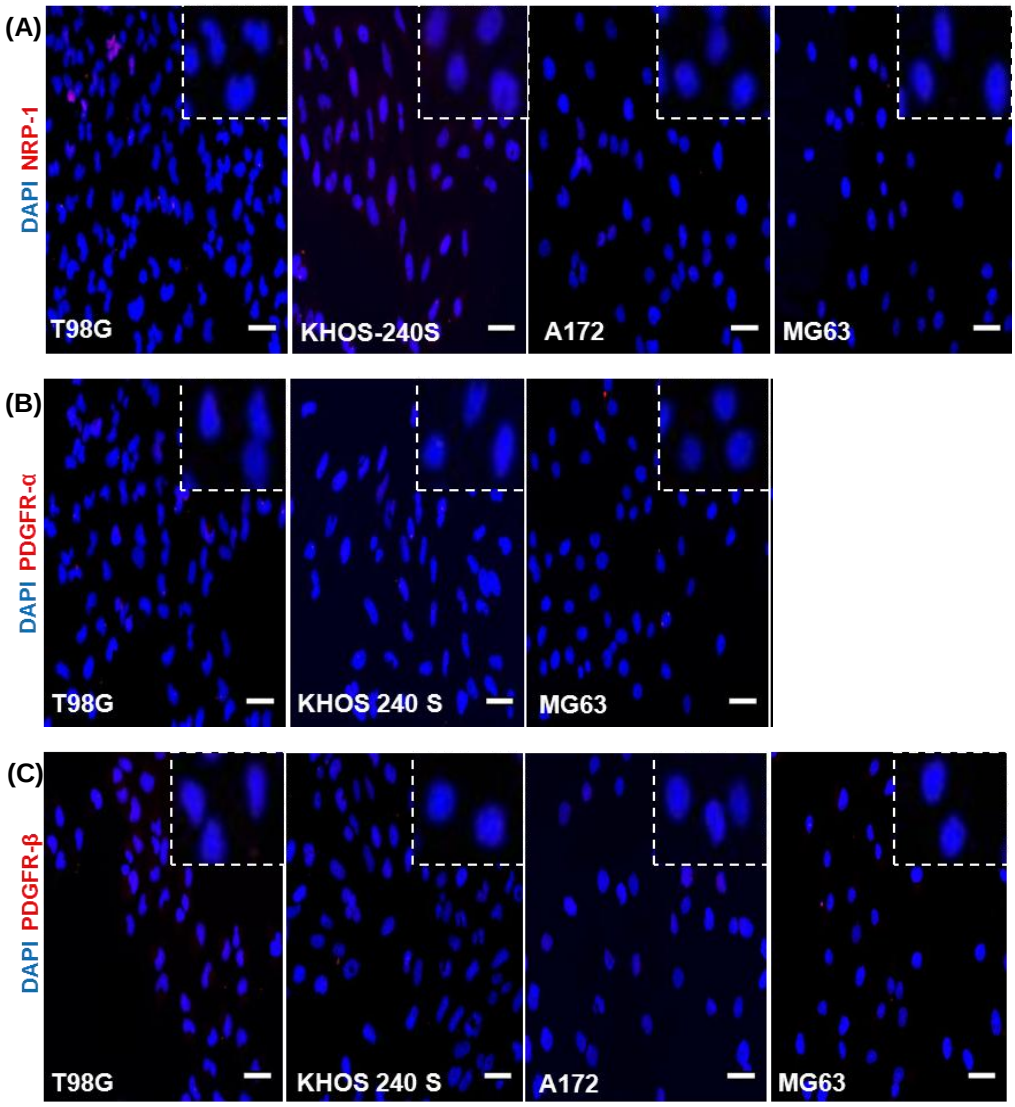

Figure 4.17: Technical PLA controls: The mesenchymal tumour cell lines were labelled with single primary antibodies

Cell lines were treated in accordance to the PLA protocol, except that one primary antibody was omitted. Row **(A)** shows the PLA signals detected using the NRP-1 MAB-38701 antibody. Row **(B)** shows the PLA signals detected by the PDGFR-α (Sc-339) antibody. Row **(C)** shows the PLA signals detected by the PDGFR-β (#3169) antibody. DAPI nuclear staining clearly indicated the number of cells in the field of view, yet only trace or no PLA signals could be visualised indicating that the non-specific background was very low for the PLA. Scale bar=50 µm. Images were collected on a widefield microscope (Leica DM RXA) using a 20x objective and captured using a Coolsnap EZ camera driven by MetaVue software. Results are representative of at least two independent experiments.

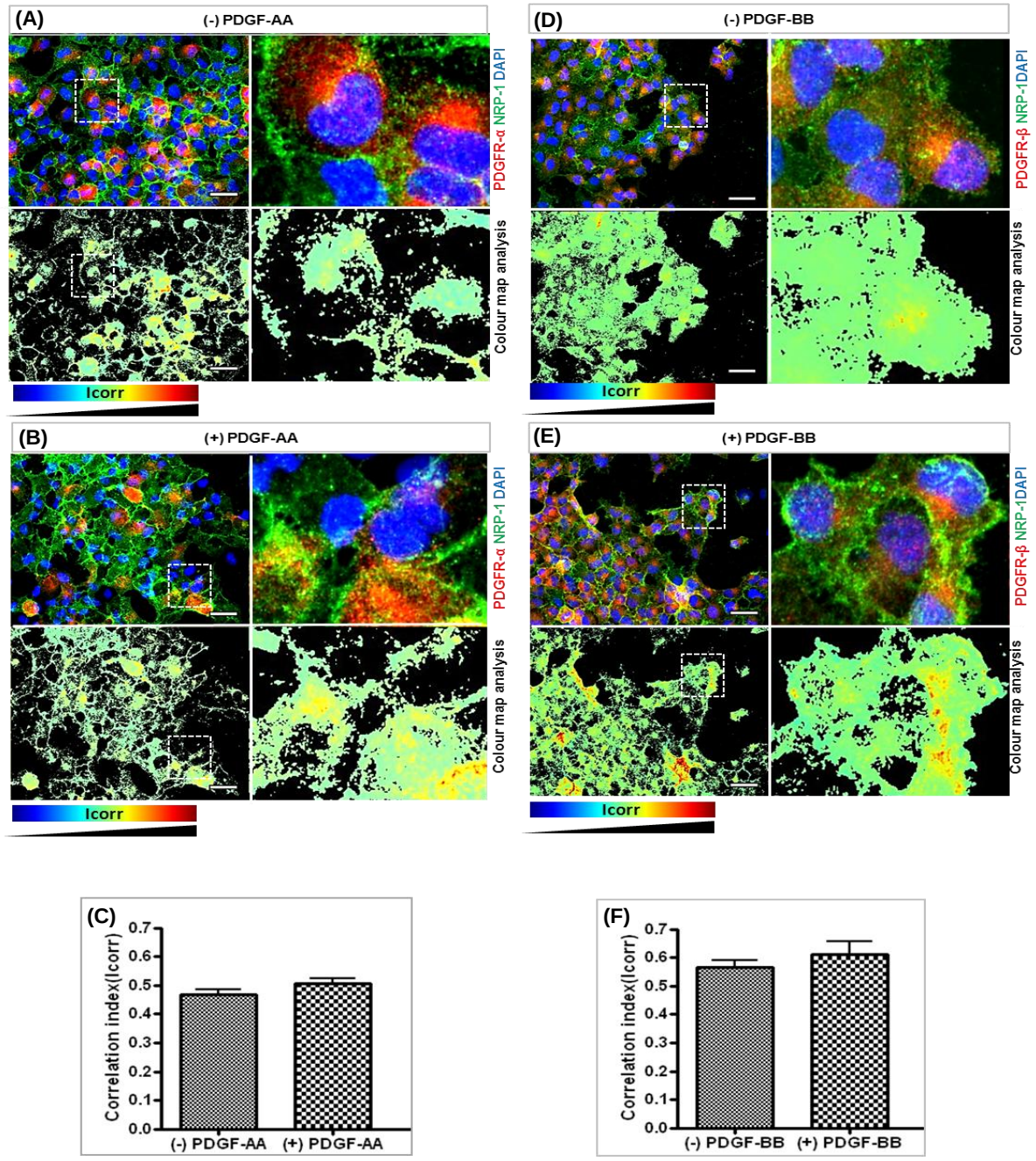

Figure 4.18: Immunofluorescence analysis of co-localisation between NRP-1 and PDGFR-α or PDGFR-β in T98G cells

The left panels illustrate the detection of NRP-1 (green), and PDGFR-α (red) in untreated control cells **(A)** or cells treated with PDGF-AA **(B)**. The right panels illustrate the detection of NRP-1 (green), and PDGFR-β (red) in untreated control cells **(D)** or cells treated with PDGF-BB **(E)**. A colour-map analysis (illustrated in the lower rows of each quadrant) has been used to calculate the correlation index (Icorr) between NRP-1 and PDGFR-α or β, with the hotter colours representing a greater degree of co-localisation. Inset the left panels, a white square outlines a magnified region to clearly visualise areas of co-localisation. Icorr values, (representative of 6 independent images and 2 experimental repeats), are represented in histograms in, **(C)** NRP-1 and PDGFR-α, and **(F)** NRP-1 and PDGFR-β. Images were collected on a widefield microscope (Leica DM RXA) using a 20x objective and captured using a Coolsnap EZ camera driven by MetaVue software. Scale bar =50 μM.

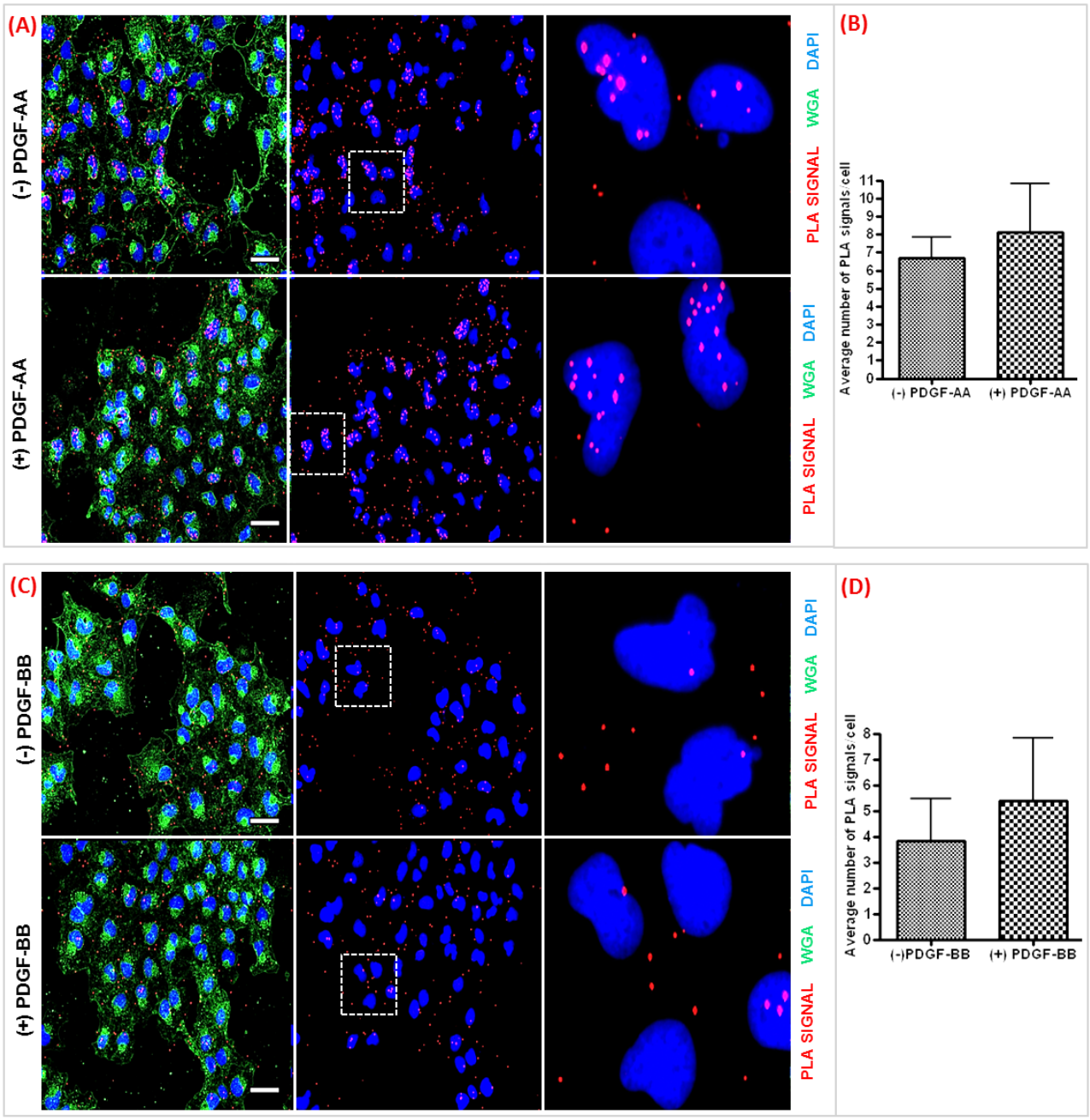

Figure 4.19: In situ PLA detection of NRP-1 and PDGFR-α or PDGFR-β interactions in T98G cells.

In **(A)** and **(C)** the left panel illustrates T98G cells treated (+/-) PDGF-AA or (+/-) PDGF-BB. The PLA signals (red) denote NRP-1: PDGFR-α or NRP-1: PDGFR-β interactions. Cells were also labelled with wheat germ agglutinin (green) to visualise the cell morphology and ensure PLA signals were localised to cells. Inset the central panel, the white dashed square outlines a magnified region (illustrated in the right panel) to clearly visualise the PLA signals. In **(B)** and **(D)** the histograms represents quantified **(B)** NRP-1: PDGFR-α; **(D)** NRP-1: PDGFR-β PLA signals (normalised to cell number). Plotted values were determined using blob finder software. Images are representative of 6 independent images and 2 experimental repeats. Images were collected on a widefield microscope (Leica DM RXA) using a 20x objective and captured using a Coolsnap EZ camera driven by MetaVue software. Scale bar=50 μm.

Immunofluorescence analysis of A172 cells illustrated that NRP-1 localisation in the cell membrane and throughout the cytoplasm. Interestingly NRP-1 clustered at certain points in the cell membrane and, in some cells NRP-1 appeared to be localised to points of cell spreading. This observation is consistent with reports that NRP-1 can interact with integrin α5β1 at sites of cell adhesion and spreading (Valdembri et al., 2009) and that NRP-1 helps to mediate the adhesion of tumour cells (Jia et al., 2010). PDGFR-β staining was punctate and distributed throughout the cytoplasm of the cell. Co-localisation analysis revealed some perinuclear co-localisation between NRP-1 and PDGFR-β, indicated by the yellow and red points on the co-localisation colour-map. PDGF-BB stimulation did not significantly affect the level of co-localisation between NRP-1 and PDGFR-β (Figure 4.20).

The PLA analysis, using A172 cells, detected an interaction between NRP-1 and PDGFR-β, which was denoted by positive PLA staining. Following PDGF-BB stimulation, a significant increase ($P<0.05$) in the number of PLA signals was recorded. This result suggested that, in A172 cells, PDGF-BB potentiated the interaction between NRP-1 and PDGFR-β. Together these data suggest that PDGF-BB may promote the interaction between NRP-1 and PDGFR-β in A172 cells however, based on the immunofluorescence analysis, the co-localisation may not occur primarily at the cell surface (Figure 4.21).

The immunofluorescence analysis of the KHOS-240S cells revealed that NRP-1 was localised throughout the cytoplasm with some membrane staining. PDGFR-α localisation was concentrated around the nucleus with no apparent cytoplasmic or membrane staining. Co-localisation mapped to a small area of the cell around the nucleus. PDGF-AA stimulation of KHOS-240S cells did not affect the degree of co-localisation between NRP-1 and PDGFR-α. PDGFR-β staining was punctate and indicated a widespread intracellular localisation of PDGFR-β in KHOS-240S cells. NRP-1 also stained throughout KHOS-240S cells with the strongest staining localised to the cell membrane. Co-localisation between NRP-1 and PDGFR-β could be detected in the perinuclear region; however, the level of co-localisation did not significantly increase after PDGF-BB stimulation (Figure 4.22).

PLA analysis revealed an interaction between PDGFR-α and NRP-1 in KHOS-240S cells. On PDGF-AA stimulation, the number of PLA signals significantly increased, suggesting that PDGF-AA potentiated the interaction between NRP-1 and PDGFR-α. The detection of PLA signals also denoted that PDGFR-β and NRP-1 interact; however, PDGF-BB did not significantly increase this interaction (Figure 4.23). Overall this result suggests that, in KHOS-240S cells, PDGF is not crucial for an interaction to occur between NRP-1 and PDGFRs, however, PDGF-AA can potentiate the interaction between PDGFR-α and NRP-1.

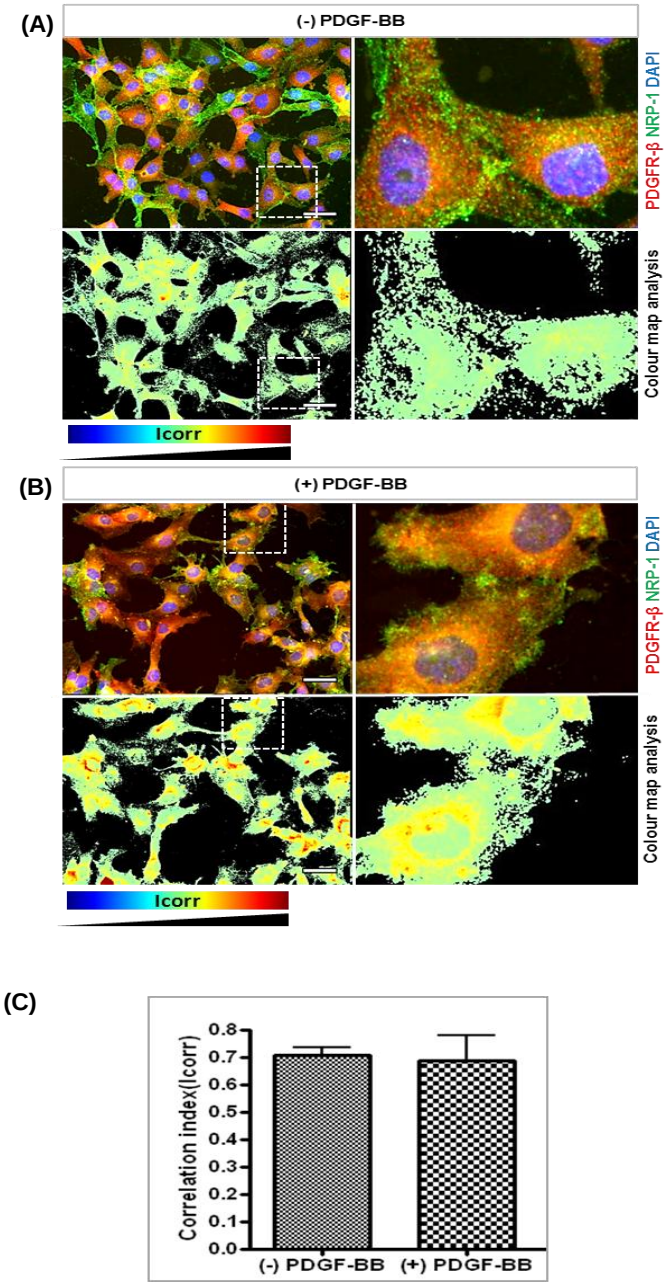

Figure 4.20: Immunofluorescence analysis of co-localisation between NRP-1 and PDGFR-β in A172 cells

The panels illustrate the detection of NRP-1 (green) and PDGFR-β (red) in untreated control cells **(A)** or cells treated with PDGF-BB **(B)**. NRP-1 clustered at points in the cell membrane and, in some cells, NRP-1 appeared to be localised at points of cell spreading. PDGFR-β staining was punctate and distributed throughout the cytoplasm, the staining was intensified /more diffuse following PDGF-BB stimulation. A colour-map analysis (illustrated in the lower rows of each quadrant) has been used to calculate the correlation index (Icorr) between NRP-1 and PDGFR- β, with the hotter colours representing a greater degree of co-localisation. Inset the left panels, the dashed white square outlines a magnified region to clearly visualise areas of co-localisation. **(C)** Icorr values, (representative of 6 independent images and 2 experimental repeats), are represented in histograms. Images were collected on a widefield microscope (Leica DM RXA) using a 20x objective and captured using a Coolsnap EZ camera driven by MetaVue software. Scale bar =50 μM.

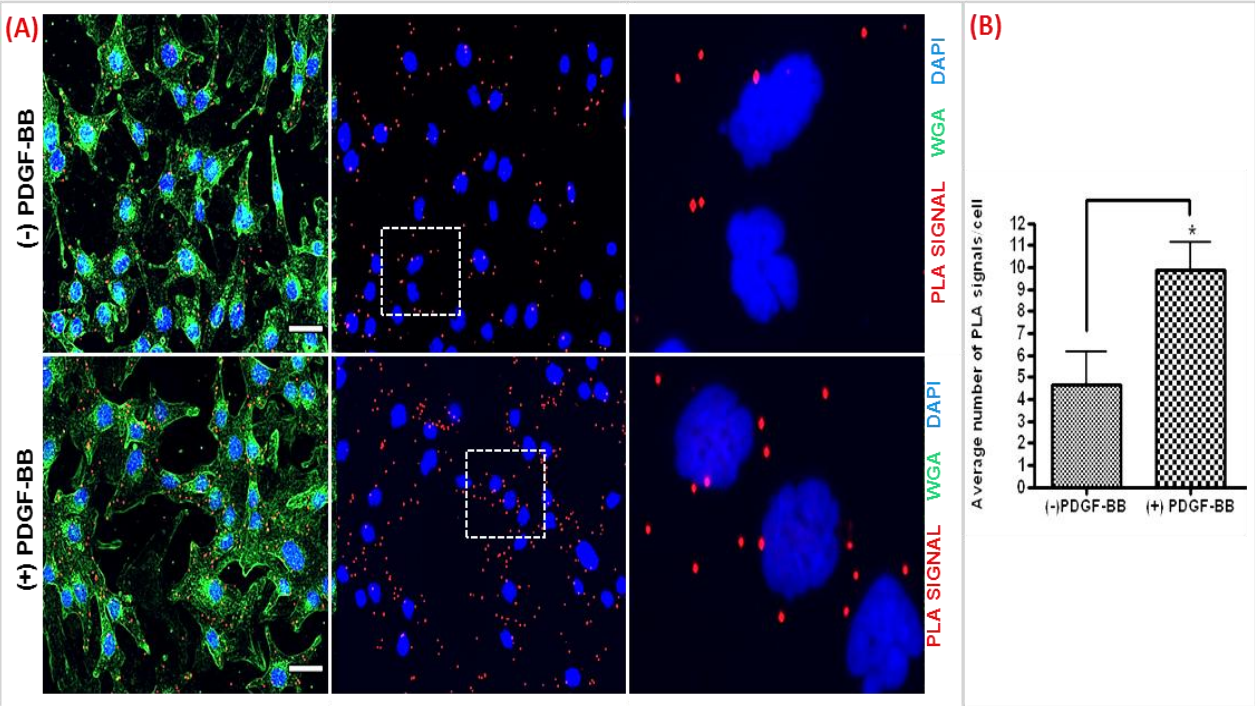

Figure 4.21: In situ PLA detection of NRP-1 and PDGFR-β interactions in A172 cells
In **(A)** the left panel illustrates the A172 cells treated (+/-) PDGF-BB. The PLA signals (red) denote NRP-1: PDGFR-β interactions. Cells were also labelled with wheat germ agglutinin (green) to visualise the cell morphology and ensure PLA signals were localised to cells. Inset the central panel, the white dashed square outlines a magnified region (illustrated in the right panel) to clearly visualise the PLA signals. In **(B)** the histogram represents quantified NRP-1: PDGFR-β PLA signals (normalised to cell number). Plotted values were determined using Blob Finder software. Asterisks * indicates significance (*P<0.05, calculated by one way ANOVA).Images are representative of 6 independent images and 2 experimental repeats. Images were collected on a widefield microscope (Leica DM RXA) using a 20x objective and captured using a Coolsnap EZ camera driven by MetaVue software. Scale bar=50 μm.

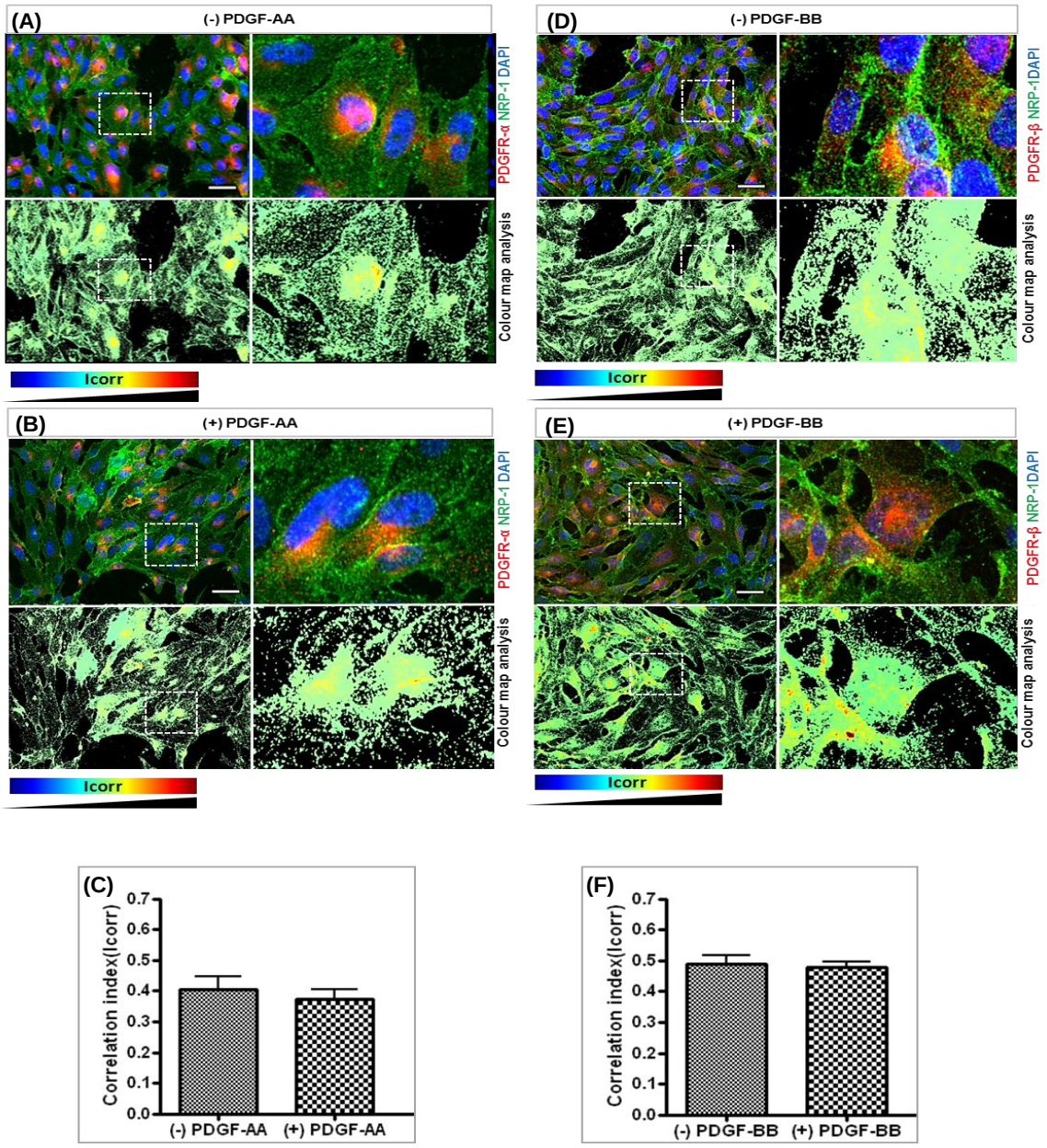

Figure 4.22: Immunofluorescence analysis of co-localisation between NRP-1 and PDGFR-α or PDGFR-β in KHOS-240S cells

The left panels illustrate the detection of NRP-1 (green) and PDGFR-α (red) in untreated control cells **(A)** or cells treated with PDGF-AA **(B)**. The right panels illustrate the detection of NRP-1 (green) and PDGFR-β (red) in untreated control cells **(D)** or cells treated with PDGF-BB **(E)**. NRP-1 localised throughout the cytoplasm with some evident membrane staining and PDGFR-α and β was localised in the peri-nuclear region of the cells. PDGF-BB intensified PDGFR-β staining compared to staining in un-treated cells. A colour-map analysis (illustrated in the lower rows of each quadrant) has been used to calculate the correlation index (Icorr) between NRP-1 and PDGFR-α or β, with the hotter colours representing a greater degree of co-localisation. Inset the left panels, a white square outlines a magnified region to clearly visualise areas of co-localisation. Icorr values, (representative of 6 independent images and 2 experimental repeats), are represented in histograms in **(C)** NRP-1 and PDGFR-α and **(F)** NRP-1 and PDGFR-β. Images were collected on a widefield microscope (Leica DM RXA) using a 20x objective and captured using a Coolsnap EZ camera driven by MetaVue software. Scale bar =50 μM.

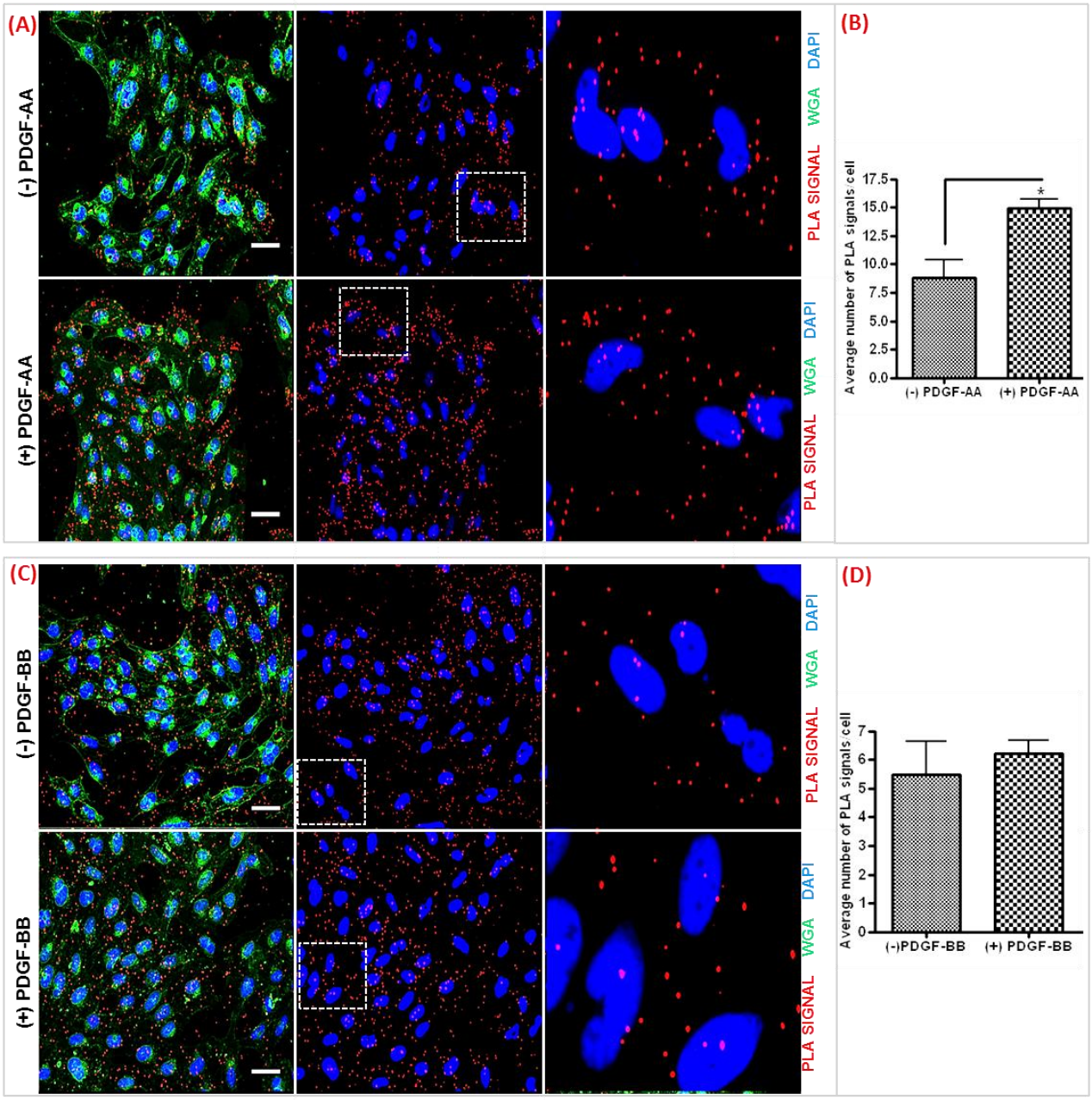

Figure 4.23: In situ PLA detection of NRP-1 and PDGFR-α or PDGFR-β interactions in KHOS-240S cells

In **(A)** and **(C)** the left panel illustrates KHOS-240S cells treated (+/-) PDGF-AA or (+/-) PDGF-BB. The PLA signals (red) denote NRP-1: PDGFR-α or NRP-1: PDGFR-β interactions. Cells were also labelled with wheat germ agglutinin (green) to visualise the cell morphology and ensure PLA signals were localised to cells. Inset the central panel, the white dashed square outlines a magnified region (illustrated in the right panel) to clearly visualise the PLA signals. In **(B)** and **(D)** the histograms represents quantified **(B)** NRP-1: PDGFR-α, **(D)** NRP-1: PDGFR-β, PLA signals (normalised to cell number). Plotted values were determined using Blob Finder software. Images are representative of 6 independent images and 2 experimental repeats. Asterisks * indicates significance (*P<0.05 calculated by one way ANOVA). Images were collected on a widefield microscope (Leica DM RXA) using a 20x objective and captured using a Coolsnap EZ camera driven by MetaVue software. Scale bar=50 μm.

Immunofluorescence analysis of the MG63 cells illustrated that NRP-1 was localised throughout the cells, however, NRP-1 was expressed in much lower levels compared to the other cell lines tested. Thus, the exposure time to detect NRP-1 in the MG63 cell line was 1500 ms, compared to 800 ms in the other cell lines. This lower expression of NRP-1 in the MG63 cells, compared to the other cell lines, was also evident in data described earlier in this chapter (Figure 4.10). PDGFR-α expression was perinuclear and polarised to one half of the MG63 cells. The co-localisation colour-map analysis highlighted that co-localisation between NRP-1 and PDGFR-α was localised around the nucleus. PDGF-AA did not significantly increase co-localisation between PDGFR-α and NRP-1 in MG63 cells. PDGFR-β localisation was cytoplasmic and perinuclear in MG63 cells and co-localisation between PDGFR- β and NRP-1 was detected. However, PDGF-BB stimulation of MG63 cells did not increase the co-localisation between NRP-1 and PDGFR-β (Figure 4.24).

The PLA analysis of the MG63 cells revealed an association between NRP-1 and PDGFR-α. When MG63 cells were stimulated with PDGF-AA, no significant difference in the number of PLA signals/cell was detected. This result suggested that the interaction between PDGFR-α and NRP-1 was not mediated by PDGF-AA. Fewer PLA signals were detected when the interaction between PDGFR-β and NRP-1 was examined and PDGF-BB did not increase the number of PLA signals (Figure 4.25). This result suggested that PDGF-BB was not involved in mediating the interaction between NRP-1 and PDGFR-β in MG63 cells. Together these results suggest that there is an association between NRP-1 and PDGFRs, yet this interaction is not mediated by PDGF growth factors.

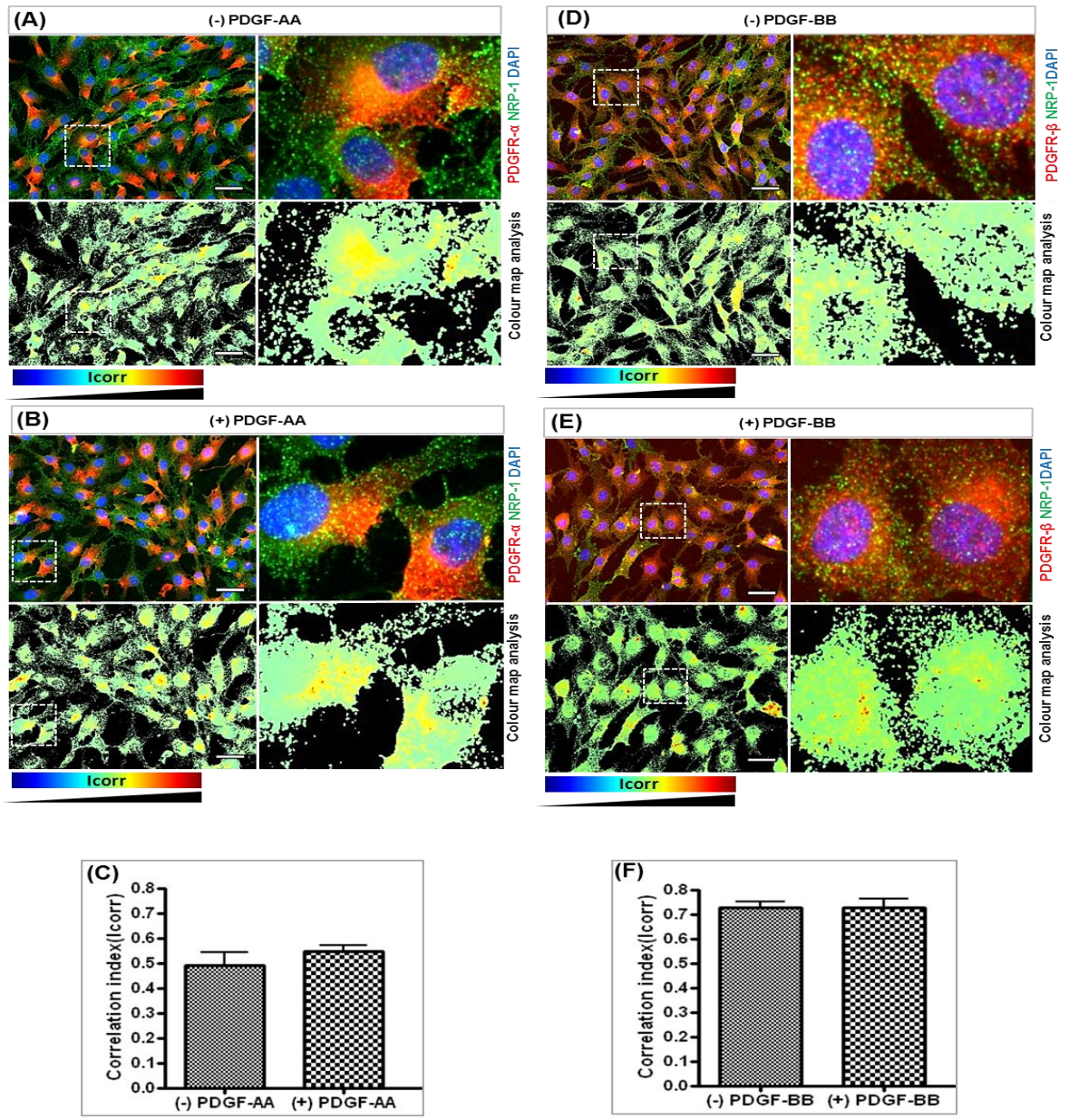

Figure 4.24: Immunofluorescence analysis of co-localisation between NRP-1 and PDGFR-α or PDGFR-β in MG63 cells

The left panels illustrate the detection of NRP-1 (green) and PDGFR-α (red) in untreated control cells **(A)** or cells treated with PDGF-AA **(B)**. The right panels illustrate the detection of NRP-1 (green) and PDGFR-β (red) in untreated control cells **(D)** or cells treated with PDGF-BB **(E)**. NRP-1 was localised throughout the cells. PDGFR-α and PDGFR-β expression was perinuclear, however PDGFR-α was polarised to one half of the MG63 cells. PDGF stimulation did not alter the staining pattern in MG63 cells. A colour-map analysis (illustrated in the lower rows of each quadrant) has been used to calculate the correlation index (Icorr) between NRP-1 and PDGFR-α or β, with the hotter colours representing a greater degree of co-localisation. Inset the left panels, a white square outlines a magnified region to clearly visualise areas of co-localisation. Icorr values, (representative of 6 independent images and 2 experimental repeats), are represented in histograms in, **(C)** NRP-1 and PDGFR-α, and **(F)** NRP-1 and PDGFR-β. Images were collected on a widefield microscope (Leica DM RXA) using a 20x objective and captured using a Coolsnap EZ camera driven by MetaVue software. Scale bar =50 μM.

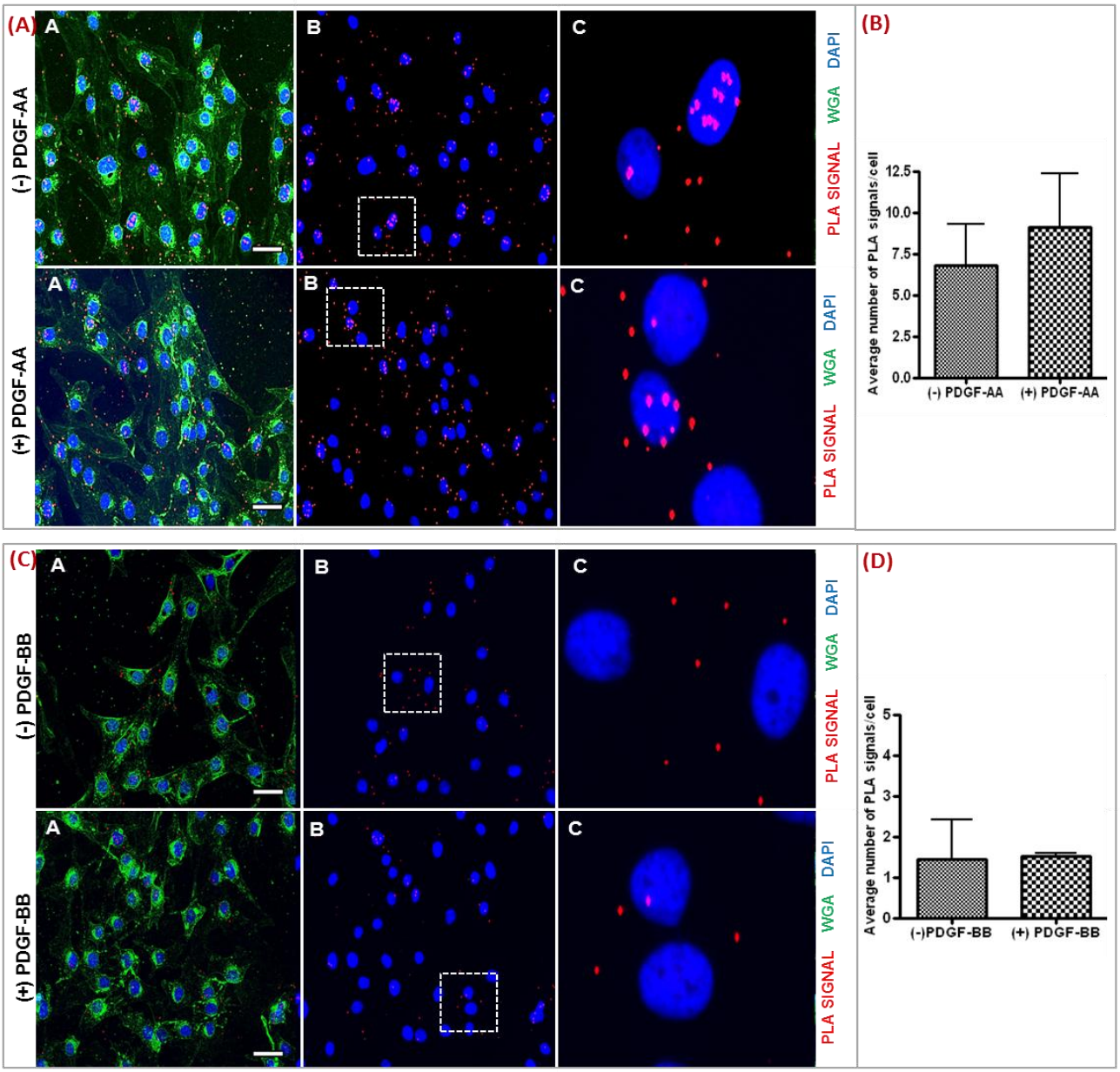

Figure 4.25: In situ PLA detection of NRP-1 and PDGFR-α or PDGFR-β in MG63 cells
In **(A)** and **(C)** the left panel illustrates MG63 cells treated (+/-) PDGF-AA or (+/-) PDGF-BB. The PLA signals (red) denote NRP-1: PDGFR-α or NRP-1: PDGFR-β interactions. Cells were also labelled with wheat germ agglutinin (green) to visualise the cell morphology and ensure PLA signals were localised to cells. Inset the central panel, the white dashed square outlines a magnified region (illustrated in the right panel) to clearly visualise the PLA signals. In **(B)** and **(D)** the histograms represents quantified **(B)** NRP-1: PDGFR-α or **(D)** NRP-1: PDGFR-β PLA signals (normalised to cell number). Plotted values were determined using Blob Finder software. Images are representative of 6 independent images and 2 experimental repeats. Images were collected on a widefield microscope (Leica DM RXA) using a 20x objective and captured using a Coolsnap EZ camera driven by MetaVue software. Scale bar=50 μm.

4.3 Summary

The results in this Chapter demonstrated that the PDGF growth factors have the capacity to bind, distinctly from VEGF-A_{165}, to the b domains of NRP-1 (Section 4.1.4). In mesenchymal tumour cells the PLA provided evidence of an interaction between NRP-1 and PDGFRs, however this interaction did not appear to be dependent on PDGF growth factors (Section 4.2.4). The NRP-1 IP results (Section 4.2.1) did not demonstrate an association between NRP-1 and PDGFR in any of the cell types assayed however, in some cell lines PDGF potentiated the interaction between NRP-1 and PDGFR. As discussed, the increased sensitivity conveyed by the PLA has previously demonstrated interactions which are not detected by co-IP.

The interactions between NRP-1 and PDGFR (in the absence of PDGF growth factors) suggest other mechanisms may also exist to control NRP-1/PDGFR crosstalk and these mechanisms may vary in different cell types. As discussed (Chapter 1, Section 1.1.1), NRP-1 often exists as a proteoglycan with either HS or CS GAGs covalently attached to NRP-1-serine-612. HS proteoglycans (HSPG) are synthesised by almost every type of animal cell and consist of repeating disaccharide units of glucuronic/iduronic acid and glucosamine that are linked to a core-protein via specific serine residues. Extensive modifications, including N-sulphation, N-deacytylation and O-sulphation at various positions of HS chains are thought to contribute to controlling the specificity of HS interactions with different proteins (Kreuger et al., 2006). Many of the growth factors which interact with NRP-1 are also reported to bind to HS, these proteins include FGF (Jastrebova et al., 2006), VEGF (Ashikari-Hada et al., 2005), HGF (Catlow et al., 2003), and PDGF (Abramsson et al., 2007; Lustig et al., 1996; Rolny et al., 2002). HS chains are reported to 'capture' and retain growth factors at the cell surface and stabilise growth factor/receptor interactions which is essential for RTK activation (Ashikari-Hada et al., 2005; Phillips et al., 2012).

In the simplest scenario, NRP-1 associated HS chains may bind growth factors to retain and orientate these ligands within close proximity of NRP and RTKs. The HS-controlled spacial orientation of specific growth factors may be conducive to the formation of complexes comprised of NRP-1/RTKs that are stabilised by a network of HS interactions. It is feasible that such interactions may regulate NRP-1/PDGFR crosstalk yet intricacies in the modifications of HS chains may control which growth factors are associated with NRP-1. A recent paper reported that knockdown of SULF enzymes, (which modify the sulphation pattern of HS in the extracellular microenvironment), distinctly controlled the activation of different RTKs. For example, SULF knockdown increased FGFR activation but inhibited the activity of PDGFR-α, IGF1Rβ, and EPHA2. This result presents interesting questions as to what mediates the specific modifications of NRP-1 associated HS chains (Phillips et al., 2012). Such variations in the NRP-1 associated HS may vary across different

cell types and may impact on NRP-1/PDGFR crosstalk through, for example, HS chains binding to PDGF growth factors and regulating their bioavailability or HS binding to other growth factors (e.g. FGF or HGF) and promoting NRP-1 interactions with their respective RTKs.

In addition to biomolecular interactions mediated by HS chains, several interactions mediated by the intracellular C-terminus of NRP-1 have also been reported. Via the C-terminal SEA motif, NRP-1 can interact with proteins including, integrin α5β1 (Valdembri et al., 2009) and p130Cas (Pellet-Many et al., 2011). Deletion of the NRP-1 C-terminal has also been reported to significantly decrease VEGFR activation (Prahst et al., 2008) and regulate the endocytic recycling of VEGFR-2 (Ballmer-Hofer et al., 2011). In the context of PDGFR crosstalk with NRP-1, intracellular interactions between the C-terminus of NRP-1 and the kinase domain of PDGFR may also be significant.

In conclusion, this Chapter outlined that NRP-1 has the capacity to bind to PDGF growth factors. Interactions between NRP-1/PDGFR were detected in all the cell types (in the absence of PDGF), however, PDGF increased the NRP-1/PDGFR interactions in some cell types. These results suggest that PDGF may potentiate NRP-1 and PDGFR interactions in some cells, however, it is likely other mechanisms possibly involving HS and the C-terminus of NRP-1 may act to stabilise NRP-1/PDGFR crosstalk. The relative contribution of these different mechanisms to NRP-1/PDGFR crosstalk may vary in different cell types and may be dependent on, the relative expression of RTKs and their ligands and the modification of NRP-1 associated HS chains in the different cell types. Although the mechanisms by which NRP-1 and PDGFR associate may vary in different cell types, the results in this Chapter indicate that NRP-1 and PDGFR interact. The next Chapter therefore, aims to assess the relevance of this interaction in mediating PDGFR kinase activity and downstream signalling.

4.3.1 Chapter 4: principal findings

- The NRP-1 b domains bind to the PDGF growth factors and this interaction is not inhibited by the VEGF-A competitive inhibitor, tuftsin.
- PLA determined that NRP-1 interacts with PDGFRs in the mesenchymal tumour cells and this is not dependent on PDGF growth factors.
- NRP-1/PDGFR interactions were not detected by co-IP, which may suggest a low frequency or transient protein interaction.

Chapter 5 – Results

PDGFR phosphorylation and signalling in mesenchymal tumour cells: the influence of NRP-1

5.0 Introduction

As detailed in Chapter 4, NRP-1 interacted with PDGFR in the mesenchymal tumour cell lines, however, PDGF only potentiated the interaction between NRP-1 and PDGFR some of the cells but not others (Chapter 4, Section 4.2.4). In addition, it was established that the different isoforms of PDGF can bind to NRP-1 (Section 4.1.3). Thus, a scenario may exist whereby PDGF is bound to both NRP-1 and PDGFR, mediating an interaction. However (as discussed in Chapter 4, Section 4.3), HS or the NRP-1 C-terminal may also contribute to such interactions and the relative contribution of these factors may vary in different cell lines. Such cell-type specific subtleties in the mechanisms of NRP-1/PDGFR crosstalk, may serve to control the kinase activity of PDGFR. Using the cell lines (selected based on their differential expression of PDGFR and NRP-1) this Chapter aims to explore if NRP-1/PDGFR crosstalk can affect the kinase activity and signalling of PDGFR.

As discussed (Chapter 1, Section 1.3), the specific interactions between different PDGF isoforms and the PDGFR-α and β subunits govern the activation of distinct and overlapping intracellular signalling pathways. The kinase activity of PDGFR is dependent on the auto-phosphorylation of conserved tyrosine residues within the intracellular kinase domain, Tyr-849 for PDGFR-α and Tyr-857 for PDGFR-β (Fantl et al., 1989; Heldin and Westermark, 1999; Kazlauskas and Cooper, 1989; Kelly et al., 1991). Kinase activation of either PDGFR-α or PDGFR-β activates several overlapping downstream pathways, for example, Ras-ERK, PI3K and PLC-γ (Chapter 1, Section 1.3). However, there are some distinctions in the specificities of PDGFR-α and PDGFR-β, for example only PDGFR-α binds to Crk and only PDGFR-β binds to GAP (Rosenkranz and Kazlauskas, 2009). Changes in PDGFR-associated proteins may be attributed to the phosphorylation of alternative tyrosine residues within PDGFR-α or β subunits. For example, in reports examining the PDGFR-α subunit, Tyr-754 is only phosphorylated when PDGFR-α/β heterodimers are formed (Rupp et al., 1994) whereas, using the PDGFR-β subunit, Tyr-771 is only phosphorylated when PDGFR-β/β homodimers occur (Ekman et al., 1999). Further to this, distinct subsets of genes are regulated by the α and β homodimers and the α/β heterodimers of PDGFR (Wu et al., 2008). These findings also translate to cellular effects, with published reports suggesting that PDGFR-β but not PDGFR-α signalling is an important mediator of cell motility (Eriksson et al., 1992) and cells expressing both PDGFR-α and β show increased chemotactic and mitogenic responses to PDGF-AB (Heidaran et al., 1991; Rupp et al., 1994).

These subtle changes in the cellular signalling induced by the different isoforms of PDGFRs may be important in NRP-1/PDGFR crosstalk. In cell types with no detectable VEGFRs, previous reports outlined that the PDGF-AA induced phosphorylation of the PDGFR- α homodimer is most significantly affected by NRP-1. Interestingly, in these studies, intricacies in NRP-1 mediated PDGFR-αα signalling existed in the different cell types despite the cells showing a similar receptor complement. In the MSCs, NRP-1 siRNA significantly decreased the phosphorylation of the PI3K binding site, Tyr-742 (Ball et al., 2010) whereas, in vascular SMCs NRP-1 siRNA significantly decreased the total phosphorylation of PDGFR-αα but did not affect the Tyr sites important for PI3K or ERK-1/2 signalling. Instead, in vascular SMCs, the phosphorylation of the Crk associated protein, p130Cas, was specifically decreased by NRP-1 siRNA. In MSCs, Ball et al (2010) also reported NRP-1 siRNA significantly decreased PDGF-BB mediated phosphorylation of PDGFR-β Tyr-751, whereas Pellet-Many et al (2011) suggested that in vascular SMCs, PDGFR-β phosphorylation was not affected by NRP-1. NRP-1 has also been demonstrated to affect PDGFR-β kinase activity and signalling in cell types expressing VEGFR-1 and VEGFR-2, for example, human aortic SMCs (Banerjee et al., 2006, 2008; Lorquet et al., 2010) and hepatic stellate cells (Cao et al., 2008; Novo et al., 2007). In both human aortic SMCs and hepatic stellate cells, NRP-1 crosstalk with PDGFR-β controlled cell migration. Cao et al (2008) also suggested that an intracellular association between NRP-1 and c- Abl kinase selectively directed PDGFR signalling towards mediating the small GTpase Rac-1, known to be central in controlling cell migration and actin remodelling.

Taken together, these studies emphasise that NRP-1 may differentially regulate PDGFR signalling and this is dependent on both the expression of different PDGFR isoforms and the specific cell type. As outlined in Chapter 3 (Section 3.4), the selected mesenchymal tumour cell lines vary in their expression of PDGFR and NRP-1 and are valuable models to examine how the receptor complement of tumour cells may differentially influence NRP-1 mediated PDGFR signalling. To examine the role of NRP-1 in regulating PDGFR phosphorylation and signalling cells were treated with NRP-1 siRNA or scrambled siRNA. It is important to highlight that only a single nucleotide sequence was targeted for NRP-1 siRNA. Thus, to rule out 'off target' siRNA effects additional, distinct NRP-1 siRNA sequences should be targeted in future work.

To ensure that the PDGF ligands were responsible for activating the PDGFR signalling the cells were treated with PDGFR small molecule inhibitors. Selected cells were treated with either 100 nM of PDGFR inhibitor V (which specifically inhibits the kinase activity of PDGFR-α and β) or 80 nM of PDGFR inhibitor IV (ATP competitive, reversible inhibitor that specifically inhibits PDGFR-α, PDGFR-β and c-Abl kinase). Given the reports that NRP-1 and c-Abl kinase interact to direct PDGFR signalling towards Rac-1 (Cao et al., 2010), the specificities of inhibitor IV and inhibitor V

provided a means to assess if c-Abl kinase was also directing PDGFR signalling in mesenchymal tumour cells.

To determine PDGFR phosphorylation a quantitative enzyme linked immune-absorbance assay (ELISA) and immunoblot analysis was used. The phosphorylation of conserved tyrosine residues within the intracellular kinase domain, Tyr-849 for PDGFR-α and Tyr-857 for PDGFR-β (Fantl et al., 1989; Heldin and Westermark, 1999; Kazlauskas and Cooper, 1989; Kelly et al., 1991), regulates the catalytic activity of PDGFR. Using a monoclonal antibody (Cell Signaling Technology, #3170), which specifically detects both pPDGFR-α Tyr-849 and pPDGFR-β Tyr-857, the kinase activity of PDGFRs was assayed by immunoblot. The Duoset ® ELISA was used to detect the phosphorylation of all PDGFR-β tyrosine residues (using a specific total PDGFR-β antibody and p-Tyr antibody) and the Pathscan ELISA (which specifically detects pPDGFR-α Tyr-849) were used to assay PDGFR activation. A schematic of each of the ELISAs is outlined in material and methods, Figure 2.0. Downstream PDGFR signalling was also analysed by immunoblot, detailed in Section 2.3.

5.1 NRP-1 does not affect the phosphorylation of PDGFR-α or PDGFR-β

In A172 and U87MG cells, the phosphorylation of PDGFR-β was examined by ELISA and immuno blot analysis. The results for these two cell lines were very similar, thus only the data for the U87MG cells is illustrated in Figure 5.0 (the A172 results are presented in Appendix, Figure 8.11). PDGF-BB stimulated a significant increase in PDGFR-β phosphorylation ($P<0.001$) and this was significantly inhibited ($P<0.001$) in cells treated with PDGFR inhibitor V. NRP-1 siRNA effectively blocked the expression of NRP in both cell lines; however, NRP-1 expression was not essential for the phosphorylation of PDGFR-β (+) PDGF-BB . Immunoblot analysis of these cell lines confirmed that NRP-1 siRNA did not inhibit the phosphorylation of PDGFR. In summary, NRP-1 is not required for PDGFR phosphorylation in A172 and U87MG cells.

In the remainder of the cell lines PDGFR-α and PDGFR-β phosphorylation was examined by ELISA and immunoblot. In all the cell lines, except MG63, PDGF-AA stimulation did not increase the phosphorylation of PDGFR-α Tyr-849 (see Appendix Figures 8.12 to 8.15). In MG63 cells, PDGF-AA induced a significant increase in PDGFR-α Tyr-849 phosphorylation ($P<0.001$), see Figure 5.2. A significant increase ($P<0.001$) in PDGFR-β phosphorylation was stimulated by PDGF-BB in KHOS-240S, MG63 and T98G cells, see Figure 5.3 for MG63 cells data (the remainder of the data is included in appendix figures) . In KHOS-240S and MG63 cells PDGF-BB also triggered a significant increase in PDGFR-α Tyr-849 phosphorylation ($P<0.001$) see Figure 5.1 for MG63 cells data (data for KHOS-240S is included in Appendix, Figure 8.14). In all the cell lines

tested, PDGFR inhibitor V attenuated PDGFR phosphorylation stimulated by PDGF-AA or PDGF-BB. NRP-1 knockdown did not attenuate PDGFR phosphorylation in any of the cell lines, as illustrated by both the ELISA and immunoblot results. However, in the MG63 cells NRP-1 siRNA treatment caused a small but significant decrease in PDGF-BB stimulated phosphorylation of PDGFR-β (Figure 5.1).

Collectively, these ELISA results suggest that mesenchymal tumour cells are more responsive to PDGF-BB than to PDGF-AA, with the exception of MG63 cells, which respond equally to both PDGF AA and PDGF-BB. Inhibitor V effectively blocks PDGF-AA and PDGF-BB mediated PDGFR phosphorylation in all the tumour cell lines. Following NRP-1 siRNA treatment, only the PDGF-BB mediated phosphorylation of PDGFR-β was blocked in the MG63 cells. However, this inhibition did not ablate PDGFR-β activation and PDGFR-β phosphorylation still increased six fold above basal levels in MG63's. In the remainder of the cell lines, NRP-1 siRNA did not inhibit the phosphorylation of PDGFR-α or PDGFR-β. In summary, these results suggest that NRP-1 is not a critical factor for PDGF stimulated activation of PDGFRs in mesenchymal tumour cells.

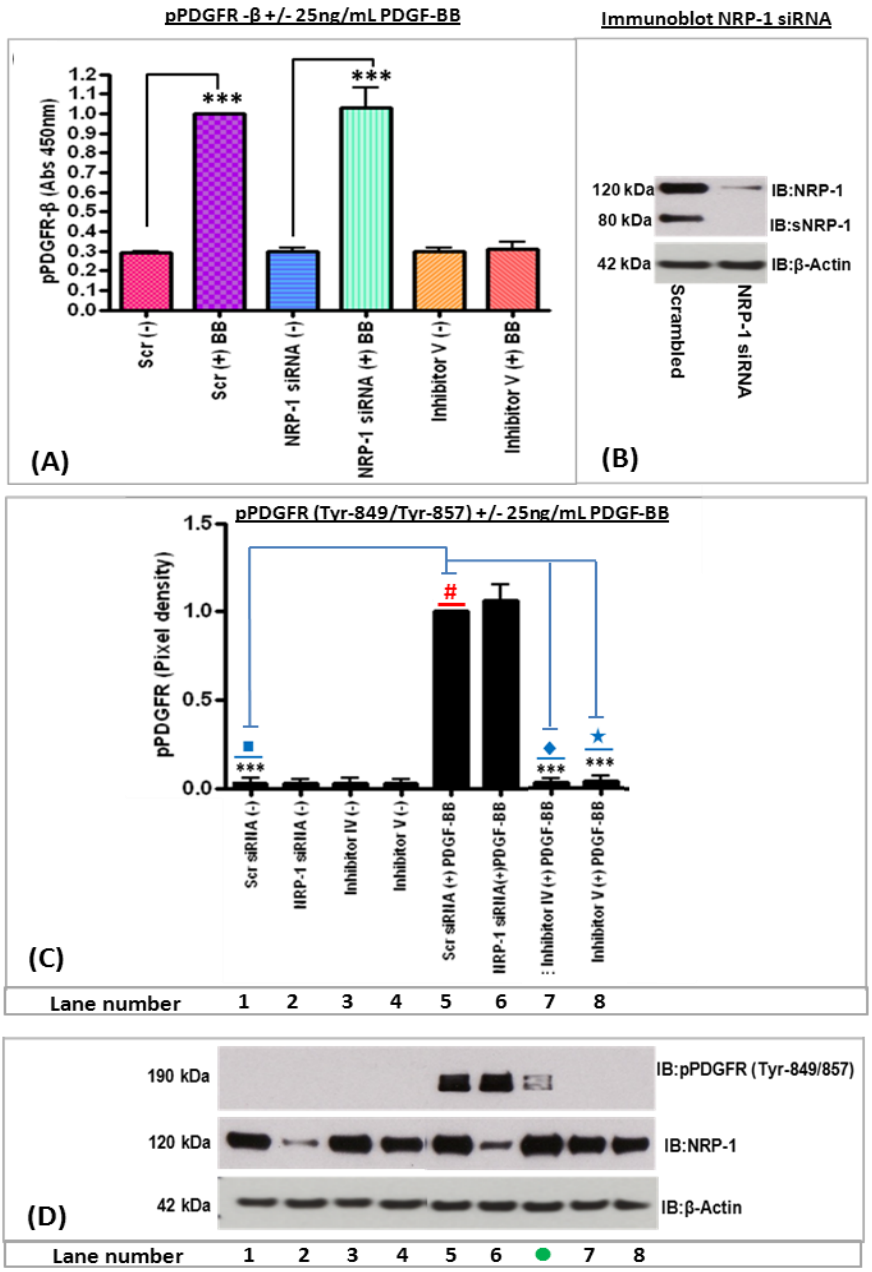

Figure 5.0: NRP-1 siRNA does not attenuate PDGFR phosphorylation in U87MG cells

(A) The ELISA results illustrate that PDGF-BB (■) stimulated a significant increase in pPDGFR-β. Inhibitor V (■) blocked pPDGFR-β and NRP-1 siRNA treatment (■) did not inhibit pPDGFR-β. **(B)** Immunoblot data illustrated that NRP-1 siRNA treatment blocks the expression of NRP-1 in U87MG cells. To quantify the levels of phosphorylated PDGFR, pixel densities were calculated using Gene Tools v3 software. **(C)** The histogram illustrates the quantified levels of pPDGFR (■) which has been expressed as a ratio relative to the Scr (+) PDGF-BB sample in lane 5 (#). Data presented is the mean value from at least two experimental repeats +/- calculated standard errors. Asterisks (*) indicate significance (calculated by one-way ANOVA, $P<0.05$*, $P<0.001$***). PDGF-BB (#) significantly increased the phosphorylation of PDGFR, relative to un-stimulated controls (■) in lane 1. PDGFR inhibitor IV (♦), inhibitor V (★) treatment significantly inhibited pPDGFR-β. NRP-1 siRNA did not inhibit the phosphorylation of PDGFR. **(D)** Immunoblots detected pPDGFR (Tyr-849/857), NRP-1 and β-Actin in U87MG cells. The data indicated between lanes 6 and 7 (●) was not used in this analysis.

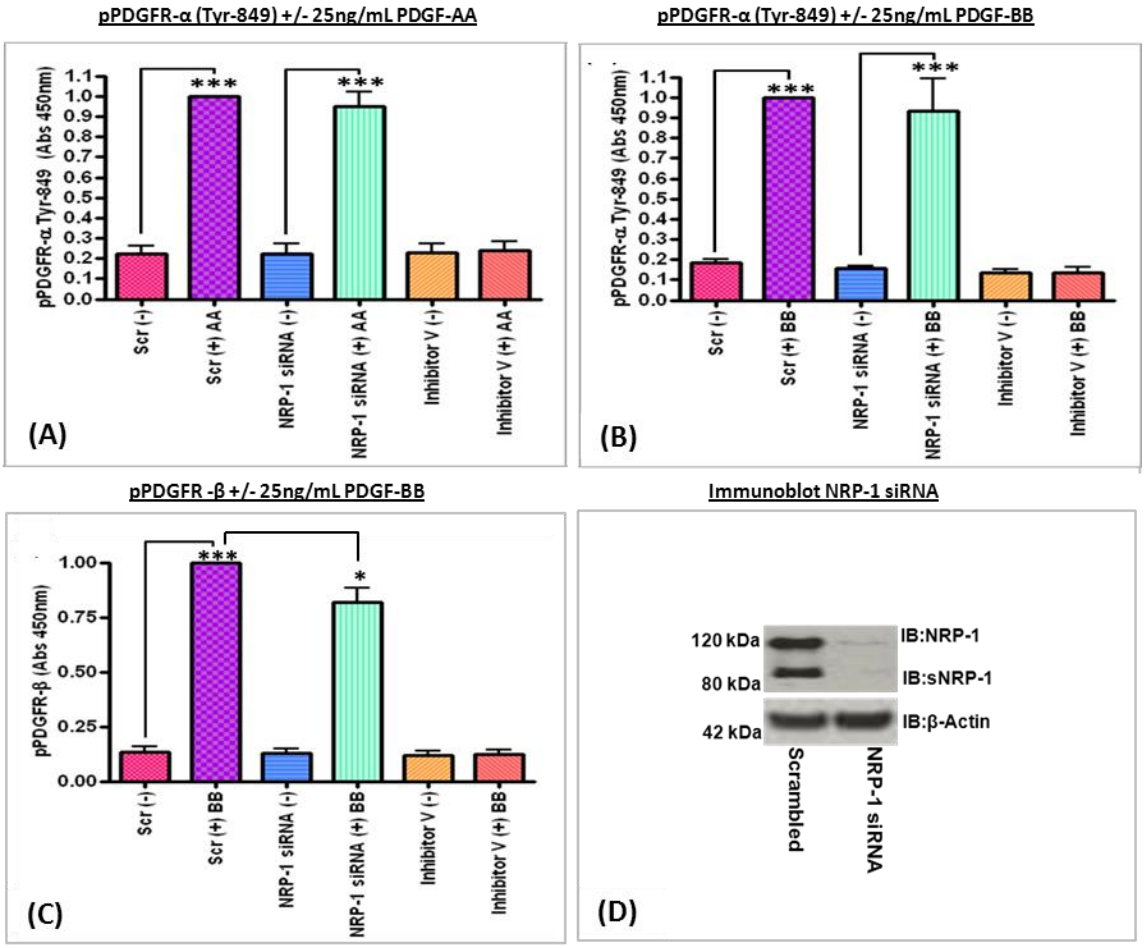

Figure 5.1: NRP-1 siRNA does not inhibit PDGFR-α phosphorylation in MG63 cells

The ELISA results presented in the histograms above illustrate that **(A)** PDGF-AA (■) or **(B)** PDGF-BB (■) stimulated a significant increase in pPDGFR-α. PDGFR inhibitor V blocked PDGFR-α phosphorylation (■) (+/-) PDGF-AA or PDGF-BB and NRP-1 siRNA treatment (■) did not inhibit the PDGF stimulated increase in pPDGFR-α levels. **(C)** PDGF-BB (■) stimulated a significant increase in pPDGFR-β and NRP-1 siRNA treatment (■) caused a small but significant decrease in pPDGFR-β. Inhibitor V (■) attenuated the phosphorylation of PDGFR-β (+/-) PDGF-BB. **(D)** The Immunoblot data illustrates that NRP-1 siRNA treatment blocks the expression of NRP-1 in MG63 cells. Asterisks (*****) indicate significance (calculated by one-way ANOVA, $P<0.05$*, $P<0.001$***).

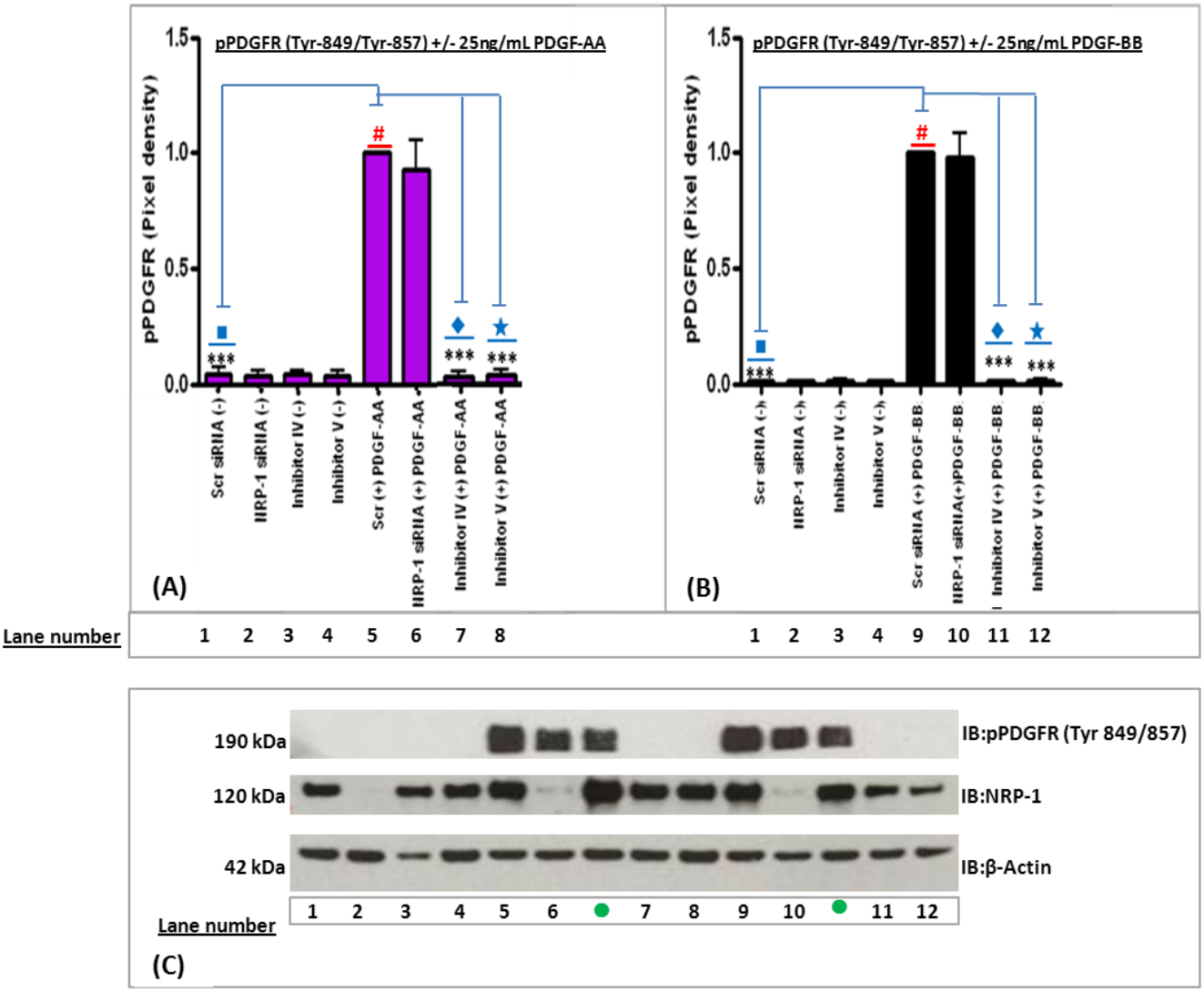

Figure 5.2: NRP-1 siRNA does not attenuate PDGFR phosphorylation in MG63 cells

To quantify the phosphorylation of PDGFR, pixel densities were calculated using Gene Tools v3 software. The histograms in **(A)** and **(B)** illustrate quantified pPDGFR levels in cells stimulated with PDGF-AA (■) or PDGF-BB (■). The values on the histograms were calculated as a ratio relative to the Scr (+) PDGF-AA in **(A)** lane 5, indicated by the # symbol or the Scr (+) PDGF-BB in **(B)** lane 5, indicated by the # symbol. Data presented is the mean value from at least two experimental repeats +/- calculated standard errors. Asterisks (*****) indicate significance (calculated by one-way ANOVA, *P*<0.05*, *P*<0.01**, *P*<0.001***). **(A)** PDGF-AA (#) significantly increased levels of pPDGFR, relative to un-stimulated controls (■). PDGFR inhibitor IV (♦), inhibitor V treatment significantly inhibited pPDGFR. **(B)** PDGF-BB (#) significantly increased PDGFR phosphorylation, relative to un-stimulated controls (■). PDGFR inhibitor IV (♦) or inhibitor V (★) treatment significantly inhibited pPDGFR. NRP-1 siRNA did not inhibit the phosphorylation of PDGFR. **(C)** Immunoblots detected pPDGFR (Tyr-849/857), NRP-1 and β-Actin in MG63 cells. The data indicated between immunoblot lanes 6/7 and 10/11 (●) was not used in this analysis.

5.2 The influence of NRP-1 on the activation of primary PDGFR-α or PDGFR-β downstream signalling pathways

The ELISA and immunoblot results detailed in the previous section suggested that NRP-1 was not essential for the phosphorylation of PDGFR-α or PDGFR-β. However, as part of the immunoblot analysis the same samples assayed for PDGFR-α and PDGFR-β phosphorylation were also tested for the activation of primary PDGFR downstream signalling pathways. Three primary PDGFR signalling pathways were selected for the immunoblot analysis, PI3K, MAPK-ERK, and PLC-γ. It was important to understand if downstream PDGFR signalling was affected by NRP-1, as previous work by Pellet-Many et al (2011) (Pellet-Many et al., 2011) reported that NRP-1/PDGFR crosstalk did not decrease the overall kinase activity of PDGFR-β, but had specific downstream effects on p130Cas phosphorylation. It was therefore, important to interrogate if NRP-1 selectively mediated the phosphorylation of specific PDGFR tyrosine residues, as such subtle effects may have not been identified through the analysis of PDGFR phosphorylation alone.

5.2.3 Phosphorylation of PLC-γ is not inhibited in NRP-1 siRNA treated cells

The phosphorylation of PLC-γ was examined by immunoblot. Phosphorylation of tyrosine residues in the C-terminus of PDGFR allows PLC-γ to bind directly to PDGFR via its two SH2 domains. PLC-γ is reported to associate with PDGFR-α Tyr-988 and Tyr-1018 (Eriksson et al., 1995) or PDGFR-β Tyr-1021 and Tyr-1091 (Valius et al., 1993). PDGFR then phosphorylates PLC-γ at three tyrosine sites, and phosphorylation of PLC-γ at Tyr-783 is essential for its catalytic activity (Kim et al., 1991). Activated PLC-γ acts on the same substrate as PI3K, PIP_2, and interestingly molecular crosstalk between PI3K and PLC-γ exists to regulate PLC-γ activity (Falasca et al., 1998). Activated PLC-γ targets PIP_2 and generates two products, IP_3 and DAG. DAG activates protein kinase-C (PKC) and IP_3 increases the accumulation of intracellular calcium (Kim et al., 2000). Activation of PLC-γ has been reported to be a rate-limiting step mediating chemotaxis of cells towards PDGF(Rönnstrand et al., 1999). PLC-γ signalling is also reported to be involved in cell spreading, motility, and cancer cell invasion (Jones et al., 2005; Rönnstrand et al., 1999).

In all the mesenchymal tumour cell lines the pattern PLC-γ phosphorylation was similar, thus, only the data for MG63 cells is presented in Figure 5.3 (the remainder of the results are detailed in the Appendix Figures 8.16 to 8.19). In all the cell lines, PDGF stimulation significantly increased the phosphorylation of PLC-γ relative to un-stimulated controls and PDGFR inhibitor IV or inhibitor V attenuated the activation of PLC-γ. However, NRP-1 siRNA treatment did not inhibit PDGF stimulated phosphorylation of pPLC-γ in any of the cell lines. In summary, these results illustrate

that stimulation or inhibition of PDGFR signalling can control the activation of PLC-γ in the mesenchymal tumour cell lines however, NRP-1 knockdown does not affect the activation of PLC-γ.

5.2.2 Regulation of the PI3K-AKT pathway in mesenchymal tumour cells

As discussed (Chapter 1, Section 1.3.1) another principal pathway activated through PDGFR phosphorylation is PI3K. On auto-phosphorylation of PDGFR-β Tyr-751 and Tyr-740 (Kashishian et al., 1992; Kazlauskas and Cooper, 1989; Kazlauskas et al., 1992), and PDGFR-α Tyr-740 or Tyr-731 (Yu et al., 1991), SH-2 domains within the p85 regulatory subunit of PI3K bind directly to specific motifs on the phosphorylated tyrosine residues. Binding of the p85 subunit to phosphorylated tyrosine residues releases the catalytic subunit of PI3K (Carpenter et al., 1993) which targets its major substrate PIP_2. PI3K phosphorylates PIP_2 and generates PIP_3, which functions as a second messenger to activate AKT. AKT phosphorylates multiple proteins involved in cell death, ultimately leading to increased cell survival and proliferation. AKT also has documented roles in regulating cell differentiation and migration (Manning and Cantley, 2007; Vivanco and Sawyers, 2002; Yoeli-Lerner et al., 2009). The tumour suppressor protein, Pten, facilitates negative regulation of the PI3K pathway. Pten is a phosphoinositide 3-phosphatase which de-phosphorylates the PI3K second messenger, PIP_3, thereby inhibiting the downstream activation of AKT (Leslie and Downes, 2002; Maehama and Dixon, 1998). Mutations and deletions of the PTEN gene are documented in a high proportion of gliomas (Knobbe et al., 2002; McDowell et al., 2011), including the glioma cell lines used in these analyses. Both U87MG and A172 cells are null for the PTEN gene (Endersby et al., 2011; Zhang et al., 2008), whereas T98G cells carry a point mutation (L42R) (Endersby et al., 2011; Kleber et al., 2008) which has been reported to result in normal to increased PTEN activity (Han et al., 2000). Such differences in Pten expression, may impact to regulate the basal levels of pAKT in the different glioma cell lines. To determine the status of the PI3K pathway, the phosphorylation of the downstream biomarker AKT was examined by immunoblot.

PDGF stimulated phosphorylation of AKT varied in the PTEN null cell lines, U87MG and A172. In U87MG cells, aberrant activation of pAKT was detected (Appendix Figure 8.20), however, in A172 cells PDGF-BB stimulated a significant elevation of pAKT ($P<0.001$), see Appendix, Figure 8.21. In both U87MG and A172 cells NRP-1 siRNA treatment did not inhibit the phosphorylation of AKT; however, PDGFR inhibitors IV and V significantly decreased the phosphorylation of AKT in A172 and U87MG cells. In summary, PDGF-BB can drive the increased phosphorylation of AKT in A172 but not U87MG cells, however, inhibition of pAKT by inhibitor IV or V indicates that (in some part)

PDGFR signalling is driving AKT phosphorylation in both cell lines, NRP-1 was not critical for AKT phosphorylation.

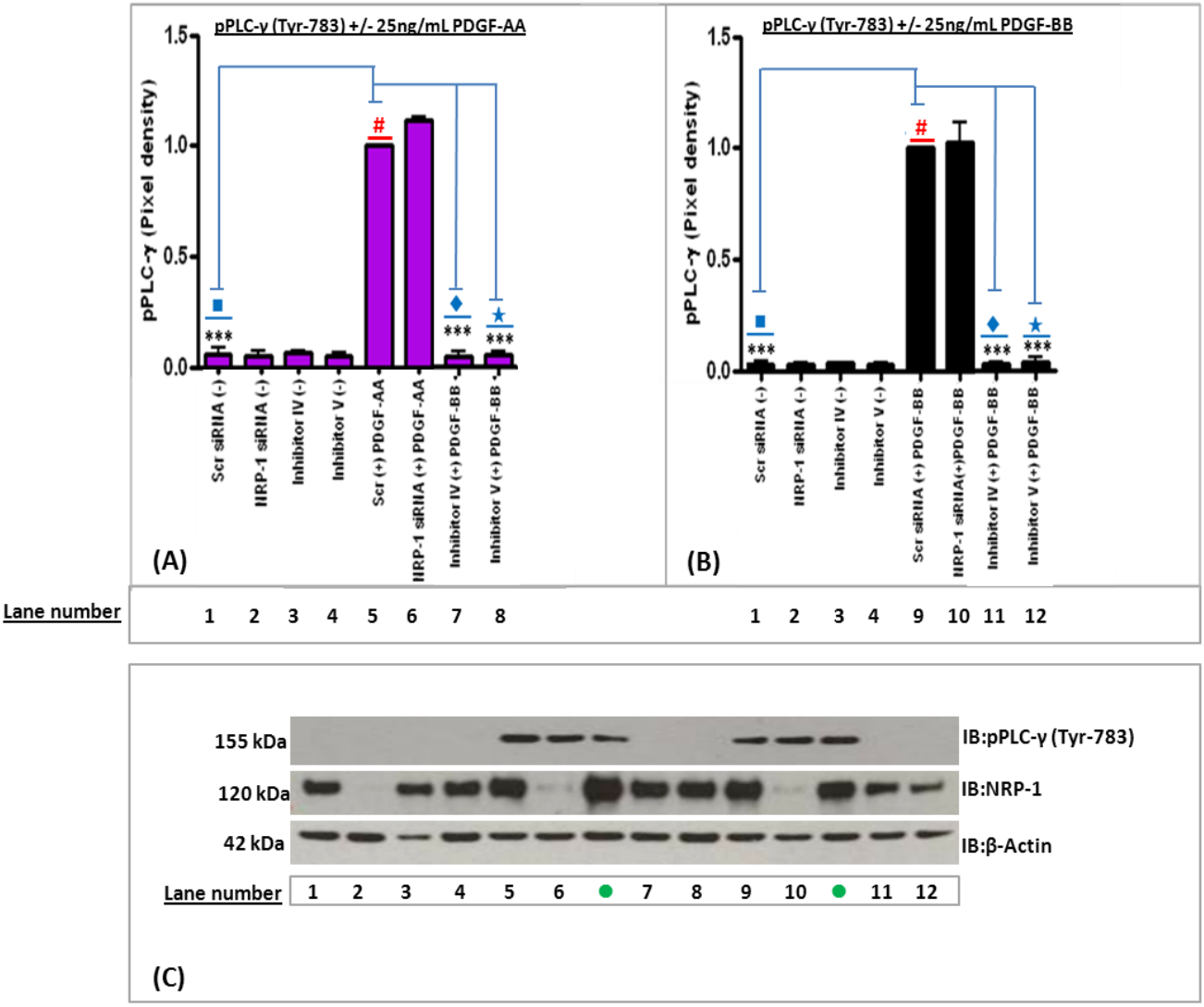

Figure 5.3: NRP-1 siRNA does not attenuate PLC-γ (Tyr-783) phosphorylation in MG63 cells
To quantify the amount of pPLC-γ (Tyr-783), pixel densities were calculated using Gene Tools v3 software. The histograms in **(A)** and **(B)** illustrate the quantified levels of pPLC-γ in cells stimulated with PDGF-AA (■) or PDGF-BB (■). The values on the histograms were calculated as a ratio relative to the Scr (+) PDGF-AA in **(A)** lane 5, indicated by the # symbol or the Scr (+) PDGF-BB in **(B)** lane 5, indicated by the # symbol. Data presented is the mean value from at least two experimental repeats +/- calculated standard errors. Asterisks (*) indicate significance (calculated by one-way ANOVA, *P*<0.001***). **(A)** PDGF-AA (#) significantly increased pPLC-γ, relative to un-stimulated controls (■). PDGFR inhibitor IV (♦), inhibitor V significantly inhibited pPLC-γ. (**B)** PDGF-BB (#) significantly increased the phosphorylation of PLC-γ, relative to un-stimulated controls (■). PDGFR inhibitor IV (♦) or inhibitor V (★) significantly inhibited pPLC-γ. NRP-1 siRNA did not inhibit the phosphorylation of PLC-γ. **(C)** Immunoblots detected pPLC-γ (Tyr-783), NRP-1 and β-Actin in MG63 cells. The data indicated between immunoblot lanes 6/7 and 10/11 (●) was not used in this analysis.

In the T98G (PTEN mutant) MG63 and KHOS-240S cells, PDGF-AA or PDGF-BB stimulated a significant increase ($P<0.001$) in AKT phosphorylation which was attenuated by PDGFR inhibitors IV or V. NRP-1 siRNA treatment significantly inhibited the increase in pAKT stimulated by PDGF-AA ($P<0.05$) but not PDGF-BB in T98G cells (Figure 5.4). In KHOS-240S cells, NRP-1 siRNA treatment significantly inhibited the increase in pAKT stimulated by PDGF-BB ($P<0.05$) but not PDGF-AA (Figure 5.5). MG63 cells were not dependent on either NRP-1 for AKT phosphorylation. Thus, in all the cell lines, PDGFR stimulation or inhibition can regulate the phosphorylation of AKT and NRP-1 is important for the maximal phosphorylation of AKT stimulated by PDGF-AA or BB in T98G and KHOS-240S cells. It should be highlighted that, although NRP-1 siRNA inhibits the PDGF stimulated increase in pAKT (in the aforementioned cells), pAKT is not depleted to basal levels (as is the case when cells are treated with PDGFR inhibitors IV or V). This suggests that, in cells treated with NRP-1 siRNA, PDGFR signalling is still functioning to some degree to stimulate AKT phosphorylation.

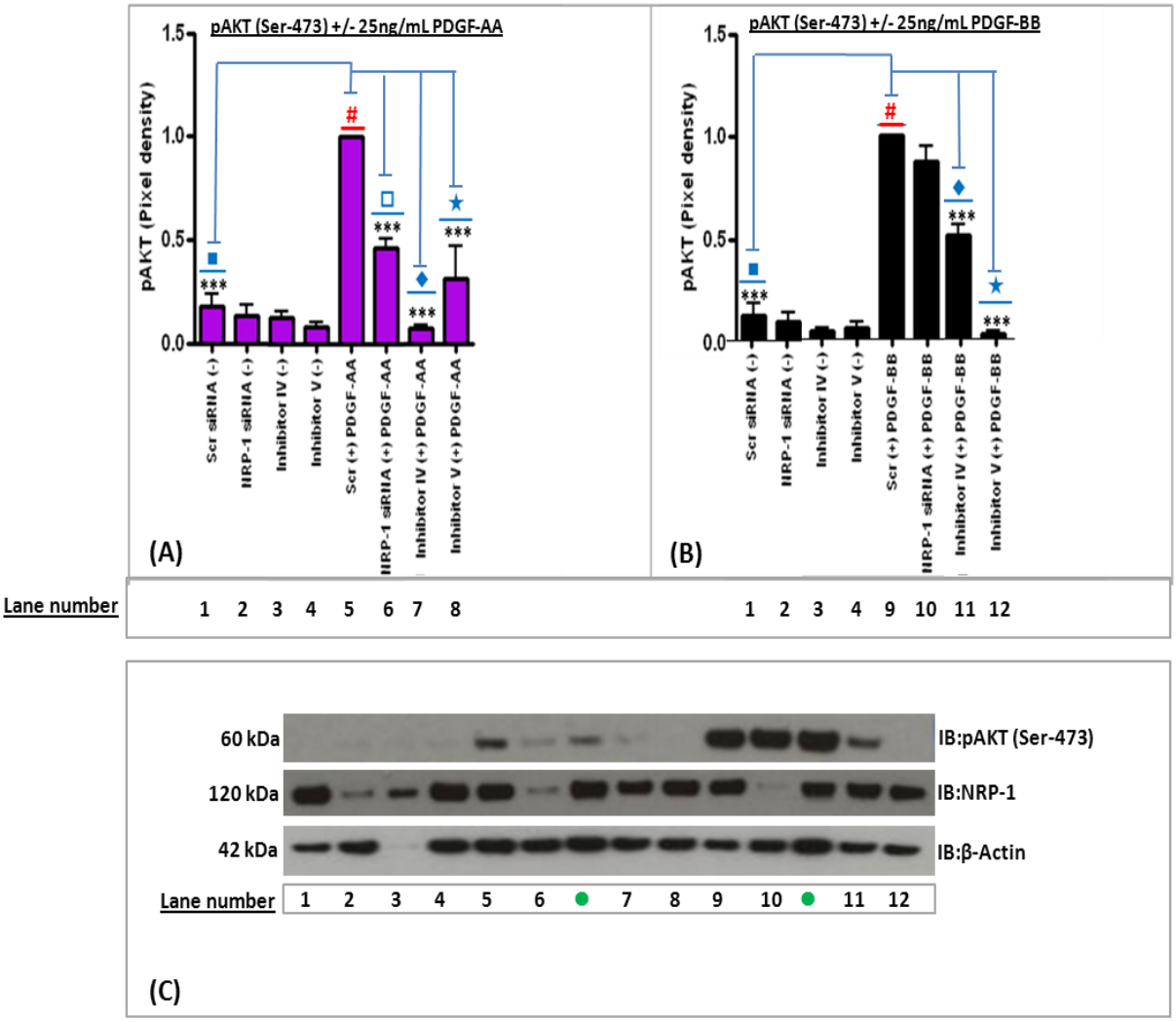

Figure 5.4: NRP-1 siRNA inhibits PDGF-AA stimulated phosphorylation of AKT (Ser-473) in T98G cells

To quantify the levels of pAKT (Ser-473) pixel densities were calculated using Gene Tools v3 software. The histograms in **(A)** and **(B)** illustrate the quantified level of pAKT in cells stimulated with PDGF-AA (■) or PDGF-BB (■).The values on the histograms were calculated as a ratio relative to the Scr (+) PDGF-AA in **(A)** lane 5, indicated by the # symbol or the Scr (+) PDGF-BB in **(B)** lane 5, indicated by the # symbol. Data presented is the mean value from at least three experimental repeats +/- calculated standard errors. Asterisks (*) indicate significance (calculated by one-way ANOVA, $P<0.05$*, $P<0.001$***). **(A)** PDGF-AA (#) significantly increased AKT phosphorylation, relative to un-stimulated controls (■). PDGFR inhibitor IV (♦), inhibitor V or NRP-1 (□) siRNA treatment significantly inhibited pAKT. **(B)** PDGF-BB (#) significantly increased the level of pAKT, relative to un-stimulated controls (■). PDGFR inhibitor IV (♦), inhibitor V (★) significantly attenuated the phosphorylation of AKT. NRP-1 siRNA did not inhibit the phosphorylation of AKT. **(C)** Immunoblots detected pAKT (Ser-473), NRP-1 and β-Actin in T98G cells. The data indicated between immunoblot lanes 6/7 and 10/11 (●) was not used in this analysis.

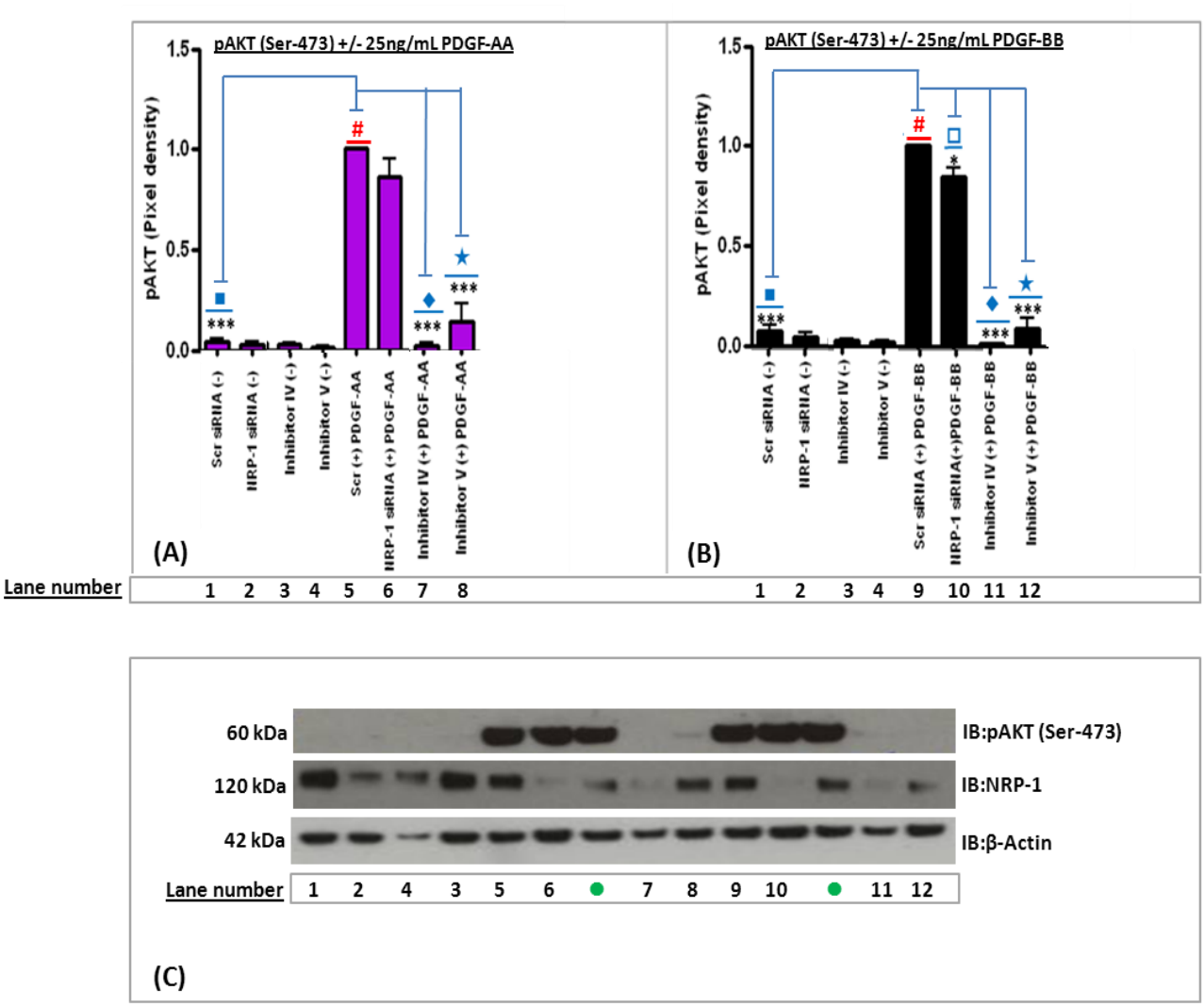

Figure 5.5: NRP-1 siRNA inhibits PDGF-BB stimulated phosphorylation of AKT (Ser-473) in KHOS-240S cells

To quantify the levels of pAKT (Ser-473) pixel densities were calculated using Gene Tools v3 software. The histograms in **(A)** and **(B)** illustrate the quantified levels of pAKT in cells stimulated with PDGF-AA (■) or PDGF-BB (■).The values on the histograms were calculated as a ratio relative to the Scr (+) PDGF-AA in **(A)** lane 5, indicated by the # symbol or the Scr (+) PDGF-BB in **(B)** lane 5, indicated by the # symbol. Data presented is the mean value from at least three experimental repeats +/- calculated standard errors. Asterisks (*) indicate significance (calculated by one-way ANOVA, $P<0.05$*, $P<0.001$***). **(A)** PDGF-AA (#) significantly increased the phosphorylation of AKT, relative to un-stimulated controls (■). PDGFR inhibitor IV (♦) or inhibitor V (★) significantly attenuated the activation of AKT. **(B)** PDGF-BB (#) significantly increased the amount of pAKT, relative to un-stimulated controls (■). PDGFR inhibitor IV (♦), inhibitor V (★) or NRP-1 (□) siRNA treatment significantly inhibited pAKT. **(C)** Immunoblots detected pAKT (Ser-473), NRP-1 and β-Actin in KHOS-240S cells. The data indicated between immunoblot lanes 6/8 and 10/12 (●) was not used in this analysis.

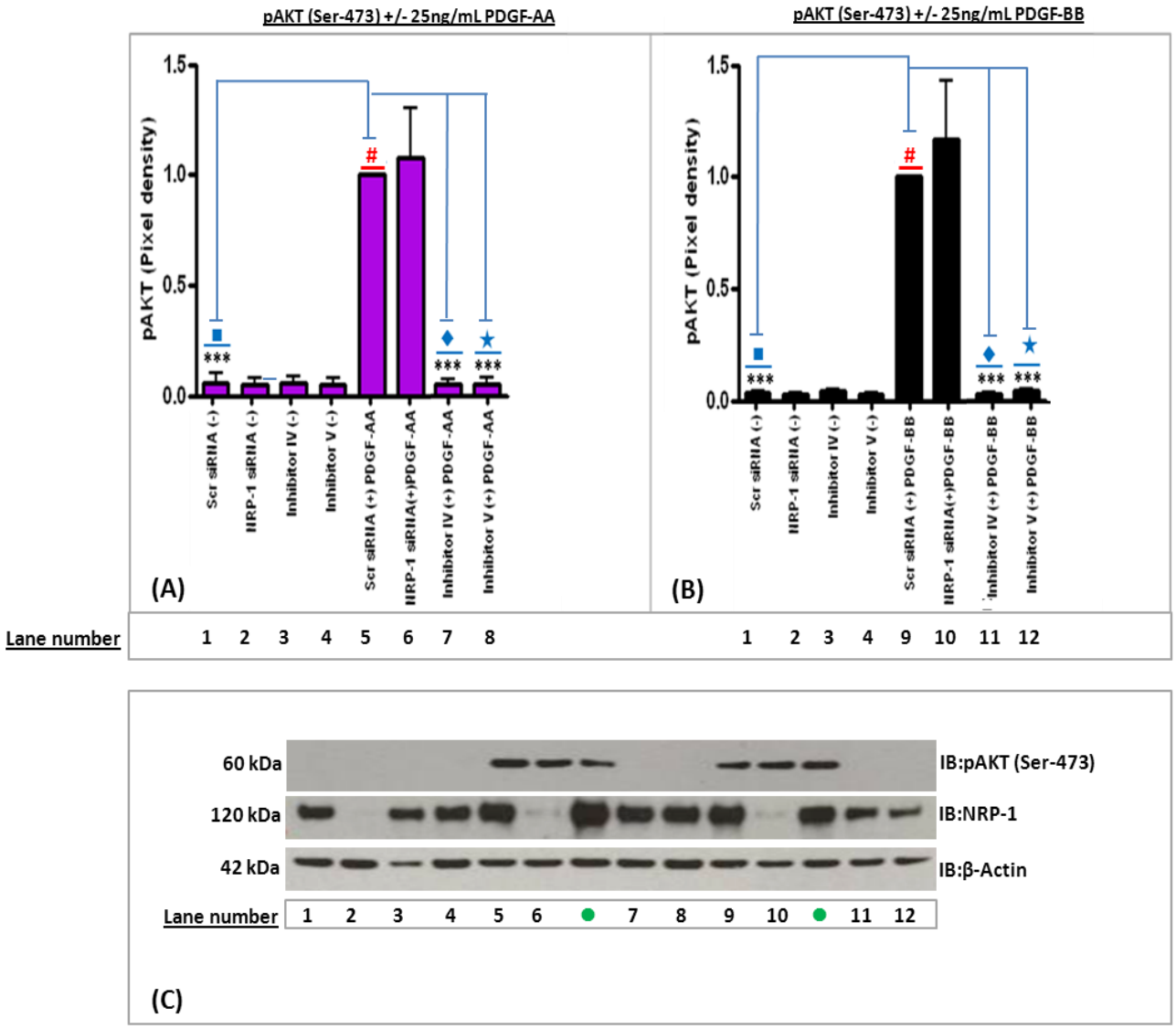

Figure 5.6: NRP-1 siRNA does not attenuate PDGF-stimulated phosphorylation of AKT in MG63 cells

To quantify the phosphorylation AKT (Ser-473) pixel densities were calculated using Gene Tools v3 software. The histograms in **(A)** and **(B)** illustrate the quantified level of pAKT in cells stimulated with PDGF-AA (■) or PDGF-BB (■). The values on the histograms were calculated as a ratio relative to the Scr (+) PDGF-AA in **(A)** lane 5, indicated by the # symbol or the Scr (+) PDGF-BB in **(B)** lane 5, indicated by the # symbol. Data presented is the mean value from at least three experimental repeats +/- calculated standard errors. Asterisks (*) indicate significance (calculated by one-way ANOVA, $P<0.001$***). **(A)** PDGF-AA (#) significantly increased the AKT phosphorylation, relative to un-stimulated controls (■) and PDGFR inhibitor IV (♦) or inhibitor V (★) significantly attenuated the phosphorylation of AKT. **(B)** PDGF-BB (#) significantly increased pAKT, relative to un-stimulated controls (■). PDGFR inhibitor IV (♦) or inhibitor V (★) significantly inhibited pAKT. NRP-1 siRNA treatment had no effect on AKT phosphorylation. **(C)** Immunoblots detected pAKT (Ser-473), NRP-1 and β-Actin in MG63 cells. The data indicated between immunoblot lanes 6/7 and 10/11 (●) was not used in this analysis.

5.2.3 Regulation of the Ras-MAPK pathway in mesenchymal tumour cells

As discussed (Chapter 1, Section 1.3.1), activation of the Ras-MAPK signalling pathway is one of the primary downstream effects of PDGFR phosphorylation. Phosphorylation of PDGFR-β Tyr-716 (Arvidsson et al., 1994) or PDGFR-α Tyr-720 (Bazenet et al., 1996) initiates the sequential activation of several molecules, cumulating in the activation of MEK which in turn activates ERK-1/2 (Sebolt-Leopold and Herrera, 2004). ERK-1/2 then activates multiple transcription factors which positively regulate cell proliferation, survival, and differentiation (Dhillon et al., 2007; Sebolt-Leopold and Herrera, 2004). The PDGF-induced phosphorylation of ERK-1/2 was examined by immunoblot in the mesenchymal tumour cells.

In U87MG and A172 cells PDGF-BB stimulated a significant increase in pERK-1 relative to un-stimulated controls ($P<0.05$ U87MG and $P<0.001$ A172) and ERK-2 phosphorylation was significantly elevated in A172 cells ($P<0.05$). NRP-1 siRNA treatment did not inhibit the activation of ERK, however ERK phosphorylation was inhibited by PDGFR inhibitor IV and V. In summary, in A172 and U87MG cells, PDGF-BB stimulated a greater increase in ERK-1 than ERK-2, (partly because basal levels of ERK-2 were higher) and NRP-1 siRNA did not inhibit ERK phosphorylation (Appendix Figures 8.22 and 8.23).

In T98G cells, PDGF-BB stimulation significantly increased the phosphorylation of ERK-1/2 ($P<0.001$, $P<0.01$ respectively) and NRP-1 siRNA significantly attenuated ERK-1/2 phosphorylation. Inhibitor IV and V blocked the phosphorylation of ERK-1/2 stimulated by PDGF-BB (Figure 5.7). Although NRP-1 siRNA treatment blocked PDGF-BB stimulated ERK-1/2 phosphorylation in T98G cells, it is important to highlight that the basal level of pERK-1/2 were also diminished. Basal levels of pERK-1/2 were also suppressed in T98G cells treated with PDGFR inhibitor IV, but not inhibitor V. Taken together this data suggests that basal phosphorylation of ERK-1/2 may be regulated via a mechanism independent of PDGFR and that c-Abl kinase maybe involved in some part in regulating pERK-1/2 in T98G cells.

Compared to the other cell lines, MG63 cells had the lowest levels of basal pERK-1/2. In both MG63 and KHOS-240S cells PDGF-AA or PDGF-BB stimulation significantly increased the pERK-1/2 relative to un-stimulated controls. PDGFR inhibitor IV or V attenuated the activation of ERK-1/2 (+PDGF-AA or BB) in all samples, with the exception of pERK-2 (+PDGF-BB) which was not blocked by inhibitor V. NRP-1 siRNA did not inhibit the activation of ERK-1/2 (+PDGF-AA or BB) in MG63 cells, however, NRP-1 siRNA treatment significantly decreased ($P<0.01$) PDGF stimulated phosphorylation of ERK-1 in KHOS-240S cells. In summary, these results show that in MG63 and KHOS-240S cells, both isoforms of PDGF stimulate ERK-1/2 phosphorylation and this can be

inhibited by PDGFR inhibitor IV or V (except in the aforementioned sample). In KHOS-240S cells, PDGF stimulated phosphorylation of ERK-1 appears to be mediated, in part, by NRP-1 (Figures 5.8 and 5.9).

To summarise, compared to PDGF-BB, PDGF-AA stimulated lower increase in pERK-1/2 levels and only cell lines with high phosphorylation of PDGFR-α (KHOS-240S and MG63) showed significant increases in pERK-1/2 following PDGF-AA stimulation. Whereas, PDGF-BB significantly increased pERK-1 in all of the cancer cell lines and pERK-2 in all except, U87MG cells. NRP-1 siRNA significantly inhibited pERK-1/2 in T98G cells and pERK-1 in KHOS-240S cells (+PDGF-AA or PDGF-BB). In all of the cells PDGFR inhibitor IV, but not inhibitor V, blocked ERK-1/2 phosphorylation (+/-PDGFs), whereas inhibitor V showed more specificity towards ERK-1. The differential effects of inhibitor IV and V suggests that blockade of c-Abl kinase is able to confer greater inhibition of the ERK pathway. Overall, these results show that in different cell types some similarities in the pattern of ERK-1/2 phosphorylation can be observed, for e.g. the effects of inhibitor IV. However, NRP-1 only affects PDGF mediated activation of pERK-1/2 in a subset of cells and in the majority of these cells, only ERK-1 is inhibited. This suggests that NRP-1 may largely control PDGF activation of ERK-1 and this is cell-type specific.

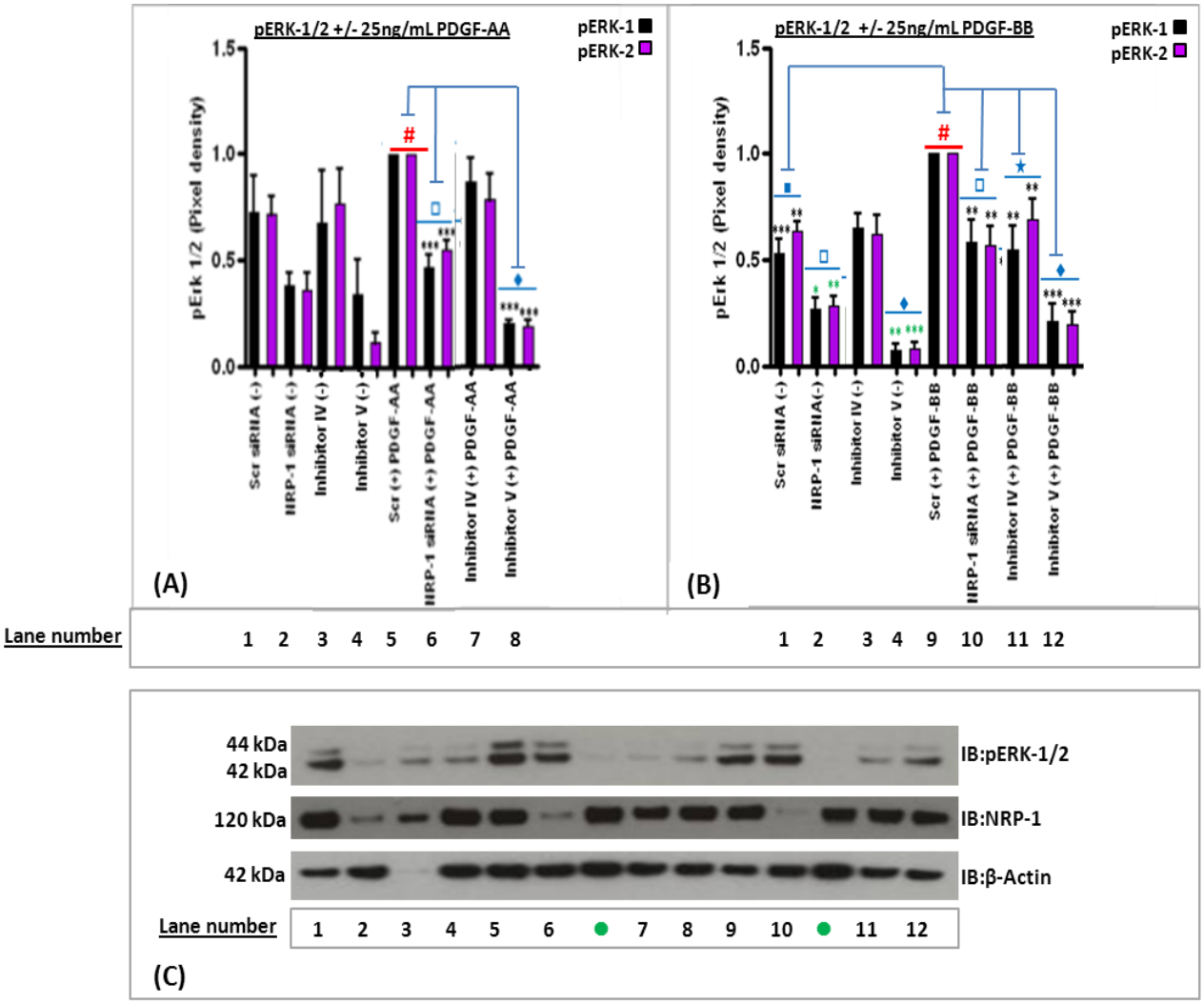

Figure 5.7: NRP-1 siRNA inhibits PDGF-stimulated phosphorylation of ERK-1/2 in T98G cells
To quantify the levels of pERK-1/2 pixel densities were calculated using Gene Tools v3 software. The histograms in **(A)** and **(B)** illustrate the quantified levels of pERK-1 (■) and pERK-2 (■) in cells stimulated with PDGF-AA or PDGF-BB. The values on the histograms were calculated as a ratio relative to the Scr (+) PDGF-AA in **(A)** lane 5, indicated by the # symbol or the Scr (+) PDGF-BB in **(B)** lane 5, indicated by the # symbol. Data presented is the mean value from at least three experimental repeats +/- calculated standard errors. Asterisks (*) indicate significance (calculated by one-way ANOVA, *P*<0.05*, *P*<0.01**, *P*<0.001***). **(A)** PDGFR inhibitor IV (♦) or NRP-1 (□) siRNA treatment of cells significantly attenuated the PDGF-AA stimulated increase in pERK-1/2. As PDGF-AA did not significantly increase the levels of pERK-1/2 in Scrambled control cells (Lane 1 v Lane 6), this suggests that ERK-1/2 phosphorylation is not driven by PDGF-AA in T98G cells. **(B)** PDGF-BB (#) significantly increased pERK-1/2 relative to un-stimulated controls (■). PDGFR inhibitor IV (♦), inhibitor V (★) or NRP-1 (□) siRNA treatment of cells significantly attenuated PDGF-BB stimulated phosphorylation of ERK-1/2. The green asterisks (*) indicate that NRP-1 siRNA treatment of cells and PDGFR inhibitor IV significantly inhibit pERK-1/2 phosphorylation in the absence of PDGF-BB. This suggests that these factors may regulate pERK-1/2 independently of PDGFR signalling. **(C)** Immunoblots detected pERK-1/2, NRP-1 and β-Actin in T98G cells. The data indicated between immunoblot lanes 6/8 and 10/12 (●) was not used in this analysis.

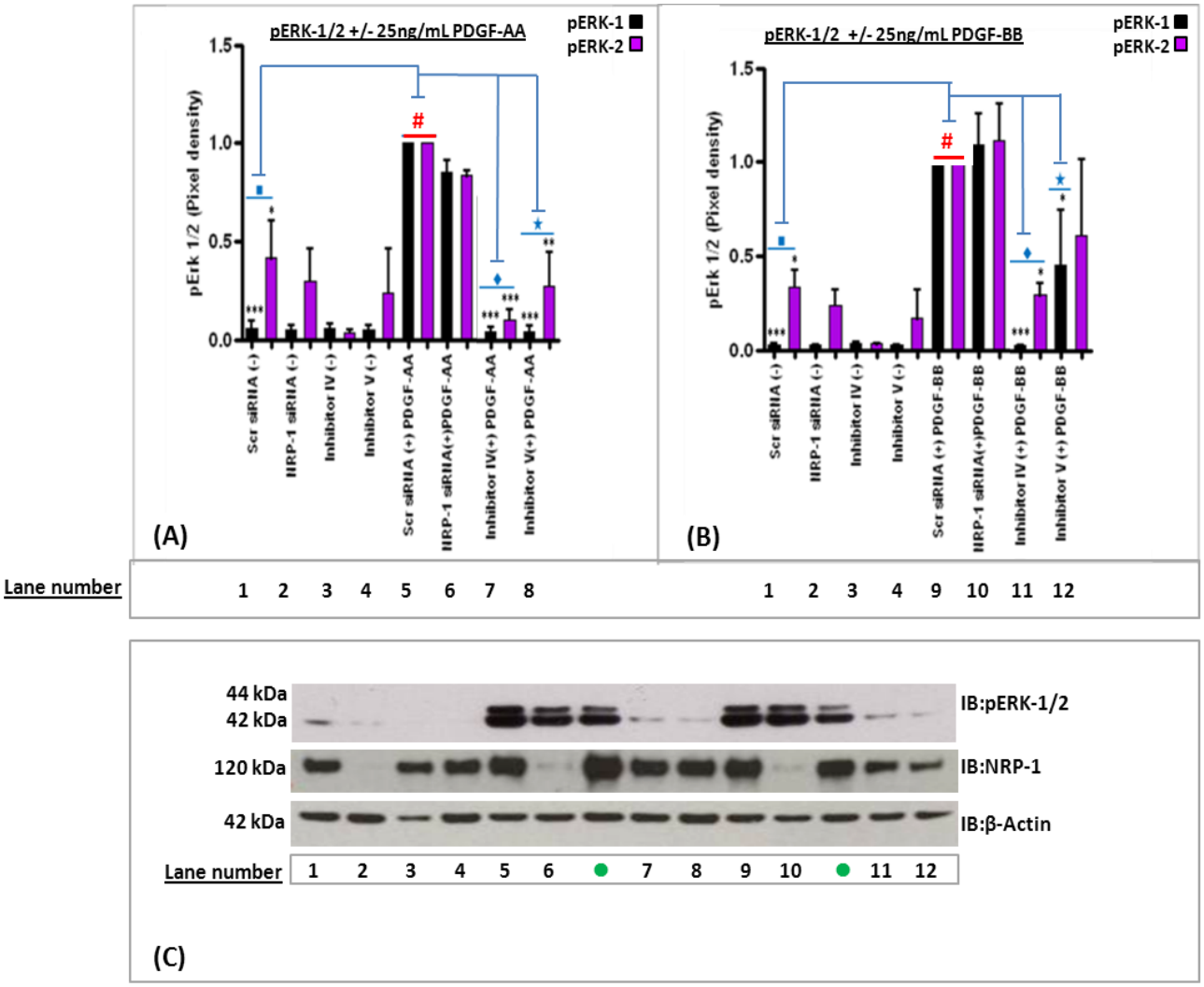

Figure 5.8: NRP-1 siRNA does not inhibit PDGF-stimulated phosphorylation of ERK-1/2 in MG63 cells

To quantify the levels of pERK-1/2 pixel densities were calculated using Gene Tools v3 software. The histograms in **(A)** and **(B)** illustrate the quantified levels of pERK-1 (■) and pERK-2 (■) in cells stimulated with PDGF-AA or PDGF-BB. The values on the histograms were calculated as a ratio relative to the Scr (+) PDGF-AA in **(A)** lane 5, indicated by the # symbol or the Scr (+) PDGF-BB in **(B)** lane 5, indicated by the # symbol. Data presented is the mean value from at least three experimental repeats +/- calculated standard errors. Asterisks (*) indicate significance (calculated by one-way ANOVA, $P<0.05$*, $P<0.01$**, $P<0.001$***). **(A)** PDGF-AA (#) significantly increased the phosphorylation of ERK-1/2 relative to un-stimulated controls (■). PDGFR inhibitor IV (♦) and inhibitor V (★) significantly attenuated pERK-1/2 levels. **(B)** PDGF-BB (#) significantly increased pERK-1/2 relative to un-stimulated controls (■). PDGFR inhibitor IV (♦), inhibitor V blocked PDGF-BB stimulated phosphorylation of ERK-1/2. NRP-1 siRNA treatment of cells did not inhibit ERK-1/2 phosphorylation. **(C)** Immunoblots detected pERK-1/2, NRP-1 and β-Actin in MG63 cells. The data indicated between immunoblot lanes 6/7 and 10/11 (●) was not used in this analysis.

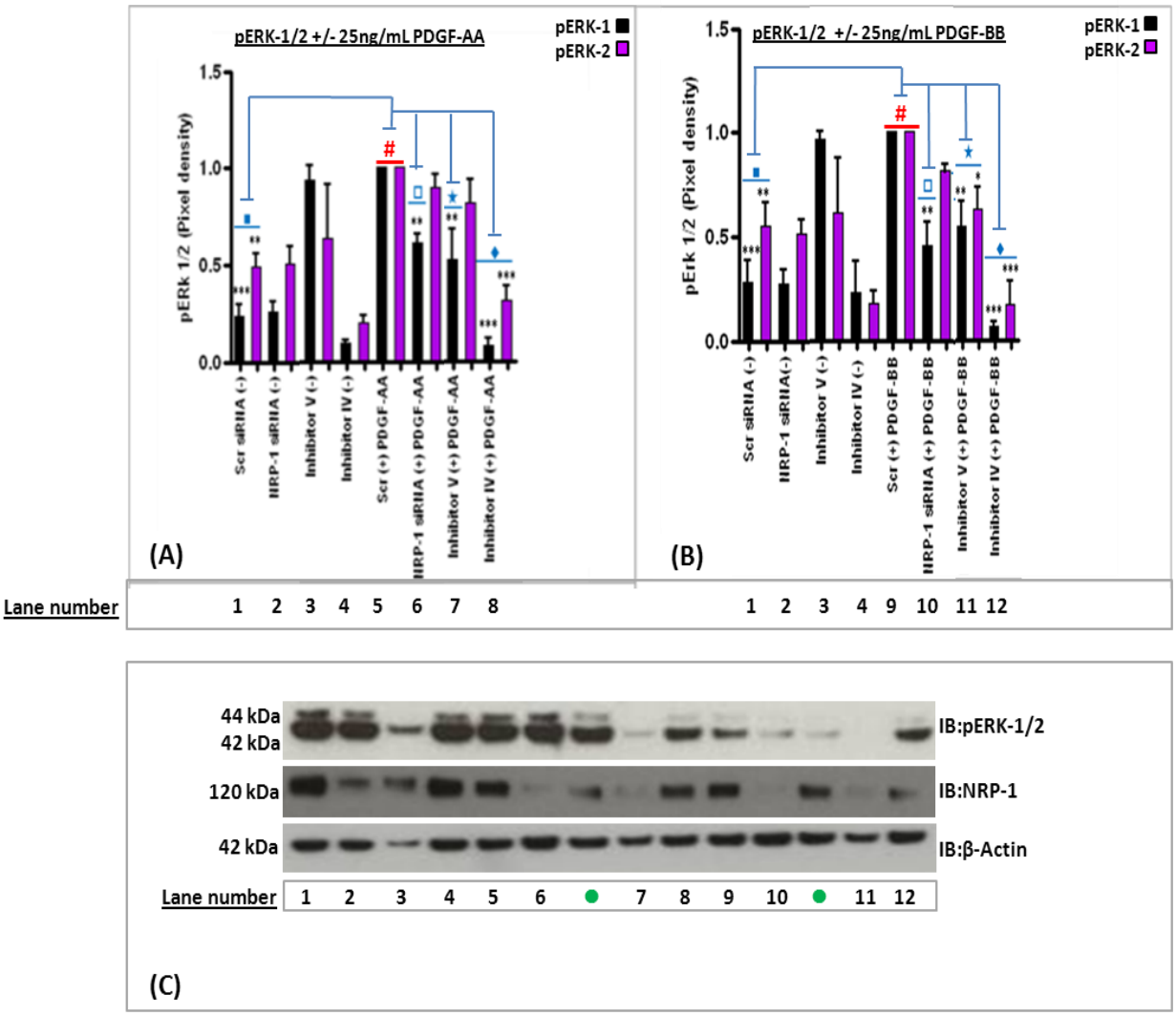

Figure 5.9: NRP-1 siRNA inhibits PDGF-stimulated phosphorylation of ERK-1/2 in KHOS-240S cells

To quantify the levels of pERK-1/2 pixel densities were calculated using Gene Tools v3 software. The histograms in **(A)** and **(B)** illustrate the quantified levels of pERK-1 (■) and pERK-2 (■) in cells stimulated with PDGF-AA or PDGF-BB. The values on the histograms were calculated as a ratio relative to the Scr (+) PDGF-AA in **(A)** lane 5, indicated by the # symbol or the Scr (+) PDGF-BB in **(B)** lane 5, indicated by the # symbol. Data presented is the mean value from at least three experimental repeats +/- calculated standard errors. Asterisks (*) indicate significance (calculated by one-way ANOVA, $P<0.05$*, $P<0.01$**, $P<0.001$***). **(A)** PDGF-AA (#) significantly increased pERK-1/2 relative to un-stimulated controls (■). PDGFR inhibitor V (★) and NRP-1 (□) siRNA treatment of cells significantly attenuated ERK-1 phosphorylation. Inhibitor IV (♦) blocked PDGF-AA stimulated phosphorylation of ERK-1/2. **(B)** PDGF-BB (#) significantly increased the levels of pERK-1/2 relative to un-stimulated controls (■) and PDGFR inhibitor IV (♦) or inhibitor V inhibited this increase in pERK-1/2. NRP-1 (□) siRNA treatment of cells inhibited the increase in pERK-1 stimulated by PDGF-BB. **(C)** Immunoblots detected pERK-1/2, NRP-1 and β-Actin in KHOS-240S cells. The data indicated between immunoblot lanes 6/7 and 10/11 (●) was not used in this analysis.

5.3 Summary

As illustrated in Chapter 4 (Section 4.2.4), PDGF potentiated the NRP-1: PDGFR interactions in some of the mesenchymal tumour cell lines but not others. It was hypothesised that, in part NRP-1s interaction with PDGF growth factors PDGFs may serve to control the kinase activity and signalling of PDGFRs. This Chapter specifically examined the contribution of NRP-1 to controlling the overall kinase activity of PDGFR and the activation of several primary downstream signalling pathways.

The results from this Chapter are summarised in Figure 5.33. In all of the cells, PDGF ligand stimulated the phosphorylation of PDGFR, AKT and PLC-γ and this was blocked by inhibitor IV or V (this was with the exception of the U87MG cells (PTEN null) that showed aberrant activation of AKT without PDGF ligand stimulation). These results illustrate that the activation status of PDGFR can determine if these downstream pathways are 'on' or 'off'. It is important to highlight that the total levels of PDGFRs and associated downstream proteins were not determined as part of this analysis. Consequently, the increased protein phosphorylation may be attributed to a change in total protein expression stimulated by PDGF. As a control, to ensure the effects on phosphorylation are not due to a change in total protein expression, total and phosphorylated protein levels should be quantified in future experiments.

The relative contribution of NRP-1 to PDGFR signalling varied in the different cell types. NRP-1 was not critical for the phosphorylation of PDGFR-α or PDGFR-β in any of the cell lines, however NRP-1 siRNA treatment inhibited PDGF-mediated activation of the PI3K-AKT and/or the Ras-ERK pathway in T98G and KHOS-240S cells but the PLC-γ pathway was not affected. This suggests that NRP-1 may exert specific subtle effects on particular PDGFR signalling pathways, without altering the overall kinase activity of the receptor and this is cell type–specific. Pellet-Many et al (2011) also documented that the phosphorylation of PDGFR-β (+PDGF-BB) was not effected by NRP-1 siRNA, yet cellular effects on migration were detected following knockdown of NRP-1 (with an underlying mechanism involving p130Cas). With this in mind, it maybe that in the certain tumour cell lines different mechanisms of NRP-1/PDGFR crosstalk exist to regulate highly specific signalling to controls cellular behaviour. To elucide which underlying factors may control the cell-type specificity of NRP-1/PDGFR crosstalk it may be advantageous to further characterise the expression of other key NRP-1 interacting proteins in these cells and also assay cellular behaviour following NRP-1 knockdown. The next therefore Chapter examines whether or not NRP-1 was essential for PDGF mediated migration or proliferation of the mesenchymal tumour cells. Such

effects on cellular behaviour may imply NRP-1/PDGFR crosstalk is regulating alternative underlying PDGFR signalling mechanisms than those examined in this Chapter.

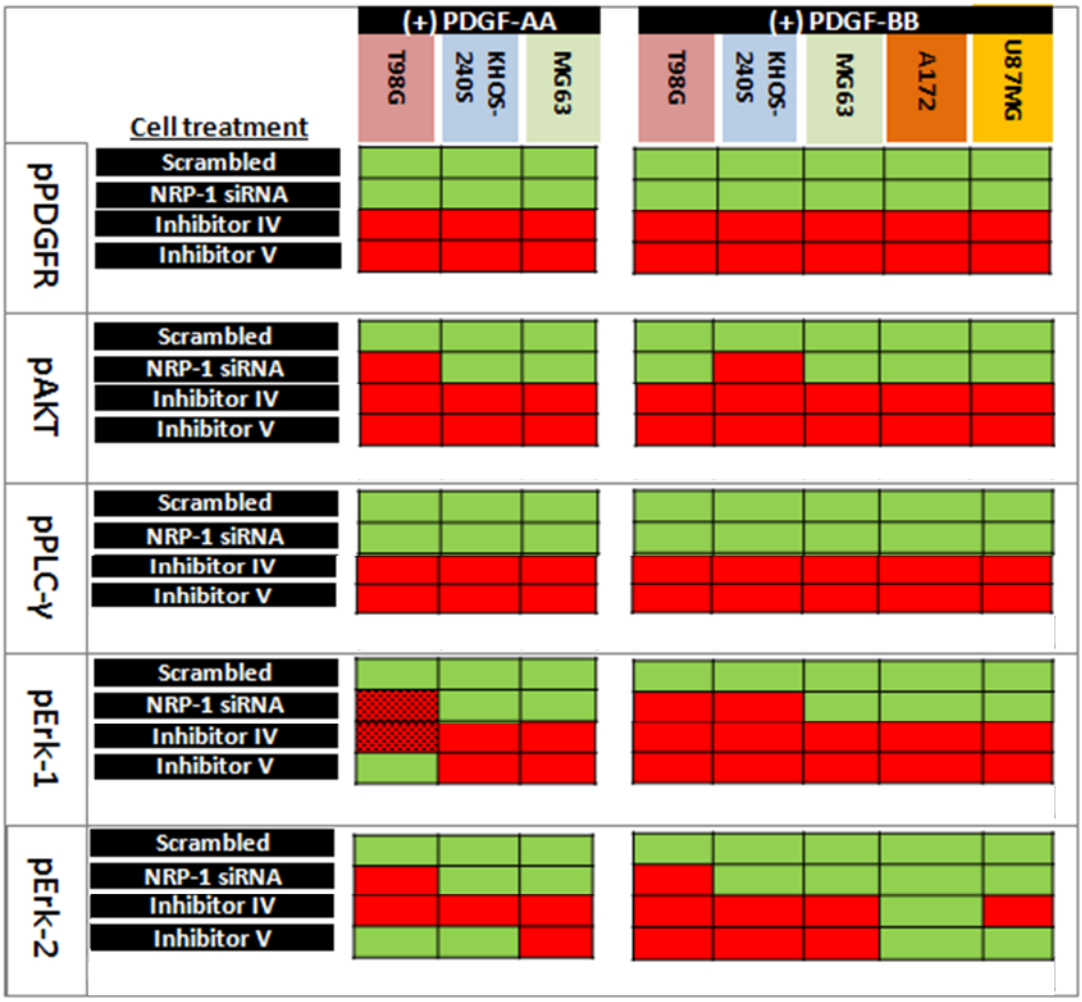

Figure 5.10: The kinase activity and signalling of PDGFRs in the mesenchymal tumour cells
The heat map details the activation status of PDGFR and primary downstream PDGFR signalling pathways in the mesenchymal tumour cells treated with either PDGF-AA or PDGF-BB. The green panels ( ) indicate significantly elevated levels of the phosphorylated proteins whereas the red panels ( ) indicate significantly reduced levels of the phosphorylated proteins in the different treatment groups stimulated with PDGF-AA (left panels) or PDGF-BB (right panels). The hashed panel ( ) indicates that in the T98G cells the phosphorylation of ERK-1 is significantly inhibited in the NRP-1 siRNA and Inhibitor IV treatment groups in both the presence and absence of the PDGF-AA ligand. The heat map clearly illustrates that PDGF-AA or PDGF-BB induced a significant increase in the levels of pPDGFR and NRP-1 siRNA did not inhibit this. NRP-1 did not affect the levels of pPLC-γ in any of the cells. NRP-1 siRNA treatment differentially effected the phosphorylation of ERK-1/2 and AKT in the panel of glioma and osteosarcoma cell lines.

5.3.1 Chapter 5: principal findings

- All the mesenchymal tumour cells show no dependence on NRP-1 for the phosphorylation of PDGFR-α and/or PDGFR-β.

- NRP-1 is not important for PDGF-stimulated phosphorylation of PLC-γ in all the mesenchymal tumour cell lines.

- In T98G, KHOS-240S and MG63 cells, NRP-1 is important for PDGF-stimulated activation of the Ras-ERK and/or PI3K-AKT signalling pathways.

Chapter 6 – Results

The influence of NRP-1/PDGFR crosstalk on the proliferation and migration of mesenchymal tumour cells

6.0 Introduction

As detailed in Chapter 5, NRP-1 knockdown does not attenuate PDGFR phosphorylation however, in some cell lines, specific effects on PDGF stimulated phosphorylation of ERK-1/2 and AKT can be detected which may suggest NRP-1 somehow directs PDGFR downstream signalling. As alluded to, previous findings have outlined that NRP-1 controls PDGF-BB stimulated downstream PDGFR signalling without affecting the phosphorylation of PDGFR (Evans et al., 2011; Pellet-Many et al., 2011) and importantly, in these studies NRP-1 knockdown attenuated cell migration towards PDGF-BB. It is feasible such novel mechanisms of NRP-1/PDGFR crosstalk may also exist to regulate the cellular behaviour of the tumour cell lines and the underlying mechanism may have not been elucidated in Chapter 5, as only selected downstream PDGFR markers were assayed. This Chapter, therefore investigated whether or not NRP-1 effected PDGFR mediated proliferation and migration of the mesenchymal tumour cells.

6.1 The influence of NRP-1 on PDGFR-mediated survival of the mesenchymal tumour cells

6.1.1 NRP-1 has no effect on PDGF-stimulated mesenchymal cancer cell survival

A primary driver of glioma and osteosarcoma proliferation is the autocrine secretion of PDGF ligands and constitutive activation PDGFR signalling (Chin et al., 1997; Hoelzinger et al., 2007; McGary et al., 2002; Ranza et al.,2007; Sulzbacher et al., 2000). This section explores whether exogenous PDGF can promote the proliferation of the mesenchymal tumour cells and whether or not NRP-1 effects this proliferation. Briefly, cells were treated with NRP-1 siRNA or Scr oligonucleotides and incubated for 72 hr with either PDGF-AA or PDGF-BB. Cell proliferation was assessed using the CyQuant® proliferation assay, which measures the cellular DNA to determine the cell number (for detailed methods see, Chapter 2, Section 2.5.1).

The proliferative response of KHOS-240S and MG63 osteosarcoma cells to PDGF ligands was very similar so only the data for KHOS-240S cells is illustrated (Figure 6.0) (data for MG63 cells is presented in the Appendix, Figure 8.26). In the osteosarcoma cells, PDGF-AA or PDGF-BB stimulated a significant increase ($P<0.05$) in cell number relative to un-stimulated controls. Relative to scrambled control cells, NRP-1 siRNA did not significantly inhibit PDGF stimulated proliferation of either KHOS-240S (Figure 6.0) or MG63 cells.

Compared to the osteosarcoma cells, the glioma cell lines exhibited a diminished proliferative response to PDGF ligands. In U87MG, T98G and A172 cells, PDGF-AA or PDGF-BB stimulated no significant increase in cell proliferation. NRP-1 siRNA treatment did not affect the survival of A172 or U87MG cells (Appendix, Figures 8.25 and 8.27, respectively). The basal level of cell proliferation showed a small but significant reduction in T98G cells treated with NRP-1 siRNA ($P<0.01$) (Figure 6.1). Together these results illustrate that, out of the glioma cell lines, only A172 proliferated in response to PDGF-BB and again NRP-1 did not block cell proliferation.

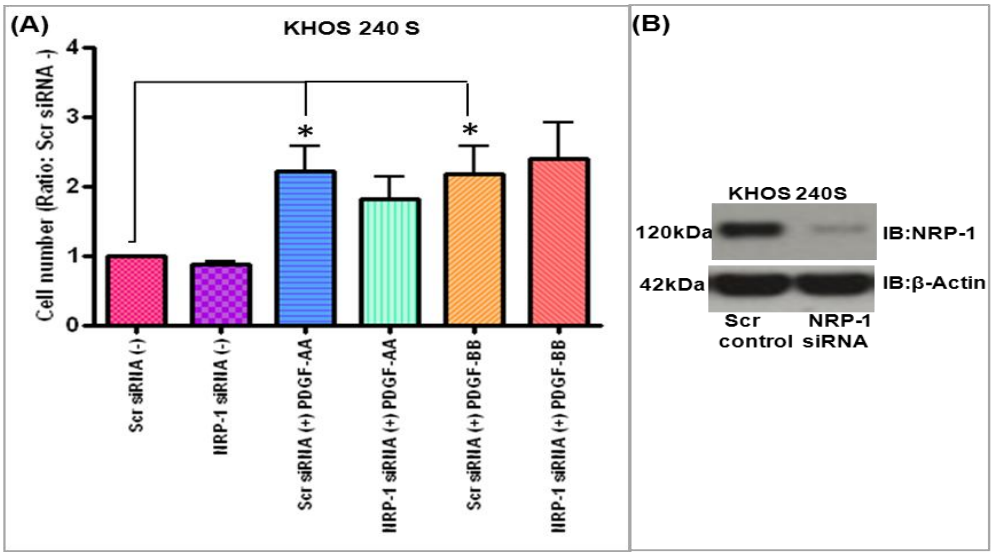

Figure 6.0: PDGF-AA or PDGF-BB stimulated KHOS-240S cell proliferation

(A) The histogram illustrates cell numbers as determined by the CyQuant® assay. Cell numbers have been expressed as a ratio relative to un-stimulated scrambled control cells (■). PDGF-AA (■) or BB (■) stimulated a significant increase in cell number relative to un-stimulated controls (■). NRP-1 siRNA (■) treatment decreased KHOS-240S cell number, though this was not significant. **(B)** The Immunoblot data illustrates that NRP-1 siRNA treatment blocks the expression of NRP-1 in KHOS-240S cells. Asterisks indicate significance relative to un-treated controls (calculated by one-way ANOVA, $P < 0.05$*).

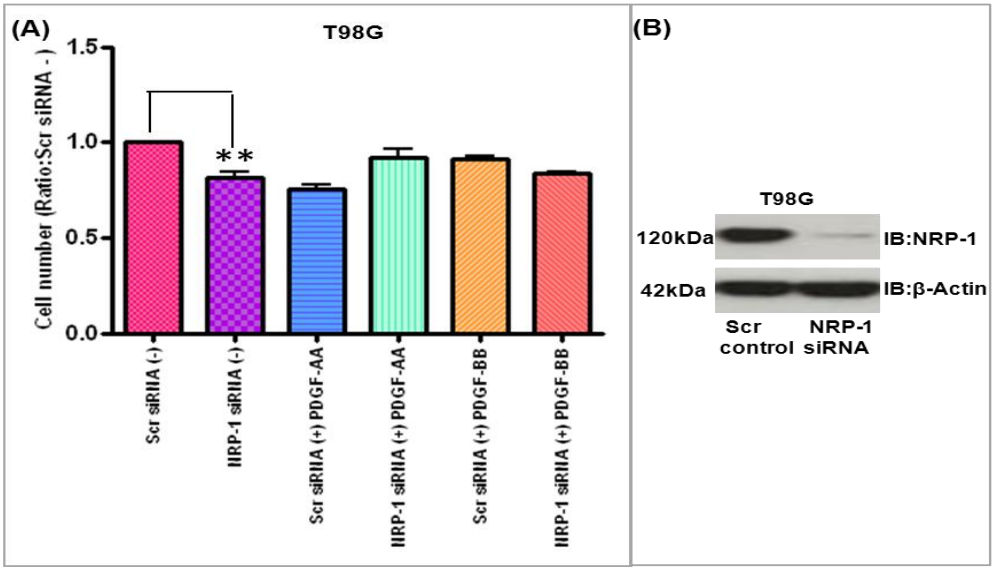

Figure 6.1: PDGF-AA or PDGF-BB stimulated an increase in T98G cell proliferation

(A)The histogram illustrates cell numbers as determined by the CyQuant® assay. Cell numbers have been expressed as a ratio relative to un-stimulated scrambled control cells (■). PDGF-AA (■) or BB (■) stimulated no significant increase in cell number relative to un-stimulated controls (■). NRP-1 siRNA (■) treatment did stimulated a small but significant decrease in basal cell survival (■). **(B)** The Immunoblot data illustrates that NRP-1 siRNA treatment blocks the expression of NRP-1 in T98G cells. Asterisks indicate significance relative to un-treated controls (calculated by one-way ANOVA, $P < 0.01$**).

6.2 PDGFR-mediated migration of the mesenchymal tumour cells: the influence of NRP-1

PDGF growth factors are known chemo attractants for a number of cell types including; smooth muscle cells (Nelson et al., 1997), fibroblasts (Seppä et al., 1982; Yu et al., 2001), stem cells (Ozaki et al., 2007), and cancer cells (Lin et al., 2009; Uren et al., 2003; Wach et al., 1996). In glioma, PDGF also promotes cell migration which is reported to be mediated through PDGFR activation of the PI3K pathway (Cattaneo et al., 2006). However, in another study PDGF-BB is reported to regulate glioma cell migration via an alternative mechanism not involving PI3K. Instead migration is controlled via a mechanism involving NRP-1, PDGF-BB and p130Cas (Evans et al., 2011). Osteosarcoma cells also show a migratory response to PDGF, with PDGF-BB and PDGF-AB inducing the greatest degree of migration (Allam et al., 1992; Celotti et al.,2006; Mehrotra et al., 2004).

This section examines the migratory response of the mesenchymal tumour cells to PDGF-AA and PDGF-BB, and whether or not NRP-1 effects PDGF-mediated cell migration. A cell-exclusion migration assay was used to quantify the migratory response of cells (see Chapter 2, Section 2.5.2). Briefly, cells were treated with scrambled oligonucleotides or NRP-1 siRNA before equal numbers of cells were plated into two separate chambers of a specific iBidi culture insert. Culture inserts were removed, leaving a cell free gap of 500 μM. Cells were treated (+/-) PDGF and the cell free gap was imaged at 0 hr, 4 hr, 8 hr and 24 hr. Using Image J, the area of the cell free gap was measured at time 0 hr and compared to the 4 hr, 8 hr and 24 hr, to quantify the percentage of migration over time.

At 4 hr and 8 hr PDGF-AA stimulated no significant increase in the migration of MG63 or KHOS-240S cells but by 24 hr PDGF-AA, had significantly potentiated ($P<0.001$) cell migration. PDGFR inhibitor V significantly inhibited PDGF-AA-stimulated migration of MG63 and KHOS-240S cells. In KHOS-240S cells treated with NRP-1 siRNA PDGF-AA stimulated migration was significantly suppressed at 24 hr ($P<0.001$), Figure 6.2. In MG63 cells NRP-1 siRNA treatment did not inhibit PDGF-AA stimulated cell migration (Appendix, Figure 8.28).

PDGF-BB stimulated a significant increase in the migration of KHOS-240S and MG63 cells at 8 hr and 24 hr and in KHOS-240S migration was also enhanced at 4 hr ($P<0.001$). Migration of MG63 cells (+PDGF-BB) was blocked by PDGFR inhibitor V ($P<0.001$) but not NRP-1 siRNA (Appendix, Figure 8.29). However, in KHOS-240S cells NRP-1 siRNA treatment significantly inhibited PDGF-BB stimulated cell migration at 4 hr ($P<0.001$), 8 hr ($P<0.05$) and 24 hr ($P<0.001$), see Figure 6.3. PDGFR inhibitor V also blocked the migration of KHOS-240S cells at 4 hr ($P<0.001$) and 24 hr ($P<0.001$), and at 8hr there was a trend for decreased migration in cells treated with inhibitor V. Together these results illustrate that PDGF growth factors stimulate the migration of both KHOS-240S and MG63 cells, with PDGF-BB stimulating a more rapid rate of migration in both cell lines. PDGF-stimulated migration was blocked through treating cells with inhibitor V, suggesting a critical role for PDGFR signalling in mediating the motility of KHOS-240S and MG63 cells. NRP-1 siRNA treatment also significantly attenuated KHOS-240S, but not MG63 cell migration, which illustrates that KHOS-240S cells show some dependence on NRP-1 for PDGF-stimulated cell motility.

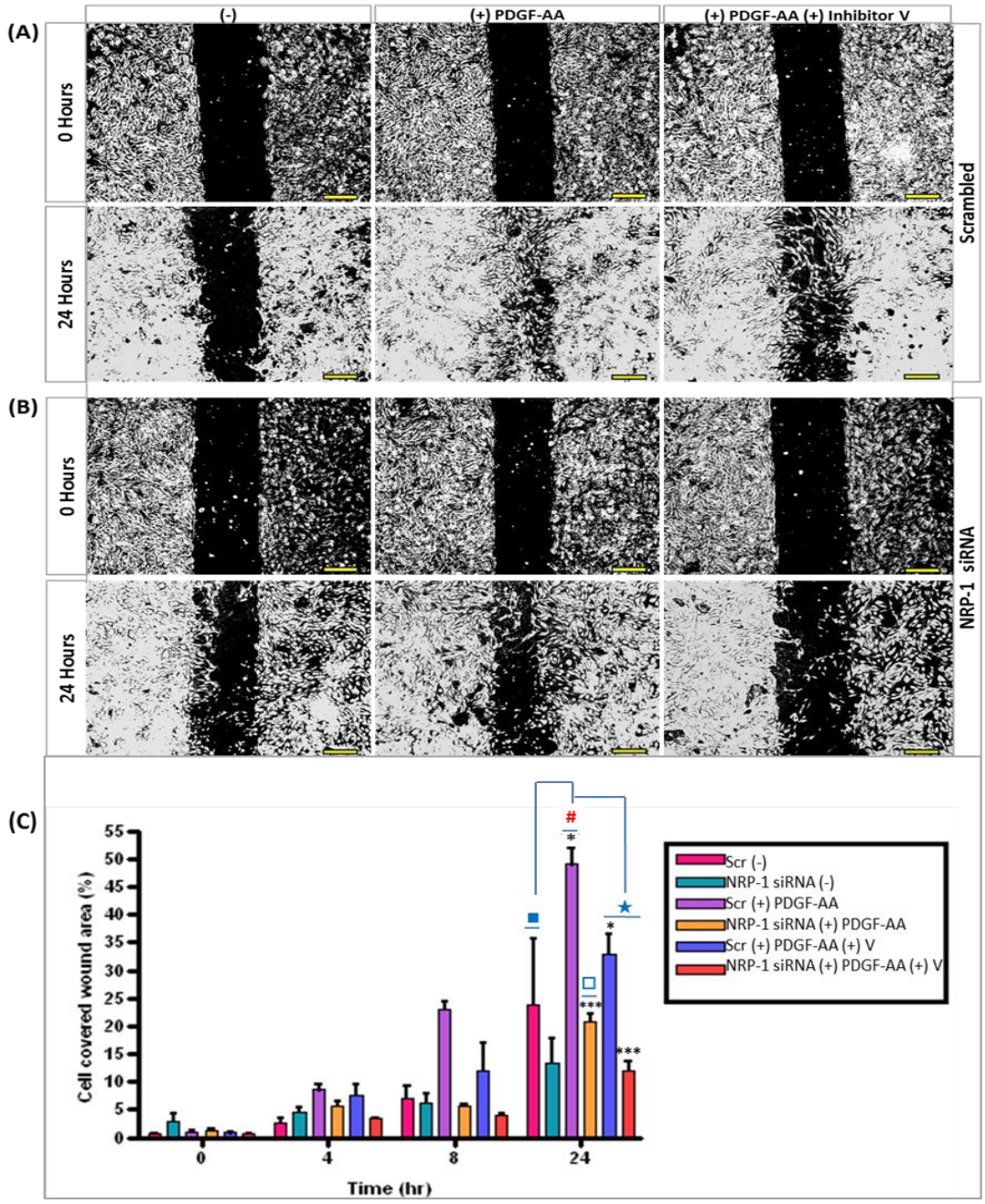

Figure 6.2: PDGF-AA stimulated the migration of KHOS-240S cells

The figures in **(A)** and **(B)** illustrate representative images taken at time 0 hr and 24 hr. Images have been converted to binary images for clear visualisation of cell-free areas. **(A)** Scrambled control or **(B)** NRP-1 siRNA treated KHOS-240S cells were left un-stimulated or stimulated with PDGF-AA (+/- PDGFR inhibitor V). The top row of panels illustrates cells imaged at 0 hr, with the corresponding 24 hr images positioned directly below. **(C)** The histogram plots the % cell covered area relative to the total area (defined at 0 hr). At 24 hr, the (#) symbol highlights that PDGF-AA induced a significant increase in KHOS-240S cell migration in scrambled control cells relative to un-stimulated controls (■). NRP-1 siRNA significantly inhibited the migration of KHOS-240S cells (+PDGF-AA) relative to scrambled controls (□). Treatment of KHOS-240S cells with inhibitor V significantly attenuated migration (★). Results are representative of at least two experimental repeats. Asterisks indicate significance relative to un-stimulated controls (calculated by one-way ANOVA, $P < 0.05$*, $P < 0.01$**, $P < 0.001$***). Scale bar=250 µm.

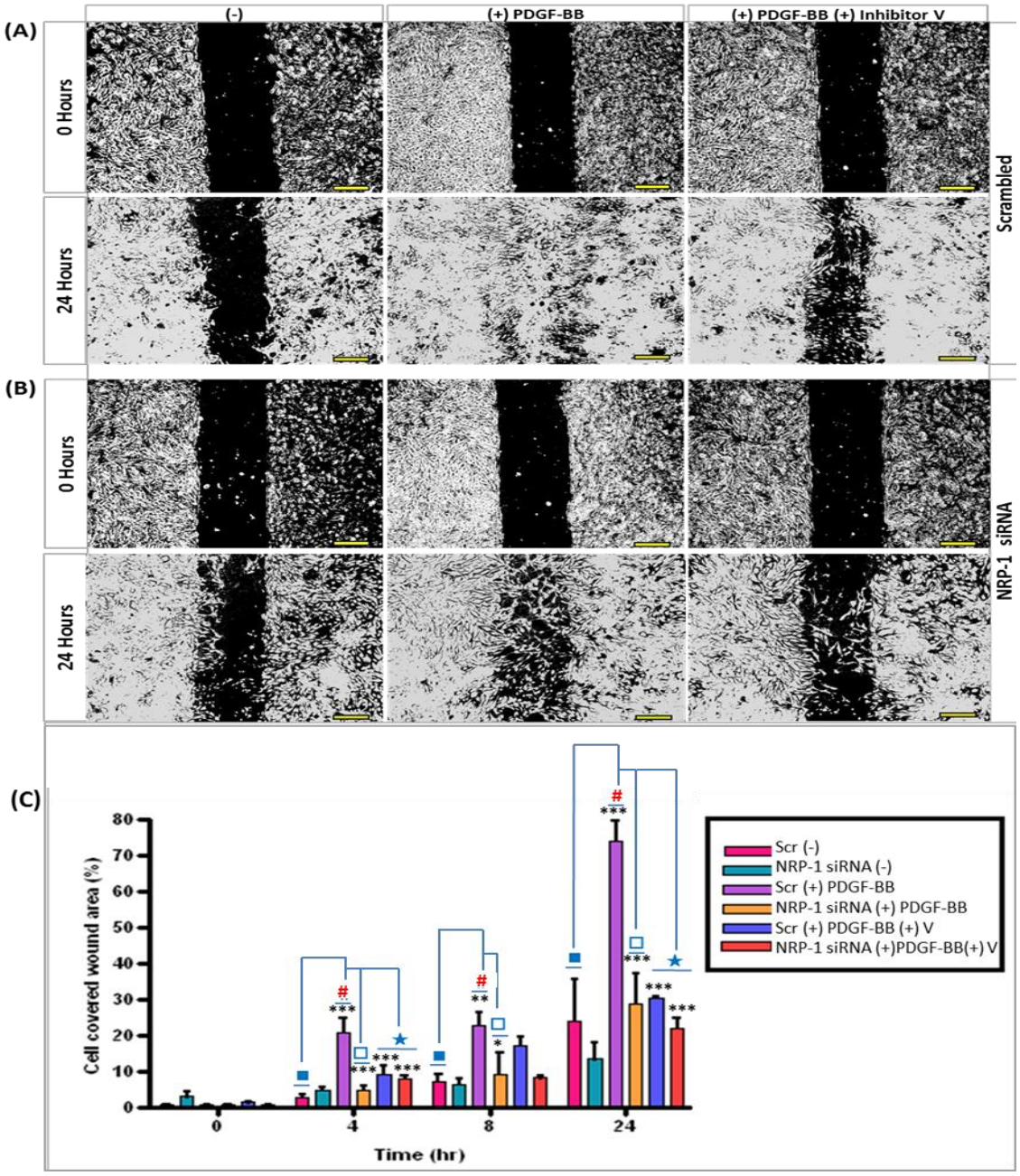

Figure 6.3: PDGF-BB stimulated the migration of KHOS-240S cells

The figures in **(A)** and **(B)** illustrate representative images taken at time 0 hr and 24 hr. Images have been converted to binary images for clear visualisation of cell-free areas. **(A)** Scrambled control or **(B)** NRP-1 siRNA treated KHOS-240S cells were left un-stimulated or stimulated with PDGF-BB (+/- PDGFR inhibitor V). The top row of panels illustrates cells imaged at 0 hr, with the corresponding 24 hr images positioned directly below. **(C)** The histogram plots the % cell covered area relative to the total area (defined at 0 hr). At 4 hr, 8 hr and 24 hr, the (#) symbol highlights that PDGF-BB induced a significant increase in KHOS-240S cell migration in scrambled control cells relative to un-stimulated controls (■). NRP-1 siRNA significantly inhibited the migration of KHOS-240S cells (+PDGF-BB) relative to scrambled controls (□) at 4 hr, 8 hr and 24 hr. Treatment of KHOS-240S cells with inhibitor V significantly attenuated migration (★) at 4hr and 24 hr. Results are representative of at least two experimental repeats. Asterisks indicate significance relative to un-stimulated controls (calculated by one-way ANOVA, $P < 0.05$*, $P < 0.01$**, $P < 0.001$***). Scale bar=250 µm.

Out of the glioma cell lines, only A172 and T98G cell migration was examined. This was because U87MG cells tended to form spheroids (which were less adherent) and the cells formed networks rather than monolayers. Thus, on removal of the iBidi cultures insert, the U87MG were frequently detached, leaving patches in the cell monolayers and unequal cell exclusion zones, therefore, the migration of U87MG cells could not be accurately determined using this method.

Based on the data in Chapter 5, which detailed that T98G cells showed little or no phosphorylation of PDGFR-α (following PDGF-AA stimulation), only the migratory response of T98G cells to PDGF-BB was examined. In T98G cells, PDGF-BB stimulated a significant increase in cell migration at 4 hr ($P<0.05$), 8 hr ($P<0.01$) and 24 hr ($P<0.01$). NRP-1 siRNA treatment of cells induced a significant decrease in the basal level of T98G cell migration at 4 hr ($P<0.05$), 8 hr ($P<0.001$) or 24 hr ($P<0.01$), however, at 4 hr and 8 hr PDGF-BB stimulation restores the migratory potential of NRP-1 siRNA treated cells. Thus, at these early time-points, PDGF-BB stimulated migration is comparable in scrambled or NRP-1 siRNA treated T98G cells. However, by 24 hr, PDGF-BB stimulated migration of T98G cells treated with NRP-1 siRNA showed a small but significant decrease ($P<0.05$) compared to scrambled controls. This might imply that NRP-1 siRNA exerts a subtle inhibitory effect on T98G migration, which cumulates over time to attenuate T98G cells migratory response to PDGF-BB (Figure 6.4).

As in the previous Chapter, only the response of A172 cells to PDGF-BB was assayed. In A172 cells, PDGF-BB stimulated no significant increase in cell migration at 4hr, 8hr or 24hr and PDGFR inhibitor V did not significantly inhibit the migration of A172 cells at the different time-points. The migration of A172 cells was low compared to the other cell lines tested, which suggested that these cells are less motile than the other cell lines. The data also shows the A172 cells do not migrate in response to PDGF-BB and basal migration is not influenced by either NRP-1 or PDGFR (Appendix, Figure 8.30).

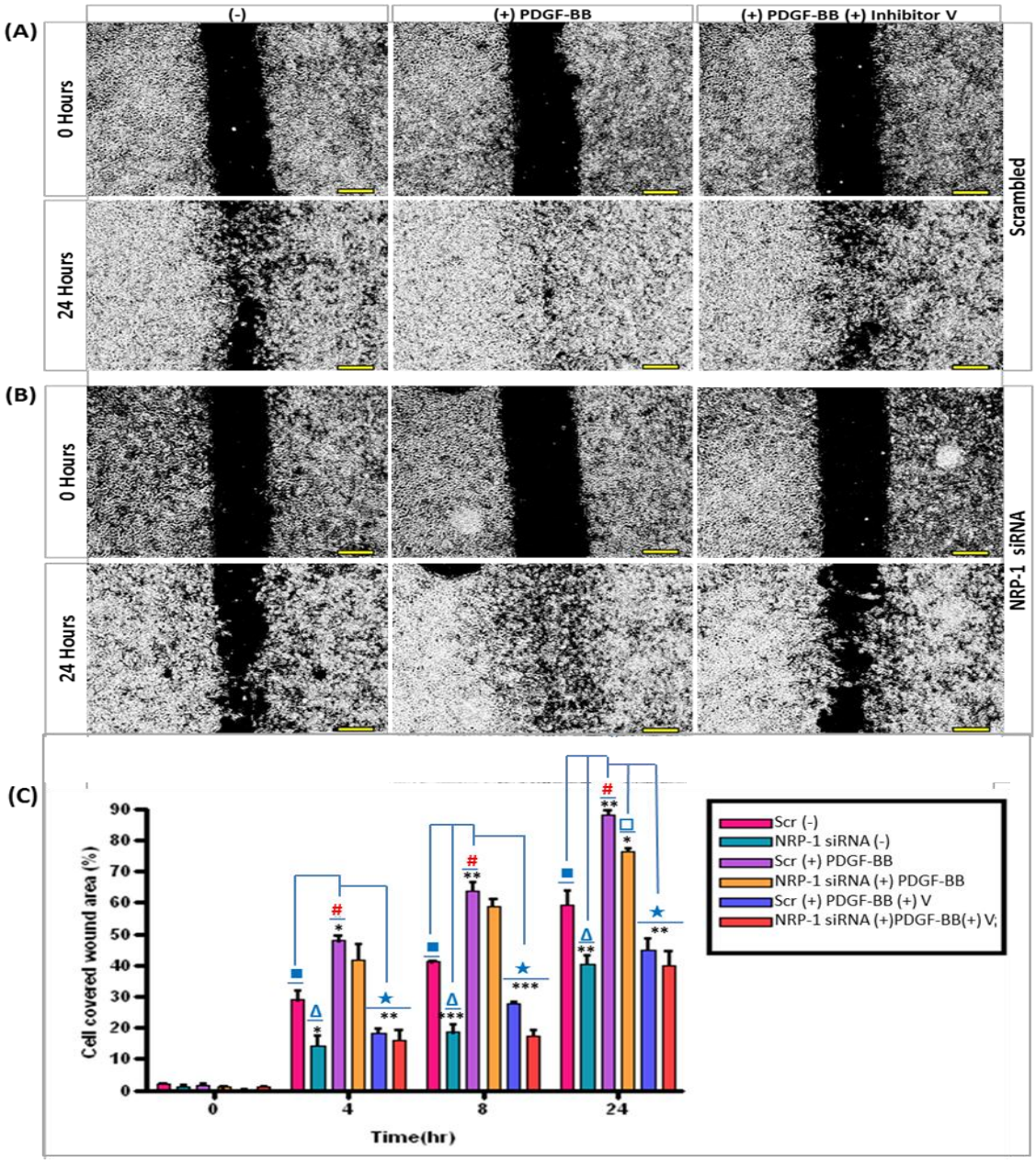

Figure 6.4: PDGF-BB stimulated the migration of T98G cells

The figures in **(A)** and **(B)** illustrate representative images taken at time 0 hr and 24 hr. Images have been converted to binary images for clear visualisation of cell-free areas. **(A)** Scrambled control or **(B)** NRP-1 siRNA treated T98G cells were left un-stimulated or stimulated with PDGF-BB (+/- PDGFR inhibitor V). The top row of panels illustrates cells imaged at 0 hr, with the corresponding 24 hr images positioned directly below. **(C)** The histogram plots the % cell covered area relative to the total area (defined at 0 hr). At 4 hr, 8 hr and 24 hr, the (#) symbol highlights that PDGF-BB induced a significant increase in T98G cell migration in scrambled control cells relative to un-stimulated controls (■). NRP-1 siRNA significantly inhibited the basal migration of T98G cells (+PDGF-BB) (Δ) relative to scrambled controls (■) at 4 hr, 8 hr and 24 hr. At 24 hr, NRP-1 siRNA blocked PDGF-BB-mediated migration of T98G cells relative to scrambled controls (#) Treatment of T98G cells with inhibitor V significantly attenuated migration (★) at 4 hr, 8 hr and 24 hr. Results are representative of at least two experimental repeats. Asterisks indicate significance relative to un-stimulated controls (calculated by one-way ANOVA, $P < 0.05$*, $P < 0.01$**, $P < 0.001$***). Scale bar=250 µm.

6.3 Summary

The results in this Chapter outlined that exogenous PDGF-AA and BB drove the proliferation of the osteosarcoma cells but not the glioma cell lines. The proliferative response of KHOS-240S or MG63 cells was not impaired by NRP-1 siRNA treatment. Thus, in these cell lines PDGF-stimulated proliferation occurs independent of NRP-1, suggesting PDGFR/NRP-1 crosstalk does not affect the survival of mesenchymal tumour cells.

The results in this Chapter detailed that exogenous PDGF ligands could stimulate the migration of all the mesenchymal tumour cell lines (except A172) and migration was blocked through inhibition of PDGFR signalling. PDGF-BB induced a more rapid rate of cell migration than PDGF-AA in the mesenchymal tumour cells. These results were consistent with other studies outlining that PDGF mediated osteoblast migration (Lind et al., 1995) and glioma cell migration (Amagasaki et al., 2006; Yamamoto et al., 1997). The paper by Amagasaki (2006) also detailed that A172 and T98G glioma cells showed comparable chemotaxis towards PDGF-BB in a Boyden chamber assay, which does not concur with the migration data collected in this Chapter. This study also determined that cells migrated, even in the absence of PDGF-BB, suggesting a high level of cell motility. Such high levels of cell motility (-PDGF) may have been partly attributed to the fibronectin used in these studies (to coat boyden chambers) as A172 and T98G cells are known to migrate towards fibronectin in a dose-dependent manner (Ohnishi et al., 1997). Boyden chambers were coated with 50 µg/mL of fibronectin (Amagasaki et al., 2006), however, fibronectin concentrations as low as 0.5µg/mL are reported to increase the chemotaxis of glioma cells. Thus, it is possible incubating glioma cell lines in a fibronectin and PDGF-BB rich environment may have positively regulated A172 cell migration and this may account for the differences in the published Boyden chamber assay results and cell-exclusion assay results documented in this Chapter.

NRP-1 was not essential for PDGF induced migration of MG63 cells, however, NRP-1 was crucial for PDGF-AA and PDGF-BB mediated migration of KHOS-240S cells. Although both KHOS-240S and MG63 cells express NRP-1, the relative expression varies with KHOS-240S cells expressing greater levels of NRP-1. It may be possible the differential expression of NRP-1 accounting for the different migratory responses of the osteosarcoma cell lines. Alternatively, MG63 cells may autonomously secrete growth factors that may over-ride any inhibitory effects induced by NRP-1. There is very little information, to date, on the role of NRP-1 in regulating the migration of osteosarcoma cells and further detailed studies are required to elucidate the mechanisms by which NRP-1 inhibits the migration of KHOS-240S cells.

In the T98G cells, NRP-1 reduced the basal levels of cell migration however; PDGF-BB was able to restore the migratory potential of T98G cells at all time-points, except 24 hr. This suggests that only the sustained inhibition of NRP-1 is able to inhibit T98G cell migration induced by PDGF-BB. A possible mechanism for this may be related to the recycling of PDGFRs. Chiarugi et al (2002) reported that 10 min exposure of cells to PDGF induced the down-regulation of cell surface PDGFR, yet by 45 min PDGFRs were re-expressed on the cell surface at their original level. Although PDGFRs were quickly recycled, sustained PDGF stimulation induced to a time-dependent decrease in pPDGFR. At 10 min pPDGFR levels peak and by 9 hr phosphorylation is significantly depleted, owing to regulation by protein tyrosine phosphatases (Chiarugi et al., 2002). With this in mind, it is feasible that following 24 hr exposure to PDGF-BB, the magnitude of PDGFR phosphorylation may have been supressed. Consequently, in T98G cells treated with NRP-1 siRNA, PDGF-BB stimulation could not overcome the inhibition of basal cell migration at 24 hr. Previous studies have also documented the importance of NRP-1 in glioma cell migration (Bagci et al., 2009).

Together these results suggest that NRP-1 significantly inhibits PDGF-mediated migration but not proliferation in a subset of mesenchymal tumour cell lines (T98G and KHOS-240S). Importantly, NRP-1/PDGFR crosstalk affected cell migration in the cell lines where either ERK and/or AKT phosphorylation was inhibited (Chapter 5). This suggests that in these cells, NRP-1 may exert inhibitory effects on cell migration through modulating the activity of known PDGFR downstream targets, rather than through mediating alternative PDGFR signalling mechanisms.

6.3.1 Chapter 6: principal findings

- The proliferation of the osteosarcoma, but not, glioma cell lines is stimulated by PDGF growth factors and NRP-1 has no influence on PDGF-mediated cell proliferation
- The majority of the mesenchymal tumour cell lines migrate in response to PDGF-AA and PDGF-BB
- KHOS-240S and T98G cells show some dependence on NRP-1 PDGF-stimulated cell migration

Chapter 7- Discussion

7.0 Discussion

RTK signalling regulates several intracellular pathways associated with tumour cell proliferation, migration, and survival. Consequently, many anti-cancer therapies have focused on targeted inhibition of the kinase activity of RTKs. Targeted therapies against multiple RTK have greater efficacy in some tumours, for example, VEGFR and PDGFR inhibition induced a greater regression of tumour vasculature compared to therapies only targeting VEGFR (Erber et al., 2004). Such multi-targeted cancer therapies against VEGFR and PDGFR destabilise tumour vessels through disrupting endothelial cell and pericyte interactions, which sensitise the tumours to anti-angiogenic therapies (Erber et al., 2004; Hasumi et al., 2007). VEGFR and PDGFR also activate convergent downstream signalling pathways (for e.g., MAP kinase-ERK) (Dhillon et al., 2007) and share a close phylogenic relationship (Gu and Gu, 2003; Kondo et al., 1998). Thus, in tumours that express both VEGFR and PDGFR, it is feasible that PDGFR signalling is able to compensate if VEGFR is inhibited, and vice versa. Such RTK co-activation networks are well documented to promote multi-drug resistance in cancer (Pillay et al., 2009; Xu and Huang, 2010) and thus, targeting multiple RTKs is an important strategy to inhibit tumour progression. NRP-1 is a well-established co-receptor for VEGFR-1 and VEGFR-2, which stabilises the VEGF ligand/ receptor complex and is important for the maximal phosphorylation of VEGFR (Fuh et al., 2000; Shraga-Heled et al., 2007; Soker et al., 2002; Whitaker et al., 2001). Ball et al (2010) also discovered that NRP-1 was essential for the kinase activity of PDGFR and PDGF mediated proliferation/migration of MSCs. The concept that NRP-1 regulates the activity of these closely related RTKs (PDGFR and VEGFR), which are both involved in tumour angiogenesis, suggested NRP-1 as a potential therapeutic cancer target. Furthermore, NRP-1 is over-expressed in many tumours and considered a negative prognostic biomarker (Bagri et al., 2009; Ellis, 2006; Miao et al., 2000). No extensive studies had investigated NRP-1/PDGFR crosstalk in tumour cells. This study therefore, provided an important opportunity to advance the understanding of NRP-1/PDGFR crosstalk and the role of this mechanism in cancer cell biology.

An initial objective of the project was to identify tumour cell lines expressing both NRP-1 and PDGFR to investigate NRP-1/PDGFR crosstalk. The results in Chapter 3 detailed that NRP-1 was expressed in both mesenchymal and epithelial tumour cell lines, yet PDGFR was only expressed in tumours with a mesenchymal phenotype. This expression pattern suggested that crosstalk involving NRP-1/PDGFR might be limited to specific types of tumours. Because NRP-1 can interact with RTKs such as VEGFR (Fuh et al., 2000; Soker et al., 2002), c-Met (Hu et al., 2007), and PDGFR (Ball et al., 2010; Cao et al., 2010; Pellet-Many et al., 2011), the relative levels of cell

surface receptors may be critical in determining the specific molecular interactions involving NRP-1. In the selected osteosarcoma and glioma tumour cell lines, NRP-1 and PDGFRs were expressed at varying levels (Chapter 3) and PDGFR signalling was reported to be a driver of tumour progression (Kubo et al., 2008; Lokker et al., 2002; McGary et al., 2002; Takeuchi et al., 2004). It is still unclear whether other NRP-1-interacting RTKs (e.g. c-Met, VEGFR) compete with PDGFR for interactions with NRP-1. Ball et al (2010) and Pellet-Many et al (2011) reported the existence of NRP-1/PDGFR crosstalk in cell types where VEGFR-1 and VEGFR-2 expression could not be detected (Ball et al., 2010; Pellet-Many et al., 2011). Yet, NRP-1/PDGFR crosstalk was also documented in hepatic stellate cells (Cao et al., 2010) and human aortic SMCs (Banerjee et al., 2006), which express both VEGFR-1 and VEGFR-2 (Banerjee et al., 2008; Lorquet et al., 2010; Novo et al., 2007). These lines of evidence suggest that VEGFR expression can be an important determinant of NRP-1/PDGFR crosstalk in some cell types but not others. To interrogate the relevance of VEGFR expression on NRP-1/PDGFR crosstalk, mesenchymal tumour cells expressing both VEGFR-1 and VEGFR-2 (U87MG), or no detectable VEGFRs (KHOS-240S), were included in the project.

Whether or not different RTKs compete or interact distinctly with NRP-1 may pre-determine if NRP-1/PDGFR interactions occur in different cell types. The second objective of the project was therefore, to explore how NRP-1/PDGFR interactions occurred in the mesenchymal tumour cells. As discussed (Chapter 4), it had been suggested that PDGF growth factors were critical in controlling the NRP-1/PDGFR crosstalk in some cell types but not others (Ball et al., 2010; Pellet-Many et al., 2011). Principal findings from this project were that PDGF growth factors have the capacity to bind, distinctly from VEGF-A_{165}, to the b domains of NRP-1 (Section 4.1.4), and in situ interactions between NRP-1 and PDGFR could be detected in the cultured tumour cell lines (Section 4.2.4). Although PDGF potentiated the interaction between NRP-1 and PDGFR in some cell lines, PDGF was not critical for these PDGFR and NRP-1 interactions to occur, implying that other mechanisms contribute to controlling NRP-1/PDGFR crosstalk. As discussed (Chapter 4), HS may be one potential candidate that may regulate NRP-1/PDGFR crosstalk. NRP-1 can act as one of the core membrane-associated proteins to which HS chains are covalently attached in the Golgi apparatus (see Chapter 1, Section 1.1.1). Serine-612 (in linker region between the b2 domain and MAM domain) serves as the attachment site for HS (Frankel et al., 2008; Shintani et al., 2006). HS can also bind to PDGF growth factors (Abramsson et al., 2007; Lustig et al., 1996; Rolny et al., 2002). Thus, a possible mechanism could involve NRP-1-associated HS promoting an indirect interaction between NRP-1 and PDGFR, which may be stabilised through intracellular interactions involving the NRP-1 C-terminus and the intracellular regions of PDGFR. The NRP-1 C-terminal SEA motif can interact with proteins such as integrin α5β1 (Valdembri et al., 2009) and p130Cas (Pellet-Many et al., 2011), and deletion of this C-terminal motif is reported to significantly decrease

VEGFR activation (Prahst et al., 2008) and to regulate the endocytic recycling of VEGFR-2 (Ballmer-Hofer et al., 2011). In the context of PDGFR crosstalk with NRP-1, intracellular interactions between the C-terminus of NRP-1 and the kinase domain of PDGFR may also be significant.

Having determined that PDGF growth factors have the capacity to bind to the b domains of NRP-1, and that interactions between NRP-1/PDGFR occur in situ, the third aim of the project sought to establish whether NRP-1/PDGFR associations controlled PDGFR kinase activity and signalling (Chapter 5). The results from Chapter 5 detailed that PDGFR signalling assays can determine if specific PDGFR downstream pathways are 'on' or 'off' in the mesenchymal tumour cell lines. PDGF stimulated the phosphorylation of PDGFR, AKT and PLC-γ and phosphorylation was blocked by inhibitor IV (inhibits PDGFRs and c-Abl) or inhibitor V (inhibits PDGFR only)(with the exception of the PTEN null U87MG cells which showed aberrant phosphorylation of AKT). NRP-1 was not essential for PDGF-stimulated phosphorylation of of PLC-γ or PDGFR in any of the cells tested. Yet, NRP-1 affected PDGFR-mediated activation of the PI3K-AKT and Ras-ERK pathway in some cell lines, e.g. KHOS-240S and T98G but not others e.g. A172 cells. Together these data suggested that NRP-1 might direct specific aspects of PDGFR signalling. Previous studies also reported that NRP-1 is not important for the total phosphorylation of PDGFR-β (Cao et al., 2010; Evans et al., 2011; Pellet-Many et al., 2011), whereas other work (in different cell types) suggests that NRP-1 is important for the phosphorylation of the PDGFR tyrosine residues important for PI3K-binding (Ball et al., 2010). Overall, these results reinforce the assertion that the effects of NRP-1 on PDGFR signalling are highly cell type specific.

The results in Chapter 5 also suggest some synergy between PDGFR, NRP-1 and the MAP-kinase ERK pathway. Inhibition of c-Abl kinase and PDGFR (using inhibitor IV) ablated the phosphorylation of ERK-1/2 and NRP-1 in some cell lines and NRP-1 knockdown significantly inhibited ERK-1/2 phosphorylation in three out of the five cell lines. A possible mechanism to explain these results may be gleaned from the finding that NRP-1 and c-Abl reside in a complex to direct PDGFR signalling towards Rac-1 (Cao et al., 2010). The guanine nucleotide exchange factor, Sos-1/2, shows specificity to activate either Rac-1 or Ras-1, thus the effects documented by Cao et al. (2010) may be related to an upstream mechanism whereby NRP-1 and c-Abl together direct PDGFR signals toward the activation of Sos-1/2. If such a mechanism exists, it is feasible that inhibition of either NRP-1 or PDGFR/c-Abl may induce a synergistic down-regulation of the other proteins involved in directing ERK-1/2 or Rac-1 activation. This possible mechanism would provide an interesting biological crosstalk whereby NRP-1 and c-Abl selectively direct the kinase activity of PDGFR. Recent insights by Cao et al. (2012) also support the hypothesis that NRP-1 is particularly important for Ras activation in tumour cells. In this study, tumour-cell-derived VEGF-A

and NRP-1 were essential for the activation of Ras, independent of VEGFR-1 or VEGFR-2. Activation of Ras was dependent on Sos-1/2 and regulated tumour cell growth (Cao et al., 2012). It has not yet been interrogated how NRP-1 and VEGF-A activate Sos-1/2, Ras (independent of VEGFR) but a possible mechanism could involve VEGF-A signalling through PDGFR-α (Ball et al., 2007b) and again, NRP-1/c-Abl directing PDGFR signalling towards of Sos-1/2, Ras.

Several studies had suggested that NRP-1/PDGFR crosstalk regulated highly specific cell signalling (e.g. p130Cas or Rac-1) without affecting the phosphorylation of PDGFR or downstream proteins (e.g. AKT or ERK-1/2) (Cao et al., 2010; Evans et al., 2011; Pellet-Many et al., 2011). In these studies, NRP-1 mediated the inhibition of PDGFR-associated signalling molecules and induced inhibitory effects on cell migration. As documented in Chapter 5, NRP-1 affected PDGFR phosphorylation and downstream signalling in some cell lines but not others. To rule out the possibility that NRP-1:PDGFR was regulating alternative signalling mechanisms (other than those examined), the final aspect of the project investigated the influence of NRP-1 on PDGF mediated proliferation and migration of tumour cells.

Results in Chapter 6 outlined that T98G, KHOS-240S and MG63 cells migrated towards PDGF-AA and PDGF-BB. In the KHOS-240S and T98G cells, NRP-1 was essential for the PDGF-stimulated migration of cells and this result is consistent with other published reports of NRP-1 regulating PDGF-mediated cell migration (Cao et al., 2010; Evans et al., 2011; Pellet-Many et al., 2011). Interestingly, NRP-1/PDGFR crosstalk affected cell migration in the same cell lines (T98G and KHOS-240S) where NRP-1/PDGFR crosstalk also affected ERK and AKT phosphorylation (Chapter 5). This result suggested that, in these cells, NRP-1 exerts inhibitory effects on cell migration partly through modulating the activity of known PDGFR downstream targets.

In summary, this study identified a subset of mesenchymal tumour cell lines expressing both NRP-1 and PDGFR-α and/or PDGFR-β, which were used to investigate NRP-1/PDGFR crosstalk. In these cell lines, NRP-1 could associate with PDGFR-α or β, however, this interaction was not dependent on PDGF ligands. NRP-1 did not control the auto-phosphorylation of PDGFR-α or β, however, in some cell lines there was evidence that NRP-1 was important for the activation of the MAPK-ERK and PI3K pathways. NRP-1 was an important mediator of cell survival in all the mesenchymal tumour cells and NRP-1 inhibited PDGF-mediated migration of some of the tumour cells. Together these results highlight that NRP-1/ PDGFR crosstalk is highly cell-type specific and that the functional significance of NRP-1/PDGFR associations may vary in different cells. The literature also reports distinct cellular effects mediated by NRP-1/PDGFR crosstalk in different cell types, and further work is needed to understand how the NRP-1/PDGFR crosstalk conveys these unique cellular effects.

7.1 Future directions

Because of the emerging roles for NRP-1 in regulating/ binding a diverse array of growth factors and RTKs, understanding what mediates the specificity of NRP-1 interactions with these molecules may be an interesting focus of future work. Evidently, the complement of NRP-1 binding molecules within specific cell types will pre-determine which interactions can occur; however, it is not clear whether NRP-1 preferentially interacts with specific molecules. The data from this project suggested that PDGF and VEGF may interact distinctly with the b domains of NRP-1, which may suggest that concurrent NRP interactions can occur within cells. As discussed (Chapter 1), NRP-1 can act as the core protein for HS chains (Shintani et al., 2006) and an interesting idea is that NRP-1 associated HS chains may mediate the specificity of NRP-1 interactions. Extensive modifications, including, N-sulphation, N-deacytylation and O-sulphation at various positions on HS strongly contribute to controlling the specificity of HS interactions with different proteins (Kreuger et al., 2006). Post-secretion of HS chains, 6-O sulphation has been shown to be particularly important in determining HS protein binding specificities and also in controlling the kinase activity of PDGFR (Kreuger et al., 2006; Phillips et al., 2012). Thus, exploring the sulphation pattern of NRP-1-bound HS may help to define the specificity of NRP-1 interactions in different cell types.

Future work should also focus on defining the direct and/or indirect association between NRP-1 and PDGFR. As alluded to, PDGFs bound to NRP-1 but did not appear to potentiate the interaction between NRP-1/PDGFR in the tumour cells (Chapter 4). The C-terminal region of NRP-1 is essential for NRP-1 and VEGFR-2 complex formation (Prahst et al., 2008) and it would be interesting to determine if deletion of the NRP-1 C-terminal also inhibited NRP-1/PDGFR associations. As discussed, NRP-1 bound HS or CS chains may stabilise the PDGFR/NRP-1 associations. A possible approach to interrogate the contribution of NRP-1-associated GAGs would be to generate cell lines expressing NRP-1 (mutated at serine-612), which would prevent GAG modification of NRP-1 (Shintani et al., 2006).

Future studies should also further define the intracellular signalling effects of NRP-1/ PDGFR crosstalk. As alluded to, the data in this report and previous reports suggest some synergy between PDGFR / NRP-1/c-Abl in directing cell signalling towards Rac-1 (Cao et al., 2010) and ERK-1/2. Thus, future studies could interrogate this pathway through examining factors upstream of ERK-1/2 and Rac-1, such as the specific PDGFR Tyr- residues associated with ERK-1/2 activation and the guanine nucleotide exchange factor, Sos-1/2. Although a recent study detailed that NRP-1 was important for the activation of Ras via a mechanism dependent on Sos-1/2, no studies to date have investigated how NRP-1 knockdown impacts on the activation of Sos-1/2.

In summary, the emerging data surrounding NRP-1 suggests that this glycoprotein/proteoglycan can participate in a diverse array of intracellular and extracellular interactions involving RTKs (Ball et al., 2010; Guo et al., 2003; Pellet-Many et al., 2011; Soker et al., 2002), growth factors (Glinka et al., 2010; West et al., 2005) and adhesion molecules (Fukasawa et al., 2007; Valdembri et al., 2009). As discussed above, understanding the factors, which mediate the specificities of NRP-1 interactions in different cell types, will be key to determine the functional significance of NRP-1/PDGFR crosstalk in cancer. To date, the literature and work in this project have suggested that, rather than mediating the overall kinase activity of PDGFR, NRP-1 has subtle effects on specific aspects of PDGFR signalling which may involve other molecules such as c-Abl kinase (Cao et al., 2010; Pellet-Many et al., 2011). Since NRP-1 and PDGFR contribute to the progression of mesenchymal tumours (Chapter 1), understanding the intricacies of NRP-1/PDGFR crosstalk in these cells will be particularly important and contribute to the development of targeted therapies.

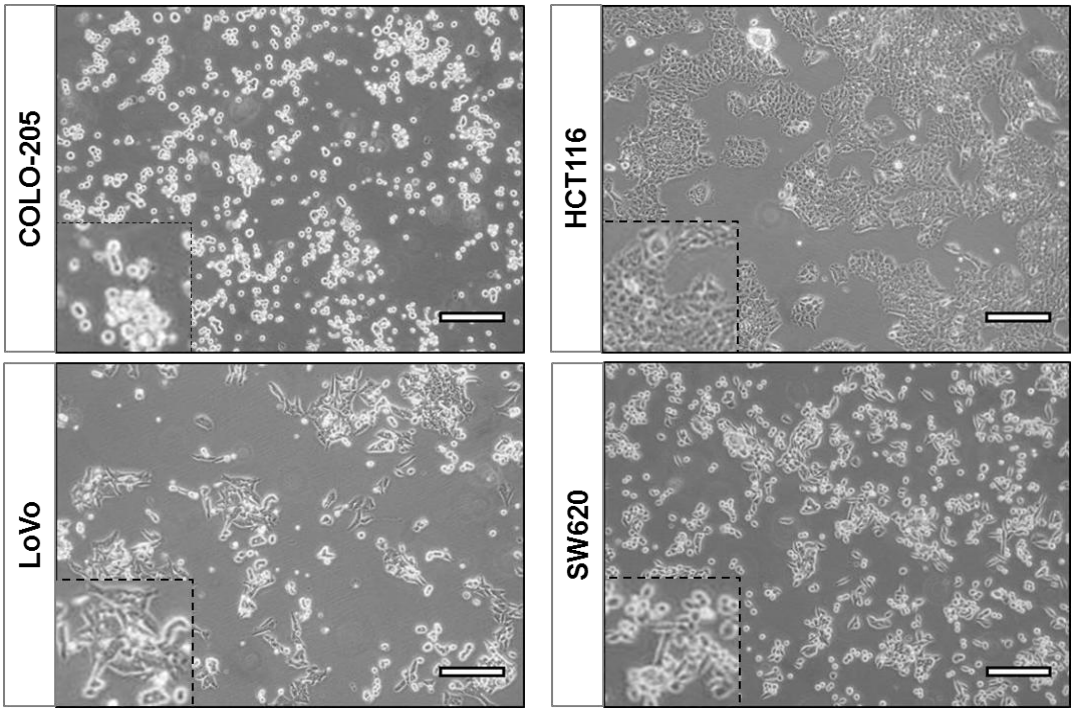

Figure 8.0: The morphology of the selected colon cancer cell lines
Colon cancer cell lines were cultured under standard conditions (Chapter 2, 2.0). Images were collected using a phase-contrast microscope (Olympus CK X41) set at 10x magnification. Enlarged cell images are illustrated in the bottom left corner of each image outlined by the dashed line (- - -). In the bottom right corner of each image scale bars are shown. Scale bar=100 μm.

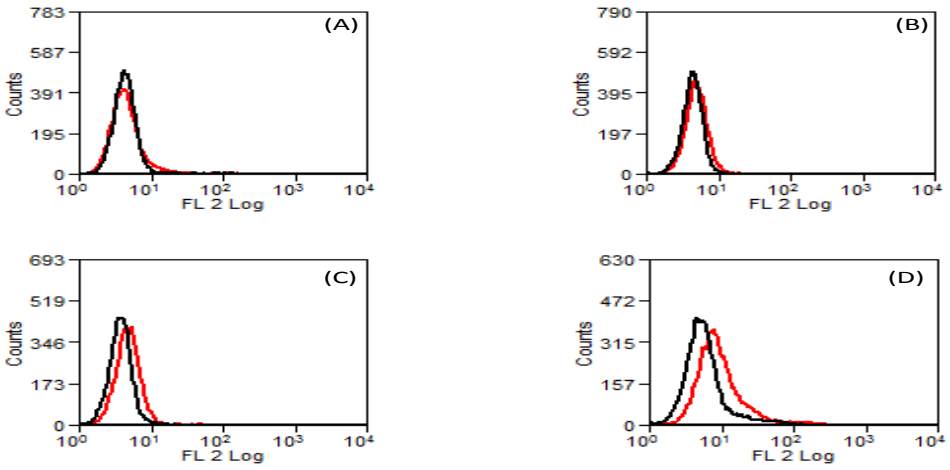

Figure 8.1: Cell surface expression of NRP-1 in the selected colon cancer cell lines
Colon cancer cell lines were cultured under standard conditions (Chapter 2, 2.0.1) and the expression of NRP-1 was determined by single colour flow cytometry (Chapter 2, 2.0.2). Analysis of **(A)** HCT116; **(B)** SW620; **(C)** COLO-205; **(D)** LoVo was performed using an anti-human mAb NRP-1 or a specific IgG control antibody (Chapter 2, Table 2.0). In each histogram, the fluorescent peak for NRP-1 (red) has been superimposed onto the peak for the isotype-matched IgG control (black).

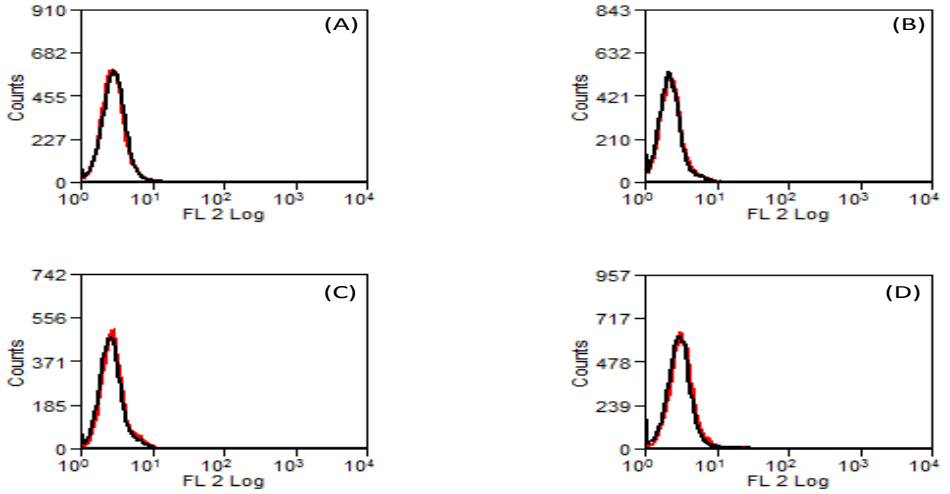

Figure 8.2: Cell surface expression of PDGFR-α in the selected colon cancer cell lines
Colon cancer cell lines were cultured under standard conditions (Chapter 2, 2.0.1) and the expression of PDGFR-α was determined by single colour flow cytometry (Chapter 2, 2.0.2). Analysis of **(A)** HCT116; **(B)** SW620; **(C)** COLO-205; **(D)** LoVo was performed using anti-human polyclonal PDGFR-α antibody or a specific IgG control antibody (Chapter 2, Table 2.0). In each histogram, the fluorescent peak for PDGFR-α (red) has been superimposed onto the peak for the isotype-matched IgG control (black).

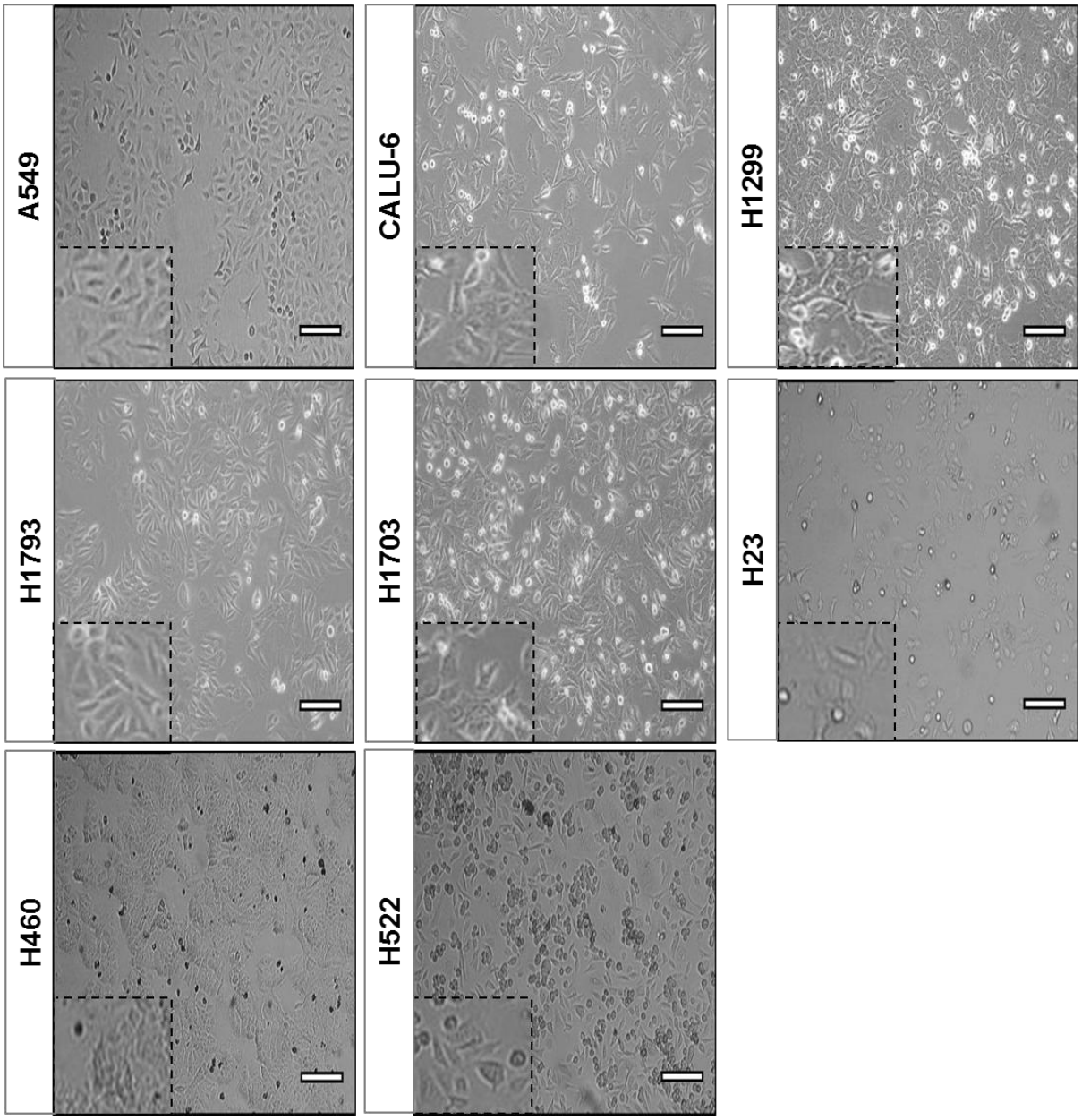

Figure 8.3: The morphology of the selected NSCLC cell lines

NSCLC cell lines were cultured under standard culture conditions (Chapter 2, 2.0). Images were collected using a phase-contrast microscope (Olympus CK X41) set at 10x magnification. Enlarged cell images are illustrated in the bottom left corner of each image outlined by the dashed line (- - -). In the bottom right corner of each image scale bars are shown. Scale bar=100 μm.

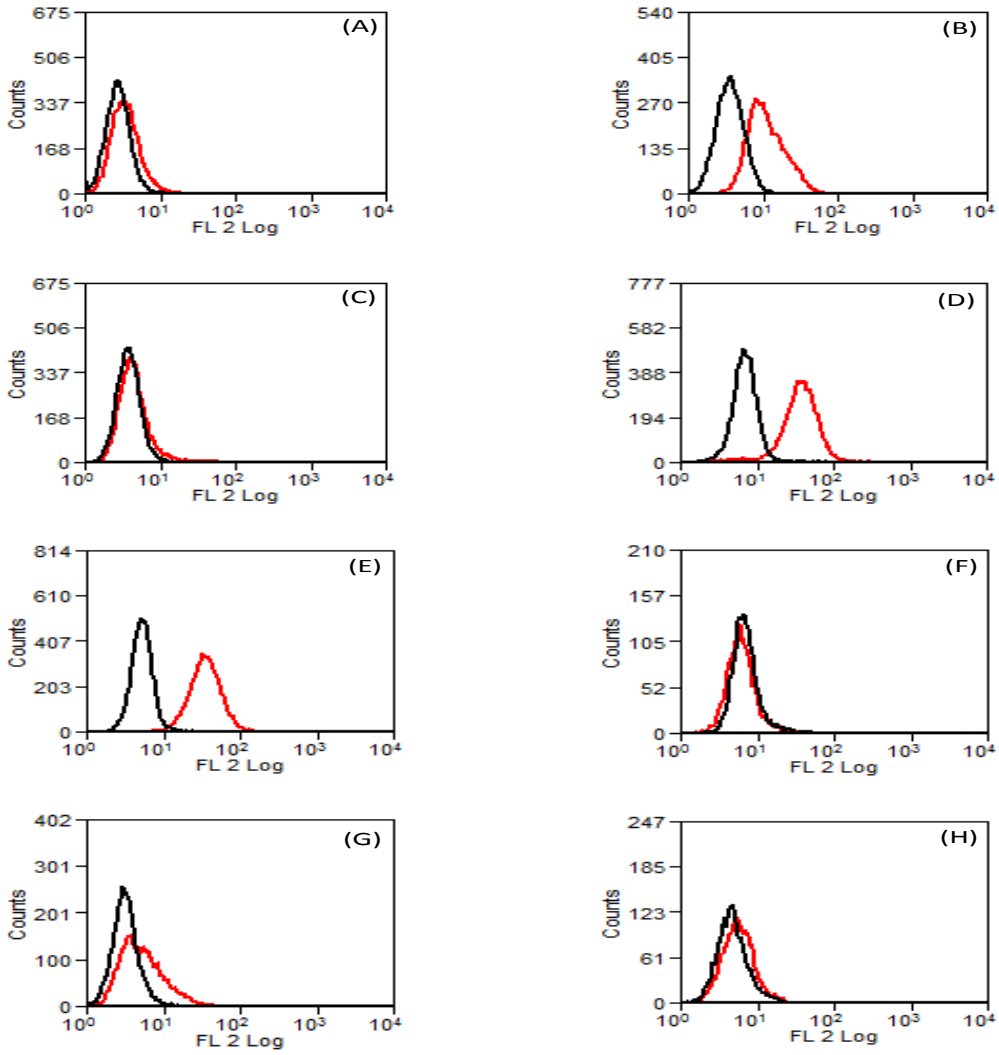

Figure 8.4: Cell surface expression of NRP-1 in the selected NSCLC cell lines

NSCLC cell lines were cultured under standard conditions (Chapter 2, 2.0.1) and the expression of NRP-1 was determined by single colour flow cytometry (Chapter 2, 2.0.2). Analysis of **(A)** H1703; **(B)** H1793; **(C)** H1299; **(D)** CALU-6; **(E)** A549; **(F)** H522; **(G)** H460; **(H)** H23 cell lines was performed using anti-human mAb against NRP-1 or a specific IgG control antibody (Chapter 2, Table 2.0). In each histogram, the fluorescent peak for NRP-1 (red) has been superimposed onto the peak for the isotype-matched IgG control (black).

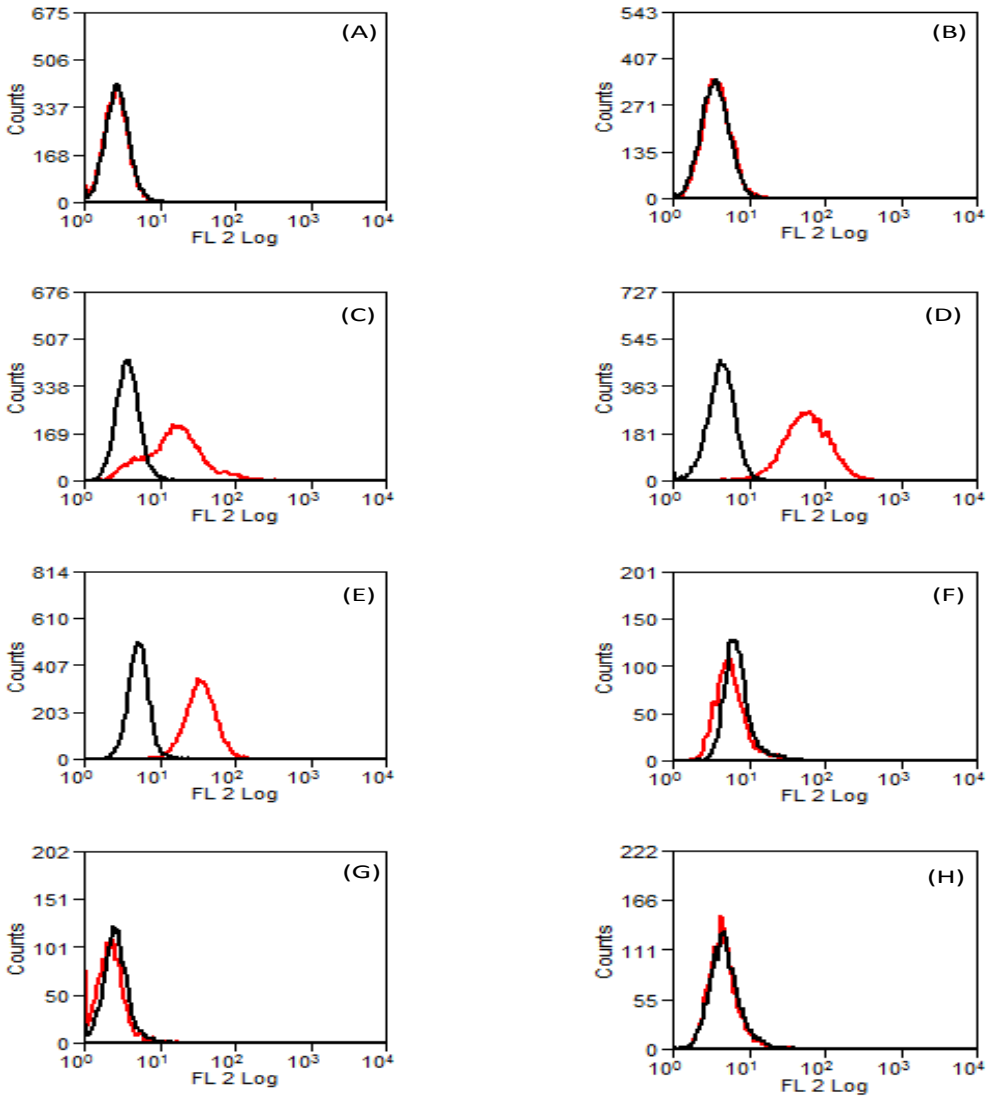

Figure 8.5: Cell surface expression of PDGFR-α in the selected NSCLC cell lines

NSCLC cell lines were cultured under standard conditions (Chapter 2, 2.0.1) and the expression of PDGFR-α was determined by single colour flow cytometry (Section 2.2). Analysis of **(A)** H1703; **(B)** H1793; **(C)** H1299; **(D)** CALU-6; **(E)** A549; **(F)** H522; **(G)** H460; **(H)** H23 cell lines was performed using anti-human polyclonal PDGFR-α Ab or a specific IgG control antibody (Chapter 2, Table 2.0). In each histogram, the fluorescent peak for PDGFR-α (red) has been superimposed onto the peak for the isotype-matched IgG control (black).

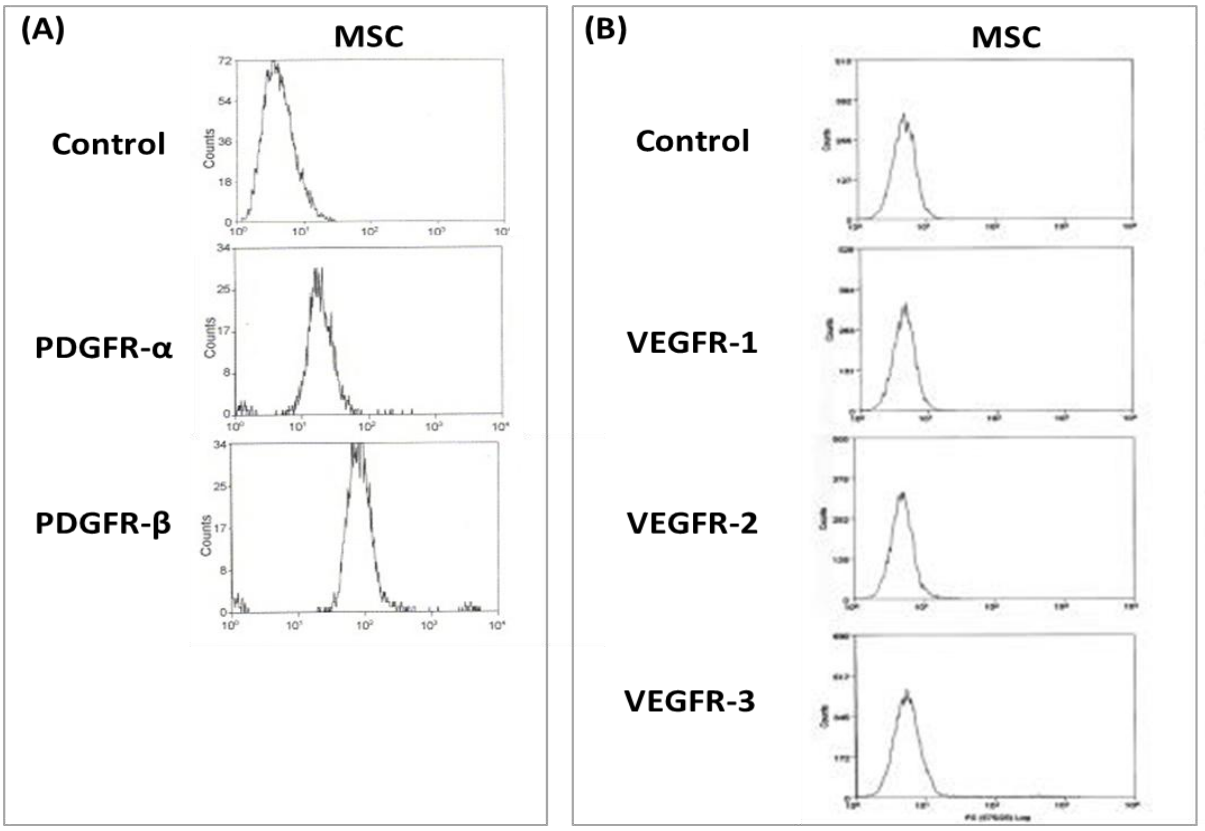

Figure 8.6: The cell surface expression of NRP-1, PDGFRs and VEGFRs in MSCs
The MSCs used in this study had previously been well characterised by single-colour flow cytometry. Data presented is adapted from published reports by Ball et al (2007a and 2007b). **(A)** Illustrates the expression of cell surface PDGFR-α and PDGFR-β in the MSCs (Ball et al., 2007a). **(B)** Illustrates no detectable expression of cell surface VEGFR-1, VEGFR-2 or VEGFR-3 in the MSCs (Ball et al., 2007b).

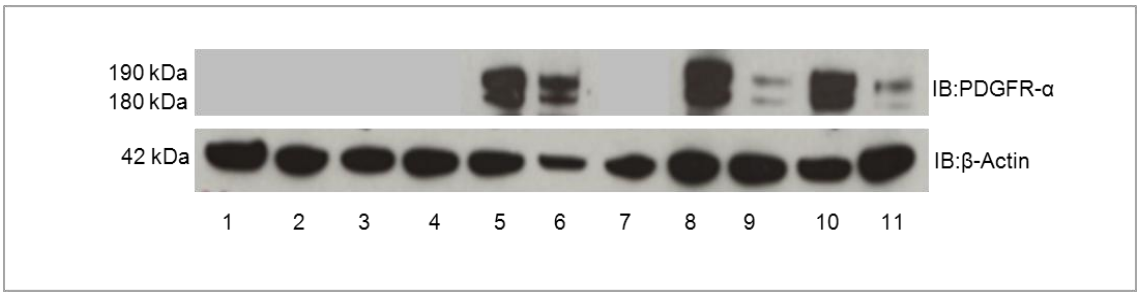

Figure 8.7: The expression of PDGFR-α in selected mesenchymal tumour cell lines
Using total cell lysates immunoblot analysis was performed using the following osteosarcoma and glioma cell lines: **(2)** Saos-2; **(3)** MG63; **(4)** KHOS 240S; **(5)** T98G; **(6)** LN229; **(7)** U118MG; **(8)** U87MG; (**9)** A172; **(10)** M059K; **(11)** M059J. Lane **(1)** shows the result for the MSC control. The PDGFR-α antibody (Table 2.0) was used to detect relative levels of PDGFR-α in the cancer cell lines and MSC control cells. For detection of PDGFR-α in the cell lines in lanes, **(5)**, **(6)**, **(8)**, (**9)**, **(10)** and **(11)** the film exposure time was 1 hour, whereas in the remainder of the cell lines the exposure time was 5 minutes (shown in Figure 3.12). Immunoblots are representative of at least two experimental repeats.

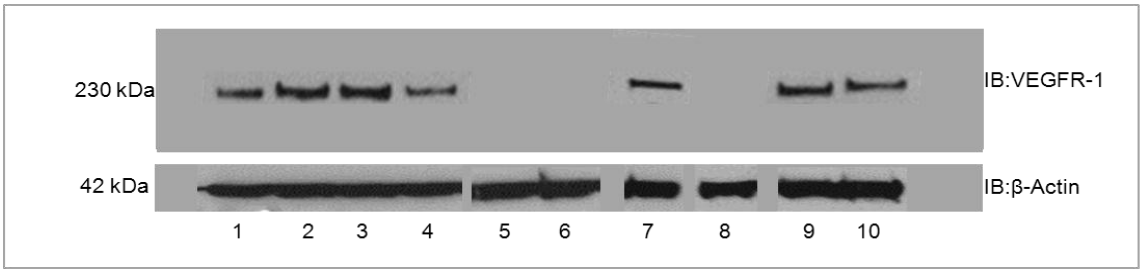

Figure 8.8: The expression of VEGFR-1 in selected mesenchymal tumour cell lines
Using total cell lysate immunoblot analysis was performed to determine the relative expression of VEGFR-1 in the following osteosarcoma and glioma cell lines: **(1)** T98G; **(2)** M059K; **(3)** LN229; **(4)** U118MG; **(5)** KHOS-240S; **(6)** M059J; **(7)** U87MG; **(8)** Saos-2; **(9)** MG63; **(10)** A172. Immunoblots represent preliminary data from one experimental repeat.

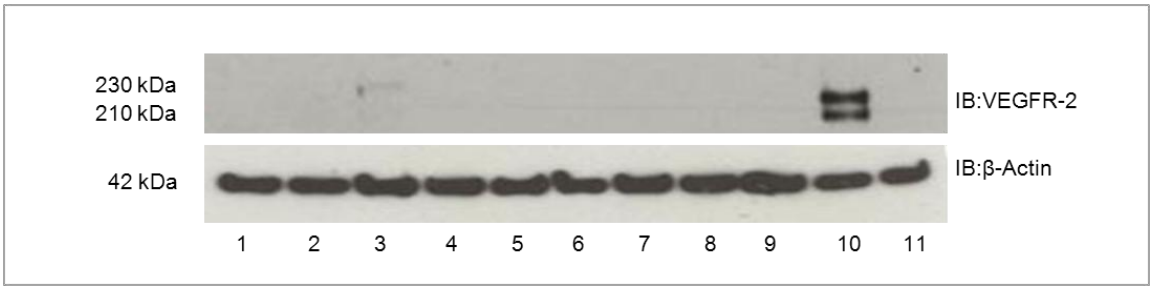

Figure 8.9: The expression of VEGFR-2 in selected mesenchymal tumour cell lines
Using total cell lysate immunoblot analysis was performed to determine the relative expression of VEGFR-2 in the following osteosarcoma and glioma cell lines: **(1)** Saos-2; (**2)** MG63; **(3)** KHOS 240-S; **(4)** T98G; **(5)** A172; **(6)** LN229; **(7)** M059J; **(8)** M059K; **(9)** U118MG; **(10)** U87MG; **(11)** MSCs. Immunoblots represent preliminary data from one experimental repeat.

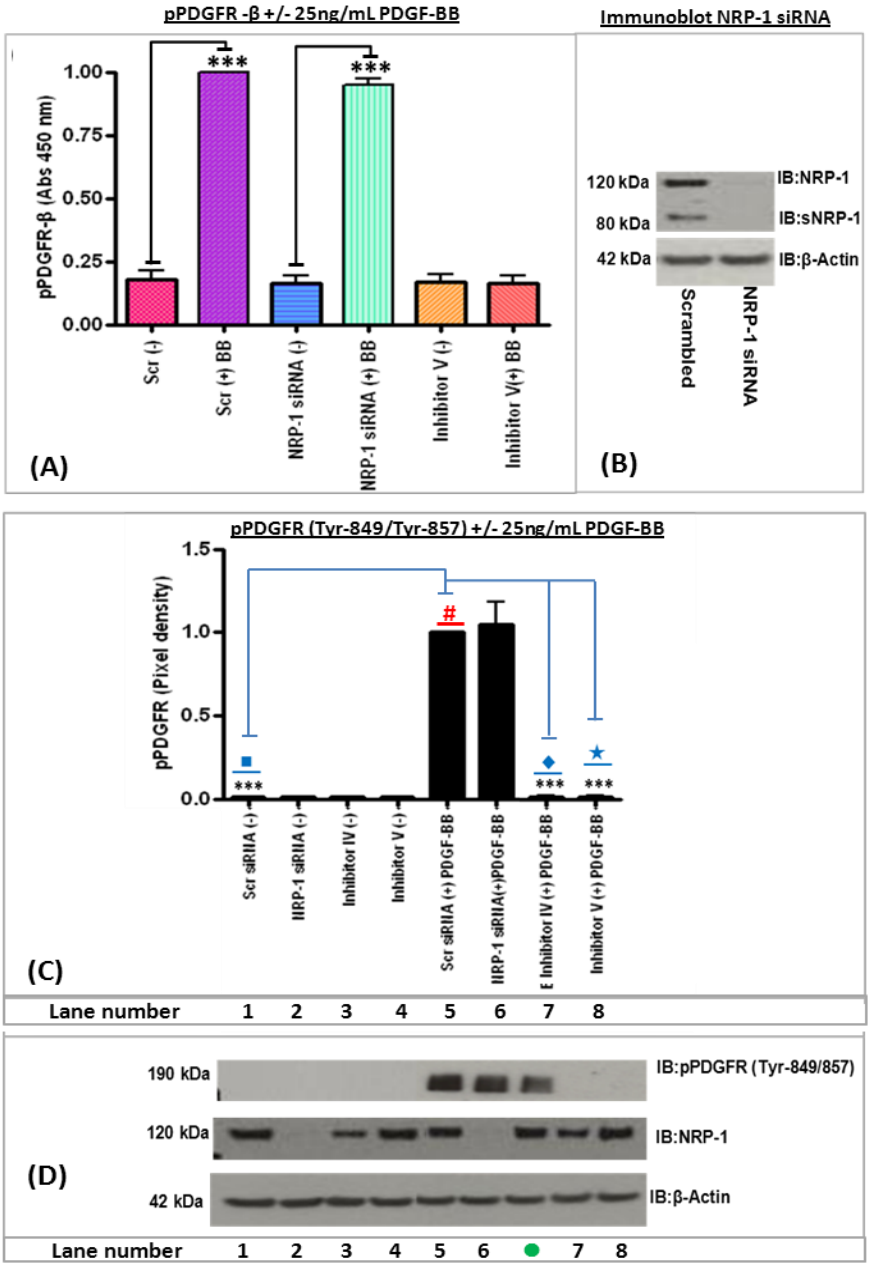

Figure 8.10: NRP-1 siRNA does not attenuate PDGFR phosphorylation in A172 cells

(A) The ELISA results illustrate that PDGF-BB (■) stimulated a significant increase in pPDGFR-β. Inhibitor V (■) blocked pPDGFR-β and NRP-1 siRNA treatment (■) did not inhibit pPDGFR-β. **(B)** Immunoblot data illustrated that NRP-1 siRNA treatment blocks the expression of NRP-1 in A172 cells. To quantify the phosphorylation of PDGFR, pixel densities were calculated using Gene Tools v3 software. **(C)** The histogram illustrates the quantified levels of pPDGFR (■) which has been expressed as a ratio relative to the Scr (+) PDGF-BB sample in lane 5 (#). Data presented is the mean value from at least two experimental repeats +/- calculated standard errors. Asterisks (*) indicate significance (calculated by one-way ANOVA, $P<0.001$***). PDGF-BB (#) significantly increased pPDGFR, relative to the un-stimulated control (■) in lane 1. PDGFR inhibitor IV (♦), inhibitor V (★) treatment significantly inhibited pPDGFR. NRP-1 siRNA did not inhibit the phosphorylation of PDGFR. **(D)** Immunoblots detected pPDGFR (Tyr-849/857), NRP-1 and β-Actin in A172 cells. The data indicated between lanes 6 and 7 (●) was not used in this analysis.

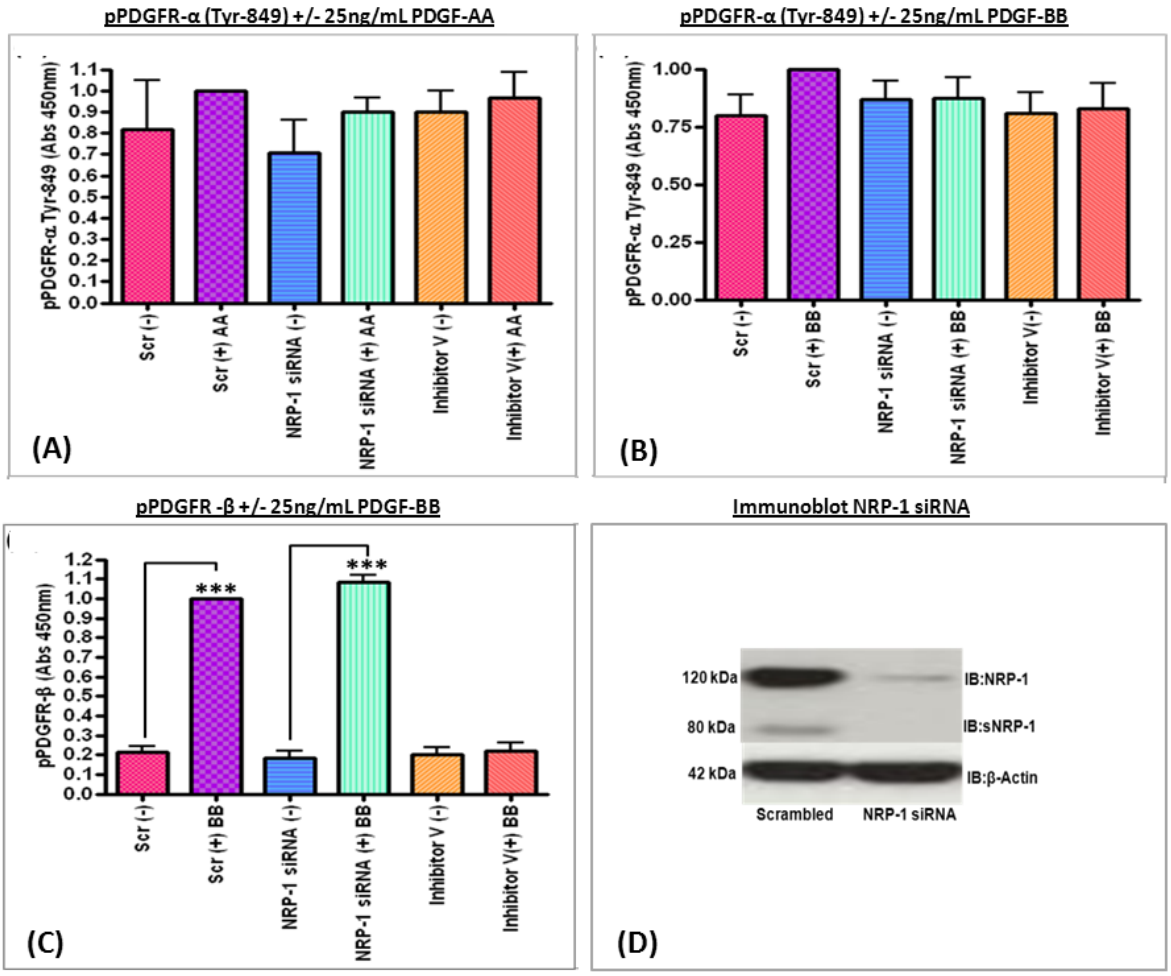

Figure 8.11: NRP-1 siRNA does not inhibit PDGFR phosphorylation in T98G cells

The ELISA results presented in the histograms above illustrate that **(A)** PDGF-AA (■) or **(B)** PDGF-BB (■) stimulated no significant increase in pPDGFR-α and PDGFR inhibitor V (■) or NRP-1 siRNA treatment (■) did not affect pPDGFR-α. **(C)** PDGF-BB (■) stimulated a significant increase in pPDGFR-β and inhibitor V (■) attenuated the phosphorylation of PDGFR-β (+/-) PDGF-BB. NRP-1 siRNA treatment (■) did not inhibit PDGF-BB- stimulated phosphorylation of PDGFR-β. **(D)** The Immunoblot data illustrates that NRP-1 siRNA treatment blocks the expression of NRP-1 in T98G cells. Asterisks (*****) indicate significance (calculated by one-way ANOVA, *P*<0.001***).

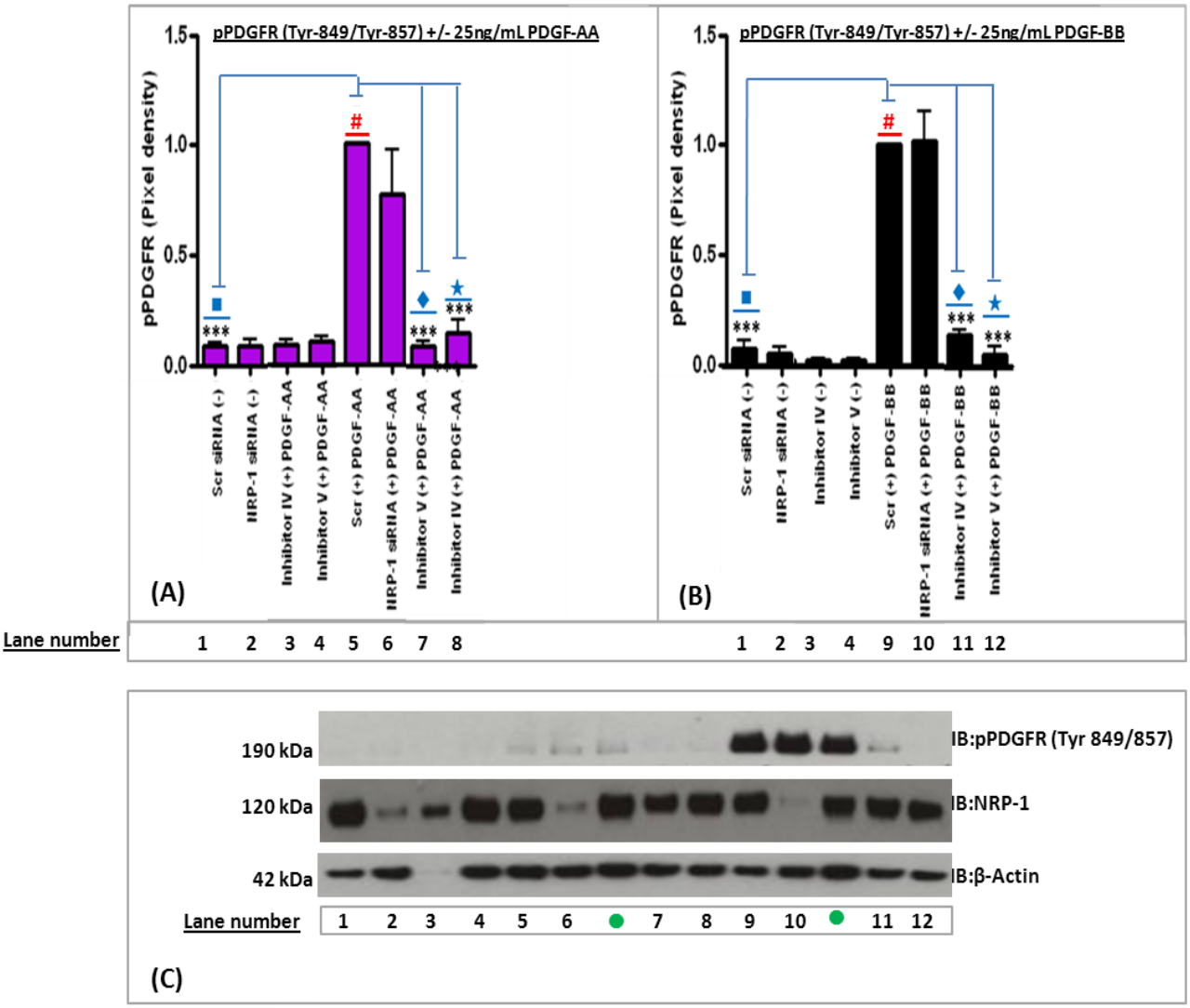

Figure 8.12: NRP-1 siRNA does not attenuate PDGFR phosphorylation in T98G cells

To quantify the phosphorylation of PDGFR, pixel densities were calculated using Gene Tools v3 software. The histograms in **(A)** and **(B)** illustrate quantified pPDGFR levels in cells stimulated with PDGF-AA (■) or PDGF-BB (■). The values on the histograms were calculated as a ratio relative to the Scr (+) PDGF-AA in **(A)** lane 5, indicated by the # symbol or the Scr (+) PDGF-BB in **(B)** lane 5, indicated by the # symbol. Data presented is the mean value from at least three experimental repeats +/- calculated standard errors. Asterisks (*****) indicate significance (calculated by one-way ANOVA, $P<0.01$**, $P<0.001$***). **(A)** PDGF-AA (#) significantly increased the pPDGFR, relative to un-stimulated controls (■). PDGFR inhibitor IV (♦) or inhibitor V (★) treatment significantly inhibited pPDGFR. **(B)** PDGF-BB (#) significantly increased the phosphorylation of PDGFR, relative to un-stimulated controls (■). PDGFR inhibitor IV (♦) or inhibitor V (★) treatment significantly inhibited pPDGFR. NRP-1 siRNA did not inhibit the phosphorylation of PDGFR. **(C)** Immunoblots detected pPDGFR (Tyr-849/857), NRP-1 and β-Actin in T98G cells. The data indicated between lanes 6 and 7 (●) and 10 and 11 (●) was not used in this analysis.

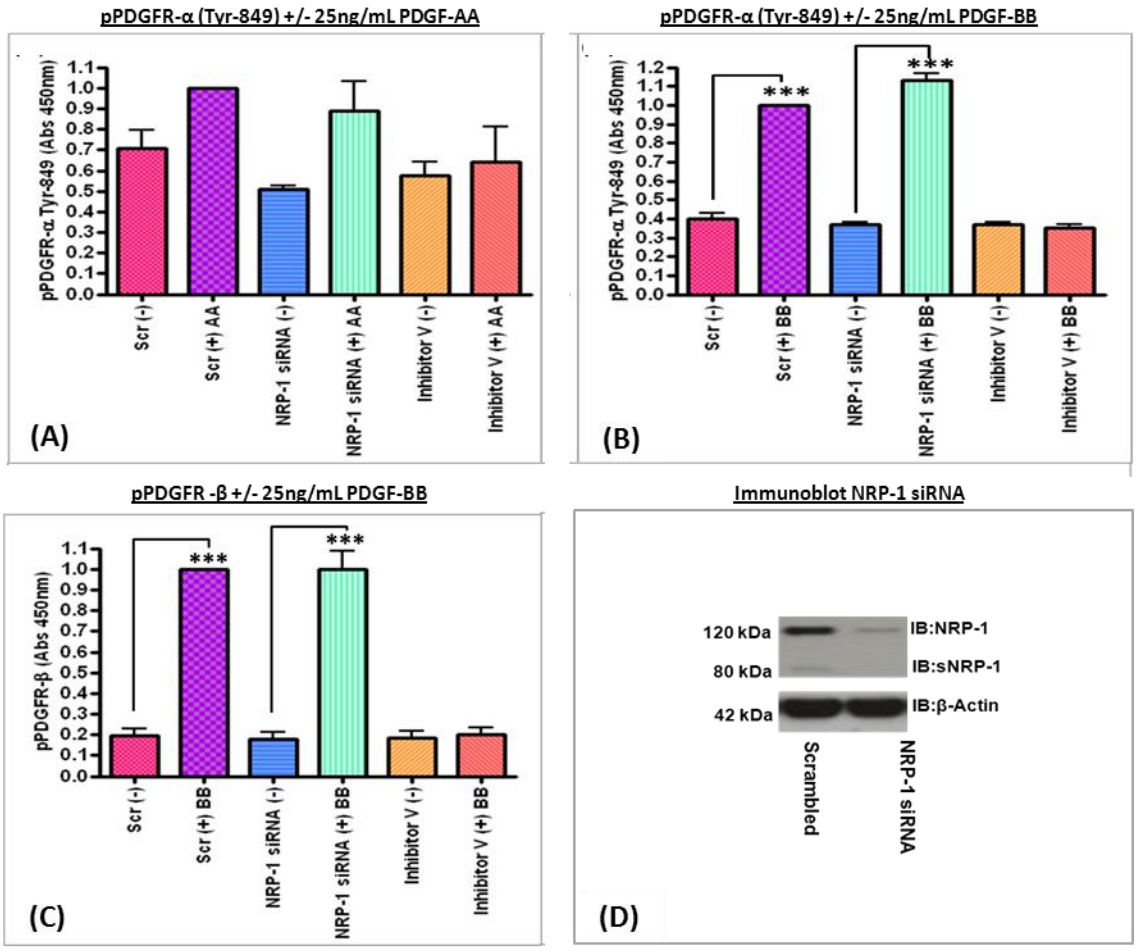

Figure 8.13: NRP-1 siRNA does not inhibit PDGFR phosphorylation in KHOS-240S cells

The ELISA results presented in the histograms above illustrate that **(A)** PDGF-AA (■) stimulated no significant increase in pPDGFR-α but **(B)** PDGF-BB (■) did significantly increased PDGFR-α phosphorylation. PDGFR inhibitor V (■) inhibited PDGF-BB stimulated phosphorylation of PDGFR-α yet, NRP-1 siRNA treatment (■) did not affect pPDGFR-α. **(C)** PDGF-BB (■) stimulated a significant increase in pPDGFR-β and inhibitor V (■) attenuated the phosphorylation of PDGFR-β (+) PDGF-BB. NRP-1 siRNA treatment (■) did not inhibit PDGF-BB- stimulated phosphorylation of PDGFR-β. **(D)** The Immunoblot data illustrates that NRP-1 siRNA treatment blocks the expression of NRP-1 in KHOS-240S cells. Asterisks (*****) indicate significance (calculated by one-way ANOVA, *P*<0.001***).

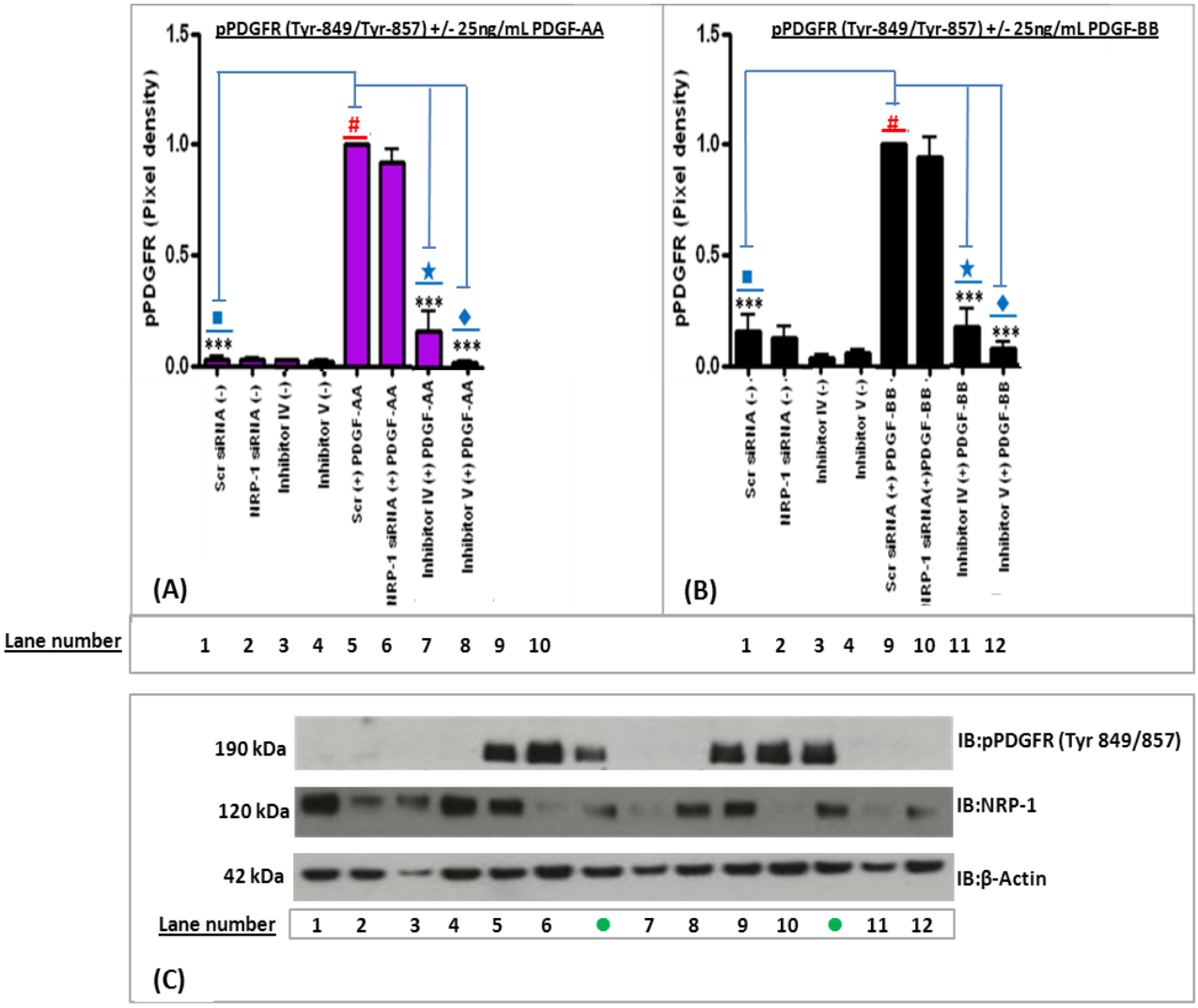

Figure 8.14: NRP-1 siRNA does not attenuate PDGFR phosphorylation in KHOS-240S cells

To quantify the phosphorylation of PDGFR, pixel densities were calculated using Gene Tools v3 software. The histograms in **(A)** and **(B)** illustrate quantified pPDGFR levels in cells stimulated with PDGF-AA (■) or PDGF-BB (■). The values on the histograms were calculated as a ratio relative to the Scr (+) PDGF-AA in **(A)** lane 5, indicated by the # symbol or the Scr (+) PDGF-BB in **(B)** lane 5, indicated by the # symbol. Data presented is the mean value from at least three experimental repeats +/- calculated standard errors. Asterisks (*****) indicate significance (calculated by one-way ANOVA, *P*<0.001***). **(A)** PDGF-AA (#) significantly increased pPDGFR, relative to un-stimulated controls (■). PDGFR inhibitor IV (♦) or inhibitor V (★) treatment significantly inhibited pPDGFR. **(B)** PDGF-BB (#) significantly increased the phosphorylation PDGFR, relative to un-stimulated controls (■). PDGFR inhibitor IV (♦), inhibitor V treatment significantly inhibited pPDGFR. NRP-1 siRNA did not inhibit the phosphorylation of PDGFR. **(C)** Immunoblots detected pPDGFR (Tyr-849/857), NRP-1 and β-Actin in KHOS-240S cells. The data indicated between lanes 6 and 7 (●) and 10 and 11 (●) was not used in this analysis.

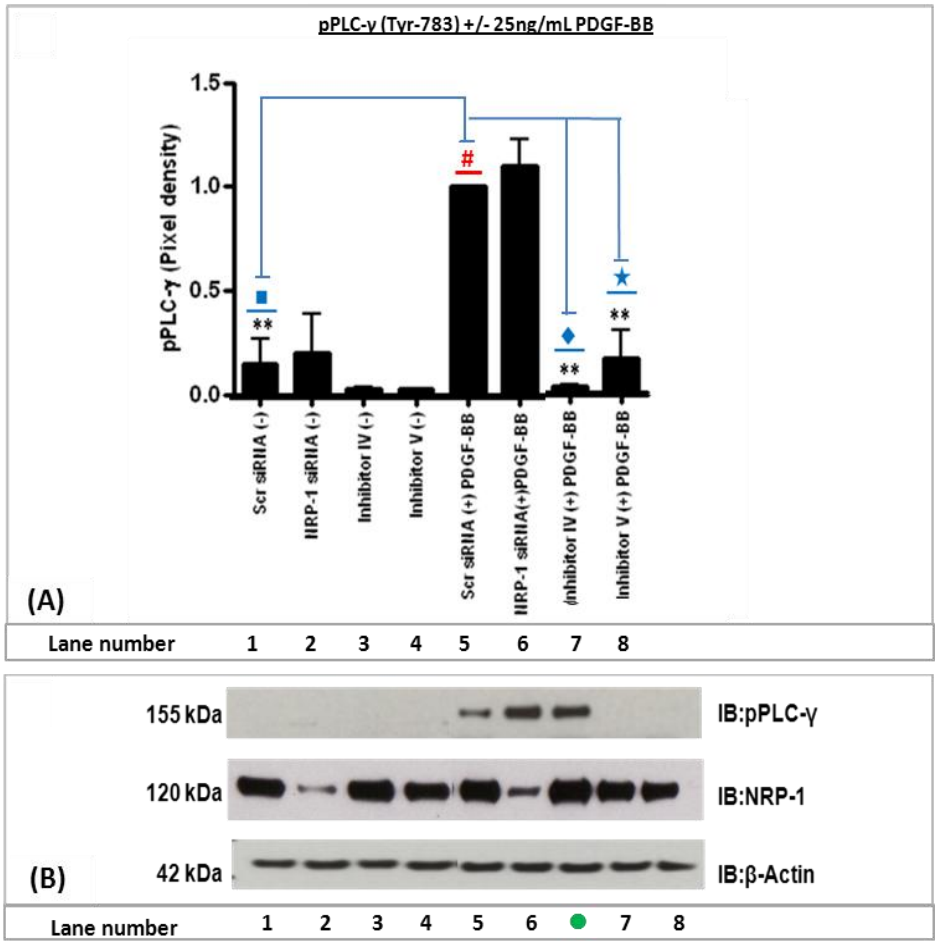

Figure 8.15: NRP-1 siRNA does not attenuate PLC-γ (Tyr-783) phosphorylation in U87MG cells

To quantify the phosphorylation of PLC-γ (Tyr-783), pixel densities were calculated using Gene Tools v3 software. The histogram in **(A)** illustrates the quantified levels of pPLC-γ in cells stimulated with PDGF-BB (■). The values have been calculated as a ratio relative to the Scr (+) PDGF sample (#) (lane 5). Data presented is the mean value from at least two experimental repeats +/- calculated standard errors. Asterisks (*) indicate significance (calculated by one-way ANOVA, $P<0.01$**). **(A)** PDGF-BB (#) significantly increased pPLC-γ, relative to un-stimulated controls (■). PDGFR inhibitor IV (♦) or inhibitor V (★) significantly inhibited pPLC-γ. NRP-1 siRNA did not inhibit the phosphorylation of PLC-γ (lane 6). **(C)** Immunoblots detected pPLC-γ (Tyr-783), NRP-1 and β-Actin in U87MG cells. Immunoblots detected pPLC-γ (Tyr-783), NRP-1 and β-Actin in U87MG cells. The data indicated between lanes 6 and 7 (●) was not used in this analysis.

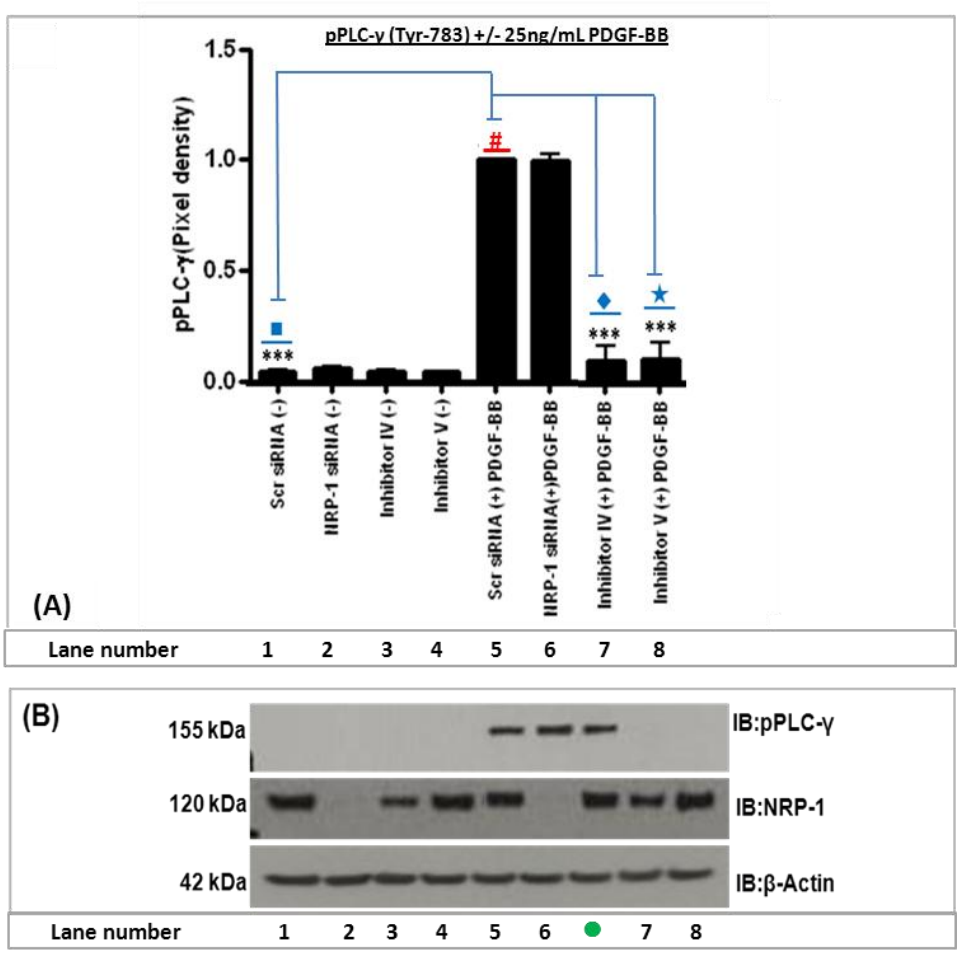

Figure 8.16: NRP-1 siRNA does not attenuate PLC-γ (Tyr-783) phosphorylation in A172 cells
To quantify the levels of pPLC-γ (Tyr-783), pixel densities were calculated using Gene Tools v3 software. The histogram in **(A)** illustrates the quantified levels of pPLC-γ in cells stimulated with PDGF-BB (■). The values have been calculated as a ratio relative to the Scr (+) PDGF sample (#) (lane 5). Data presented is the mean value from at least two experimental repeats +/- calculated standard errors. Asterisks (*) indicate significance (calculated by one-way ANOVA, *P*<0.001***). **(A)** PDGF-BB (#) significantly increased the phosphorylation of PLC-γ, relative to un-stimulated controls (■). PDGFR inhibitor IV (♦) or inhibitor V (★) significantly inhibited pPLC-γ. NRP-1 siRNA did not inhibit the phosphorylation of PLC-γ (lane 6). **(C)** Immunoblots detected pPLC-γ (Tyr-783), NRP-1 and β-Actin in A172 cells. The data indicated between lanes 6 and 7 (●) was not used in this analysis.

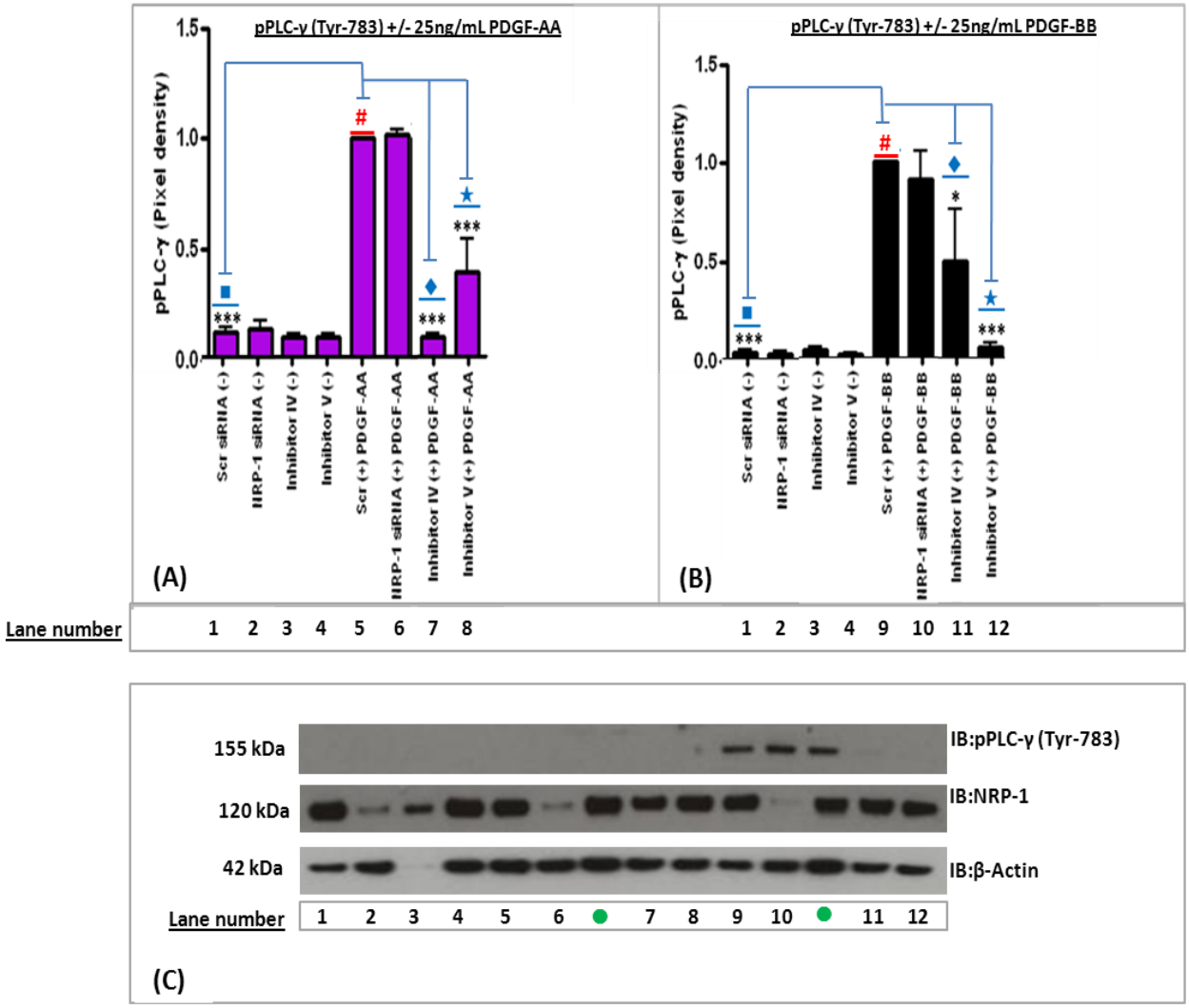

Figure 8.17: NRP-1 siRNA does not attenuate PLC-γ (Tyr-783) phosphorylation in T98G cells
To quantify the phosphorylation of PLC-γ (Tyr-783), pixel densities were calculated using Gene Tools v3 software. The histograms in **(A)** and **(B)** illustrate the quantified levels of pPLC-γ in cells stimulated with PDGF-AA (■) or PDGF-BB (■). The values on the histograms were calculated as a ratio relative to the Scr (+) PDGF-AA in **(A)** lane 5, indicated by the # symbol or the Scr (+) PDGF-BB in **(B)** lane 5, indicated by the # symbol. Data presented is the mean value from at least three experimental repeats +/- calculated standard errors. Asterisks (*) indicate significance (calculated by one-way ANOVA, $P<0.05$*, $P<0.001$***). **(A)** PDGF-AA (#) significantly increased pPLC-γ, relative to un-stimulated controls (■). PDGFR inhibitor IV (♦), inhibitor V significantly inhibited pPLC-γ. (**B)** PDGF-BB (#) significantly increased the phosphorylation of PLC-γ, relative to un-stimulated controls (■). PDGFR inhibitor IV (♦) or inhibitor V (★) significantly inhibited pPLC-γ. NRP-1 siRNA did not inhibit the phosphorylation of PLC-γ. **(C)** Immunoblots detected pPLC-γ (Tyr-783), NRP-1 and β-Actin in T98G cells. The data indicated between lanes 6 and 7 (●) and 10 and 11 (●) was not used in this analysis.

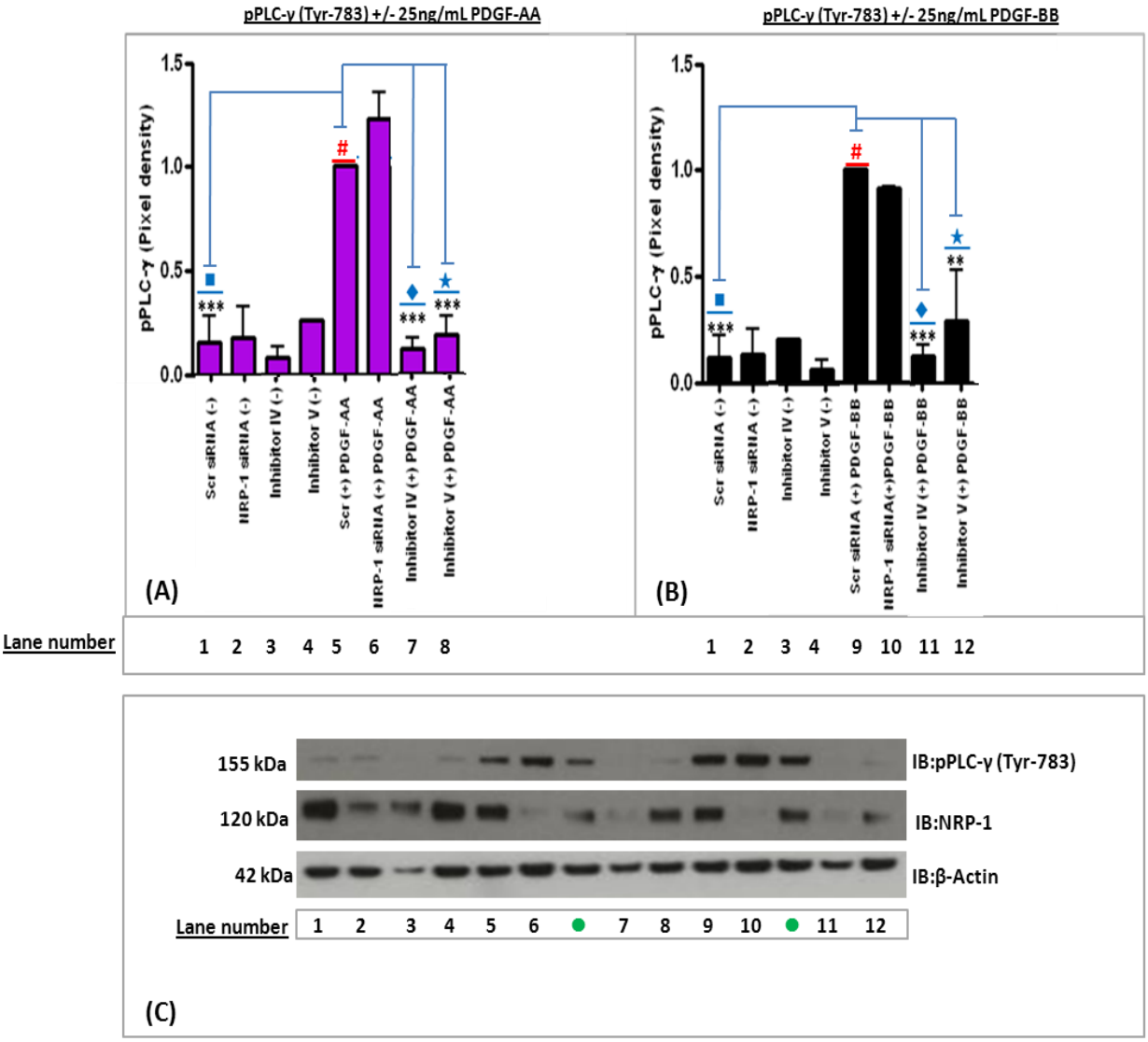

Figure 8.18: NRP-1 siRNA does not attenuate PLC-γ (Tyr-783) phosphorylation in KHOS-240S cells

To quantify the phosphorylation of PLC-γ (Tyr-783), pixel densities were calculated using Gene Tools v3 software. The histograms in **(A)** and **(B)** illustrate the quantified levels of pPLC-γ in cells stimulated with PDGF-AA (■) or PDGF-BB (■). The values on the histograms were calculated as a ratio relative to the Scr (+) PDGF-AA in **(A)** lane 5, indicated by the # symbol or the Scr (+) PDGF-BB in **(B)** lane 5, indicated by the # symbol. Data presented is the mean value from at least three experimental repeats +/- calculated standard errors. Asterisks (*) indicate significance (calculated by one-way ANOVA, $P<0.01$**, $P<0.001$***). **(A)** PDGF-AA (#) significantly increased pPLC-γ, relative to un-stimulated controls (■). PDGFR inhibitor IV (♦), inhibitor V significantly inhibited pPLC-γ. **(B)** PDGF-BB (#) significantly increased the phosphorylation of PLC-γ, relative to un-stimulated controls (■). PDGFR inhibitor IV (♦) or inhibitor V (★) significantly inhibited pPLC-γ. NRP-1 siRNA did not inhibit the phosphorylation of PLC-γ. **(C)** Immunoblots detected pPLC-γ (Tyr-783), NRP-1 and β-Actin in KHOS-240S cells. The data indicated between lanes 6 and 8 (●) and 10 and 12 (●) was not used in this analysis.

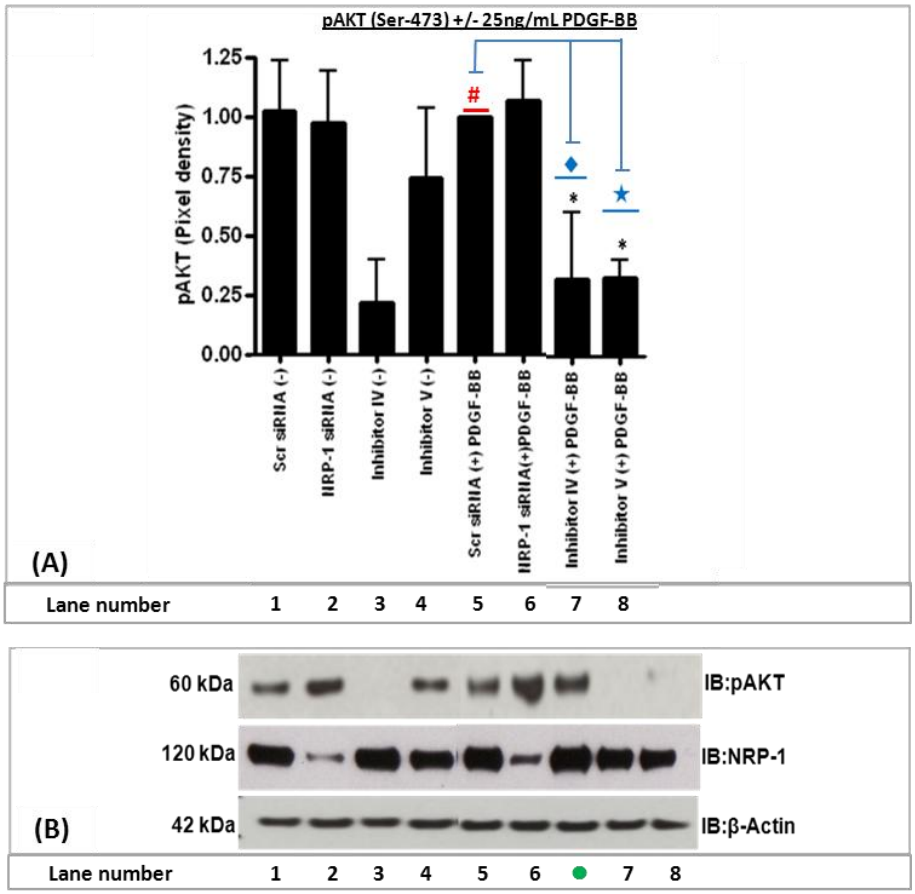

Figure 8.19: NRP-1 siRNA does not inhibits PDGF-stimulated phosphorylation of AKT (Ser-473) in U87MG cells

To quantify the levels of pAKT (Ser-473) pixel densities were calculated using Gene Tools v3 software. The histogram in **(A)** illustrates the quantified levels of pAKT in cells stimulated with PDGF-BB (■). The values have been calculated as a ratio relative to the Scr (+) PDGF sample (#) (Lane 5). Data presented is the mean value from at least two experimental repeats +/- calculated standard errors. Asterisks (*) indicate significance (calculated by one-way ANOVA, $P<0.05$*). **(B)** PDGF-BB (#) stimulation did not significantly increased the phosphorylation of AKT, relative to un-stimulated controls (■) and NRP-1 siRNA treatment of cells did not inhibit pAKT. PDGFR inhibitor IV (♦) or inhibitor V (★) treatment significantly attenuated AKT phosphorylation. **(C)** Immunoblots detected pAKT (Ser-473), NRP-1 and β-Actin in U87MG cells. The data indicated between lanes 6 and 7 (●) was not used in this analysis.

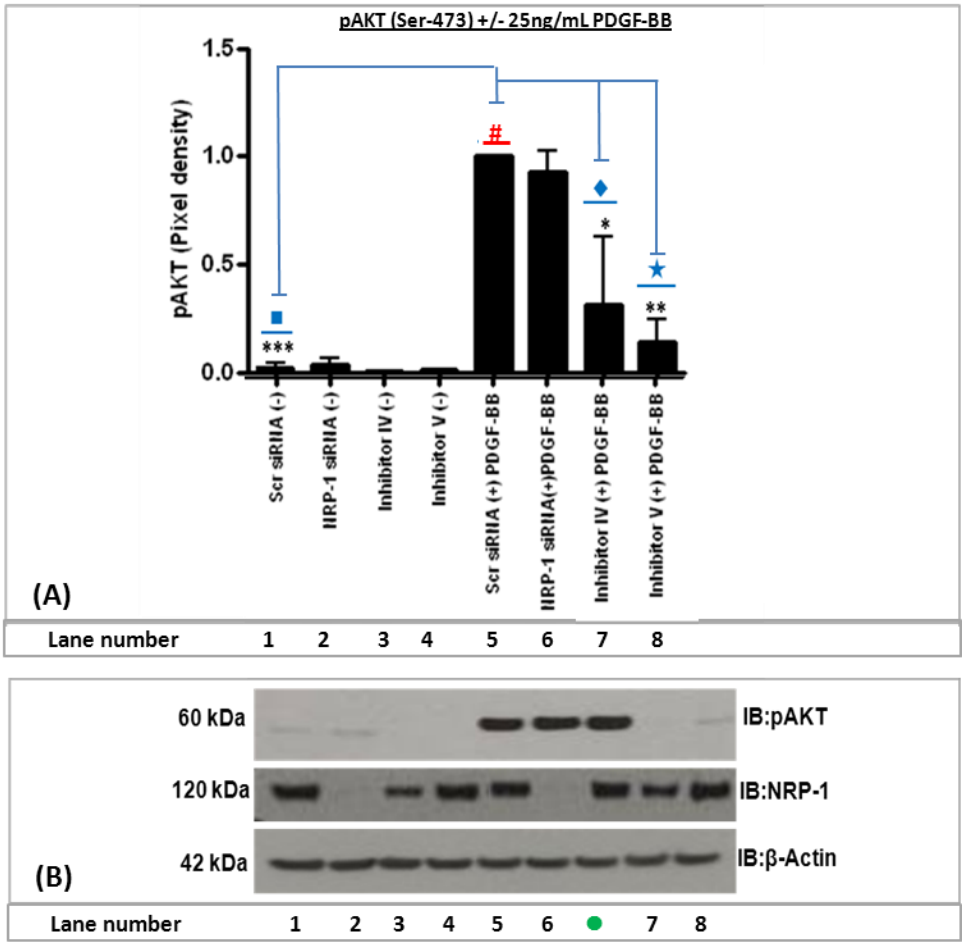

Figure 8.20: NRP-1 siRNA does not inhibits PDGF-stimulated phosphorylation of AKT (Ser-473) in A172 cells

To quantify the levels of pAKT (Ser-473) pixel densities were calculated using Gene Tools v3 software. The histogram in **(A)** illustrates the quantified levels of pAKT in cells stimulated with PDGF-BB (■). The values have been calculated as a ratio relative to the Scr (+) PDGF sample (#) (Lane 5). Data presented is the mean value from at least two experimental repeats +/- calculated standard errors. Asterisks (*) indicate significance (calculated by one-way ANOVA, *P*<0.05*, *P*<0.01** *P*<0.001***). **(B)** PDGF-BB (#) stimulation significantly increased the phosphorylation of AKT, relative to un-stimulated controls (■) and NRP-1 siRNA treatment of cells did not inhibit pAKT. PDGFR inhibitor IV (♦) or inhibitor V (★) treatment significantly attenuated AKT phosphorylation. **(C)** Immunoblots detected pAKT (Ser-473), NRP-1 and β-Actin in A172 cells. The data indicated between lanes 6 and 7 (●) was not used in this analysis.

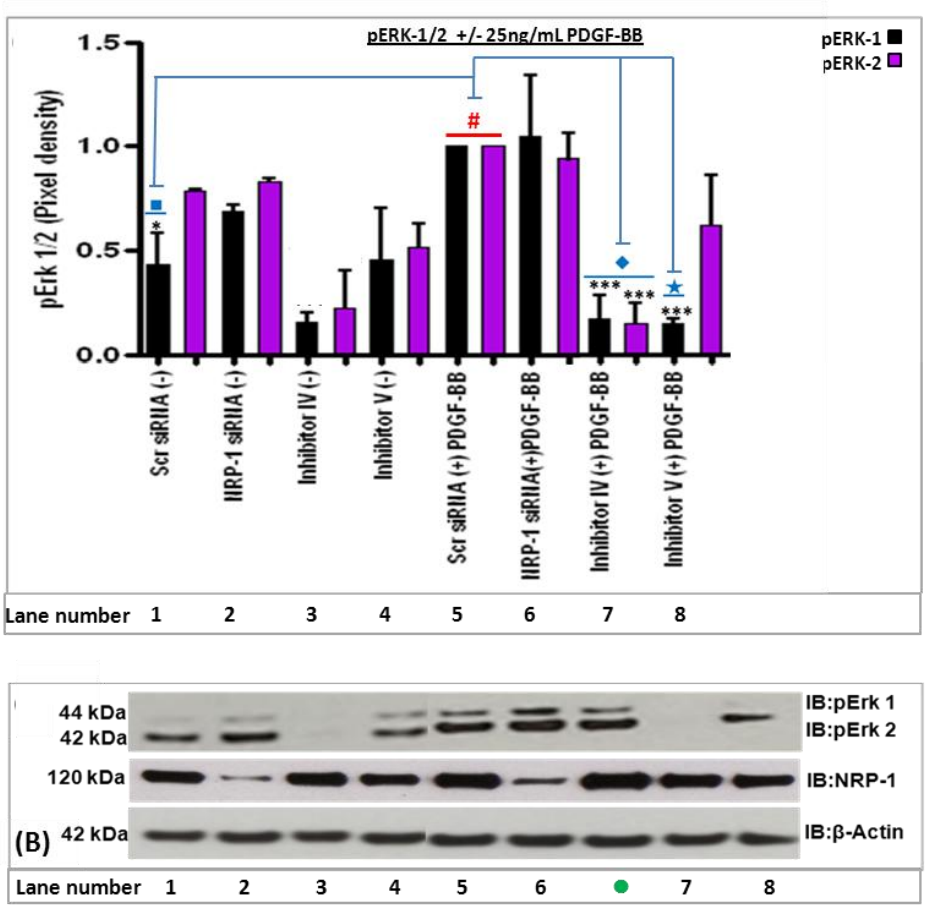

Figure 8.21: NRP-1 siRNA does not inhibit PDGF-stimulated phosphorylation of ERK-1/2 in U87MG cells

To quantify the levels of pERK-1/2 pixel densities were calculated using Gene Tools v3 software. The histograms in **(A)** illustrates the quantified levels of pERK-1 (■) and pERK-2 (■) in cells stimulated with PDGF-BB. The values have been calculated as a ratio relative to the Scr (+) PDGF-BB sample (#). Data presented is the mean value from at least two experimental repeats +/- calculated standard errors. Asterisks (*) indicate significance (calculated by one-way ANOVA, $P<0.05$*, $P<0.001$***). **(B)** PDGF-BB (#) significantly increased the phosphorylation of pERK-1 relative to un-stimulated controls (■). PDGFR inhibitor IV (♦) significantly attenuated PDGF-BB-stimulated phosphorylation of ERK-1/2 and inhibitor V (★) blocked pERK-1 (+PDGF-BB). NRP-1 siRNA treatment did not inhibit PDGF-BB stimulated phosphorylation of ERK-1/2 in U87MG cells. **(C)** Immunoblots detected pERK-1/2, NRP-1 and β-Actin in U87MG cells. The data indicated between lanes 6 and 7 (●) was not used in this analysis.

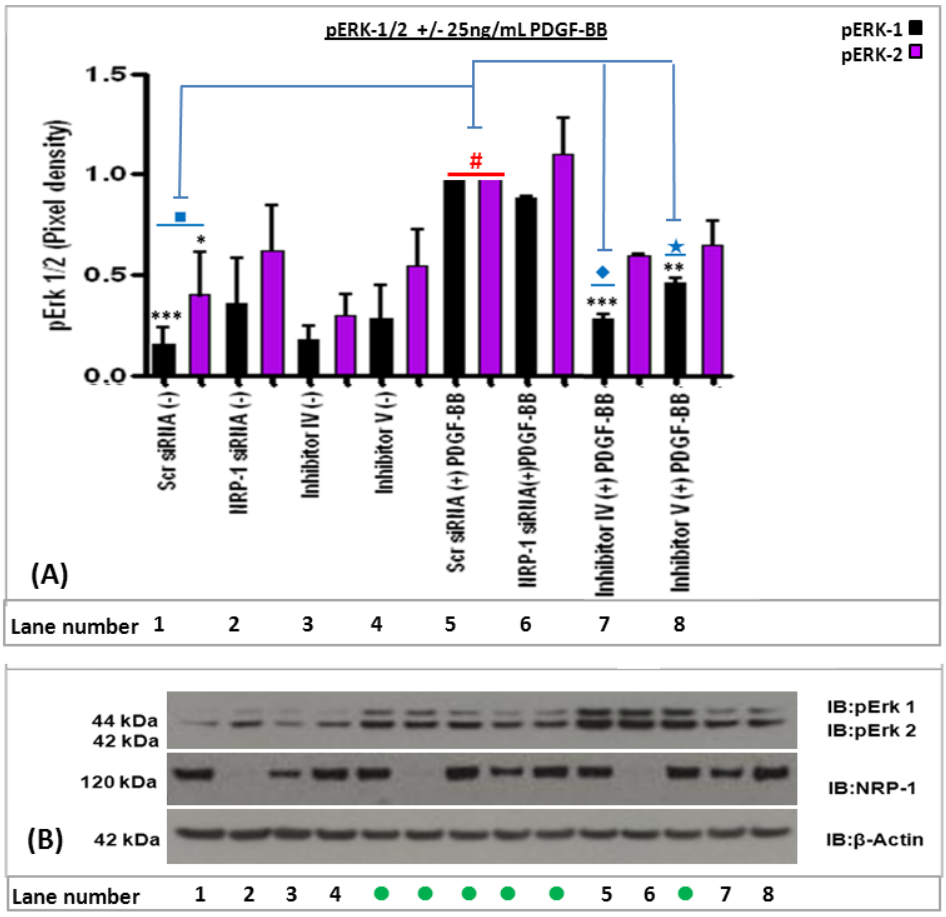

Figure 8.22: NRP-1 siRNA does not inhibit PDGF-stimulated phosphorylation of ERK-1/2 in A172 cells

To quantify the levels of pERK-1/2 pixel densities were calculated using Gene Tools v3 software. The histograms in **(A)** illustrates the quantified levels of pERK-1 (■) and pERK-2 (■) in cells stimulated with PDGF-BB. The values have been calculated as a ratio relative to the Scr (+) PDGF-BB sample (#). Data presented is the mean value from at least two experimental repeats +/- calculated standard errors. Asterisks (*) indicate significance (calculated by one-way ANOVA, *P*<0.05*, *P*<0.01**, *P*<0.001***). **(B)** PDGF-BB (#) significantly increased pERK-1/2 relative to un-stimulated controls (■). PDGFR inhibitor IV (♦) or inhibitor V (★) significantly attenuated PDGF-BB-stimulated phosphorylation of ERK-1. NRP-1 siRNA treatment did not inhibit PDGF-BB stimulated phosphorylation of ERK-1/2 in A172 cells. **(C)** Immunoblots detected pERK-1/2, NRP-1 and β-Actin in A172 cells. The data indicated between lanes 4 and 5 (●) and 6 and 7 (●) was not used in this analysis.

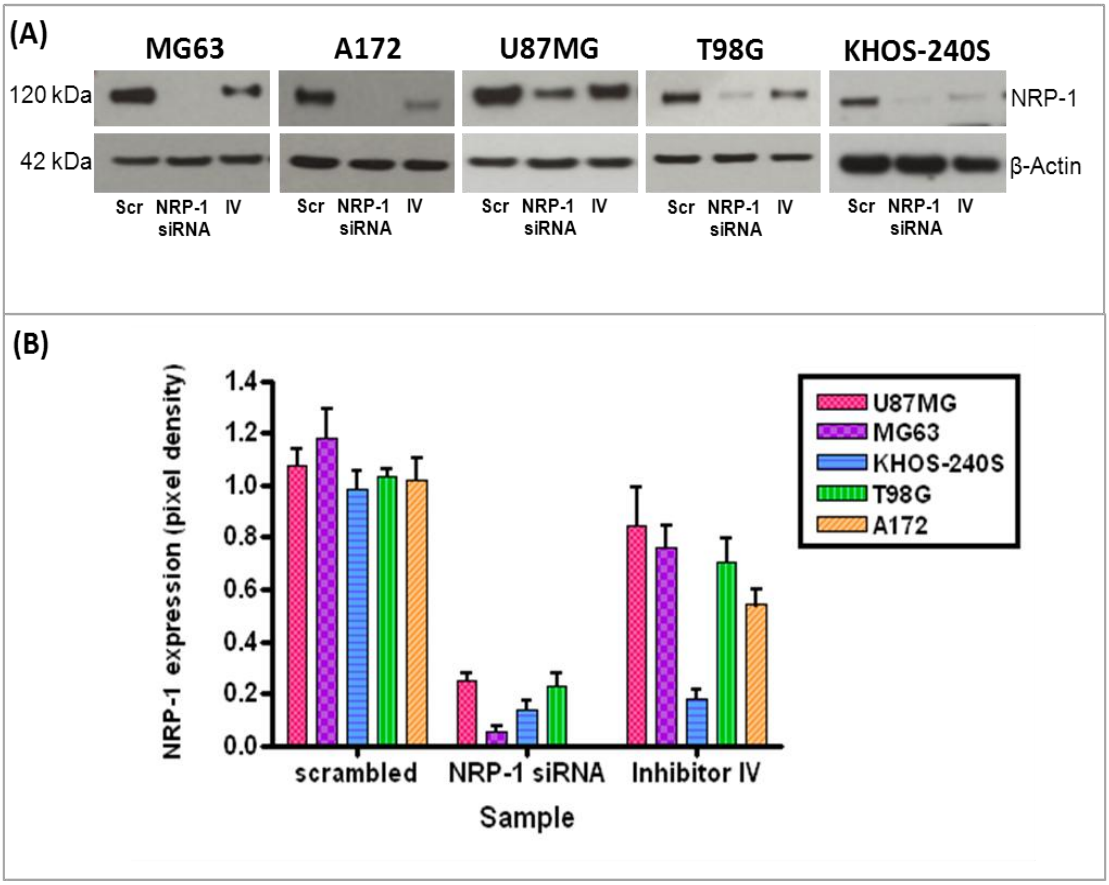

Figure 8.23: IB detection of NRP-1 expression in cells treated with NRP-1 siRNA or PDGFR inhibitor IV

The expression of NRP-1 was detected by immunoblot in tumour cell lines treated with scrambled oligonucleotides, NRP-1 siRNA or 80 nM of PDGFR inhibitor IV. **(A)** Illustrates the immunoblots for NRP-1 with β-Actin as a loading control in each of the cell lines**. (B)** The bar chart illustrates the quantified expression of NRP-1 that has been normalised to β-Actin. Data presented are the mean values from at least two experimental repeats (+/-) calculated standard errors. NRP-1 siRNA effectively attenuates the expression of NRP-1 in the different cell lines. PDGFR inhibitor IV also decreases the expression of NRP-1 in a number of the cell lines, with the most pronounced inhibition of NRP-1 expression in KHOS-240S and A172 cells.

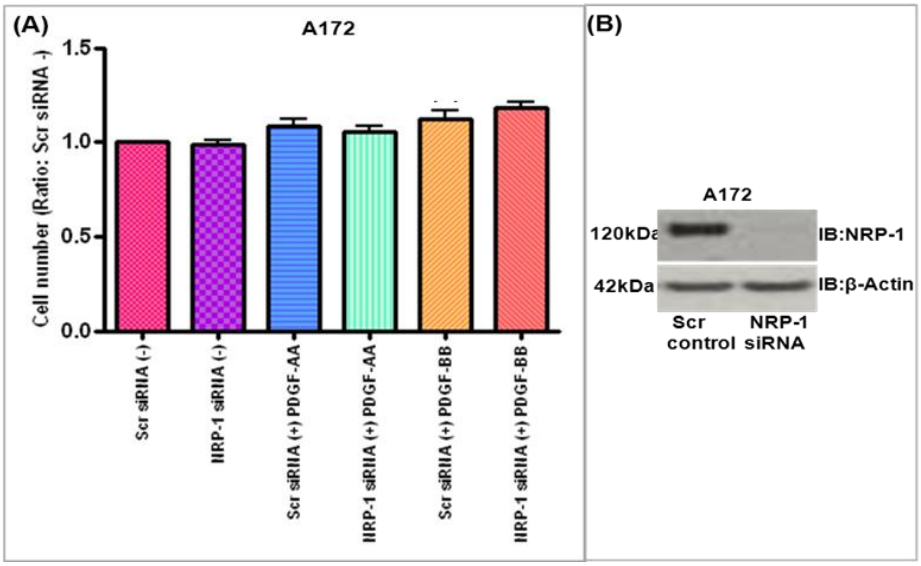

Figure 8.24: PDGF-AA or PDGF-BB does not stimulate A172 cell proliferation
(A) The histogram illustrates cell numbers as determined by the CyQuant® assay. Cell numbers have been expressed as a ratio relative to un-stimulated scrambled control cells (■). PDGF-AA (■) or BB (■) did not stimulate any increase in cell number. NRP-1 siRNA (■) treatment also had no effect on A172 cell number. **(B)** The Immunoblot data illustrates that NRP-1 siRNA treatment blocks the expression of NRP-1 in A172 cells.

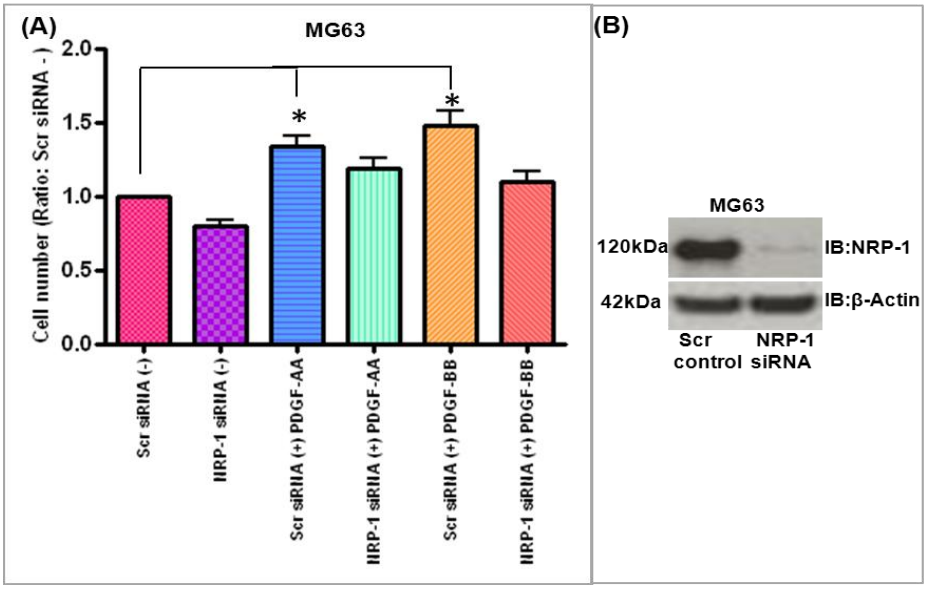

Figure 8.25: PDGF-AA or PDGF-BB stimulated increased MG63 cell proliferation
(A) The histogram illustrates cell numbers as determined by the CyQuant® assay. Cell numbers have been expressed as a ratio relative to un-stimulated scrambled control cells (■). PDGF-AA (■) or BB (■) stimulated a significant increase in cell number relative to un-stimulated controls (■). NRP-1 siRNA (■) treatment decreased MG63 cell number, though this was not significant. **(B)** The Immunoblot data illustrates that NRP-1 siRNA treatment blocks the expression of NRP-1 in MG63 cells. Asterisks indicate significance relative to un-treated controls (calculated by one-way ANOVA, $P < 0.05$*).

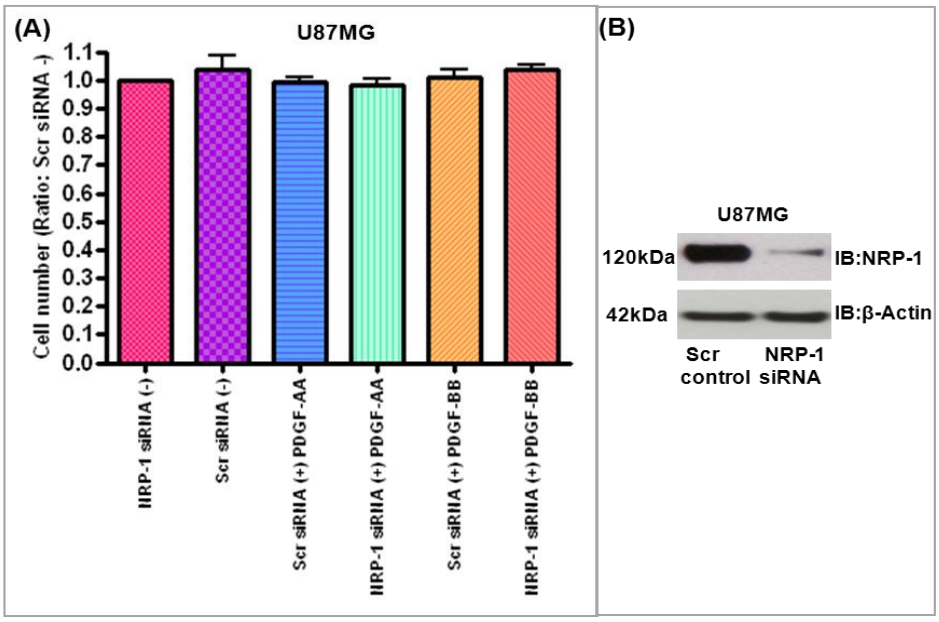

Figure 8.26: PDGF-AA or PDGF-BB does not stimulate U87MG cell proliferation

(A) The histogram illustrates cell numbers as determined by the CyQuant® assay. Cell numbers have been expressed as a ratio relative to un-stimulated scrambled control cells (■). PDGF-AA (■) or BB (■) did not stimulate any increase in cell number. NRP-1 siRNA (■) treatment also had no effect on U87MG cell number. **(B)** The Immunoblot data illustrates that NRP-1 siRNA treatment blocks the expression of NRP-1 in U87MG cells.

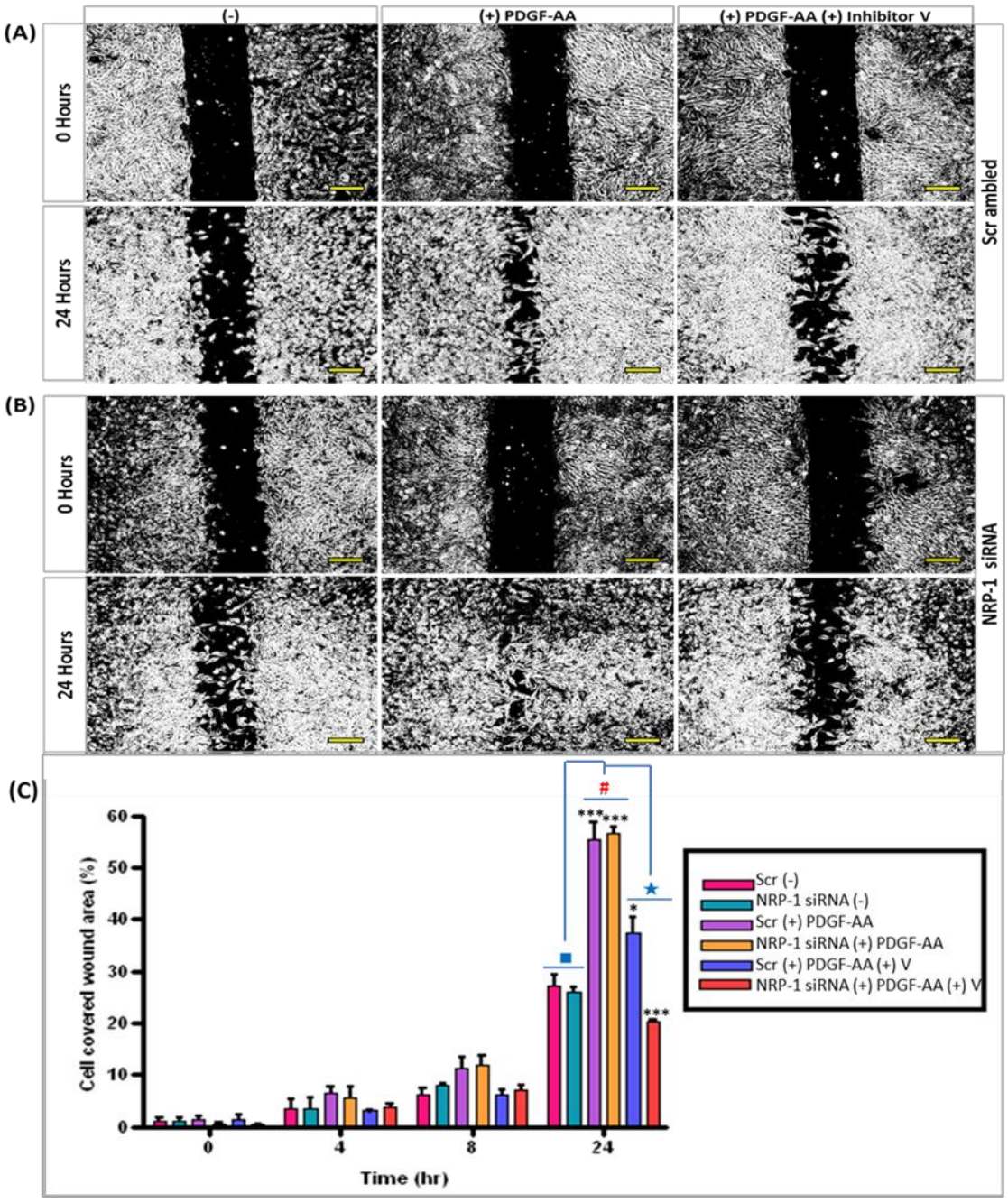

Figure 8.27: PDGF-AA stimulation does not increase the migration of MG63 cells
The figures in **(A)** and **(B)** illustrate representative images taken at time 0 hr and 24 hr. Images have been converted to binary images for clear visualisation of cell-free areas. **(A)** Scrambled control or **(B)** NRP-1 siRNA treated MG63 cells were left un-stimulated or stimulated with PDGF-AA (+/- PDGFR inhibitor V). The top row of panels illustrates cells imaged at 0 hr, with the corresponding 24 hr images positioned directly below. **(C)** The histogram plots the % cell covered area relative to the total area (defined at 0 hr). At 24 hr, the (#) symbol highlights that PDGF-AA induced a significant increase in MG63 migration in either scrambled control or NRP-1 siRNA treated cells relative to un-stimulated controls (■). Treatment of MG63 cells with inhibitor V significantly attenuated migration (★). Results are representative of at least two experimental repeats. Asterisks indicate significance relative to un-stimulated controls (calculated by one-way ANOVA, $P < 0.05$*, $P < 0.01$**, $P < 0.001$***). Scale bar=250 µm.

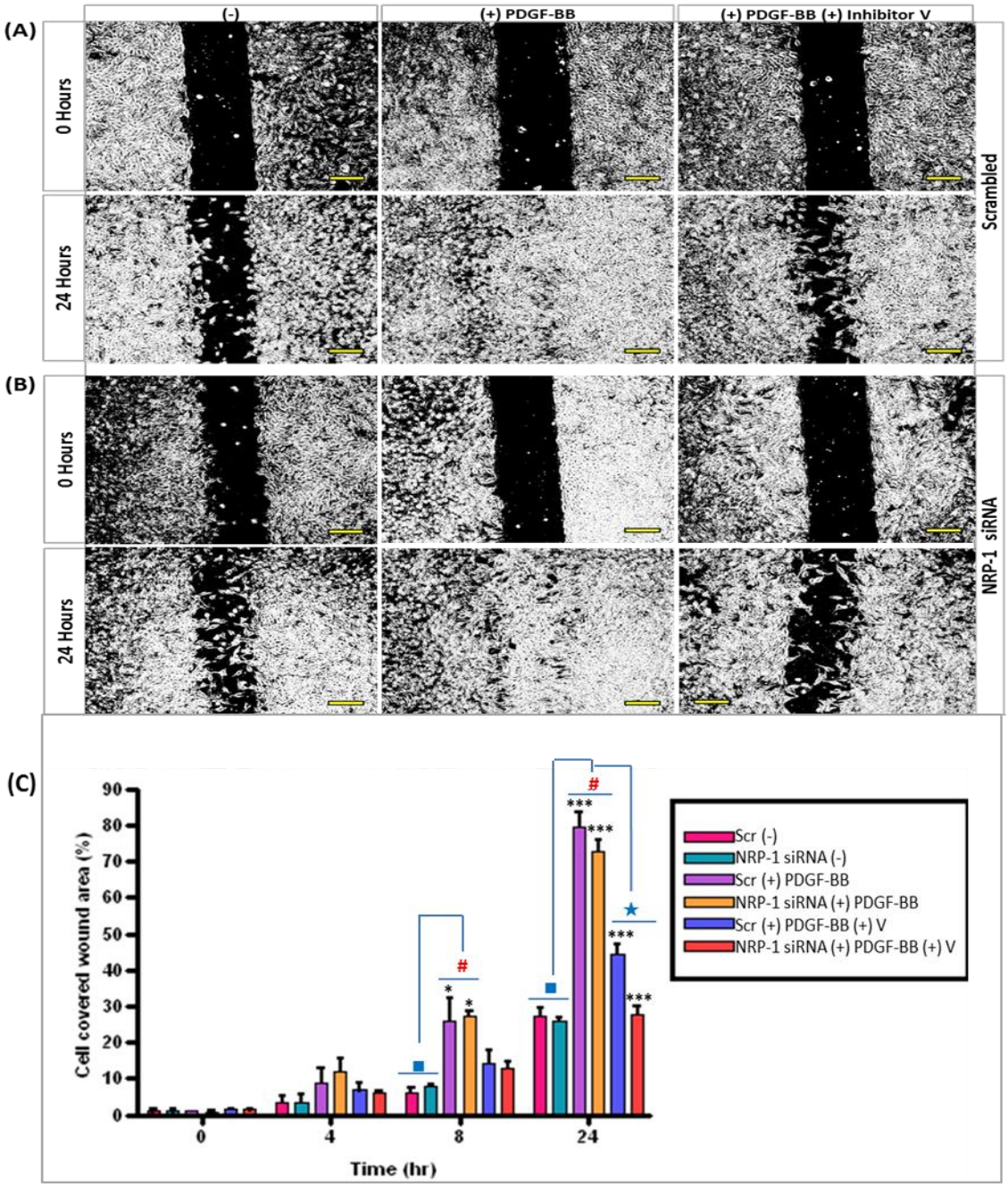

Figure 8.28: PDGF-BB does not stimulate the migration of MG63 cells

The figures in **(A)** and **(B)** illustrate representative images taken at time 0 hr and 24 hr. Images have been converted to binary images for clear visualisation of cell-free areas. **(A)** Scrambled control or **(B)** NRP-1 siRNA treated MG63 cells were left un-stimulated or stimulated with PDGF-BB (+/- PDGFR inhibitor V). The top row of panels illustrates cells imaged at 0 hr, with the corresponding 24 hr images positioned directly below. **(C)** The histogram plots the % cell covered area relative to the total area (defined at 0 hr). At 8 hr and 24 hr, the (#) symbol highlights that PDGF-BB induced a significant increase in MG63 migration in either scrambled control or NRP-1 siRNA treated cells relative to un-stimulated controls (■). Treatment of MG63 cells with inhibitor V significantly attenuated cell migration (★). Results are representative of at least two experimental repeats. Asterisks indicate significance relative to un-stimulated controls (calculated by one-way ANOVA, $P < 0.05$*, $P < 0.001$***). Scale bar=250 µm.

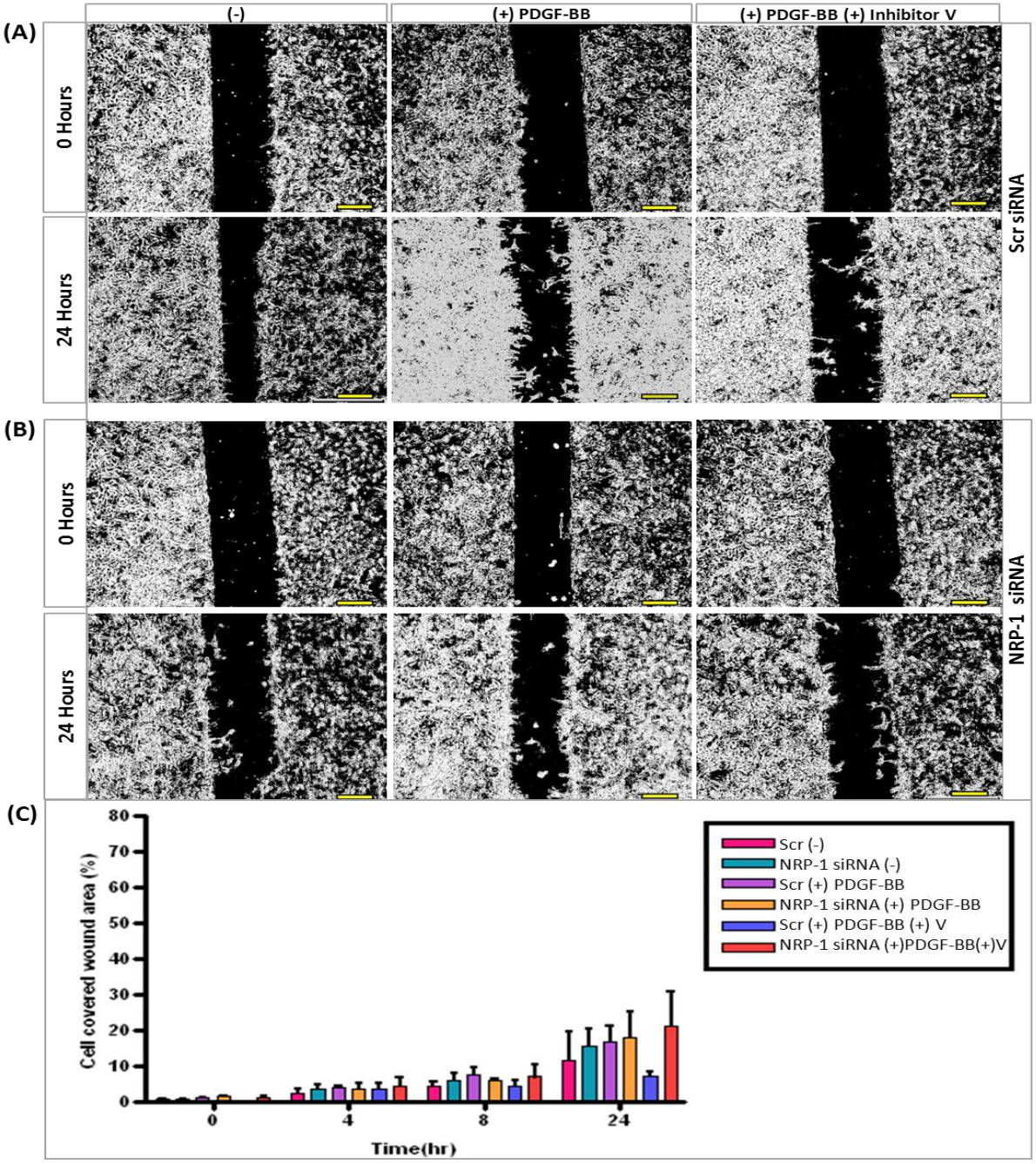

Figure 8.29: PDGF-BB does not stimulate the migration of A172 cells

The figures in **(A)** and **(B)** illustrate representative images taken at time 0 hr and 24 hr. Images have been converted to binary images for clear visualisation of cell-free areas. **(A)** Scrambled control or **(B)** NRP-1 siRNA treated A172 cells were left un-stimulated or stimulated with PDGF-BB (+/- PDGFR inhibitor V). The top row of panels illustrates cells imaged at 0 hr, with the corresponding 24 hr images positioned directly below. **(C)** The histogram plots the % cell covered area relative to the total area (defined at 0 hr). At 4 hr, 8 hr and 24 hr PDGF-BB did not induced a significant increase in A172 cell migration relative to un-stimulated controls .Scale bar=250 µm.

Chapter 9- References

Abramsson A, Kurup S, Busse M, Yamada S, Lindblom P, Schallmeiner E, Stenzel D, Sauvaget D, Ledin J, Ringvall M *et al***.** (2007). Defective N-sulfation of heparan sulfate proteoglycans limits PDGF-BB binding and pericyte recruitment in vascular development. *Genes & development*, **21**: 316–31.

Akagi M, Kawaguchi M, Liu W, McCarty MF, Takeda A, Fan F, Stoeltzing O, Parikh AA, Jung YD, Bucana CD *et al*. (2003). Induction of neuropilin-1 and vascular endothelial growth factor by epidermal growth factor in human gastric cancer cells. *British Journal of Cancer*, **88**: 796–802.

Alam A, Herault JP, Barron P, Favier B, Fons P, Delesque-Touchard N, Senegas I, Laboudie P, Bonnin J, Cassan C *et al*. (2004). Heterodimerization with vascular endothelial growth factor receptor-2 (VEGFR-2) is necessary for VEGFR-3 activity. *Biochemical and biophysical research communications*, **324**:,909–15.

Allalou A and Wählby C (2009). BlobFinder, a tool for fluorescence microscopy image cytometry. *Computer methods and programs in biomedicine*, **94**: 58–65.

Allalunis-Turner MJ, Barron GM, Day RS, Dobler KD, and Mirzayans R (1993). Isolation of two cell lines from a human malignant glioma specimen differing in sensitivity to radiation and chemotherapeutic drugs. *Radiation research*, **134**: 349–54.

Allam M, Martinet N, and Martinet Y (1992). Differential migratory response of U-2 OS osteosarcoma cell to the various forms of platelet-derived growth factor. *Biochimie*, **74:**, 183–6.

Alonso G, Koegl M, Mazurenko N, and Courtneidge SA (1995). Sequence requirements for binding of Src family tyrosine kinases to activated growth factor receptors. *The Journal of biological chemistry*, **270**: 9840–8.

Alonso V, de Gortázar AR, Ardura JA, Andrade-Zapata I, Alvarez-Arroyo MV, and Esbrit P (2008). Parathyroid hormone-related protein (107-139) increases human osteoblastic cell survival by activation of vascular endothelial growth factor receptor-2. *Journal of cellular physiology*, **217**: 717–27.

Amagasaki K, Kaneto H, Heldin CH, and Lennartsson J (2006). c-Jun N-terminal kinase is necessary for platelet-derived growth factor-mediated chemotaxis in primary fibroblasts. *The Journal of biological chemistry*, **281**: 22173–9.

Amin DN, Bielenberg DR, Lifshits E, Heymach JV, and Klagsbrun M (2008). Targeting EGFR activity in blood vessels is sufficient to inhibit tumor growth and is accompanied by an increase in VEGFR-2 dependence in tumor endothelial cells. *Microvascular research*, **76**:15–22.

Ansel JC, Tiesman JP, Olerud JE, Krueger JG, Krane JF, Tara DC, Shipley GD, Gilbertson D, Usui ML, and Hart CE (1993). Human keratinocytes are a major source of cutaneous platelet-derived growth factor. *The Journal of clinical investigation*, **92**: 671–8.

Antipenko A, Himanen JP, van Leyen K, Nardi-Dei V, Lesniak J, Barton WA, Rajashankar KR, Lu M, Hoemme C, Püschel AW *et al*. (2003). Structure of the semaphorin-3A receptor binding module. *Neuron*, **39**: 589–98.

Antoniades HN, Galanopoulos T, Neville-Golden J, Kiritsy CP, and Lynch SE (1991). Injury induces in vivo expression of platelet-derived growth factor (PDGF) and PDGF receptor mRNAs in skin epithelial cells and PDGF mRNA in connective tissue fibroblasts. *Proceedings of the National Academy of Sciences of the United States of America*, **88**: 565–9.

Antoniades HN, Scher CD, and Stiles CD (1979). Purification of human platelet-derived growth factor. *Proceedings of the National Academy of Sciences of the United States of America*, **76**: 1809–13.

Apostolova N, Gomez-Sucerquia LJ, Gortat A, Blas-Garcia A, and Esplugues JV (2011). Compromising mitochondrial function with the antiretroviral drug efavirenz induces cell survival-promoting autophagy. *Hepatology (Baltimore, Md.)*, **54**: 1009–19.

Arvidsson AK, Rupp E, Nånberg E, Downward J, Rönnstrand L, Wennström S, Schlessinger J, Heldin CH, and Claesson-Welsh, L (1994). Tyr-716 in the platelet-derived growth factor beta-receptor kinase insert is involved in GRB2 binding and Ras activation. *Molecular and cellular biology*, **14**: 6715–26.

Ashikari-Hada S, Habuchi H, Kariya Y, and Kimata K (2005). Heparin regulates vascular endothelial growth factor165-dependent mitogenic activity, tube formation, and its receptor phosphorylation of human endothelial cells. Comparison of the effects of heparin and modified heparins. *The Journal of biological chemistry*, **280**: 31508–15.

Ataliotis P and Mercola M (1997). Distribution and functions of platelet-derived growth factors and their receptors during embryogenesis. *International review of cytology*, **172**: 95–127.

Autiero M, Waltenberger J, Communi D, Kranz A, Moons L, Lambrechts D, Kroll J, Plaisance S, De Mol M, Bono F *et al.* (2003). Role of PlGF in the intra- and intermolecular cross talk between the VEGF receptors Flt1 and Flk1. *Nature medicine*, **9**: 936–43.

Bachelder RE, Crago A, Chung J, Wendt MA, Shaw LM, Robinson G, and Mercurio AM (2001). Vascular Endothelial Growth Factor Is an Autocrine Survival Factor for Neuropilin-expressing Breast Carcinoma Cells. *Cancer Res.*, **61**: 5736–5740.

Bagci T, Wu JK, Pfannl R, Ilag LL, and Jay DG (2009). Autocrine semaphorin 3A signaling promotes glioblastoma dispersal. *Oncogene*, **28**: 3537–50.

Bagri A, Tessier-Lavigne M, and Watts RJ (2009). Neuropilins in tumor biology. *Clinical cancer research : an official journal of the American Association for Cancer Research*, **15**: 1860–4.

Balasubramaniam V, Le Cras TD, Ivy DD, Grover TR, Kinsella JP, and Abman SH (2003). Role of platelet-derived growth factor in vascular remodeling during pulmonary hypertension in the ovine fetus. *American journal of physiology. Lung cellular and molecular physiology*, **284**: L826–33.

Ball SG, Bayley C, Shuttleworth CA, and Kielty CM (2010). Neuropilin-1 regulates platelet-derived growth factor receptor signalling in mesenchymal stem cells. *The Biochemical journal*, **427**: 29–40.

Ball SG, Shuttleworth CA, and Kielty CM (2007a). Platelet-derived growth factor receptor-alpha is a key determinant of smooth muscle alpha-actin filaments in bone marrow-derived mesenchymal stem cells. *The international journal of biochemistry & cell biology*, **39**: 379–91.

Ball SG, Shuttleworth CA, and Kielty CM (2007b). Vascular endothelial growth factor can signal through platelet-derived growth factor receptors. *The Journal of cell biology*, **177**: 489–500.

Ballmer-Hofer K, Andersson AE, Ratcliffe LE, and Berger P (2011). Neuropilin-1 promotes VEGFR-2 trafficking through Rab11 vesicles thereby specifying signal output. *Blood*, **118**: 816–26.

Banai S, Wolf Y, Golomb G, Pearle A, Waltenberger J, Fishbein I, Schneider A, Gazit A, Perez L, Huber R *et al.* (1998). PDGF-receptor tyrosine kinase blocker AG1295 selectively attenuates smooth muscle cell growth in vitro and reduces neointimal formation after balloon angioplasty in swine. *Circulation*, **97**: 1960–9.

Banerjee S, Mehta S, Haque I, Sengupta K, Dhar K, Kambhampati S, Van Veldhuizen PJ, and Banerjee SK (2008). VEGF-A165 induces human aortic smooth muscle cell migration by activating neuropilin-1-VEGFR1-PI3K axis. *Biochemistry*, **47**: 3345–51.

Banerjee S, Sengupta K, Dhar K, Mehta S, D'Amore PA, Dhar G, and Banerjee SK (2006). Breast cancer cells secreted platelet-derived growth factor-induced motility of vascular smooth muscle cells is mediated through neuropilin-1. *Molecular carcinogenesis*, **45**: 871–80.

Banks-Schlegel SP, Gazdar AF, and Harris CC (1985). Intermediate filament and cross-linked envelope expression in human lung tumor cell lines. *Cancer research*, **45**: 1187–97.

Bannerman P, Ara J, Hahn A, Hong L, McCauley E, Friesen K, and Pleasure D (2008). Peripheral nerve regeneration is delayed in neuropilin 2-deficient mice. *Journal of neuroscience research*, **86**: 3163–9.

Barleon B, Sozzani S, Zhou D, Weich HA, Mantovani A, and Marmé D (1996). Migration of human monocytes in response to vascular endothelial growth factor (VEGF) is mediated via the VEGF receptor flt-1. *Blood*, **87**: 3336–43.

Barr MP, Byrne AM, Duffy AM, Condron CM, Devocelle M, Harriott P, Bouchier-Hayes DJ, and Harmey JH (2005). A peptide corresponding to the neuropilin-1-binding site on VEGF(165) induces apoptosis of neuropilin-1-expressing breast tumour cells. *British journal of cancer*, **92**: 328–33.

Bauer EA, Cooper TW, Huang JS, Altman J, and Deuel TF (1985). Stimulation of in vitro human skin collagenase expression by platelet-derived growth factor. *Proceedings of the National Academy of Sciences of the United States of America*, **82**: 4132–6.

Bauman JE, Eaton KD, and Martins RG (2007). Antagonism of platelet-derived growth factor receptor in non-small cell lung cancer: rationale and investigations. *Clinical cancer research : an official journal of the American Association for Cancer Research*, **13**: 4632–6.

Bazenet CE, Gelderloos JA, and Kazlauskas A (1996). Phosphorylation of tyrosine 720 in the platelet-derived growth factor alpha receptor is required for binding of Grb2 and SHP-2 but not for activation of Ras or cell proliferation. *Molecular and cellular biology*, **16**: 6926–36.

Beck B, Driessens G, Goossens S, Youssef KK, Kuchnio A, Caauwe A, Sotiropoulou PA, Loges S, Lapouge G, Candi A *et al.* (2011). A vascular niche and a VEGF-Nrp1 loop regulate the initiation and stemness of skin tumours. *Nature*, **478**: 399–403.

Bennasroune A, Gardin A, Aunis D, Crémel G, and Hubert P (2004). Tyrosine kinase receptors as attractive targets of cancer therapy. *Critical reviews in oncology/hematology*, **50**: 23–38.

Bergsten E, Uutela M, Li X, Pietras K, Ostman A, Heldin CH, Alitalo K, and Eriksson U (2001). PDGF-D is a specific, protease-activated ligand for the PDGF beta-receptor. *Nature cell biology*, **3**: 512–6.

Bergé M, Allanic D, Bonnin P, de Montrion C, Richard J, Suc M, Boivin JF, Contrerès JO, Lockhart BP, Pocard M *et al.* (2011). Neuropilin-1 is upregulated in hepatocellular carcinoma and contributes to tumour growth and vascular remodelling. *Journal of Hepatology*, **55**: 866–875.

Betsholtz C, Johnsson A, Heldin CH, Westermark B, Lind P, Urdea MS, Eddy R, Shows TB, Philpott K, Mellor AL et al. (1986). cDNA sequence and chromosomal localization of human platelet-derived growth factor A-chain and its expression in tumour cell lines. *Nature*, **320**: 695–699.

Bigner DD, Bigner SH, Pontén J, Westermark B, Mahaley MS, Ruoslahti E, Herschman H, Eng LF, and Wikstrand CJ (1981). Heterogeneity of Genotypic and phenotypic characteristics of fifteen permanent cell lines derived from human gliomas. *Journal of neuropathology and experimental neurology*, **40**: 201–29.

Billiau A, Cassiman JJ, Willems D, Verhelst M, and Heremans H (1975). In vitro cultivation of human tumor tissues. *Oncology*, **31**: 257–72.

Billiau A, Edy VG, Heremans H, Van Damme J, Desmyter J, Georgiades JA, and De Somer P (1977). Human interferon: mass production in a newly established cell line, MG-63. *Antimicrobial agents and chemotherapy*, **12**: 11–5.

Bonthron DT, Morton CC, Orkin SH, and Collins T (1988). Platelet-derived growth factor A chain: gene structure, chromosomal location, and basis for alternative mRNA splicing. *Proceedings of the National Academy of Sciences of the United States of America*, **85**: 1492–6.

Bork P and Beckmann G (1993). The CUB domain. A widespread module in developmentally regulated proteins. *Journal of molecular biology*, **231**: 539–45.

Bork P, Doerks T, Springer TA, and Snel B (1999). Domains in plexins: links to integrins and transcription factors. *Trends in biochemical sciences*, **24**: 261–3.

Bos JL (1995). A target for phosphoinositide 3-kinase: Akt/PKB. *Trends in biochemical sciences*, **20**: 441–2.

Boström H, Willetts K, Pekny M, Levéen P, Lindahl P, Hedstrand H, Pekna M, Hellström M, Gebre-Medhin S, Schalling M *et al.* (1996). PDGF-A signaling is a critical event in lung alveolar myofibroblast development and alveogenesis. *Cell*, **85**: 863–73.

Boucher P, Gotthardt M, Li WP, Anderson RGW, and Herz J (2003). LRP: role in vascular wall integrity and protection from atherosclerosis. *Science (New York, N.Y.)*, **300**: 329–32.

Boucher P, Liu P, Gotthardt M, Hiesberger T, Anderson RGW, and Herz J (2002). Platelet-derived growth factor mediates tyrosine phosphorylation of the cytoplasmic domain of the low Density lipoprotein receptor-related protein in caveolae. *The Journal of biological chemistry*, **277**: 15507–13.

Bovenkamp DE, Goishi K, Bahary N, Davidson AJ, Zhou Y, Becker T, Becker CG, Zon LI, and Klagsbrun M (2004). Expression and mapping of duplicate neuropilin-1 and neuropilin-2 genes in developing zebrafish. *Gene expression patterns : GEP*, **4**: 361–70.

Brattain MG, Fine WD, Khaled FM, Thompson J, and Brattain DE (1981). Heterogeneity of malignant cells from a human colonic carcinoma. *Cancer research*, **41**: 1751–6.

Brave SR, Ratcliffe K, Wilson Z, James NH, Ashton S, Wainwright A, Kendrew J, Dudley P, Broadbent N, Sproat G *et al.* (2011). Assessing the activity of cediranib, a VEGFR-2/3 tyrosine kinase inhibitor, against VEGFR-1 and members of the structurally related PDGFR family. *Molecular cancer therapeutics*, **10**: 861–73.

Broome MA and Hunter T (1997). The PDGF receptor phosphorylates Tyr 138 in the c-Src SH3 domain in vivo reducing peptide ligand binding. *Oncogene*, **14**: 17–34.

Bronzert D, Pantazis H, Antoniades H *et al.* (1987). Synthesis and secretion of platelet-derived growth factor by human breast cancer cell lines. *Proceedings of the National Academy of Sciences of the United States of America*, **84**: 5763.

Brower M, Carney DN, Oie HK, Gazdar AF, and Minna JD (1986). Growth of cell lines and clinical specimens of human non-small cell lung cancer in a serum-free defined medium. *Cancer research*, **46**: 798–806.

Brusselmans K, Bono F, Collen D, Herbert JM, Carmeliet P, and Dewerchin M (2005). A novel role for vascular endothelial growth factor as an autocrine survival factor for embryonic stem cells during hypoxia. *The Journal of biological chemistry*, **280**: 3493–9.

Burgess A, Vigneron S, Brioudes E, Labbé JC, Lorca T, and Castro A (2010). Loss of human Greatwall results in G2 arrest and multiple mitotic defects due to deregulation of the cyclin B-Cdc2/PP2A balance. *Proceedings of the National Academy of Sciences of the United States of America*, **107**: 12564–9.

Busse M, Feta A, Presto J, Wilén M, Grønning M, Kjellén L, and Kusche-Gullberg M (2007). Contribution of EXT1, EXT2, and EXTL3 to heparan sulfate chain elongation. *The Journal of biological chemistry*, **282**: 32802–10.

Cackowski FC, Xu L, Hu B, and Cheng SY (2004). Identification of two novel alternatively spliced Neuropilin-1 isoforms. *Genomics*, **84**: 82–94.

Cai H and Reed RR (1999). Cloning and characterization of neuropilin-1-interacting protein: a PSD-95/Dlg/ZO-1 domain-containing protein that interacts with the cytoplasmic domain of neuropilin-1. *The Journal of neuroscience : the official journal of the Society for Neuroscience*, **19**: 6519–27.

Calver AR, Hall AC, Yu WP, Walsh FS, Heath JK, Betsholtz C, and Richardson WD (1998). Oligodendrocyte population dynamics and the role of PDGF in vivo. *Neuron*, **20**: 869–82.

Calzolari F and Malatesta P (2010). Recent insights into PDGF-induced gliomagenesis. *Brain pathology (Zurich, Switzerland)*, **20**: 527–38.

Cao S, Yaqoob U, Das A, Shergill U, Jagavelu K, Huebert RC, Routray C, Abdelmoneim S, Vasdev M, Leof E *et al.* (2010). Neuropilin-1 promotes cirrhosis of the rodent and human liver by enhancing PDGF/TGF-beta signaling in hepatic stellate cells. *The Journal of clinical investigation*, **120**: 2379–94.

Cao Y, Ji WR, Qi P, and Rosin A (1997). Placenta growth factor: identification and characterization of a novel isoform generated by RNA alternative splicing. *Biochemical and biophysical research communications*, **235**: 493–8.

Cao Y, Wang L, Nandy D, Zhang Y, Basu A, Radisky D, and Mukhopadhyay D (2008). Neuropilin-1 Upholds Dedifferentiation and Propagation Phenotypes of Renal Cell Carcinoma Cells by Activating Akt and Sonic Hedgehog Axes. *Cancer Research*, **68**: 8667–8672.

Cao, Y, Wang E, Pal K, Dutta SK, Bar-Sagi D and Mukhopadhyay D (2012). VEGF exerts an angiogenesis-independent function in cancer cells to promote their malignant progression. *Cancer research*, **72**: 3912-8

Carpenter CL, Auger KR, Chanudhuri M, Yoakim M, Schaffhausen B, Shoelson S and Cantley LC (1993). Phosphoinositide 3-kinase is activated by phosphopeptides that bind to the SH2 domains of the 85-kDa subunit. *The Journal of biological chemistry*, **268**: 9478–83.

Castro-Rivera E, Ran S, Brekken RA, and Minna JD (2008). Semaphorin 3B inhibits the phosphatidylinositol 3-kinase/Akt pathway through neuropilin-1 in lung and breast cancer cells. *Cancer research*, **68**: 8295–303.

Catalano A, Caprari P, Moretti S, Faronato M, Tamagnone L, and Procopio A (2006). Semaphorin-3A is expressed by tumor cells and alters T-cell signal transduction and function. *Blood*: **107**: 3321–9.

Catlow K, Deakin J, Delehedde M, Fernig D, Gallagher J, Pavao M, and Lyon M (2003). Hepatocyte growth factor/scatter factor and its interaction with heparan sulphate and dermatan sulphate*. Biochemical society transactions*.**31**: 352-53

Cattaneo MG, Gentilini D, and Vicentini LM (2006). Deregulated human glioma cell motility: inhibitory effect of somatostatin. *Molecular and cellular endocrinology*, **256**: 34–9.

Celotti F, Colciago A, Negri-Cesi P, Pravettoni A, Zaninetti R, and Sacchi MC (2006). Effect of platelet-rich plasma on migration and proliferation of SaOS-2 osteoblasts: role of platelet-derived growth factor and transforming growth factor-beta. *Wound repair and regeneration : official publication of the Wound Healing Society [and] the European Tissue Repair Society*, **14**: 195–202.

Chazotte B (2011). Labeling membrane glycoproteins or glycolipids with fluorescent wheat germ agglutinin. *Cold Spring Harbor protocols*.

Chen H, Chédotal A, He Z, Goodman CS, and Tessier-Lavigne M (1997). Neuropilin-2, a novel member of the neuropilin family, is a high affinity receptor for the semaphorins Sema E and Sema IV but not Sema III. *Neuron*, **19**: 547–59.

Chen R, Jiang X, Sun D, Han G, Wang F, Ye M, Wang L, and Zou H (2009). Glycoproteomics Analysis of Human Liver Tissue by Combination of Multiple Enzyme Digestion and Hydrazide Chemistry research articles. 651–661.

Chen YC, Chang CN, Hsu HC, Chiou SJ, Lee LT, and Hseu TH (2009). Sennoside B inhibits PDGF receptor signaling and cell proliferation induced by PDGF-BB in human osteosarcoma cells. *Life sciences*, **84**: 915–22.

Chen YL, Wu YY, Chung YC, Chao YC, Yang SC, Shih JY, Yuan A, Hong TM, and Yang PC (2006). Neuropilin-1 and lung cancer progression: Potential role of targeting neuropilin-1 as an anti-tumor strategy. *AACR Meeting Abstracts*, **385.**

Chiara F, Bishayee S, Heldin CH, and Demoulin JB (2004a). Autoinhibition of the platelet-derived growth factor beta-receptor tyrosine kinase by its C-terminal tail. *The Journal of biological chemistry*, **279**: 19732–8.

Chiara F, Goumans MJ, Forsberg H, Ahgrén A, Rasola A, Aspenström P, Wernstedt C, Hellberg C, Heldin CH, and Heuchel R (2004b). A gain of function mutation in the activation loop of platelet-derived growth factor beta-receptor deregulates its kinase activity. *The Journal of biological chemistry*, **279**: 42516–27.

Chiarugi P, Cirri P, Taddei ML, Talini D, Doria L, Fiaschi T, Buricchi F, Giannoni E, Camici G, Raugei G *et al*. (2002). New perspectives in PDGF receptor downregulation: the main role of phosphotyrosine phosphatases. *J. Cell Sci.*, **115**: 2219–2232.

Chin LS, Murray SF, Zitnay KM, and Rami B (1997). K252a inhibits proliferation of glioma cells by blocking platelet-derived growth factor signal transduction. *Clinical Cancer Research*, **3**: 771–776.

Cho HY, Cutchins EC, Rhim JS, and Huebner RJ (1976). Revertants of human cells transformed by murine sarcoma virus. *Science (New York, N.Y.)*, **194**: 951–3.

Christinger HW, Fuh G, de Vos AM, and Wiesmann C (2004). The crystal structure of placental growth factor in complex with domain 2 of vascular endothelial growth factor receptor-1. *The Journal of biological chemistry*, **279**: 10382–8.

Claesson-Welsh L (1994). Platelet-derived growth factor receptor signals. *The Journal of biological chemistry*, **269**: 32023–6.

Claesson-Welsh L, Eriksson A, Morén A, Severinsson L, Ek B, Ostman A, Betsholtz C and Heldin CH (1988). cDNA cloning and expression of a human platelet-derived growth factor (PDGF) receptor specific for B-chain-containing PDGF molecules. *Molecular and cellular biology*, **8**: 3476–86.

Clark RA, Folkvord JM, Hart CE, Murray MJ, and McPherson JM (1989). Platelet isoforms of platelet-derived growth factor stimulate fibroblasts to contract collagen matrices. *The Journal of clinical investigation*, **84**: 1036–40.

Corbel C, Lemarchandel V, Thomas-Vaslin V, Pelus AS, Agboton C, and Roméo PH (2007). Neuropilin 1 and CD25 co-regulation during early murine thymic differentiation. *Developmental and comparative immunology*, **31**:1082–94.

Cordes N, Hansmeier B, Beinke C, Meineke V, and van Beuningen D (2003). Irradiation differentially affects substratum-dependent survival, adhesion, and invasion of glioblastoma cell lines. *British journal of cancer*, **89**: 2122–32.

Craven RJ, Xu LH, Weiner TM, Fridell YW, Dent GA, Srivastava S, Varnum B, Liu ET, and Cance WG (1995). Receptor tyrosine kinases expressed in metastatic colon cancer. *International journal of cancer.***60**: 791–7.

Cébe Suarez S, Pieren M, Cariolato L, Arn S, Hoffmann U, Bogucki A, Manlius C, Wood J, and Ballmer-Hofer K (2006). A VEGF-A splice variant defective for heparan sulfate and neuropilin-1 binding shows attenuated signaling through VEGFR-2. *Cellular and molecular life sciences : CMLS*, **63**: 2067–77.

Dai C, Celestino JC, Okada Y, Louis DN, Fuller GN, and Holland EC (2001). PDGF autocrine stimulation dedifferentiates cultured astrocytes and induces oligodendrogliomas and oligoastrocytomas from neural progenitors and astrocytes in vivo. *Genes & development*, **15**: 1913–25.

Dalla-Favera R, Gallo RC, Giallongo A, and Croce CM (1982). Chromosomal localization of the human homolog (c-sis) of the simian sarcoma virus onc gene. *Science.* **218**: 686–8.

Dallas NA, Gray MJ, Xia L, Fan F, van Buren G, Gaur P, Samuel S, Lim SJ, Arumugam T, Ramachandran V *et al.* (2008). Neuropilin-2-Mediated Tumor Growth and Angiogenesis in Pancreatic Adenocarcinoma. *Clinical Cancer Research*, **14**: 8052–8060.

Danilenko DM, Ring BD, Tarpley JE, Morris B, Van GY, Morawiecki A, Callahan W, Goldenberg M, Hershenson S, and Pierce GF (1995). Growth factors in porcine full and partial thickness burn repair. Differing targets and effects of keratinocyte growth factor, platelet-derived growth factor-BB, epidermal growth factor, and neu differentiation factor. *The American journal of pathology*, **147**: 1261–77.

DeMali KA, Godwin SL, Soltoff SP, and Kazlauskas A (1999). Multiple roles for Src in a PDGF-stimulated cell. *Experimental cell research*, **253**: 271–9.

Dhar K, Dhar G, Majumder M, Haque I, Mehta S, Van Veldhuizen PJ, Banerjee SK, and Banerjee S (2010). Tumor cell-derived PDGF-B potentiates mouse mesenchymal stem cells-pericytes transition and recruitment through an interaction with NRP-1. *Molecular cancer*, **9**: 209.

Dhillon AS, Hagan S, Rath O, and Kolch W (2007). MAP kinase signalling pathways in cancer. *Oncogene*, **26**: 3279–90.

Ding H, Wu X, Kim I, Tam PP, Koh GY, and Nagy A (2000). The mouse Pdgfc gene: dynamic expression in embryonic tissues during organogenesis. *Mechanisms of development*, **96**: 209–13.

Ding W, Knox TR, Tschumper RC, Wu W, Schwager SM, Boysen JC, Jelinek DF, and Kay NE (2010). Platelet-derived growth factor (PDGF)-PDGF receptor interaction activates bone marrow-derived mesenchymal stromal cells derived from chronic lymphocytic leukemia: implications for an angiogenic switch. *Blood*, **116**: 2984–93.

Dixelius J, Makinen T, Wirzenius M, Karkkainen MJ, Wernstedt C, Alitalo K and Claesson-Welsh L (2003). Ligand-induced vascular endothelial growth factor receptor-3 (VEGFR-3) heterodimerization with VEGFR-2 in primary lymphatic endothelial cells regulates tyrosine phosphorylation sites. *The Journal of biological chemistry*, **278**: 40973–9.

Dong J, Grunstein J, Tejada M, Peale F, Frantz G, Liang WC, Bai W, Yu L, Kowalski J, Liang X *et al.* (2004). VEGF-null cells require PDGFR alpha signaling-mediated stromal fibroblast recruitment for tumorigenesis. *The EMBO journal*, **23**: 2800–10.

Donnem T, Al-Saad S, Al-Shibli K, Andersen S, Busund LT, and Bremnes RM (2008). Prognostic Impact of Platelet-Derived Growth Factors in Non-small Cell Lung Cancer Tumor and Stromal Cells. *Journal of Thoracic Oncology*, **3**: 963–970.

Dormer A and Beck G (2005). Evolutionary analysis of human vascular endothelial growth factor, angiopoietin, and tyrosine endothelial kinase involved in angiogenesis and immunity. *In silico biology*, **5**: 323–39.

Doucette T, Rao G, Yang Y, Gumin J, Shinojima N, Bekele BN, Qiao W, Zhang W, and Lang FF (2011). Mesenchymal stem cells display tumor-specific tropism in an RCAS/Ntv-a glioma model. *Neoplasia (New York, N.Y.)*, **13**: 716–25.

Dougher-Vermazen M, Hulmes JD, Böhlen P, and Terman BI (1994). Biological activity and phosphorylation sites of the bacterially expressed cytosolic domain of the KDR VEGF-receptor. *Biochemical and biophysical research communications*, **205**: 728–38.

Drewinko B, Romsdahl MM, Yang LY, Ahearn MJ, and Trujillo JM (1976). Establishment of a human carcinoembryonic antigen-producing colon adenocarcinoma cell line. *Cancer research*, **36**: 467–75.

Ekman S, Thuresson ER, Heldin CH, and Rönnstrand L (1999). Increased mitogenicity of an alphabeta heterodimeric PDGF receptor complex correlates with lack of RasGAP binding. *Oncogene*, **18**: 2481–8.

Ellis LM (2006). The role of neuropilins in cancer. *Molecular cancer therapeutics*, **5**:1099–107.

Ellis LM and Hicklin DJ (2009). Resistance to Targeted Therapies: Refining Anticancer Therapy in the Era of Molecular Oncology. *Clinical cancer research : an official journal of the American Association for Cancer Research*, **15**: 7471–7478.

Ellis LM and Hicklin DJ (2008). VEGF-targeted therapy: mechanisms of anti-tumour activity. *Nature reviews. Cancer*, **8**: 579–91.

Embil JM, Papp K, Sibbald G, Tousignant J, Smiell JM, Wong B, and Lau CY (2000). Recombinant human platelet-derived growth factor-BB (becaplermin) for healing chronic lower extremity diabetic ulcers: an open-label clinical evaluation of efficacy. *Wound repair and regeneration : official publication of the Wound Healing Society [and] the European Tissue Repair Society*, **8**: 162–8.

Eming SA and Krieg T (2006). Molecular Mechanisms of VEGF-A Action during Tissue Repair. *Journal of Investigative Dermatology Symposium Proceedings*, **11**: 79–86.

Endersby R and Baker SJ (2008). PTEN signaling in brain: neuropathology and tumorigenesis. *Oncogene*, **27**: 5416–30.

Endersby R, Zhu X, Hay N, Ellison DW, and Baker SJ (2011). Nonredundant functions for Akt isoforms in astrocyte growth and gliomagenesis in an orthotopic transplantation model. *Cancer research*, **71**: 4106–16.

Erben P, Horisberger K, Muessle B, Müller MC, Treschl A, Ernst T, Kähler G, Ströbel P, Wenz F, Kienle P *et al.* (2008). mRNA expression of platelet-derived growth factor receptor-beta and C-KIT: correlation with pathologic response to cetuximab-based chemoradiotherapy in patients with rectal cancer. *International journal of radiation oncology*. **72**: 1544–50.

Erber R, Thurnher A, Katsen AD, Groth G, Kerger H, Hammes HP, Menger MD, Ullrich A, and Vajkoczy P (2004). Combined inhibition of VEGF and PDGF signaling enforces tumor vessel regression by interfering with pericyte-mediated endothelial cell survival mechanisms. *FASEB journal : official publication of the Federation of American Societies for Experimental Biology*, **18**: 338–40.

Eriksson A, Nånberg E, Rönnstrand L, Engström U, Hellman U, Rupp E, Carpenter G, Heldin CH and Claesson-Welsh L (1995). Demonstration of functionally different interactions between phospholipase C-gamma and the two types of platelet-derived growth factor receptors. *The Journal of biological chemistry*, **270**: 7773–81.

Eriksson A, Siegbahn A, Westermark B, Heldin CH, and Claesson-Welsh L (1992). PDGF alpha- and beta-receptors activate unique and common signal transduction pathways. *The EMBO journal*, **11**: 543–50.

Evans IM, Yamaji M, Britton G, Pellet-Many C, Lockie C, Zachary IC, and Frankel P (2011). Neuropilin-1 signaling through p130Cas tyrosine phosphorylation is essential for growth factor-dependent migration of glioma and endothelial cells. *Molecular and cellular biology*, **31**: 1174–85.

Falasca M, Logan SK, Lehto VP, Baccante G, Lemmon MA, and Schlessinger J (1998). Activation of phospholipase C gamma by PI 3-kinase-induced PH domain-mediated membrane targeting. *The EMBO journal*, **17**: 414–22.

Fan F, Samuel S, Gaur P, Lu J, Dallas NA, Xia L, Bose D, Ramachandran V, and Ellis LM (2011). Chronic exposure of colorectal cancer cells to bevacizumab promotes compensatory pathways that mediate tumour cell migration. *British journal of cancer*, **104**:1270–7.

Fantl WJ, Escobedo JA and Williams LT (1989). Mutations of the platelet-derived growth factor receptor that cause a loss of ligand-induced conformational change, subtle changes in kinase activity, and impaired ability to stimulate DNA synthesis. *Molecular and cellular biology*, **9**: 4473–8.

Ferns GA, Raines EW, Sprugel KH, Motani AS, Reidy M A and Ross R (1991). Inhibition of neointimal smooth muscle accumulation after angioplasty by an antibody to PDGF. *Science (New York, N.Y.)*, **253**: 1129–32.

Fogh J (1978). Cultivation, characterization, and identification of human tumor cells with emphasis on kidney, testis, and bladder tumors. *National Cancer Institute monograph*, 5–9.

Fogh J, Fogh JM, and Orfeo T (1977). One hundred and twenty-seven cultured human tumor cell lines producing tumors in nude mice. *Journal of the National Cancer Institute*, **59**: 221–6.

Fomchenko EI, Dougherty JD, Helmy KY, Katz AM, Pietras A, Brennan C, Huse JT, Milosevic A, and Holland EC (2011). Recruited cells can become transformed and overtake PDGF-induced murine gliomas in vivo during tumor progression. *PloS one*, **6**: 5763-7.

Fong GH, Rossant J, Gertsenstein M, and Breitman ML (1995). Role of the Flt-1 receptor tyrosine kinase in regulating the assembly of vascular endothelium. *Nature*, **376**: 66–70.

Frankel P, Pellet-Many C, Lehtolainen P, D'Abaco GM, Tickner ML, Cheng L, and Zachary IC (2008). Chondroitin sulphate-modified neuropilin 1 is expressed in human tumour cells and modulates 3D invasion in the U87MG human glioblastoma cell line through a p130Cas-mediated pathway. *EMBO reports*, **9**: 983–9.

Fredriksson L, Li H, and Eriksson U (2004). The PDGF family: four gene products form five dimeric isoforms. *Cytokine & growth factor reviews*, **15**: 197–204.

Fruttiger M, Karlsson L, Hall AC, Abramsson A, Calver AR, Boström H, Willetts K, Bertold CH, Heath JK, Betsholtz C *et al.* (1999). Defective oligodendrocyte development and severe hypomyelination in PDGF-A knockout mice. *Development.* **126**: 457–67.

Fuh G, Garcia KC, and de Vos AM (2000). The interaction of neuropilin-1 with vascular endothelial growth factor and its receptor flt-1. *The Journal of biological chemistry*, **275**: 26690–5.

Fujisawa H, Takagi S, and Hirata T (1995). Growth-associated expression of a membrane protein, neuropilin, in Xenopus optic nerve fibers. *Developmental neuroscience*, **17**: 343–9.

Fujita H, Zhang B, Sato K, Tanaka J, and Sakanaka M (2001). Expressions of neuropilin-1, neuropilin-2 and semaphorin 3A mRNA in the rat brain after middle cerebral artery occlusion. *Brain research*, **914**: 1–14.

Fukahi K. (2004). Aberrant Expression of Neuropilin-1 and -2 in Human Pancreatic Cancer Cells. *Clinical Cancer Research*, **10**: 581–590.

Fukasawa M, Matsushita AKM (2007). Neuropilin-1 interacts with integrin β1 and modulates pancreatic cancer cell growth, survival and invasion. *Cancer Biology & Therapy*, **6**: 1184–1191.

Furuhashi M (2004). Platelet-Derived Growth Factor Production by B16 Melanoma Cells Leads to Increased Pericyte Abundance in Tumors and an Associated Increase in Tumor Growth Rate. *Cancer Research*, **64**: 2725–2733.

Gagnon ML, Bielenberg DR, Gechtman Z, Miao HQ, Takashima S, Soker S, and Klagsbrun M (2000). Identification of a natural soluble neuropilin-1 that binds vascular endothelial growth factor: In vivo expression and antitumor activity. *Proceedings of the National Academy of Sciences of the United States of America*, **97**: 2573–8.

Gant JC, Thibault O, Blalock EM, Yang J, Bachstetter A, Kotick J, Schauwecker PE, Hauser KF, Smith GM, Mervis R *et al.* (2009). Decreased number of interneurons and increased seizures in neuropilin 2 deficient mice: implications for autism and epilepsy. *Epilepsia*, **50**: 629–45.

García-Olivas R, Hoebeke J, Castel S, Reina M, Fager G, Lustig F, and Vilaró S (2003). Differential binding of platelet-derived growth factor isoforms to glycosaminoglycans. *Histochemistry and cell biology*, **120**: 371–82.

Gavrilescu LC and Van Etten RA (2007). Production of replication-defective retrovirus by transient transfection of 293T cells. *Journal of visualized experiments : JoVE*, **550**.

Gazdar AF, Carney DN, Russell EK, Sims HL, Baylin SB, Bunn PA, Guccion JG, and Minna JD (1980). Establishment of continuous, clonable cultures of small-cell carcinoma of lung which have amine precursor uptake and decarboxylation cell properties. *Cancer research*, **40**: 3502–7.

Gelderloos JA, Rosenkranz S, Bazenet C, and Kazlauskas A (1998). A role for Src in signal relay by the platelet-derived growth factor alpha receptor. *The Journal of biological chemistry*, **273**: 5908–15.

Gerber HP, Condorelli F, Park J, and Ferrara N (1997). Differential transcriptional regulation of the two vascular endothelial growth factor receptor genes. Flt-1, but not Flk-1/KDR, is up-regulated by hypoxia. *The Journal of biological chemistry*, **272**: 23659–67.

Germeyer A, Hamilton AE, Laughlin LS, Lasley BL, Brenner RM, Giudice LC, and Nayak NR (2005). Cellular expression and hormonal regulation of neuropilin-1 and -2 messenger ribonucleic Acid in the human and rhesus macaque endometrium. *The Journal of clinical endocrinology and metabolism*, **90**: 1783–90.

Gherardi E, Love CA, Esnouf RM, and Jones EY (2004). The sema domain. *Current opinion in structural biology*, **14**: 669–78.

Giaccone G, Battey J, Gazdar AF, Oie H, Draoui M, and Moody TW (1992). Neuromedin B is present in lung cancer cell lines. *Cancer research*, **52**: 2732s–2736.

Giard DJ, Aaronson SA, Todaro GJ, Arnstein P, Kersey JH, Dosik H, and Parks WP (1973). In vitro cultivation of human tumors: establishment of cell lines derived from a series of solid tumors. *Journal of the National Cancer Institute*, **51**: 1417–23.

Giger RJ, Cloutier JF, Sahay A, Prinjha RK, Levengood DV, Moore SE, Pickering S, Simmons D, Rastan S, Walsh FS *et al.* (2000). Neuropilin-2 is required in vivo for selective axon guidance responses to secreted semaphorins. *Neuron*, **25**: 29–41.

Giger RJ, Urquhart ER, Gillespie SK, Levengood DV, Ginty DD, and Kolodkin AL (1998). Neuropilin-2 is a receptor for semaphorin IV: insight into the structural basis of receptor function and specificity. *Neuron*, **21**: 1079–92.

Gilbertson DG, Duff ME, West JW, Kelly JD, Sheppard PO, Hofstrand PD, Gao Z, Shoemaker K, Bukowski TR, Moore M *et al.* (2001). Platelet-derived growth factor C (PDGF-C), a novel growth factor that binds to PDGF alpha and beta receptor. *The Journal of biological chemistry*, **276**: 27406–14.

Giovannetti E, Mey V, Danesi R, Basolo F, Barachini S, Deri M, and Del Tacca M (2005). Interaction between gemcitabine and topotecan in human non-small-cell lung cancer cells: effects on cell survival, cell cycle and pharmacogenetic profile. *British journal of cancer*, **92**: 681–9.

Glinka Y, Stoilova S, Mohammed N, and Prud'homme GJ (2010). Neuropilin-1 exerts co-receptor function for TGF-beta-1 on the membrane of cancer cells and enhances responses to both latent and active TGF-beta. *Carcinogenesis*, **32**: 613–621.

Gnessi L, Basciani S, Mariani S, Arizzi M, Spera G, Wang C, Bondjers C, Karlsson L, and Betsholtz C (2000). Leydig cell loss and spermatogenic arrest in platelet-derived growth factor (PDGF)-A-deficient mice. *The Journal of cell biology*, **149**: 1019–26.

Goel HL, Pursell B, Standley C, Fogarty K, and Mercurio AM (2012). Neuropilin-2 regulates α6β1 integrin in the formation of focal adhesions and signaling. *Journal of cell science*, **125**: 497–506.

Gondi CS, Veeravalli KK, Gorantla B, Dinh DH, Fassett D, Klopfenstein JD, Gujrati M, and Rao JS (2010). Human umbilical cord blood stem cells show PDGF-D-dependent glioma cell tropism in vitro and in vivo. *Neuro-oncology*, **12**: 453–65.

Goodman C, Kolodkin AL, Luo Y, Püschel AW, and Raper J (1999). Unified Nomenclature for the Semaphorins/Collapsins. *Cell*, **97**: 551–552.

Goretzki L, Burg MA, Grako KA, and Stallcup WB (1999). High-affinity binding of basic fibroblast growth factor and platelet-derived growth factor-AA to the core protein of the NG2 proteoglycan. *The Journal of biological chemistry*, **274**: 16831–7.

Grandclement C, Pallandre JR, Valmary Degano S, Viel E, Bouard A, Balland J, Rémy-Martin JP, Simon B, Rouleau A, Boireau W *et al.* (2011). Neuropilin-2 expression promotes TGF-β1-mediated epithelial to mesenchymal transition in colorectal cancer cells. *PloS one*, **6**.

Gronwald RG, Grant FJ, Haldeman BA, Hart CE, O'Hara PJ, Hagen FS, Ross R, Bowen-Pope DF, and Murray MJ (1988). Cloning and expression of a cDNA coding for the human platelet-derived growth factor receptor: evidence for more than one receptor class. *Proceedings of the National Academy of Sciences of the United States of America*, **85**: 3435–9.

Gschwind A, Fischer OM, and Ullrich A (2004). The discovery of receptor tyrosine kinases: targets for cancer therapy. *Nature reviews. Cancer*, **4**: 361–70.

Gu C, Rodriguez ER, Reimert DV, Shu T, Fritzsch B, Richards LJ, Kolodkin AL and Ginty DD (2003). Neuropilin-1 Conveys Semaphorin and VEGF Signaling during Neural and Cardiovascular Development. *Developmental Cell*, **5**: 45–57.

Gu J and Gu X (2003). Natural history and functional divergence of protein tyrosine kinases. *Gene*, **317**: 49–57.

Gu L, Brian J, Whitaker GB, Perman B, Leahy DJ, Rosenbaum JS, Ginty DD and Kolodkin AL (2002). Characterization of neuropilin-1 structural features that confer binding to semaphorin 3A and vascular endothelial growth factor 165. *The Journal of biological chemistry*, **277**: 18069–76.

Gualandris A, Noghero A, Geuna M, Arese M, Valdembri D, Serini G, and Bussolino F (2009). Microenvironment drives the endothelial or neural fate of differentiating embryonic stem cells coexpressing neuropilin-1 and Flk-1. *FASEB journal : official publication of the Federation of American Societies for Experimental Biology*, **23**: 68–78.

Guo P, Hu B, Gu W, Xu L, Wang D, Huang HJS, Cavenee WK, and Cheng SY (2003). Platelet-derived growth factor-B enhances glioma angiogenesis by stimulating vascular endothelial growth factor expression in tumor endothelia and by promoting pericyte recruitment. *The American journal of pathology*, **162**: 1083–93.

Gömöri E, Fülöp Z, Mészáros I, Dóczi T, and Matolcsy A (2002). Microsatellite analysis of primary and recurrent glial tumors suggests different modalities of clonal evolution of tumor cells. *Journal of neuropathology and experimental neurology*, **61**: 396–402.

Hamada H, Kobune M, Nakamura K, Kawano Y, Kato K, Honmou O, Houkin K, Matsunaga T and Niitsu Y (2005). Mesenchymal stem cells (MSC) as therapeutic cytoreagents for gene therapy. *Cancer science*, **96**: 149–56.

Hambardzumyan D, Cheng YK, Haeno H, Holland EC, and Michor F (2011). The probable cell of origin of NF1- and PDGF-driven glioblastomas. *PloS one*, **6**.

Hamdan R, Zhou Z, and Kleinerman ES (2011). SDF-1 Induces PDGF-B Expression and the Differentiation of Bone Marrow Cells into Pericytes. *Molecular Cancer Research*, **9**: 1462–1470.

Hamerlik P, Lathia JD, Rasmussen R, Wu Q, Bartkova J, Lee M, Moudry P, Bartek J, Fischer W, Lukas J, Rich JN (2012). Autocrine VEGF-VEGFR2-Neuropilin-1 signaling promotes glioma stem-like cell viability and tumor growth. *J Exp Med.*, **209**: 507–20.

Han SY, Kato H, Kato S, Suzuki T, Shibata H, Ishii S, Shiiba K, Matsuno S, Kanamaru R, and Ishioka C (2000). Functional evaluation of PTEN missense mutations using in vitro phosphoinositide phosphatase assay. *Cancer research*, **60**: 3147–51.

Hanahan D and Weinberg RA (2011). Hallmarks of cancer: the next generation. *Cell*, **144**: 646–74.

Handa A, Tokunaga T, Tsuchida T, Lee YH, Kijima H, Yamazaki H, Ueyama Y, Fukuda H, and Nakamura M (2000). Neuropilin-2 expression affects the increased vascularization and is a prognostic factor in osteosarcoma. *International journal of oncology*, **17**: 291–5.

Hansel DE, Wilentz RE, Yeo CJ, Schulick RD, Montgomery E and Maitra A (2004). Expression of neuropilin-1 in high-grade dysplasia, invasive cancer, and metastases of the human gastrointestinal tract. *The American journal of surgical pathology*, **28**: 347–56.

Harlan JM, Thompson PJ, Ross RR, and Bowen-Pope DF (1986). Alpha-thrombin induces release of platelet-derived growth factor-like molecule(s) by cultured human endothelial cells. *The Journal of cell biology*, **103**: 1129–33.

Harper J, Gerstenfeld LC, and Klagsbrun M (2001). Neuropilin-1 expression in osteogenic cells: down-regulation during differentiation of osteoblasts into osteocytes. *Journal of cellular biochemistry*, **81**: 82–92.

Hassan SE, Bekarev M, Kim MY, Lin J, Piperdi S, Gorlick R, and Geller DS (2012). Cell surface receptor expression patterns in osteosarcoma. *Cancer*, **118**: 740–9.

Hasumi Y, Kłosowska-Wardega A, Furuhashi M, Ostman A, Heldin CH, and Hellberg C (2007). Identification of a subset of pericytes that respond to combination therapy targeting PDGF and VEGF signaling. *International journal of cancer. Journal international du cancer*, **121**, 2606–14.

Hata N, Shinojima N, Gumin J, Yong R, Marini F, Andreeff M and Lang FF (2010). Platelet-derived growth factor BB mediates the tropism of human mesenchymal stem cells for malignant gliomas. *Neurosurgery*, **66**: 144–56.

Hausser HJ and Brenner RE (2005). Phenotypic instability of Saos-2 cells in long-term culture. *Biochemical and biophysical research communications*, **333**: 216–22.

Hawkins PT, Eguinoa A, Qiu RG, Stokoe D, Cooke FT, Walters R, Wennström S, Claesson-Welsh L, Evans T, and Symons M (1995). PDGF stimulates an increase in GTP-Rac via activation of phosphoinositide 3-kinase. *Current biology*, **5**: 393–403.

He Z and Tessier-Lavigne M (1997). Neuropilin is a receptor for the axonal chemorepellent Semaphorin III. *Cell*, **90**: 739–51.

Heidaran MA, Mahadevan D, and Larochelle WJ (1995). Beta PDGFR-IgG chimera demonstrates that human beta PDGFR Ig-like domains 1 to 3 are sufficient for high affinity PDGF BB binding. *FASEB journal : official publication of the Federation of American Societies for Experimental Biology*, **9**: 140–5.

Heidaran MA, Pierce JH, Yu JC, Lombardi D, Artrip JE, Fleming TP, Thomason A, and Aaronson SA (1991). Role of alpha beta receptor heterodimer formation in beta platelet-derived growth factor (PDGF) receptor activation by PDGF-AB. *J. Biol. Chem.*, **266**: 20232–20237.

Heldin CH, Westermark B, and Wasteson A (1979). Platelet-derived growth factor: purification and partial characterization. *Proceedings of the National Academy of Sciences of the United States of America*, **76**: 3722–6.

Heldin CH and Westermark B (1999). Mechanism of Action and In Vivo Role of Platelet-Derived Growth Factor. *Physiol Rev*, **79**: 1283–1316.

Hellström M, Kalén M, Lindahl P, Abramsson A, and Betsholtz C (1999). Role of PDGF-B and PDGFR-beta in recruitment of vascular smooth muscle cells and pericytes during embryonic blood vessel formation in the mouse. *Development,* **126**: 3047–55.

Herzog Y, Kalcheim C, Kahane N, Reshef R, and Neufeld G (2001). Differential expression of neuropilin-1 and neuropilin-2 in arteries and veins. *Mechanisms of development*, **109**: 115–9.

Hillman RT, Feng BY, Ni J, Woo WM, Milenkovic L, Hayden-Gephart MG, Teruel MN, Oro AE, Chen JK, and Scott MP(2011). Neuropilins are positive regulators of Hedgehog signal transduction. *Genes & development*, **25**: 2333–46.

Hirota S, Ohashi A, Nishida T, Isozaki K, Kinoshita K, Shinomura Y, and Kitamura Y (2003). Gain-of-function mutations of platelet-derived growth factor receptor alpha gene in gastrointestinal stromal tumors. *Gastroenterology*, **125**: 660–7.

Hochman E, Castiel A, Jacob-Hirsch J, Amariglio N, and Izraeli S (2006). Molecular pathways regulating pro-migratory effects of Hedgehog signaling. *The Journal of biological chemistry*, **281**: 33860–70.

Hoelzinger DB, Demuth T, and Berens ME (2007). Autocrine factors that sustain glioma invasion and paracrine biology in the brain microenvironment. *Journal of the National Cancer Institute*, **99**: 1583–93.

Holden JA, Willmore-Payne C, Coppola D, Garrett CR, and Layfield LJ (2007). High-resolution melting amplicon analysis as a method to detect c-kit and platelet-derived growth factor receptor alpha activating mutations in gastrointestinal stromal tumors. *American journal of clinical pathology*, **128**: 230–8.

Holmes DIR and Zachary I (2005). The vascular endothelial growth factor (VEGF) family: angiogenic factors in health and disease. *Genome biology*, **6**: 209.

Hong TM, Chen YL, Wu YY, Yuan A, Chao YC, Chung YC, Wu MH, Yang SC, Pan SH, Shih JY, *et al.* (2007a). Targeting neuropilin 1 as an antitumor strategy in lung cancer. *Clinical cancer research : an official journal of the American Association for Cancer Research*, **13**: 4759–68.

Hong X, Jiang F, Kalkanis SN, Zhang ZG, Zhang X, Zheng X, Mikkelsen T, Jiang H and Chopp M (2007b). Decrease of endogenous vascular endothelial growth factor may not affect glioma cell proliferation and invasion. *Journal of experimental therapeutics & oncology*, **6**: 219–29.

Hooshmand-Rad R, Yokote K, Heldin CH, and Claesson-Welsh L (1998). PDGF alpha-receptor mediated cellular responses are not dependent on Src family kinases in endothelial cells. *Journal of cell science*, **111:** 607–14.

Hsu S, Huang F, and Friedman E (1995). Platelet-derived growth factor-B increases colon cancer cell growth in vivo by a paracrine effect. *J Cell Physiol.* **165**: 239–45.

Hu B, Guo P, Bar-Joseph I, Imanishi Y, Jarzynka MJ, Bogler O, Mikkelsen T, Hirose T, Nishikawa R, and Cheng SY (2007). Neuropilin-1 promotes human glioma progression through potentiating the activity of the HGF/SF autocrine pathway. *Oncogene*, **26**: 5577–86.

Hughes DC (2001). Alternative splicing of the human VEGFGR-3/FLT4 gene as a consequence of an integrated human endogenous retrovirus. *Journal of molecular evolution*, **53**: 77–9.

Humbert M, Monti G, Fartoukh M, Magnan A, Brenot F, Rain B, Capron F, Galanaud P, Duroux P, Simonneau G *et al.* (1998). Platelet-derived growth factor expression in primary pulmonary hypertension: comparison of HIV seropositive and HIV seronegative patients. *The European respiratory journal : official journal of the European Society for Clinical Respiratory Physiology*, **11**: 554–9.

Hurst NJ, Najy AJ, Ustach CV, Movilla L, and Kim HR (2012). Platelet-derived growth factor-C (PDGF-C) activation by serine proteases: implications for breast cancer progression. *The Biochemical journal*, **441**: 909–18.

Hurwitz H, Fehrenbacher L, Novotny W, Cartwright T, Hainsworth J, Heim W, Berlin, J, Baron A, Griffing S, Holmgren E *et al.* (2004). Bevacizumab plus irinotecan, fluorouracil, and leucovorin for metastatic colorectal cancer. *The New England journal of medicine*, **350**: 2335–42.

Huse M and Kuriyan J (2002). The conformational plasticity of protein kinases. *Cell*, **109**: 275–82.

Hägerstrand D, Hesselager G, Achterberg S, Wickenberg BU, Kowanetz M, Kastemar M, Heldin CH, Isaksson A, Nistér M, and Ostman A (2006). Characterization of an imatinib-sensitive subset of high-grade human glioma cultures. *Oncogene*, **25**: 4913–22.

Inoue, Takanari and Meyer T (2008). Synthetic activation of endogenous PI3K and Rac identifies an AND-gate switch for cell polarization and migration. *PloS one*, **3.**

Irusta PM, Luo, Yue, Bakht O, Lai CC, Smith SO, and DiMaio D. (2002). Definition of an inhibitory juxtamembrane WW-like domain in the platelet-derived growth factor beta receptor. *The Journal of biological chemistry*, **277**: 38627–34.

Ishii N, Maier D, Merlo A, Tada M, Sawamura Y, Diserens AC, and Van Meir EG. (1999). Frequent co-alterations of TP53, p16/CDKN2A, p14ARF, PTEN tumor suppressor genes in human glioma cell lines. *Brain pathology (Zurich, Switzerland)*, **9**: 469–79.

Jackson EL, Garcia-Verdugo JM, Gil-Perotin S, Roy M, Quinones-Hinojosa A, VandenBerg S, and Alvarez-Buylla A. (2006). PDGFR alpha-positive B cells are neural stem cells in the adult SVZ that form glioma-like growths in response to increased PDGF signaling. *Neuron*, **51**: 187–99.

Jane EP, Premkumar DR, Addo-Yobo SO, and Pollack IF. (2009). Abrogation of mitogen-activated protein kinase and Akt signaling by vandetanib synergistically potentiates histone deacetylase inhibitor-induced apoptosis in human glioma cells. *The Journal of pharmacology and experimental therapeutics*, **331**: 327–37.

Jaskolski F, Mulle C, and Manzoni OJ. (2005). An automated method to quantify and visualize colocalized fluorescent signals. *Journal of neuroscience methods*, **146**: 42–9.

Jastrebovav N, Vanwildemeersch M, Rapraeger AC, Giménez-Gallego G, Lindahl U, and Spillmann D. (2006). Heparan sulfate-related oligosaccharides in ternary complex formation with fibroblast growth factors 1 and 2 and their receptors. *The Journal of biological chemistry*, **281**: 26884–92.

Jawad Z. and Paoli M. (2002). Novel sequences propel familiar folds. *Structure (London, England : 1993)*, **10**: 447–54.

Jawien A, Bowen-Pope DF, Lindner V, Schwartz SM, and Clowes AW. (1992). Platelet-derived growth factor promotes smooth muscle migration and intimal thickening in a rat model of balloon angioplasty. *The Journal of clinical investigation*, **89**: 507–11.

Jia H, Cheng L, Tickner M, Bagherzadeh A, Selwood D, and Zachary I. (2010). Neuropilin-1 antagonism in human carcinoma cells inhibits migration and enhances chemosensitivity. *British journal of cancer*, **102**: 541–52.

Jia, Haiyan, Bagherzadeh, Azadeh, Hartzoulakis B, Jarvis A, Löhr M, Shaikh S, Aqil R, Cheng, Lili, Tickner, Michelle, Esposito D, et al. (2006). Characterization of a bicyclic peptide neuropilin-1 (NP-1) antagonist (EG3287) reveals importance of vascular endothelial growth factor exon 8 for NP-1 binding and role of NP-1 in KDR signaling. *The Journal of biological chemistry*, **281**: 13493–502.

Jiang Y, Boije M, Westermark, Bengt, and Uhrbom L. (2011). PDGF-B Can sustain self-renewal and tumorigenicity of experimental glioma-derived cancer-initiating cells by preventing oligodendrocyte differentiation. *Neoplasia (New York, N.Y.)*, **13**: 492–503.

Johnsson A, Heldin CH, Wasteson A, Westermark B, Deuel TF, Huang JS, Seeburg PH, Gray A, Ullrich A, and Scrace G. (1984). The c-sis gene encodes a precursor of the B chain of platelet-derived growth factor. *The EMBO journal*, **3**: 921–8.

Jones EAV, Yuan L, Breant C, Watts RJ, and Eichmann A. (2008). Separating genetic and hemodynamic defects in neuropilin 1 knockout embryos. *Development (Cambridge, England)*, **135**: 2479–88.

Jones NP, Peak J, Brader S, Eccles SA, and Katan M. (2005). PLCgamma1 is essential for early events in integrin signalling required for cell motility. *Journal of cell science*, **118**: 2695–706.

Joukov V, Kaipainen A, Jeltsch M, Pajusola K, Olofsson B, Kumar V, Eriksson U, and Alitalo K. (1997). Vascular endothelial growth factors VEGF-B and VEGF-C. *Journal of cellular physiology*, **173**: 211–5.

Joukov V, Sorsa T, Kumar V, Jeltsch M, Claesson-Welsh L, Cao Y, Saksela O, Kalkkinen N, and Alitalo K. (1997). Proteolytic processing regulates receptor specificity and activity of VEGF-C. *The EMBO journal*, **16**: 3898–911.

Kaipainen A, Korhonen J, Mustonen T, van Hinsbergh VW, Fang GH, Dumont D, Breitman M, and Alitalo K. (1995). Expression of the fms-like tyrosine kinase 4 gene becomes restricted to lymphatic endothelium during development. *Proceedings of the National Academy of Sciences of the United States of America*, **92**: 3566–70.

Kamiya T, Kawakami T, Abe Y, Nishi M, Onoda N, Miyazaki N, Oida Y, Yamazaki, Hitoshi, Ueyama, Yoshito, and Nakamura M. (2006). The preserved expression of neuropilin (NRP) 1 contributes to a better prognosis in colon cancer. *Oncology Reports*, **15**: 369.

Karaman MW, Herrgard S, Treiber DK, Gallant P, Atteridge CE, Campbell BT, Chan KW, Ciceri P, Davis MI, Edeen PT, et al. (2008). A quantitative analysis of kinase inhibitor selectivity. *Nature biotechnology*, **26**: 127–32.

Karayan-Tapon L, Wager M, Guilhot J, Levillain P, Marquant C, Clarhaut J, Potiron V, and Roche J. (2008). Semaphorin, neuropilin and VEGF expression in glial tumours: SEMA3G, a prognostic marker? *British Journal of Cancer*, **99**: 1153–1160.

Karlsson L, Bondjers C, and Betsholtz C. (1999). Roles for PDGF-A and sonic hedgehog in development of mesenchymal components of the hair follicle. *Development (Cambridge, England)*, **126**: 2611–21.

Karlsson L, Lindahl P, Heath JK, and Betsholtz C. (2000). Abnormal gastrointestinal development in PDGF-A and PDGFR-(alpha) deficient mice implicates a novel mesenchymal structure with putative instructive properties in villus morphogenesis. *Development (Cambridge, England)*, **127**: 3457–66.

Kashishian A, Kazlauskas A, and Cooper JA. (1992). Phosphorylation sites in the PDGF receptor with different specificities for binding GAP and PI3 kinase in vivo. *The EMBO journal*, **11**: 1373–82.

Kashiwagi H, Shiraga M, Kato H, Kamae T, Yamamoto N, Tadokoro S, Kurata Y, Tomiyama Y, and Kanakura Y (2005). Negative regulation of platelet function by a secreted cell repulsive protein, semaphorin 3A. *Blood*, **106**: 913–21.

Kawai T, Hiroi S, and Torikata C (1997). Expression in lung carcinomas of platelet-derived growth factor and its receptors. *Laboratory investigation; a journal of technical methods and pathology*, **77**: 431–6.

Kawakami A, Kitsukawa T, Takagi S, and Fujisawa H (1996). Developmentally regulated expression of a cell surface protein, neuropilin, in the mouse nervous system. *Journal of neurobiology*, **29**: 1–17.

Kawakami T, Tokunaga T, Hatanaka H, Kijima H, Yamazaki H, Abe Y, Osamura Y, Inoue H, Ueyama Y, and Nakamura M (2002). Neuropilin 1 and neuropilin 2 co-expression is significantly correlated with increased vascularity and poor prognosis in nonsmall cell lung carcinoma. *Cancer*, **95**: 2196–201.

Kawasaki T, Kitsukawa T, Bekku Y, Matsuda Y, Sanbo M, Yagi T, and Fujisawa H (1999). A requirement for neuropilin-1 in embryonic vessel formation. *Development (Cambridge, England)*, **126**: 4895–902.

Kazlauskas A and Cooper JA (1989). Autophosphorylation of the PDGF receptor in the kinase insert region regulates interactions with cell proteins. *Cell*, **58**: 1121–33.

Kazlauskas A, Kashishian A, Cooper JA, and Valius M (1992). GTPase-activating protein and phosphatidylinositol 3-kinase bind to distinct regions of the platelet-derived growth factor receptor beta subunit. *Molecular and cellular biology*, **12**: 2534–44.

Kelly J, Haldeman B, Grant F, Murray M, Seifert R, Bowen-Pope D, Cooper J, and Kazlauskas A (1991). Platelet-derived growth factor (PDGF) stimulates PDGF receptor subunit dimerization and intersubunit trans-phosphorylation. *J. Biol. Chem.*, **266**: 8987–8992.

Kendall RL and Thomas KA (1993). Inhibition of vascular endothelial cell growth factor activity by an endogenously encoded soluble receptor. *Proceedings of the National Academy of Sciences of the United States of America*, **90**, 10705–9.

Keramati AR, Singh R, Lin A, Faramarzi S, Ye Z, Mane S, Tellides G, Lifton RP, and Mani A (2011). Wild-type LRP6 inhibits, whereas atherosclerosis-linked LRP6R611C increases PDGF-dependent vascular smooth muscle cell proliferation. *Proceedings of the National Academy of Sciences of the United States of America*, **108**: 1914–8.

Kim HK, Kim JW, Zilberstein A, Margolis B, Kim JG, Schlessinger J, and Rhee SG (1991). PDGF stimulation of inositol phospholipid hydrolysis requires PLC-gamma 1 phosphorylation on tyrosine residues 783 and 1254. *Cell*, **65**, 435–41.

Kim MJ, Kim E, Ryu SH, and Suh PG (2000). The mechanism of phospholipase C-gamma1 regulation. *Experimental & molecular medicine*, **32**: 101–9.

Kitadai, Y, Sasaki T, Kuwai T, Nakamura T, Bucana CD, Hamilton SR, and Fidler IJ (2006). Expression of activated platelet-derived growth factor receptor in stromal cells of human colon carcinomas is associated with metastatic potential. *International journal of cancer. Journal international du cancer*, **119**: 2567–74.

Kitsukawa T, Shimizu M, Sanbo M, Hirata T, Taniguchi M, Bekku Y, Yagi T, and Fujisawa H (1997). Neuropilin-semaphorin III/D-mediated chemorepulsive signals play a crucial role in peripheral nerve projection in mice. *Neuron*, **19**: 995–1005.

Kitsukawa T, Shimono A, Kawakami A, Kondoh H, and Fujisawa H (1995). Overexpression of a membrane protein, neuropilin, in chimeric mice causes anomalies in the cardiovascular system, nervous system and limbs. *Development*, **121**: 4309–18.

Kleber S, Sancho-Martinez I, Wiestler B, Beisel A, Gieffers C, Hill O, Thiemann M, Mueller Wolf, Sykora, J, Kuhn A *et al.* (2008). Yes and PI3K bind CD95 to signal invasion of glioblastoma. *Cancer cell*, **13**: 235–48.

Knobbe CB, Merlo A, and Reifenberger G (2002). Pten signaling in gliomas. *Neuro-oncology*, **4**: 196–211.

Kohler N. and Lipton A (1974). Platelets as a source of fibroblast growth-promoting activity. *Experimental cell research*, **87**: 297–301.

Kolodkin AL, Levengood DV, Rowe EG, Tai YT, Giger RJ, and Ginty DD (1997). Neuropilin is a semaphorin III receptor. *Cell*, **90**: 753–62.

Kolodkin AL, Matthes DJ, and Goodman CS (1993). The semaphorin genes encode a family of transmembrane and secreted growth cone guidance molecules. *Cell*, **75**: 1389–99.

Kondo K, Hiratsuka S, Subbalakshmi E, Matsushime H, and Shibuya M (1998). Genomic organization of the flt-1 gene encoding for vascular endothelial growth factor (VEGF) receptor-1 suggests an intimate evolutionary relationship between the 7-Ig and the 5-Ig tyrosine kinase receptors. *Gene*, **208**: 297–305.

Koos B, Paulsson J, Jarvius M, Sanchez BC, Wrede B, Mertsch S, Jeibmann A, Kruse A, Peters O, Wolff JE *et al.* (2009). Platelet-derived growth factor receptor expression and activation in choroid plexus tumors. *The American journal of pathology*, **175**: 1631–7.

Koppel AM, Feiner L, Kobayashi H, and Raper JA (1997). A 70 amino acid region within the semaphorin domain activates specific cellular response of semaphorin family members. *Neuron*, **19**: 531–7.

Krampert M, Heldin CH, and Heuchel RL (2008). A gain-of-function mutation in the PDGFR-beta alters the kinetics of injury response in liver and skin. *Laboratory investigation; a journal of technical methods and pathology*, **88**: 1204–14.

Kreuger J, Spillmann D, Li J, and Lindahl U (2006). Interactions between heparan sulfate and proteins: the concept of specificity. *The Journal of cell biology*, **174**: 323–7.

Kreuter M, Woelke K, Bieker R, Schliemann C, Steins M, Buechner T, Berdel WE, and Mesters RM (2006). Correlation of neuropilin-1 overexpression to survival in acute myeloid leukemia. *Leukemia : official journal of the Leukemia Society of America, Leukemia Research Fund, U.K*, **20**: 1950–4.

Kubo T, Piperdi S, Rosenblum J, Antonescu CR, Chen W, Kim HS, Huvos AG, Sowers R, Meyers PA, Healey JH *et al* (2008). Platelet-derived growth factor receptor as a prognostic marker and a therapeutic target for imatinib mesylate therapy in osteosarcoma. *Cancer*, **112**: 2119–29.

LaRochelle WJ, Jeffers M, McDonald WF, Chillakuru RA, Giese NA, Lokker NA, Sullivan C, Boldog FL, Yang M, Vernet C *et al.* (2001). PDGF-D, a new protease-activated growth factor. *Nature cell biology*, **3**: 517–21.

LaRochelle WJ, May-Siroff M, Robbins KC, and Aaronson SA (1991). A novel mechanism regulating growth factor association with the cell surface: identification of a PDGF retention domain. *Genes & development*, **5**: 1191–9.

Lamalice L, Houle F, and Huot J (2006). Phosphorylation of Tyr1214 within VEGFR-2 triggers the recruitment of Nck and activation of Fyn leading to SAPK2/p38 activation and endothelial cell migration in response to VEGF. *The Journal of biological chemistry*, **281**: 34009–20.

Lantuéjoul S, Constantin B, Drabkin H, Brambilla C, Roche J, and Brambilla E (2003). Expression of VEGF, semaphorin SEMA3F, and their common receptors neuropilins NP1 and NP2 in preinvasive bronchial lesions, lung tumours, and cell lines. *The Journal of pathology*, **200**: 336–47.

Latil A, Bièche I, Pesche S, Valéri A, Fournier G, Cussenot O, and Lidereau R (2000). VEGF overexpression in clinically localized prostate tumors and neuropilin-1 overexpression in metastatic forms. *International Journal of Cancer*, **89**: 167–171.

Lee P, Goishi K, Davidson AJ, Mannix R, Zon L, and Klagsbrun M (2002). Neuropilin-1 is required for vascular development and is a mediator of VEGF-dependent angiogenesis in zebrafish. *Proceedings of the National Academy of Sciences of the United States of America*, **99**: 10470–5.

Lee S, Jilani SM, Nikolova GV, Carpizo D, and Iruela-Arispe ML (2005). Processing of VEGF-A by matrix metalloproteinases regulates bioavailability and vascular patterning in tumors. *The Journal of cell biology*, **169**: 681–91.

Leibovitz A, Stinson JC, McCombs WB, McCoy CE, Mazur KC, and Mabry ND (1976). Classification of human colorectal adenocarcinoma cell lines. *Cancer research*, **36**: 4562–9.

le Noble F, Moyon D, Pardanaud L, Yuan L, Djonov V, Matthijsen R, Bréant C, Fleury V, and Eichmann A (2004). Flow regulates arterial-venous differentiation in the chick embryo yolk sac. *Development,* **131**: 361–75.

Leslie NR and Downes CP (2002). PTEN: The down side of PI 3-kinase signalling. *Cellular signalling*, **14**: 285–95.

Leveen P, Pekny M, Gebre-Medhin S, Swolin B, Larsson E, and Betsholtz C (1994). Mice deficient for PDGF B show renal, cardiovascular, and hematological abnormalities. *Genes & Development*, **8**: 1875–1887.

Lewis CD, Olson NE, Raines EW, Reidy MA, and Jackson CL (2001). Modulation of smooth muscle proliferation in rat carotid artery by platelet-derived mediators and fibroblast growth factor-2. *Platelets*, **12**: 352–8.

Li H and Wang C (2011). Post-transcriptional regulation of PDGFα-receptor in O-2A progenitor cells. *International journal of clinical and experimental medicine*, **4**: 241–51.

Li W, Nishimura R, Kashishian A, Batzer AG, Kim WJ, Cooper JA, and Schlessinger J (1994). A new function for a phosphotyrosine phosphatase: linking GRB2-Sos to a receptor tyrosine kinase. *Molecular and cellular biology*, **14**: 509–17.

Li X, Pontén A, Aase K, Karlsson L, Abramsson A, Uutela, M, Bäckström G, Hellström M, Boström H, Li H *et al.* (2000). PDGF-C is a new protease-activated ligand for the PDGF alpha-receptor. *Nature cell biology*, **2**: 302–9.

Lieber M, Smith B, Szakal A, Nelson-Rees W, and Todaro G (1976). A continuous tumor-cell line from a human lung carcinoma with properties of type II alveolar epithelial cells. *International journal of cancer. Journal international du cancer*, **17**: 62–70.

Lierman E, Michaux L, Beullens E, Pierre P, Marynen P, Cools J, and Vandenberghe P (2009). FIP1L1-PDGFRalpha D842V, a novel panresistant mutant, emerging after treatment of FIP1L1-PDGFRalpha T674I eosinophilic leukemia with single agent sorafenib. *Leukemia : official journal of the Leukemia Society of America, Leukemia Research Fund, U.K*, **23**: 845–51.

Lin AH, Eliceiri BP, and Levin EG (2009). FAK mediates the inhibition of glioma cell migration by truncated 24 kDa FGF-2. *Biochemical and biophysical research communications*, **382**: 503–7.

Lind M, Deleuran B, Thestrup-Pedersen K, Søballe K, Eriksen EF, and Bünger C (1995). Chemotaxis of human osteoblasts. Effects of osteotropic growth factors. *APMIS : acta pathologica, microbiologica, et immunologica Scandinavica*, **103**: 140–6.

Lind T (1998). The Putative Tumor Suppressors EXT1 and EXT2 Are Glycosyltransferases Required for the Biosynthesis of Heparan Sulfate. *Journal of Biological Chemistry*, **273**: 26265–26268.

Lindahl P, Hellström M, Kalén M, Karlsson L, Pekny M, Pekna M, Soriano P, and Betsholtz C (1998). Paracrine PDGF-B/PDGF-Rbeta signaling controls mesangial cell development in kidney glomeruli. *Development,* **125**: 3313–22.

Lindahl P, Johansson BR, Levéen P, and Betsholtz C (1997). Pericyte loss and microaneurysm formation in PDGF-B-deficient mice. *Science (New York, N.Y.)*, **277**: 242–5.

Lindahl P, Karlsson L, Hellström M, Gebre-Medhin S, Willetts K, Heath JK, and Betsholtz C (1997). Alveogenesis failure in PDGF-A-deficient mice is coupled to lack of distal spreading of alveolar smooth muscle cell progenitors during lung development. *Development,* **124**: 3943–53.

Lo Buono N, Parrotta R, Morone S, Bovino P, Nacci G, Ortolan E, Horenstein AL, Inzhutova A, Ferrero E, and Funaro A (2011). The CD157-integrin partnership controls transendothelial migration and adhesion of human monocytes. *The Journal of biological chemistry*, **286**: 18681–91.

Loizos N, Xu Y, Huber J, Liu, Meilin LD, Finnerty B, Rolser R, Malikzay A, Persaud A, Corcoran E *et al.* (2005). Targeting the platelet-derived growth factor receptor alpha with a neutralizing human monoclonal antibody inhibits the growth of tumor xenografts: implications as a potential therapeutic target. *Molecular cancer therapeutics*, **4**: 369–79.

Lokker NA (1997). Functional Importance of Platelet-derived Growth Factor (PDGF) Receptor Extracellular Immunoglobulin-like Domains. IDENTIFICATION OF PDGF BINDING SITE AND NEUTRALIZING MONOCLONAL ANTIBODIES. *Journal of Biological Chemistry*, **272**: 33037–33044.

Lokker NA, Sullivan CM, Hollenbach SJ, Israel MA, and Giese NA (2002). Platelet-derived Growth Factor (PDGF) Autocrine Signaling Regulates Survival and Mitogenic Pathways in Glioblastoma Cells : Evidence That the Novel PDGF-C and PDGF-D Ligands May Play a Role in the Development of Brain Tumors. *Cancer research,* **62**: 3729-3735.

Lorquet S, Berndt S, Blacher S, Gengoux E, Peulen O, Maquoi E, Noël A, Foidart JM, Munaut C, and Péqueux C (2010). Soluble forms of VEGF receptor-1 and -2 promote vascular maturation via mural cell recruitment. *FASEB journal : official publication of the Federation of American Societies for Experimental Biology*, **24**: 3782–95.

Louis DN, Ohgaki H, Wiestler OD, Cavenee WK, Burger PC, Jouvet A, Scheithauer BW, and Kleihues P (2007). The 2007 WHO classification of tumours of the central nervous system. *Acta neuropathologica*, **114:** 97–109.

Love CA, Harlos K, Mavaddat N, Davis SJ, Stuart DI, Jones EY, and Esnouf RM (2003). The ligand-binding face of the semaphorins revealed by the high-resolution crystal structure of SEMA4D. *Nature structural biology*, **10**: 843–8.

Lu L, Zhang L, Xiao Z, Lu S, Yang R, and Han ZC (2008). Neuropilin-1 in acute myeloid leukemia: Expression and role in proliferation and migration of leukemia cells. *Leukemia & Lymphoma*, **49**: 331–338.

Luo Y, Raible D, and Raper JA (1993). Collapsin: a protein in brain that induces the collapse and paralysis of neuronal growth cones. *Cell*, **75**: 217–27.

Lustig F, Hoebeke J, Ostergren-Lundèn G, Velge-Roussel F, Bondjers G, Olsson U, Rüetschi U, and Fager G (1996). Alternative Splicing Determines the Binding of Platelet-Derived Growth Factor. *Biochemistry*, **2960**: 12077–12085.

Lyden D, Hattori K, Dias S, Costa C, Blaikie P, Butros L, Chadburn A, Heissig B, Marks W, Witte L *et al.* (2001). Impaired recruitment of bone-marrow-derived endothelial and hematopoietic precursor cells blocks tumor angiogenesis and growth. *Nature medicine*, **7**: 1194–201.

M Stürzl WK (1992). Expression of platelet-derived growth factor and its receptor in AIDS-related Kaposi sarcoma in vivo suggests paracrine and autocrine mechanisms of tumor maintenance. *Proceedings of the National Academy of Sciences of the United States of America*, **89**: 7046.

Maehama T and Dixon JE (1998). The tumor suppressor, PTEN/MMAC1, dephosphorylates the lipid second messenger, phosphatidylinositol 3,4,5-trisphosphate. *The Journal of biological chemistry*, **273**: 13375–8.

Maglione D, Guerriero V, Viglietto G, Ferraro MG, Aprelikova O, Alitalo K, Del Vecchio S, Lei KJ, Chou JY, and Persico MG (1993). Two alternative mRNAs coding for the angiogenic factor, placenta growth factor (PlGF), are transcribed from a single gene of chromosome 14. *Oncogene*, **8**: 925–31.

Magnusson PU, Looman C, Ahgren A, Wu Y, Claesson-Welsh L, and Heuchel RL (2007). Platelet-derived growth factor receptor-beta constitutive activity promotes angiogenesis in vivo and in vitro. *Arteriosclerosis, thrombosis, and vascular biology*, **27**: 2142–9.

Makinen T, Olofsson B, Karpanen T, Hellman U, Soker S, Klagsbrun M, Eriksson U, and Alitalo K (1999). Differential binding of vascular endothelial growth factor B splice and proteolytic isoforms to neuropilin-1. *The Journal of biological chemistry*, **274**: 21217–22.

Mamluk R, Gechtman Z, Kutcher ME, Gasiunas N, Gallagher J, and Klagsbrun M (2002). Neuropilin-1 binds vascular endothelial growth factor 165, placenta growth factor-2, and heparin via its b1b2 domain. *The Journal of biological chemistry*, **277**: 24818–25.

Manning BD and Cantley LC (2007). AKT/PKB signaling: navigating downstream. *Cell*, **129**: 1261–74.

Marte BM and Downward J (1997). PKB/Akt: connecting phosphoinositide 3-kinase to cell survival and beyond. *Trends in biochemical sciences*, **22**: 355–8.

Martinho O, Longatto-Filho A, Lambros MB, Martins A, Pinheiro C, Silva A, Pardal F, Amorim J, Mackay A, Milanezi F *et al.* (2009). Expression, mutation and copy number analysis of platelet-derived growth factor receptor A (PDGFRA) and its ligand PDGFA in gliomas. *British journal of cancer*, **101**: 973–82.

Matsui T, Heidaran M, Miki T, Popescu N, La Rochelle W, Kraus M, Pierce J, and Aaronson S (1989). Isolation of a novel receptor cDNA establishes the existence of two PDGF receptor genes. *Science,* **243**: 800–4.

Matsumoto T, Bohman S, Dixelius J, Berge T, Dimberg A, Magnusson P, Wang L, Wikner C, Qi JH, Wernstedt C *et al.* (2005). VEGF receptor-2 Y951 signaling and a role for the adapter molecule TSAd in tumor angiogenesis. *The EMBO journal*, **24**: 2342–53.

Matsushita A, Götze T, and Korc M (2007). Hepatocyte growth factor-mediated cell invasion in pancreatic cancer cells is dependent on neuropilin-1. *Cancer research*, **67**: 10309–16.

Matthies AM, Low QE, Lingen MW, and DiPietro LA (2002). Neuropilin-1 participates in wound angiogenesis. *The American journal of pathology*, **160**: 289–96.

Mayr-Wohlfart U, Waltenberger J, Hausser H, Kessler S, Günther KP, Dehio C, Puhl W, and Brenner RE (2002). Vascular endothelial growth factor stimulates chemotactic migration of primary human osteoblasts. *Bone*, **30**: 472–477.

McAllister RM, Gardner MB, Greene AE, Bradt C, Nichols WW, and Landing BH (1971). Cultivation in vitro of cells derived from a human osteosarcoma. *Cancer*, **27**: 397–402.

McCarty MF, Somcio RJ, Stoeltzing O, Wey J, Fan F, Liu W, Bucana C, and Ellis LM (2007). Overexpression of PDGF-BB decreases colorectal and pancreatic cancer growth by increasing tumor pericyte content. *Journal of Clinical Investigation*, **117**: 2114–2122.

McColl BK, Paavonen K, Karnezis T, Harris NC, Davydova N, Rothacker J, Nice EC, Harder KW, Roufail S, Hibbs ML *et al.* (2007). Proprotein convertases promote processing of VEGF-D, a critical step for binding the angiogenic receptor VEGFR-2. *FASEB journal : official publication of the Federation of American Societies for Experimental Biology*, **21**: 1088–98.

McDonald NQ and Hendrickson WA (1993). A structural superfamily of growth factors containing a cystine knot motif. *Cell*, **73**: 421–4.

McDowell KA, Riggins GJ, and Gallia GL (2011). Targeting the AKT pathway in glioblastoma. *Current pharmaceutical design*, **17**: 2411–20.

McGary EC, Weber K, Mills L, Doucet M, Lewis V, Lev DC, Fidler IJ, and Bar-Eli M (2002). Inhibition of platelet-derived growth factor-mediated proliferation of osteosarcoma cells by the novel tyrosine kinase inhibitor STI571. *Clinical cancer research : an official journal of the American Association for Cancer Research*, **8**: 3584–91.

Mehrotra M, Krane SM, Walters K, and Pilbeam C (2004). Differential regulation of platelet-derived growth factor stimulated migration and proliferation in osteoblastic cells. *Journal of cellular biochemistry*, **93**: 741–52.

Mendez MG, Kojima SI, and Goldman RD (2010). Vimentin induces changes in cell shape, motility, and adhesion during the epithelial to mesenchymal transition. *The FASEB journal : official publication of the Federation of American Societies for Experimental Biology*, **24**: 1838–51.

Miao HQ, Lee P, Lin H, Soker S, and Klagsbrun M (2000). Neuropilin-1 expression by tumor cells promotes tumor angiogenesis and progression. *The FASEB journal : official publication of the Federation of American Societies for Experimental Biology*, **14**: 2532–9.

Migdal M, Huppertz B, Tessler S, Comforti A, Shibuya M, Reich R, Baumann H, and Neufeld G (1998). Neuropilin-1 is a placenta growth factor-2 receptor. *The Journal of biological chemistry*, **273**: 22272–8.

Miller K, Wang M, Gralow J, Dickler M, Cobleigh M, Perez EA, Shenkier T, Cella D, and Davidson NE (2007). Paclitaxel plus bevacizumab versus paclitaxel alone for metastatic breast cancer. *The New England journal of medicine*, **357**: 2666–76.

Mishra PJ, Mishra PJ, Humeniuk R, Medina DJ, Alexe G, Mesirov JP, Ganesan S, Glod JW, and Banerjee D (2008). Carcinoma-associated fibroblast-like differentiation of human mesenchymal stem cells. *Cancer research*, **68**: 4331–9.

Miyazawa K, Bäckström G, Leppänen O, Persson C, Wernstedt C, Hellman U, Heldin CH, and Ostman A (1998). Role of immunoglobulin-like domains 2-4 of the platelet-derived growth factor alpha-receptor in ligand-receptor complex assembly. *The Journal of biological chemistry*, **273**: 25495–502.

Mizui M and Kikutani H (2008). Neuropilin-1: the glue between regulatory T cells and dendritic cells? *Immunity*, **28**: 302–3.

Mondy JS, Lindner V, Miyashiro JK, Berk BC, Dean RH, and Geary RL (1997). Platelet-derived growth factor ligand and receptor expression in response to altered blood flow in vivo. *Circulation research*, **81**: 320–7.

Mori S, Rönnstrand L, Yokote K, Engström A, Courtneidge SA, Claesson-Welsh L, and Heldin CH (1993). Identification of two juxtamembrane autophosphorylation sites in the PDGF beta-receptor; involvement in the interaction with Src family tyrosine kinases. *The EMBO journal*, **12**: 2257–64.

Morrison-Graham K, Schatteman GC, Bork T, Bowen-Pope DF, and Weston JA (1992). A PDGF receptor mutation in the mouse (Patch) perturbs the development of a non-neuronal subset of neural crest-derived cells. *Development (Cambridge, England)*, **115**: 133–42.

Mueller W, Lass U, Herms J, Kuchelmeister K, Bergmann M, and von Deimling A (2001). Clonal analysis in glioblastoma with epithelial differentiation. *Brain pathology,* **11**: 39–43.

Mukherjee S, Tessema M, and Wandinger-Ness A (2006). Vesicular trafficking of tyrosine kinase receptors and associated proteins in the regulation of signaling and vascular function. *Circulation research*, **98**: 743–56.

Muller YA (1997). Vascular endothelial growth factor: Crystal structure and functional mapping of the kinase domain receptor binding site. *Proceedings of the National Academy of Sciences*, **94**: 7192–7197.

Mustoe TA, Pierce GF, Morishima C, and Deuel TF (1991). Growth factor-induced acceleration of tissue repair through direct and inductive activities in a rabbit dermal ulcer model. *The Journal of clinical investigation*, **87**: 694–703.

Nakamura TM, Takahashi T, Kalb RG, and Strittmatter SM (1998). Neuropilin-1 extracellular domains mediate semaphorin D/III-induced growth cone collapse. *Neuron*, **21**: 1093–100.

Naldini L, Vigna E, Ferracini R, Longati P, Gandino L, Prat M, and Comoglio PM (1991). The tyrosine kinase encoded by the MET proto-oncogene is activated by autophosphorylation. *Molecular and cellular biology*, **11**: 1793–803.

Nash AD, Baca M, Wright C, and Scotney PD (2006). The biology of vascular endothelial growth factor-B (VEGF-B). *Pulmonary pharmacology & therapeutics*, **19**: 61–9.

Negoro N, Kanayama Y, Haraguchi M, Umetani N, Nishimura M, Konishi Y, Iwai J, Okamura M, Inoue T and Takeda T (1995). Blood pressure regulates platelet-derived growth factor A-chain gene expression in vascular smooth muscle cells in vivo. An autocrine mechanism promoting hypertensive vascular hypertrophy. *The Journal of clinical investigation*, **95**: 1140–50.

Nelson PR, Yamamura S, and Kent KC (1997). Platelet-derived growth factor and extracellular matrix proteins provide a synergistic stimulus for human vascular smooth muscle cell migration. *Journal of Vascular Surgery*, **26:** 104–112.

Neufeld G (2002). The Neuropilins Multifunctional Semaphorin and VEGF Receptors that Modulate Axon Guidance and Angiogenesis. *Trends in Cardiovascular Medicine*, **12**: 13–19.

Neufeld and Kessler O (2008). The semaphorins: versatile regulators of tumour progression and tumour angiogenesis. *Nature reviews. Cancer*, **8**: 632–45.

Neufeld G, Shraga-Heled N, Lange T, Guttmann-Raviv N, Herzog Y, and Kessler O (2005). Semaphorins in cancer. *Frontiers in bioscience : a journal and virtual library*, **10**: 751–760.

Nevins M, Camelo M, Nevins ML, Schenk RK, and Lynch SE (2003). Periodontal regeneration in humans using recombinant human platelet-derived growth factor-BB (rhPDGF-BB) and allogenic bone. *Journal of periodontology*, **74**: 1282–92.

Newton CS, Loukinova E, Mikhailenko I, Ranganathan S, Gao Y, Haudenschild C, and Strickland DK (2005). Platelet-derived growth factor receptor-beta (PDGFR-beta) activation promotes its association with the low density lipoprotein receptor-related protein (LRP). Evidence for co-receptor function. *The Journal of biological chemistry*, **280**: 27872–8.

Nilsson I, Bahram F, Li X, Gualandi L, Koch S, Jarvius M, Söderberg O, Anisimov A, Kholová I, Pytowski B *et al.* (2010). VEGF receptor 2/-3 heterodimers detected in situ by proximity ligation on angiogenic sprouts. *The EMBO journal*, **29**: 1377–88.

Nilsson I, Shibuya M, and Wennström S (2004). Differential activation of vascular genes by hypoxia in primary endothelial cells. *Experimental cell research*, **299**: 476–85.

Nobes CD and Hall A (1995). Rho, rac and cdc42 GTPases: regulators of actin structures, cell adhesion and motility. *Biochemical Society transactions*, **23**: 456–9.

Novo E, Cannito S, Zamara E, Valfrè di Bonzo L, Caligiuri A, Cravanzola C, Compagnone A, Colombatto S, Marra F, Pinzani M *et al.* (2007). Proangiogenic cytokines as hypoxia-dependent factors stimulating migration of human hepatic stellate cells. *The American journal of pathology*, **170**: 1942–53.

Ochiumi T, Kitadai Y, Tanaka S, Akagi M, Yoshihara M, and Chayama K (2006). Neuropilin-1 is involved in regulation of apoptosis and migration of human colon cancer. *International journal of oncology*, **29**: 105–16.

Ohnishi T, Arita N, Hiraga S, Taki T, Izumoto S, Fukushima Y, and Hayakawa T (1997). Fibronectin-mediated cell migration promotes glioma cell invasion through chemokinetic activity. *Clinical & experimental metastasis*, **15**: 538–46.

Okada M, Nadanaka S, Shoji N, Tamura JI, and Kitagawa H (2010). Biosynthesis of heparan sulfate in EXT1-deficient cells. *The Biochemical journal*, **428**: 463–71.

Olofsson B (1996). Vascular endothelial growth factor B, a novel growth factor for endothelial cells. *Proceedings of the National Academy of Sciences*, **93**: 2576–2581.

Olofsson B, Pajusola K, von Euler G, Chilov D, Alitalo K, and Eriksson U (1996). Genomic organization of the mouse and human genes for vascular endothelial growth factor B (VEGF-B) and characterization of a second splice isoform. *The Journal of biological chemistry*, **271**: 19310–7.

Omura T, Heldin CH, and Ostman A (1997). Immunoglobulin-like domain 4-mediated receptor-receptor interactions contribute to platelet-derived growth factor-induced receptor dimerization. *The Journal of biological chemistry*, **272**: 12676–82.

Orr-Urtreger A and Lonai P (1992). Platelet-derived growth factor-A and its receptor are expressed in separate, but adjacent cell layers of the mouse embryo. *Development,* **115**: 1045–58.

Osada H, Tokunaga T, Nishi M, Hatanaka H, Abe Y, Tsugu A, Kijima H, Yamazaki H, Ueyama Y, and Nakamura M (2004). Overexpression of the neuropilin 1 (NRP1) gene correlated with poor prognosis in human glioma. *Anticancer research*, **24**: 547–52.

Ostman A, Andersson M, Betsholtz C, Westermark B, and Heldin CH (1991). Identification of a cell retention signal in the B-chain of platelet-derived growth factor and in the long splice version of the A-chain. *Cell regulation*, **2**: 503–12.

Ostman A, Thyberg J, Westermark B and Heldin CH (1992). PDGF-AA and PDGF-BB biosynthesis: proprotein processing in the Golgi complex and lysosomal degradation of PDGF-BB retained intracellularly. *The Journal of cell biology*, **118**: 509–19.

Ostman A (2004). PDGF receptors-mediators of autocrine tumor growth and regulators of tumor vasculature and stroma. *Cytokine & growth factor reviews*, **15**: 275–86.

Ottino P, Finley J, Rojo E, Ottlecz A, Lambrou GN, Bazan HE, and Bazan NG (2004). Hypoxia activates matrix metalloproteinase expression and the VEGF system in monkey choroid-retinal endothelial cells: Involvement of cytosolic phospholipase A2 activity. *Molecular vision*, **10**: 341–50.

Ozaki Y, Nishimura M, Sekiya K, Suehiro F, Kanawa M, Nikawa H, Hamada T, and Kato Y. (2007). Comprehensive analysis of chemotactic factors for bone marrow mesenchymal stem cells. *Stem cells and development*, **16**: 119–29.

Pallaoro A, Braun GB, and Moskovits M (2011). Quantitative ratiometric discrimination between noncancerous and cancerous prostate cells based on neuropilin-1 overexpression. *Proceedings of the National Academy of Sciences of the United States of America*, **108**: 16559–64.

Palmieri SL, Payne J, Stiles CD, Biggers JD, and Mercola M (1992). Expression of mouse PDGF-A and PDGF alpha-receptor genes during pre- and post-implantation development: evidence for a developmental shift from an autocrine to a paracrine mode of action. *Mechanisms of development*, **39**: 181–91.

Pan H, Wanami LS, Dissanayake TR, and Bachelder RE (2009). Autocrine semaphorin3A stimulates alpha2 beta1 integrin expression/function in breast tumor cells. *Breast cancer research and treatment*, **118**: 197–205.

Pan Q, Chathery Y, Wu Y, Rathore N, Tong RK, Peale F, Bagri A, Tessier-Lavigne M, Koch AW, and Watts RJ (2007). Neuropilin-1 binds to VEGF121 and regulates endothelial cell migration and sprouting. *The Journal of biological chemistry*, **282**: 24049–56.

Parikh AA, Fan F, Liu WB, Ahmad SA, Stoeltzing O, Reinmuth N, Bielenberg D, Bucana CD, Klagsbrun M, and Ellis LM (2004). Neuropilin-1 in human colon cancer: expression, regulation, and role in induction of angiogenesis. *The American journal of pathology*, **164**: 2139–51.

Park JE, Chen HH, Winer J, Houck KA, and Ferrara N (1994). Placenta growth factor. Potentiation of vascular endothelial growth factor bioactivity, in vitro and in vivo, and high affinity binding to Flt-1 but not to Flk-1/KDR. *The Journal of biological chemistry*, **269**: 25646–54.

Park JE, Keller GA, and Ferrara N (1993). The vascular endothelial growth factor (VEGF) isoforms: differential deposition into the subepithelial extracellular matrix and bioactivity of extracellular matrix-bound VEGF. *Molecular biology of the cell*, **4**: 1317–26.

Parker MW, Xu P, Li X, and Vander Kooi CW (2012). Structural basis for the selective vascular endothelial growth factor-A (VEGF-A) binding to neuropilin-1. *The Journal of biological chemistry*, **287**: 11082–11089.

Pavelock K, Braas K, Ouafik L, Osol G, and May V (2001). Differential expression and regulation of the vascular endothelial growth factor receptors neuropilin-1 and neuropilin-2 in rat uterus. *Endocrinology*, **142**: 613–22.

Pellet-Many C, Frankel P, Evans IM, Herzog B, Jünemann-Ramírez M, and Zachary IC (2011). Neuropilin-1 mediates PDGF stimulation of vascular smooth muscle cell migration and signalling via p130Cas. *The Biochemical journal*, **435**: 609–18.

Pellet-Many C, Frankel P, Jia H, and Zachary I (2008). Neuropilins: structure, function and role in disease. *The Biochemical journal*, **411**: 211–26.

Pennock S and Kazlauskas A (2012). VEGF-A competitively inhibits PDGF-dependent activation of PDGF receptor and subsequent signaling events and cellular responses. *Molecular and cellular biology*, **32**: 1955-66

Phillips JJ, Huillard E, Robinson AE, Ward A, Lum DH, Polley MY, Rosen SD, Rowitch DH, and Werb Z (2012). Heparan sulfate sulfatase SULF2 regulates PDGFRα signaling and growth in human and mouse malignant glioma. *The Journal of clinical investigation*, **122**: 911–22.

Piccirillo SG, Combi R, Cajola L, Patrizi A, Redaelli S, Bentivegna A, Baronchelli S, Maira, G, Pollo B, Mangiola A *et al.* (2009). Distinct pools of cancer stem-like cells coexist within human glioblastomas and display different tumorigenicity and independent genomic evolution. *Oncogene*, **28**: 1807–11.

Pierce GF, Mustoe TA, Senior RM, Reed J, Griffin GL, Thomason A, and Deuel TF (1988). In vivo incisional wound healing augmented by platelet-derived growth factor and recombinant c-sis gene homodimeric proteins. *The Journal of experimental medicine*, **167**: 974–87.

Pierce GF, Tarpley JE, Allman RM, Goode PS, Serdar CM, Morris B, Mustoe TA, and Vande Berg J (1994). Tissue repair processes in healing chronic pressure ulcers treated with recombinant platelet-derived growth factor BB. *The American journal of pathology*, **145**: 1399–410.

Pietras K, Pahler J, Bergers G, and Hanahan D (2008). Functions of paracrine PDGF signaling in the proangiogenic tumor stroma revealed by pharmacological targeting. *PLoS medicine*, **5**: e19.

Pillay V, Allaf L, Wilding AL, Donoghue JF, Court NW, Greenall SA, Scott AM, and Johns TG (2009). The plasticity of oncogene addiction: implications for targeted therapies directed to receptor tyrosine kinases. *Neoplasia,* **11**: 448–58, 2 p following 458.

Plouët J, Moro F, Bertagnolli S, Coldeboeuf N, Mazarguil H, Clamens S, and Bayard F (1997). Extracellular cleavage of the vascular endothelial growth factor 189-amino acid form by urokinase is required for its mitogenic effect. *The Journal of biological chemistry*, **272**: 13390–6.

Pollock RA and Richardson WD (1992). The alternative-splice isoforms of the PDGF A-chain differ in their ability to associate with the extracellular matrix and to bind heparin in vitro. *Growth factors,* **7**, 267–77.

Popkov M, Jendreyko N, Gonzalez-Sapienza G, Mage RG, Rader C, and Barbas CF (2004). Human/mouse cross-reactive anti-VEGF receptor 2 recombinant antibodies selected from an immune b9 allotype rabbit antibody library. *Journal of immunological methods*, **288**: 149–64.

Potapova O, Laird AD, Nannini MA, Barone A, Li G, Moss KG, Cherrington JM, and Mendel DB (2006). Contribution of individual targets to the antitumor efficacy of the multitargeted receptor tyrosine kinase inhibitor SU11248. *Molecular cancer therapeutics*, **5**: 1280–9.

Prahst C, Héroult M, Lanahan AA, Uziel N, Kessler O, Shraga-Heled N, Simons M, Neufeld G, and Augustin HG (2008). Neuropilin-1-VEGFR-2 complexing requires the PDZ-binding domain of neuropilin-1. *The Journal of biological chemistry*, **283**: 25110–4.

Raica M and Cimpean AM (2010). Platelet-Derived Growth Factor (PDGF)/PDGF Receptors (PDGFR) Axis as Target for Antitumor and Antiangiogenic Therapy. *Pharmaceuticals*, **3**: 572–599.

Raines EW and Ross R (1992). Compartmentalization of PDGF on extracellular binding sites dependent on exon-6-encoded sequences. *The Journal of cell biology*, **116**: 533–43.

Raines EW (2004). PDGF and cardiovascular disease. *Cytokine & growth factor reviews*, **15**: 237–54.

Ranza E, Facoetti A, Morbini P, Benericetti E, and Nano R (2007). Exogenous platelet-derived growth factor (PDGF) induces human astrocytoma cell line proliferation. *Anticancer research*, **27**: 2161–6.

Raskopf E, Vogt A, Standop J, Sauerbruch T (2010). Inhibition of neuropilin-1 by RNA-interference and its angiostatic potential in the treatment of hepatocellular carcinoma. *Z Gastroenterol*, **48**: 21–27.

Reinmuth N, Liersch R, Raedel M, Fehrmann F, Fehrmann N, Bayer M, Schwoeppe C, Kessler T, Berdel W, Thomas M *et al.* (2009). Combined anti-PDGFRalpha and PDGFRbeta targeting in non-small cell lung cancer. *International journal of cancer. Journal international du cancer*, **124**: 1535–44.

Reza JN, Gavazzi I, and Cohen J (1999). Neuropilin-1 is expressed on adult mammalian dorsal root ganglion neurons and mediates semaphorin3a/collapsin-1-induced growth cone collapse by small diameter sensory afferents. *Molecular and cellular neurosciences*, **14**: 317–26.

Rhim JS, Cho HY, and Huebner RJ (1975). Non-producer human cells induced by murine sarcoma virus. *International journal of cancer. Journal international du cancer*, **15**: 23–9.

Ridley AJ and Hall A (1992a). Distinct patterns of actin organization regulated by the small GTP-binding proteins Rac and Rho. *Cold Spring Harbor symposia on quantitative biology*, **57**: 661–71.

Ridley AJ, Paterson HF, Johnston CL, Diekmann D, and Hall A (1992b). The small GTP-binding protein rac regulates growth factor-induced membrane ruffling. *Cell*, **70**: 401–10.

Robinson CJ and Stringer SE (2001). The splice variants of vascular endothelial growth factor (VEGF) and their receptors. *Journal of cell science*, **114**: 853–65.

Robinson SD, Reynolds LE, Kostourou V, Reynolds AR, da Silva RG, Tavora B, Baker M, Marshall JF, and Hodivala-Dilke KM. (2009). Alphav beta3 integrin limits the contribution of neuropilin-1 to vascular endothelial growth factor-induced angiogenesis. *The Journal of biological chemistry*, **284**: 33966–81.

Rodan SB, Imai Y, Thiede MA, Wesolowski G, Thompson D, Bar-Shavit Z, Shull S, Mann K, and Rodan GA (1987). Characterization of a human osteosarcoma cell line (Saos-2) with osteoblastic properties. *Cancer research*, **47**: 4961–6.

Rolny C, Spillmann D, Lindahl U, and Claesson-Welsh L (2002). Heparin amplifies platelet-derived growth factor (PDGF)- BB-induced PDGF alpha -receptor but not PDGF beta -receptor tyrosine phosphorylation in heparan sulfate-deficient cells. Effects on signal transduction and biological responses. *The Journal of biological chemistry*, **277**: 19315–21.

Rorsman F, Bywater M, Knott TJ, Scott J, and Betsholtz C (1988). Structural characterization of the human platelet-derived growth factor A-chain cDNA and gene: alternative exon usage predicts two different precursor proteins. *Molecular and cellular biology*, **8**: 571–7.

Rosenkranz S and Kazlauskas A (2009). Evidence for Distinct Signaling Properties and Biological Responses Induced by the PDGF Receptor α and β Subtypes.*Growth factors,* **16:** 201-216.

Roskoski R (2007a). Sunitinib: a VEGF and PDGF receptor protein kinase and angiogenesis inhibitor. *Biochemical and biophysical research communications*, **356**: 323–8.

Roskoski R. (2007b). Vascular endothelial growth factor (VEGF) signaling in tumor progression. *Critical reviews in oncology/hematology*, **62**: 179–213.

Ross R, Glomset J, Kariya B, and Harker L. (1974). A platelet-dependent serum factor that stimulates the proliferation of arterial smooth muscle cells in vitro. *Proceedings of the National Academy of Sciences of the United States of America*, **71**: 1207–10.

Rossignol M, Beggs AH, Pierce EA, and Klagsbrun M (1999). Human neuropilin-1 and neuropilin-2 map to 10p12 and 2q34, respectively. *Genomics*, **57**: 459–60.

Rossignol M, Gagnon ML, and Klagsbrun M (2000). Genomic organization of human neuropilin-1 and neuropilin-2 genes: identification and distribution of splice variants and soluble isoforms. *Genomics*, **70**: 211–22.

Roth L, Nasarre C, Dirrig-Grosch S, Aunis D, Crémel G, Hubert P, and Bagnard D (2008). Transmembrane domain interactions control biological functions of neuropilin-1. *Molecular biology of the cell*, **19**: 646–54.

Rubin K, Tingström A, Hansson GK, Larsson E, Rönnstrand L, Klareskog L, Claesson-Welsh L, Heldin CH, Fellström B, and Terracio L (1988). Induction of B-type receptors for platelet-derived growth factor in vascular inflammation: possible implications for development of vascular proliferative lesions. *Lancet*, **1**: 1353–6.

Rupp E, Siegbahn A, Rönnstrand L, Wernstedt C, Claesson-Welsh L, and Heldin CH (1994). A unique autophosphorylation site in the platelet-derived growth factor alpha receptor from a heterodimeric receptor complex. *European journal of biochemistry / FEBS*, **225**: 29–41.

Rushing EC, Stine MJ, Hahn SJ, Shea S, Eller MS, Naif A, Khanna S, Westra WH, Jungbluth AA, Busam KJ *et al.* (2012). Neuropilin-2: a novel biomarker for malignant melanoma? *Human pathology*, **43**: 381–9.

Rutherford RB, Niekrash CE, Kennedy JE, and Charette MF (1992). Platelet-derived and insulin-like growth factors stimulate regeneration of periodontal attachment in monkeys. *Journal of periodontal research*, **27**: 285–90.

Rönnstrand L, Siegbahn A, Rorsman C, Johnell M, Hansen K, and Heldin CH (1999). Overactivation of phospholipase C-gamma1 renders platelet-derived growth factor beta-receptor-expressing cells independent of the phosphatidylinositol 3-kinase pathway for chemotaxis. *The Journal of biological chemistry*, **274**: 22089–94.

Sait SN, Dougher-Vermazen M, Shows TB, and Terman BI (1995). The kinase insert domain receptor gene (KDR) has been relocated to chromosome 4q11-->q12. *Cytogenetics and cell genetics*, **70**: 145–6.

Salikhova A, Wang L, Lanahan AA, Liu M, Simons M, Leenders, WP, Mukhopadhyay D, and Horowitz A (2008). Vascular endothelial growth factor and semaphorin induce neuropilin-1 endocytosis via separate pathways. *Circulation research*, **103**:71–9.

Samuel S, Gaur P, Fan F, Xia L, Gray MJ, Dallas NA, Bose D, Rodriguez-Aguayo C, Lopez-Berestein G, Plowman G *et al.* (2011). Neuropilin-2 Mediated β-Catenin Signaling and Survival in Human Gastro-Intestinal Cancer Cell Lines. *PLoS ONE*, **6**: 23208.

Sanchez-Carbayo ND (2003). Gene Discovery in Bladder Cancer Progression using cDNA Microarrays. *The American Journal of Pathology*, **163**: 505.

Sandler A, Gray R, Perry MC, Brahmer J, Schiller JH, Dowlati A, Lilenbaum R, and Johnson DH (2006). Paclitaxel-carboplatin alone or with bevacizumab for non-small-cell lung cancer. *The New England journal of medicine*, **355**: 2542–50.

Sarment DP, Cooke JW, Miller SE, Jin Q, McGuire MK, Kao RT, McClain PK, McAllister BS, Lynch SE, and Giannobile WV (2006). Effect of rhPDGF-BB on bone turnover during periodontal repair. *Journal of clinical periodontology*, **33**: 135–40.

Sasportas LS, Kasmieh R, Wakimoto H, Hingtgen S, van de Water JA, Mohapatra G, Figueiredo JL, Martuza RL, Weissleder R, and Shah K (2009). Assessment of therapeutic efficacy and fate of engineered human mesenchymal stem cells for cancer therapy. *Proceedings of the National Academy of Sciences of the United States of America*, **106**: 4822–7.

Schatteman GC, Morrison-Graham K, van Koppen A, Weston JA, and Bowen-Pope DF (1992). Regulation and role of PDGF receptor alpha-subunit expression during embryogenesis. *Development*, **115**: 123–31.

Schermuly RT, Dony E, Ghofrani HA, Pullamsetti S, Savai R, Roth M, Sydykov A, Lai YJ, Weissmann N, Seeger W *et al.* (2005). Reversal of experimental pulmonary hypertension by PDGF inhibition. *The Journal of clinical investigation*, **115**: 2811–21.

Schlessinger J and Bar-Sagi D (1994). Activation of Ras and Other Signaling Pathways by Receptor Tyrosine Kinases. *Cold Spring Harbor Symposia on Quantitative Biology*, **59**: 173–179.

Schuch G, Machluf M, Bartsch G, Nomi M, Richard H, Atala A and Soker S (2002). In vivo administration of vascular endothelial growth factor (VEGF) and its antagonist, soluble neuropilin-1, predicts a role of VEGF in the progression of acute myeloid leukemia in vivo. *Blood*, **100**: 4622–8.

Sebolt-Leopold JS and Herrera R (2004). Targeting the mitogen-activated protein kinase cascade to treat cancer. *Nature reviews. Cancer*, **4**: 937–47.

Seger R and Krebs EG (1995). The MAPK signaling cascade. *FASEB journal : official publication of the Federation of American Societies for Experimental Biology*, **9**: 726–35.

Selvaraj SK, Giri RK, Perelman N, Johnson C, Malik P and Kalra VK (2003). Mechanism of monocyte activation and expression of proinflammatory cytochemokines by placenta growth factor. *Blood*, **102**: 1515–24.

Semple TU, Quinn LA, Woods LK and Moore GE (1978). Tumor and lymphoid cell lines from a patient with carcinoma of the colon for a cytotoxicity model. *Cancer research*, **38**: 1345–55.

Senes A, Gerstein M and Engelman DM (2000). Statistical analysis of amino acid patterns in transmembrane helices: the GxxxG motif occurs frequently and in association with beta-branched residues at neighboring positions. *Journal of molecular biology*, **296**: 921–36.

Sennino B, Falcón BL, McCauley D, Le T, McCauley T, Kurz JC, Haskell A, Epstein DM and McDonald DM (2007). Sequential loss of tumor vessel pericytes and endothelial cells after inhibition of platelet-derived growth factor B by selective aptamer AX102. *Cancer research*, **67**: 7358–67.

Seppä H, Grotendorst G, Seppä S, Schiffmann E and Martin GR (1982). Platelet-derived growth factor in chemotactic for fibroblasts. *The Journal of cell biology*, **92**: 584–8.

Shalaby F, Rossant J, Yamaguchi TP, Gertsenstein M, Wu XF, Breitman ML and Schuh AC (1995). Failure of blood-island formation and vasculogenesis in Flk-1-deficient mice. *Nature*, **376**: 62–6.

Shibuya M, Yamaguchi S, Yamane A, Ikeda T, Tojo A, Matsushime H and Sato M (1990). Nucleotide sequence and expression of a novel human receptor-type tyrosine kinase gene (flt) closely related to the fms family. *Oncogene*, **5**: 519–24.

Shim AH, Liu H, Focia PJ, Chen X, Lin PC and He X (2010). Structures of a platelet-derived growth factor/propeptide complex and a platelet-derived growth factor/receptor complex. *Proceedings of the National Academy of Sciences of the United States of America*, **107**: 11307–12.

Shimokado K, Raines EW, Madtes DK, Barrett TB, Benditt EP and Ross R (1985). A significant part of macrophage-derived growth factor consists of at least two forms of PDGF. *Cell*, **43**: 277–86.

Shinkai A, Ito M, Anazawa H, Yamaguchi S, Shitara K and Shibuya M (1998). Mapping of the sites involved in ligand association and dissociation at the extracellular domain of the kinase insert domain-containing receptor for vascular endothelial growth factor. *The Journal of biological chemistry*, **273**: 31283–8.

Shintani Y, Takashima S, Asano Y, Kato H, Liao Y, Yamazaki S, Tsukamoto O, Seguchi O, Yamamoto H, Fukushima T *et al.* (2006). Glycosaminoglycan modification of neuropilin-1 modulates VEGFR2 signaling. *The EMBO journal*, **25**: 3045–55.

Shraga-Heled N, Kessler O, Prahst C, Kroll J, Augustin H and Neufeld G (2007). Neuropilin-1 and neuropilin-2 enhance VEGF121 stimulated signal transduction by the VEGFR-2 receptor. *FASEB journal : official publication of the Federation of American Societies for Experimental Biology*, **21**: 915–26.

Siegfried G, Basak A, Cromlish JA, Benjannet S, Marcinkiewicz J, Chrétien M, Seidah NG and Khatib AM (2003). The secretory proprotein convertases furin, PC5, and PC7 activate VEGF-C to induce tumorigenesis. *The Journal of clinical investigation*, **111**: 1723–1732.

Siegfried G, Basak A, Prichett-Pejic W, Scamuffa N, Ma L, Benjannet S, Veinot JP, Calvo F, Seidah N and Khatib AM (2005). Regulation of the stepwise proteolytic cleavage and secretion of PDGF-B by the proprotein convertases. *Oncogene*, **24**: 6925–35.

Siegfried G, Khatib AM, Benjannet S, Chretien M and Seidah NG (2003). The Proteolytic Processing of Pro-Platelet-derived Growth Factor-A at RRKR86 by Members of the Proprotein Convertase Family Is Functionally Correlated to Platelet-derived Growth Factor-A-induced Functions and Tumorigenicity. *Cancer Res.*, **63**: 1458–1463.

Soker S, Miao H, Nomi M, Takashima S and Klagsbrun M(2002). VEGF165 mediates formation of complexes containing VEGFR-2 and neuropilin-1 that enhance VEGF165-receptor binding. *Journal of cellular biochemistry*, **85**: 357–68.

Soker S, Takashima S, Miao HQ, Neufeld G and Klagsbrun M (1998). Neuropilin-1 is expressed by endothelial and tumor cells as an isoform-specific receptor for vascular endothelial growth factor. *Cell*, **92**: 735–45.

Soriano P (1994). Abnormal kidney development and hematological disorders in PDGF beta-receptor mutant mice. *Genes & development*, **8**: 1888–96.

Soriano P (1997). The PDGF alpha receptor is required for neural crest cell development and for normal patterning of the somites. *Development,* **124**: 2691–700.

Springer TA (2002). Predicted and experimental structures of integrins and beta-propellers. *Current opinion in structural biology*, **12**: 802–13.

Stacker SA, Stenvers K, Caesar C, Vitali A, Domagala T, Nice E, Roufail S, Simpson RJ, Moritz R, Karpanen T *et al.* (1999). Biosynthesis of vascular endothelial growth factor-D involves proteolytic processing which generates non-covalent homodimers. *The Journal of biological chemistry*, **274**: 32127–36.

Steed DL (1995). Clinical evaluation of recombinant human platelet-derived growth factor for the treatment of lower extremity diabetic ulcers. Diabetic Ulcer Study Group. *Journal of vascular surgery : official publication, the Society for Vascular Surgery [and] International Society for Cardiovascular Surgery, North American Chapter*, **21**: 71–8; discussion 79–81.

Stein GH (1979). T98G: an anchorage-independent human tumor cell line that exhibits stationary phase G1 arrest in vitro. *Journal of cellular physiology*, **99**: 43–54.

Stephenson JM, Banerjee S, Saxena NK, Cherian R and Banerjee SK (2002). Neuropilin-1 is differentially expressed in myoepithelial cells and vascular smooth muscle cells in preneoplastic and neoplastic human breast: a possible marker for the progression of breast cancer. *International journal of cancer. Journal international du cancer*, **101**: 409–14.

Stover EH, Chen J, Folens C, Lee BH, Mentens N, Marynen P, Williams IR, Gilliland DG and Cools J (2006). Activation of FIP1L1-PDGFRalpha requires disruption of the juxtamembrane domain of PDGFRalpha and is FIP1L1-independent. *Proceedings of the National Academy of Sciences of the United States of America*, **103**: 8078–83.

Straume O and Akslen LA (2003). Increased Expression of VEGF-Receptors (FLT-1, KDR, NRP-1) and Thrombospondin-1 is Associated with Glomeruloid Microvascular Proliferation, an Aggressive Angiogenic Phenotype, in Malignant Melanoma. *Angiogenesis*, **6**: 295–301.

Sulzbacher I, Träxler M, Mosberger I, Lang S and Chott A (2000). Platelet-derived growth factor-AA and -alpha receptor expression suggests an autocrine and/or paracrine loop in osteosarcoma. *Modern pathology : an official journal of the United States and Canadian Academy of Pathology, Inc*, **13**: 632–7.

Suzuki K, Kumanogoh A and Kikutani H (2008). Semaphorins and their receptors in immune cell interactions. *Nature immunology*, **9**: 17–23.

Suzuki S, Heldin CH and Heuchel RL (2007). Platelet-derived growth factor receptor-beta, carrying the activating mutation D849N, accelerates the establishment of B16 melanoma. *BMC cancer*, **7**: 224.

Swan DC, McBride OW, Robbins KC, Keithley DA, Reddy EP and Aaronson SA (1982). Chromosomal mapping of the simian sarcoma virus onc gene analogue in human cells. *Proceedings of the National Academy of Sciences of the United States of America*, **79**: 4691–5.

Szerlip NJ, Pedraza A, Chakravarty D, Azim M, McGuire J, Fang Y, Ozawa T, Holland EC, Huse JT, Jhanwar S *et al.* (2012). Intratumoral heterogeneity of receptor tyrosine kinases EGFR and PDGFRA amplification in glioblastoma defines subpopulations with distinct growth factor response. *Proceedings of the National Academy of Sciences of the United States of America*, **109**: 3041–6.

Söderberg O, Gullberg M, Jarvius M, Ridderstråle K, Leuchowius KJ, Jarvius J, Wester K, Hydbring P, Bahram F, Larsson LG *et al.* (2006). Direct observation of individual endogenous protein complexes in situ by proximity ligation. *Nature methods*, **3**: 995–1000.

Söderberg O, Leuchowius KJ, Gullberg M, Jarvius M, Weibrecht I, Larsson LG and Landegren U (2008). Characterizing proteins and their interactions in cells and tissues using the in situ proximity ligation assay. *Methods*, **45**: 227–32.

Takagi S, Hirata T, Agata K, Mochii M, Eguchi G and Fujisawa H (1991). The A5 antigen, a candidate for the neuronal recognition molecule, has homologies to complement components and coagulation factors. *Neuron*, **7**: 295–307.

Takagi S, Kasuya Y, Shimizu M, Matsuura T, Tsuboi M, Kawakami A and Fujisawa H (1995). Expression of a cell adhesion molecule, neuropilin, in the developing chick nervous system. *Developmental biology*, **170**: 207–22.

Takahashi T, Nakamura F, Jin Z, Kalb RG and Strittmatter SM (1998). Semaphorins A and E act as antagonists of neuropilin-1 and agonists of neuropilin-2 receptors. *Nature neuroscience*, **1**: 487–93.

Takahashi T and Shibuya M (1997). The 230 kDa mature form of KDR/Flk-1 (VEGF receptor-2) activates the PLC-gamma pathway and partially induces mitotic signals in NIH3T3 fibroblasts. *Oncogene*, **14**: 2079–89.

Takahashi T, Yamaguchi S, Chida K and Shibuya M (2001). A single autophosphorylation site on KDR/Flk-1 is essential for VEGF-A-dependent activation of PLC-gamma and DNA synthesis in vascular endothelial cells. *The EMBO journal*, **20**: 2768–78.

Takashima S, Kitakaze M, Asakura M, Asanuma H, Sanada S, Tashiro F, Niwa H, Miyazaki Ji J, Hirota S, Kitamura Y *et al.* (2002). Targeting of both mouse neuropilin-1 and neuropilin-2 genes severely impairs developmental yolk sac and embryonic angiogenesis. *Proceedings of the National Academy of Sciences of the United States of America*, **99**: 3657–62.

Takayama Y, May P, Anderson RG and Herz J (2005). Low density lipoprotein receptor-related protein 1 (LRP1) controls endocytosis and c-CBL-mediated ubiquitination of the platelet-derived growth factor receptor beta (PDGFR beta). *The Journal of biological chemistry*, **280**: 18504–10.

Takeuchi H, Kanzawa T, Kondo Y and Kondo S (2004). Inhibition of platelet-derived growth factor signalling induces autophagy in malignant glioma cells. *British journal of cancer*, **90**: 1069–75.

Tallquist MD, Weismann KE, Hellström M and Soriano P (2000). Early myotome specification regulates PDGFA expression and axial skeleton development. *Development*, **127**: 5059–70.

Taniguchi M, Masuda T, Fukaya M, Kataoka H, Mishina M, Yaginuma H., Watanabe M and Shimizu T (2005). Identification and characterization of a novel member of murine semaphorin family. *Genes to cells : devoted to molecular & cellular mechanisms*, **10**: 785–92.

Tao Q, Spring SC and Terman BI (2003). Characterization of a new alternatively spliced neuropilin-1 isoform. *Angiogenesis*, **6**: 39–45.

Tejada ML (2006). Tumor-Driven Paracrine Platelet-Derived Growth Factor Receptor Signaling Is a Key Determinant of Stromal Cell Recruitment in a Model of Human Lung Carcinoma. *Clinical Cancer Research*, **12**: 2676–2688.

Terman BI, Carrion ME, Kovacs E, Rasmussen BA, Eddy RL and Shows TB (1991). Identification of a new endothelial cell growth factor receptor tyrosine kinase. *Oncogene*, **6**: 1677–83.

Thomson S, Petti F, Sujka-Kwok I, Epstein D and Haley JD (2008). Kinase switching in mesenchymal-like non-small cell lung cancer lines contributes to EGFR inhibitor resistance through pathway redundancy. *Clinical & experimental metastasis*, **25**: 843–54.

Tischer E, Mitchell R, Hartman T, Silva M, Gospodarowicz D, Fiddes JC and Abraham JA (1991). The human gene for vascular endothelial growth factor. Multiple protein forms are encoded through alternative exon splicing. *The Journal of biological chemistry*, **266**: 11947–54.

Tomizawa Y, Sekido Y, Kondo M, Gao B, Yokota J, Roche J, Drabkin H, Lerman MI, Gazdar AF and Minna JD (2001). Inhibition of lung cancer cell growth and induction of apoptosis after reexpression of 3p21.3 candidate tumor suppressor gene SEMA3B. *Proceedings of the National Academy of Sciences of the United States of America*, **98**: 13954–9.

Tordjman R, Ortéga N, Coulombel L, Plouët J, Roméo PH and Lemarchandel V (1999). Neuropilin-1 is expressed on bone marrow stromal cells: a novel interaction with hematopoietic cells? *Blood*, **94**: 2301–9.

Tsao AS, Wei W, Kuhn E, Spencer L, Solis LM, Suraokar M, Lee JJ, Hong WK and Wistuba I I. (2011). Immunohistochemical overexpression of platelet-derived growth factor receptor-beta (PDGFR-β) is associated with PDGFRB gene copy number gain in sarcomatoid non-small-cell lung cancer. *Clinical lung cancer*, **12**: 369–74.

Uhrbom L, Hesselager G, Nistér M and Westermark B (1998). Induction of brain tumors in mice using a recombinant platelet-derived growth factor B-chain retrovirus. *Cancer research*, **58**: 5275–9.

Uren A, Merchant MS, Sun CJ, Vitolo MI, Sun Y, Tsokos M, Illei PB, Ladanyi M, Passaniti A, Mackall C *et al.* (2003). Beta-platelet-derived growth factor receptor mediates motility and growth of Ewing's sarcoma cells. *Oncogene*, **22**: 2334–42.

Ustach CV, Huang W, Conley-LaComb MK, Lin CY, Che M, Abrams J and Kim HR (2010). A novel signaling axis of matriptase/PDGF-D/ß-PDGFR in human prostate cancer. *Cancer research*, **70**: 9631–40.

Ustach CV and Kim HR (2005). Platelet-derived growth factor D is activated by urokinase plasminogen activator in prostate carcinoma cells. *Molecular and cellular biology*, **25**: 6279–88.

Uutela M, Laurén J, Bergsten E, Li X, Horelli-Kuitunen N, Eriksson U and Alitalo K (2001). Chromosomal location, exon structure, and vascular expression patterns of the human PDGFC and PDGFD genes. *Circulation*, **103**: 2242–7.

Valdembri D, Caswell PT, Anderson KI, Schwarz JP, König I, Astanina E, Caccavari F, Norman JC, Humphries MJ, Bussolino F *et al.* (2009). Neuropilin-1/GIPC1 signaling regulates alpha5beta1 integrin traffic and function in endothelial cells. *PLoS biology*, **7**: e25.

Vales A, Kondo R, Aichberger KJ, Mayerhofer M, Kainz B, Sperr WR, Sillaber C, Jäger U and Valent P (2007). Myeloid leukemias express a broad spectrum of VEGF receptors including neuropilin-1 (NRP-1) and NRP-2. *Leukemia & Lymphoma*, **48**: 1997–2007.

Valius M, Bazenet C and Kazlauskas A (1993). Tyrosines 1021 and 1009 are phosphorylation sites in the carboxy terminus of the platelet-derived growth factor receptor beta subunit and are required for binding of phospholipase C gamma and a 64-kilodalton protein, respectively. *Molecular and cellular biology*, **13**: 133–43.

Vander Kooi CW, Jusino MA, Perman B, Neau DB, Bellamy HD and Leahy DJ (2007). Structural basis for ligand and heparin binding to neuropilin B domains. *Proceedings of the National Academy of Sciences of the United States of America*, **104**: 6152–7.

Vanveldhuizen PJ, Zulfiqar M, Banerjee S, Cherian R, Saxena NK, Rabe A, Thrasher JB and Banerjee SK (2003). Differential expression of neuropilin-1 in malignant and benign prostatic stromal tissue. *Oncology reports*, **10**: 1067–71.

Veracini L, Franco M, Boureux A, Simon V, Roche S and Benistant C (2006). Two distinct pools of Src family tyrosine kinases regulate PDGF-induced DNA synthesis and actin dorsal ruffles. *Journal of cell science*, **119**: 2921–34.

Vermeulen L, de Sousa e Melo F, Richel DJ and Medema JP (2012). The developing cancer stem-cell model: clinical challenges and opportunities. *The lancet oncology*, **13**: e83–9.

Vitt UA, Hsu SY and Hsueh AJ (2001). Evolution and classification of cystine knot-containing hormones and related extracellular signaling molecules. *Molecular endocrinology (Baltimore, Md.)*, **15**: 681–94.

Vivanco I and Sawyers CL (2002). The phosphatidylinositol 3-Kinase AKT pathway in human cancer. *Nature reviews. Cancer*, **2**: 489–501.

Vlahovic G, Rabbani ZN, Herndon JE, Dewhirst MW and Vujaskovic Z (2006). Treatment with Imatinib in NSCLC is associated with decrease of phosphorylated PDGFR-beta and VEGF expression, decrease in interstitial fluid pressure and improvement of oxygenation. *British journal of cancer*, **95**: 1013–9.

Wach F, Eyrich AM, Wustrow T, Krieg T and Hein R (1996). Comparison of migration and invasiveness of epithelial tumor and melanoma cells in vitro. *Journal of dermatological science*, **12**: 118–26.

Walker LN, Bowen-Pope DF, Ross R and Reidy MA (1986). Production of platelet-derived growth factor-like molecules by cultured arterial smooth muscle cells accompanies proliferation after arterial injury. *Proceedings of the National Academy of Sciences of the United States of America*, **83**: 7311–5.

Wang J, Coltrera MD and Gown AM (1994). Cell Proliferation in Human Soft Tissue Tumors Correlates with Platelet-derived Growth Factor B Chain Expression : An Immunohistochemical and in Situ Hybridization Study. **54:** 560–564.

Wardega P, Heldin, Carl-Henrik and Lennartsson J (2010). Mutation of tyrosine residue 857 in the PDGF beta-receptor affects cell proliferation but not migration. *Cellular signalling*, **22**: 1363–8.

Wehler TC, Frerichs K, Graf C, Drescher D, Schimanski K, Biesterfeld S, Berger MR, Kanzler S, Junginger T, Galle PR *et al*. (2008). PDGFR α / ß expression correlates with the metastatic behavior of human colorectal cancer : A possible rationale for a molecular targeting strategy. **19:** 697–704.

West DC, Rees CG, Duchesne L, Patey SJ, Terry CJ, Turnbull JE, Delehedde, Maryse, Heegaard CW, Allain F, Vanpouille C *et al*. (2005). Interactions of multiple heparin binding growth factors with neuropilin-1 and potentiation of the activity of fibroblast growth factor-2. *The Journal of biological chemistry*, **280**: 13457–64.

Westermark B, Heldin CH, and Nistér M (1995). Platelet-derived growth factor in human glioma. *Glia*, **15**: 257–63.

Westermark B and Wasteson A (1976). A platelet factor stimulating human normal glial cells. *Experimental cell research*, **98**: 170–4.

Wey JS, Gray MJ, Fan F, Belcheva A, McCarty MF, Stoeltzing O, Somcio R, Liu W, Evans DB, Klagsbrun M *et al.* (2005). Overexpression of neuropilin-1 promotes constitutive MAPK signalling and chemoresistance in pancreatic cancer cells. *British journal of cancer*, **93**: 233–41.

Whitaker, Limberg BJ and Rosenbaum JS (2001). Vascular endothelial growth factor receptor-2 and neuropilin-1 form a receptor complex that is responsible for the differential signaling potency of VEGF(165) and VEGF(121). *The Journal of biological chemistry*, **276**: 25520–31.

White MF, Shoelson SE, Keutmann H and Kahn CR (1988). A cascade of tyrosine autophosphorylation in the beta-subunit activates the phosphotransferase of the insulin receptor. *The Journal of biological chemistry*, **263**: 2969–80.

Wiesmann C, Fuh G, Christinger HW, Eigenbrot C, Wells JA, and de Vos AM (1997). Crystal structure at 1.7 A resolution of VEGF in complex with domain 2 of the Flt-1 receptor. *Cell*, **91**: 695–704.

Woolard J, Bevan HS, Harper SJ, David O and Bates DO (2009). Molecular diversity of VEGF-A as a regulator of its biological activity. *Microcirculation (New York, N.Y. : 1994)*, **16**: 572–92.

Wright WC, Daniels WP and Fogh J (1981). Distinction of seventy-one cultured human tumor cell lines by polymorphic enzyme analysis. *Journal of the National Cancer Institute*, **66**: 239–47.

von Wronski MA, Raju N, Pillai R, Bogdan NJ, Marinelli ER, Nanjappan P, Ramalingam K, Arunachalam T, Eaton S, Linder KE *et al*. (2006). Tuftsin binds neuropilin-1 through a sequence similar to that encoded by exon 8 of vascular endothelial growth factor. *The Journal of biological chemistry*, **281**: 5702–10.

Wu E, Palmer N, Tian Z, Moseman AP, Galdzicki M, Wang, Xuetao, Berger B, Zhang, Hongbing and Kohane IS (2008). Comprehensive dissection of PDGF-PDGFR signaling pathways in PDGFR genetically defined cells. *PloS one*, **3**: e3794.

Wu LW, Mayo LD, DunbarJD, Kessler KM, Ozes ON, Warren RS and Donner DB (2000). VRAP is an adaptor protein that binds KDR, a receptor for vascular endothelial cell growth factor. *The Journal of biological chemistry*, **275**: 6059–62.

Wülfing C and Rupp F (2002). Neuropilin-1: another neuronal molecule in the “immunological synapse”. *Nature immunology*, **3**: 418–9.

Xiao D and He J (2010). Epithelial mesenchymal transition and lung cancer. *Journal of thoracic disease*, **2**: 154–9.

Xu AM and Huang PH (2010). Receptor tyrosine kinase coactivation networks in cancer. *Cancer research*, **70**: 3857–60.

Yamada H, Yanagisawa K, Tokumaru S, Taguchi A, Nimura Y, Osada, Hirotaka, Nagino M and Takahashi T (2008). Detailed characterization of a homozygously deleted region corresponding to a candidate tumor suppressor locus at 21q11-21 in human lung cancer. *Genes, chromosomes & cancer*, **47**: 810–8.

Yamada Y, Takakura N, Yasue H, Ogawa H, Fujisawa H and Suda T (2001). Exogenous clustered neuropilin 1 enhances vasculogenesis and angiogenesis. *Blood*, **97**: 1671–8.

Yamamoto S, Wakimoto H, Aoyagi M, Hirakawa K and Hamada H (1997). Modulation of Motility and Proliferation of Glioma Cells by Hepatocyte Growth Factor. *Cancer Science*, **88**: 564–577.

Yamasaki Y, Miyoshi K, Oda N, Watanabe M, Miyake H, Chan J, Wang X, Sun L, Tang C, McMahon G *et al*. (2001). Weekly dosing with the platelet-derived growth factor receptor tyrosine kinase inhibitor SU9518 significantly inhibits arterial stenosis. *Circulation research*, **88**: 630–6.

Yang L, Lin C, Sun SY, Zhao S and Liu ZR (2007). A double tyrosine phosphorylation of P68 RNA helicase confers resistance to TRAIL-induced apoptosis. *Oncogene*, **26**: 6082–92.

Yang W, Ahn H, Hinrichs M, Torry RJ and Torry DS (2003). Evidence of a novel isoform of placenta growth factor (PlGF-4) expressed in human trophoblast and endothelial cells. *Journal of reproductive immunology*, **60**: 53–60.

Yang YH, Rhim JS, Rasheed S, Klement V and Roy-Burman P (1979). Reversion of Kirsten sarcoma virus transformed human cells: elimination of the sarcoma virus nucleotide sequences. *The Journal of general virology*, **43**: 447–51.

Yang, Yan, Yuzawa S and Schlessinger J (2008). Contacts between membrane proximal regions of the PDGF receptor ectodomain are required for receptor activation but not for receptor dimerization. *Proceedings of the National Academy of Sciences of the United States of America*, **105**: 7681–6.

Yasuoka H, Kodama R, Tsujimoto M, Yoshidome K, Akamatsu H, Nakahara M, Inagaki M, Sanke T and Nakamura Y (2009). Neuropilin-2 expression in breast cancer: correlation with lymph node metastasis, poor prognosis, and regulation of CXCR4 expression. *BMC Cancer*, **9**: 220.

Yeh HJ, Ruit KG, Wang YX, Parks WC, Snider WD and Deuel TF (1991). PDGF A-chain gene is expressed by mammalian neurons during development and in maturity. *Cell*, **64**: 209–16.

Yoeli-Lerner M, Chin YR, Hansen CK and Toker A (2009). Akt/protein kinase b and glycogen synthase kinase-3beta signaling pathway regulates cell migration through the NFAT1 transcription factor. *Molecular cancer research : MCR*, **7**: 425–32.

Yu JC, Heidaran MA, Pierce JH, Gutkind JS, Lombardi D, Ruggiero M and Aaronson SA (1991). Tyrosine mutations within the alpha platelet-derived growth factor receptor kinase insert domain abrogate receptor-associated phosphatidylinositol-3 kinase activity without affecting mitogenic or chemotactic signal transduction. *Molecular and cellular biology*, **11**: 3780–5.

Yu J, Moon A and Kim HR (2001). Both platelet-derived growth factor receptor (PDGFR)-alpha and PDGFR-beta promote murine fibroblast cell migration. *Biochemical and biophysical research communications*, **282**: 697–700.

Yuan L, Moyon D, Pardanaud L, Bréant C, Karkkainen MJ, Alitalo, Kari and Eichmann A (2002). Abnormal lymphatic vessel development in neuropilin 2 mutant mice. *Development (Cambridge, England)*, **129**: 4797–806.

Yuqing Zhang CC (2010). ZIP4 Upregulates the Expression of Neuropilin-1, Vascular Endothelial Growth Factor, and Matrix Metalloproteases in Pancreatic Cancer Cell Lines and Xenografts. *Cancer biology & therapy*, **9**: 236.

Zacchigna S, Pattarini L, Zentilin L, Moimas S, Carrer A, Sinigaglia M, Arsic N, Tafuro S, Sinagra G and Giacca M (2008). Bone marrow cells recruited through the neuropilin-1 receptor promote arterial formation at the sites of adult neoangiogenesis in mice. *The Journal of clinical investigation*, **118**: 2062–75.

Zhang R, Banik NL and Ray SK (2008). Differential sensitivity of human glioblastoma LN18 (PTEN-positive) and A172 (PTEN-negative) cells to Taxol for apoptosis. *Brain research*, **1239**: 216–25.

Zhang S, Zhau HE, Osunkoya AO, Iqbal S, Yang X, Fan S, Chen Z, Wang R, Marshall FF, Chung LW *et al.* (2010). Vascular endothelial growth factor regulates myeloid cell leukemia-1 expression through neuropilin-1-dependent activation of c-MET signaling in human prostate cancer cells. *Molecular Cancer*, **9**: 9.

Zhang, Yujun, He, Xiangjun, Liu, Yulan, Ye Y, Zhang, Hui, He P, Zhang Q, Dong L, Liu, Yujing and Dong, Jianqiang (2011). microRNA-320a inhibits tumor invasion by targeting neuropilin 1 and is associated with liver metastasis in colorectal cancer. *Oncology Reports*, **27**: 685.

Zheng S, Chen LR, Wang HJ and Chen SZ (2007). Analysis of mutation and expression of c-kit and PDGFR-alpha gene in gastrointestinal stromal tumor. *Hepato-gastroenterology*, **54**: 2285–90.

Zhu JJ, Leon SP, Folkerth RD, Guo SZ, Wu JK and Black PM. (1997). Evidence for clonal origin of neoplastic neuronal and glial cells in gangliogliomas. *The American journal of pathology*, **151**: 565–71.